A mathematical model for IL6-induced differentiation of neural progenitor cells on a micropatterned polymer substrate

by

Cory Lee Howk

A dissertation submitted to the graduate faculty

in partial fulfillment of the requirements for the degree of

DOCTOR OF PHILOSOPHY

Major: Applied Mathematics

Program of Study Committee:
Howard Levine, Co-major Professor
Michael Smiley, Co-major Professor
Anastasios Matzavinos
Marit Nilsen-Hamilton
Jeffrey Essner

Iowa State University

Ames, Iowa

2010

DEDICATION

I would like to dedicate this thesis to my (future) wife Diane Wilson. Without your love and support, I would not have been able to complete this work. I would also like to dedicate this thesis to the memory of Dr. Larry Pearson, Department of Mathematics and Statistics, Minnesota State University, Mankato.

TABLE OF CONTENTS

LIST OF TABLES

LIST OF FIGURES

CHAPTER 1. Introduction and Experimental Results

No matter how complex a multicellular organism is, its embryonic development begins with a single cell, the fertilized ovum. This cell's DNA contains the blueprints for every cell type that exists in the mature organism. It divides and proliferates, forming a small cluster of 16 identical cells termed the *morula*. These cells continue dividing, eventually forming the *blastocyst*. The exterior cells of the blastocyst form the *trophoblast*, and the interior cells are termed the *inner cell mass (ICM)*. The ICM eventually becomes the embryo as it continues through embryogenesis, but the trophoblast develops into the embryonic portion of the placenta. This is the first occurrence during development of *differentiation*. Differentiation is the process by which these cells begin to express genes specific to a certain cell type. As development progresses, the cells of the ICM start to follow different paths. The descendents of these cells eventually become neurons, osteocytes, endothelial cells, and every other specific cell type in the mature organism. The different types of cells can be identified via the proteins they express and the behaviors they exhibit. The path the uncommitted cells choose depends on signals in their environment.

Cells express receptors for many different molecules. Activation of these receptors can initiate signal transduction cascades that can induce the cell to start transcribing different regions of DNA, depending on which receptors are activated. Activation of different receptors (or combinations of receptors) can therefore result in a myriad of possible protein combinations that can be expressed by the cell. The cells that are uncommitted to any pathway are termed *stem cells*. A *progenitor cell* is a stem cell that has chosen a general path, such as that leading to a neural-type cell. However, the progenitor cell has not yet chosen a specific fate. For example, the progenitor cell that has committed to the neural pathway could still become

either a neuron or an astrocyte. Some of these stem and progenitor cells still exist in the adult organism. They are used by the body to repair itself in the event of injury. It is in this capacity that we would like to better understand these cells. Specifically, how do these cells differentiate? What determines their fate?

The pathway of interest here is that of the differentiation of neural progenitor cells into neurons. During embryonic development, neurogenesis occurs throughout the neural tube, the precursor of the brain. These *neuroepithelial* cells can become any type of neural cell, depending on the specific transcription factors they express. The cells are exposed to different gradients of bone morphogenetic proteins (BMPs), Sonic hedgehog (Shh), and Wnt proteins, among other inductive signalling molecules. The interactions of these molecules, both with each other and with the cells of the neural tube, determine the type of neural cell they become. However, in the mature organism neurogenesis primarily occurs in two regions of the adult brain: the subventricular zone ([2]) and the dentate gyrus of the hippocampus ([17]). A better understanding of this mechanism within the mature organism could potentially lead to procedures to repair or regenerate a damaged retina. One such investigation into neural progenitor cell differentiation is given in [44]. In this investigation adult rat hippocampal progenitor cells (AHPCs) are exposed to hippocampal astrocytes and laminin under various conditions. The percentage of AHPCs expressing class III β-tubulin (TUJ1) is measured. TUJ1 is an early neuronal marker, indicating that these cells have begun to differentiate into neurons.

Experiments were performed over two types of polystyrene substrates: one substrate was smooth, and the other had microgrooves etched into the plate. Results were gathered for four experimental conditions: control, noncontact coculture, contact coculture, and conditioned media. In all experiments performed, the polystyrene substrate was first coated with laminin. For the control experiment (1), AHPCs were plated on the laminin. For the contact coculture experiment (2), astrocytes were plated on the laminin and grown for two days, after which AHPCs were plated on the astrocytes in direct contact with them. For the noncontact coculture experiment (3), AHPCs were plated on the laminin and the astrocytes were held in an

Table 1.1 Percent observed differentiation (TUJ1 expression level)

Experiment	AHPC cells only (1)	AHPC+Astrocyte in contact (2)	AHPC+Astrocyte in non contact (3)	AHPC in Astrocyte secreted media (4)
Patterned	16%	35%	75%	38%
Non patterned	17%	20%	73%	41%

Table 1.2 Percent observed differentiation (TUJ1 expression level)

IL6 added (ng/mL)	0	.00001	.0001	.001	.01	.1	1	10	100
	19%	20%	20%	27%	25%	31%	37%	35%	36%

insert above the AHPCs, allowing diffusion of chemicals but preventing direct contact. For the conditioned media experiment (4), AHPCs were plated on the laminin and astrocytes were cultured separately. The media from the astrocyte culture, containing astrocyte secreted factors, was then fed to the AHPCs every 24 hours for six days. The percentages of cells that express TUJ1 after six days for each of these experiments are shown in Table 1.1.

Once it was hypothesized that the soluble extracellular protein interleukin-6 (IL6) was inducing differentiation, a second set of experiments was performed, where certain concentrations of IL6 were added to the control experiment on the smooth substrate every 48 hours ([41]). The percentages of cells that express TUJ1 after six days for each of these experiments are shown in Table 1.2.

It was also shown in [44] that when the cells differentiate into early neurons they sprout neuritic extensions that tend to align parallel to the grooves on the patterned substrate, but which radiate out from the cell randomly on the smooth substrate with no bias in their alignment. When cultured with astrocytes, the neurites also exhibited a tendancy to align with astrocyte cytoskeletal filaments. However, not much movement of the cell body itself is observed during these experiments.

The goals of this dissertation are to derive a biologically-reasonable mathematical model

that simulates these experimental results and to analyze the resultant model in order to help guide future research in this area. In Chapter 2 a brief review of cellular communication is provided, and the protein IL6 is introduced. Chapter 3 focuses on a system of ordinary differential equations (ODEs) used to model the kinetics of the biological mechanism for IL6-induced differentiation of AHPCs. This system models the cellular densities and chemical concentrations present over the six day period of the biological experiment. It is referred to as the population model throughout the dissertation, as the densities/concentrations are proportional to the numbers of cells/molecules. A sensitivity analysis for the population model is performed in Chapter 4 in order to examine how sensitive the output for the percentage of cells that differentiate is to each parameter in the ODE system. Chapter 5 looks beyond the first six days to examine the long-term behavior of the system. Steady state concentrations are calculated for each species, and their stability is analyzed. This is attempted through local linearization around each steady state, and in one case is studied globally throughout the biologically feasible region through the use of a Lyapunov function. In Chapter 6 the population model is expanded to include spatial variation and is explored under various chemotactic conditions. Chapter 7 presents discussions of the numerical methods used to generate the data in chapter 6. Finally, chapter 8 is a discussion of conclusions of this research and areas for future work.

CHAPTER 2. Cellular Communication

Cellular communication can occur either through direct contact or via diffusible signalling molecules. These diffusible signals could include paracrine (short-range) factors like IL6, which bind to surface receptors and initiate signal transduction cascades, or hormones like estrogen, which diffuse through the cytosolic membrane and bind to a protein receptor, which then binds directly to DNA. Some paracrine factors and hormones could also bind to surface receptors and open ion channels. Direct contact between a cell and extracellular matrix proteins such as fibronectin and laminin could include integrin binding, which can both mediate cellular adhesion and migration, or initiate a signal transduction cascade. Binding can also occur between adjacent cells through the use of cadherins. This cell-cell binding can initiate signal transduction cascades in one or both cells. Possible responses to these signals include alterred gene expression, increased proliferation, or even migration toward/away from the signal. Biological systems can use various combinations of these mechanisms, resulting in the great complexity of biological responses that exists in nature. In the hypothesized mechanism for AHPC differentiation into neurons, astrocytes secrete the cytokine interleukin-6, inducing differentiation via a pathway for this diffusible signalling molecule. It is also proposed here that the secretion rate is modulated via direct contact between astrocytes and the AHPC target cells.

2.1 Cytokines and Interleukin-6

The signalling molecule hypothesized to induce differentiation in this biological system is a cytokine. Cytokines are small soluble messenger proteins or peptides important for cell-to-cell communication in immunological responses, hemapoiesis, neurogenesis, and embryogenesis. They typically have a small mass of between 8 and 30 kDa (kiloDaltons) and act over short

distances as autocrine or paracrine factors. They typically act at very low concentrations. Their activity is often redundant, in that similar cellular responses may be obtained through binding by several different cytokines. The cytokine family includes interleukins (IL), interferons (INF), tumor necrosis factors (TNF), colony-stimulating factors, and growth factors. Many of the processes during embryonic development are regulated by cytokines. They are also used in the immune system both as messengers between cells in defense reactions and also as chemoattractants during the process of inflammation. ([29],[15])

Interleukins are a group of cytokines that were initially discovered as messengers between white blood cells (leukocytes). They have since been found to be produced by other cell types. They have many uses during development. For example, during embryogenesis muscles form through a response to IL-4, which myotubes secrete to attract additional myoblasts. During hemapoiesis, IL-3 promotes the survival and proliferation of erythroid progenitor cells. During mammalian birth, IL-1β activates enzymes that stimulate production of the prostaglandin hormones that are responsible for uterine contractions. ([20])

The cytokine of most interest here is interleukin-6 (IL6). IL6 has many varied applications. It is used for growth promotion of myeloma cells and hematopoietic progenitors, promotion of thrombopoiesis, induction of neuronal survival and differentiation, and the differentiation of mouse myeloid leukemia cell line M1 to the macrophage cell line. It is often expressed at points of inflammation. It is also expressed by Schwann cells at points of lesion when the hypoglossal nerve is injured. The related cytokine IL6R is detectable in the nerve cell bodies. ([54])

In the IL6 pathway, IL6 first binds to one receptor. This receptor complex then binds to another receptor, initiating a signal transduction cascade. IL6 binds to an IL6 receptor (IL6R) on the surface of the target cell, attaching to the extracellular α-subunit. The cytosolic portion is comprised of only 82 amino acids, and is not involved in signalling. This complex must then associate with two transmembrane gp130 receptors in order to initiate a signal transduction cascade inside the cell. Once the complex associates with a gp130 homodimer, protein tyrosine kinases of the JAK family are activated. These JAKs are associated with the cytoplasmic region of gp130. They phosphorylate tyrosine residues on gp130, allowing STAT3 to associate

with gp130, which is then itself phosphorylated. STAT3 dimerizes with another phosphorylated STAT3, and this dimer relocates to the nucleus, where it binds to corresponding regions of DNA to activate transcription of neighboring genes. The RAS/MAPK signalling pathway may also be activated by stimulation of gp130. ([35],[54])

Whereas all cells express gp130 receptors on their surface, not all cells express the surface IL6 receptor. To bind to these cells, IL6 must use a mechanism known as *transsignalling*. During transsignalling, IL6 first binds to a soluble IL6 receptor (sIL6Rα). The {IL6:sIL6Rα} complex then induces the homodimerization of gp130 receptors on another cell, binding to the complex, and initiating the cascade. It is named transsignalling because sIL6Rα can be produced by a different cell than the cell to which the complex binds. Hence sIL6Rα acts as a paracrine factor. There are two known mechanisms by which it can be produced. It could be formed due to alternative splicing of the mRNA for the IL6 receptor, or it could be formed by proteolysis of the extracellular α-subunit of a surface IL6 receptor, a process known as shedding. The ligand binding domain is identical both on the surface IL6R and the soluble sIL6Rα, and as a result the binding affinity of IL6 is nearly identical in either case. Neither IL6 nor the IL6 receptor alone can bind to gp130 to initiate the signal cascade; they first must be bound as a complex. Hence, since the cytosolic portion of the surface IL6R does not contribute to the cascade, sIL6Rα acts as an agonist for IL6 signalling. ([35])

In addition to sIL6Rα, there also exists a soluble gp130 receptor (sgp130). sgp130 is generated either by a cell shedding the extracellular domain or as a result of alternative splicing of the mRNA for the gp130 receptor. sgp130 acts as an inhibitor to the {IL6:sIL6Rα} complex since it can bind the complex but lacks the cytosolic portion of the gp130 dimer needed to initiate the signal transduction cascade. Hence it is an antagonist to IL6 signalling in systems utilizing this pathway. The {IL6:sIL6Rα} complex can bind to either gp130 or sgp130, however the {IL6:IL6R} complex associates rapidly with two molecules of gp130, and steric hinderance prevents sgp130 from associating with {IL6:IL6R}. Therefore sgp130 is not an antagonist to IL6 signalling via this pathway. ([24])

2.2 Cell Migration

The migration of cells is a common occurrence in nature. It can be seen everywhere, e.g., the migration of bacteria, the movements of mesenchymal cells during embryogenesis, and the movement of neutrophils toward bacteria within a mature organism with an active immune system. Since cell movements occur in such varied locations in nature, it is not surprising that multiple mechanisms for movement have evolved over time. An excellent reference for cell movements is [9].

Swimming and crawling are two common forms of movement. *Swimming* is the propulsion of cells through a solution due to the beating of surface appendages. *Crawling* is the motion of a cell over a surface due to alternating cycles of extension and contraction, which are often visible by deformation of the cellular surface. This motion is aided by anchorage of the cell to the surface by use of integrin proteins.

Escherichia Coli swim by use of between six and ten flagella, each rotated by its own molecular motor in the cell wall. Mammalian sperm possess just one flaggelum, which is bent by the actions of proteins (including dynein) within the flagellum. *Paramecium* swim by the coordinated movement of thousands of cilia on the cell surface, driving water over the cell in a coordinated fashion.

Most migratory cells of the mammalian body move by crawling instead of swimming. This occurs through the use of filopodia, lamellipodia, and pseudopodia. They are related structures, comprising actin filaments that polymerize, pushing on the plasma membrane and causing a protrusion to develop. Filopodia can be considered to be one dimensional protrusions, lamellipodia are two dimensional, and pseudopodia are three dimensional. Epithelial cells, fibroblasts, and some neurons use lamellipodia, and migrating growth cones use lamellipodia and filopodia. Amoebae commonly use pseudopodia. The protrusion attaches to the substrate by forming focal adhesions around integrins. Corticol contraction propels the cell's contents forward in an effort to relieve some of the tension formed by exerting the protrusion and forming the focal adhesion. Finally, focal adhesions at the rear of the cell are disassembled.

Migratory cells undergo random motion, but in the presence of certain stimulatory chem-

icals they can undergo directed movement. Receptors on the surface of the lamellipodia or filopodia detect chemicals in their environment. *Chemotaxis* is the process by which cells migrate in response to a gradient in a certain chemical in the vicinity of the cell. Binding of a chemoattractant leads to a greater increase in actin polymerization within the area of highest chemoattractant concentration. As the distribution of actin becomes greater in this area, the protrusions become localized to this area, and the cell moves in this direction. This is an especially important process during the formation of neuritic processes, and most dramatically within the axon. The growth cone of the axon forms a lamellipodium and uses many filopodia to explore its environment. The growth cone must use these guidance cues to lead the axon very long distances (relative to cell size) in order to find its proper location within the organism.

CHAPTER 3. Population Model for Cellular Differentiation

The goal of this chapter is to build a system of ordinary differential equations modeling the essential features of the IL6 mechanism discussed in Chapter 2. This mechanism includes two signalling pathways: pathway #1, which uses surface receptors, and pathway #2, which uses soluble receptors. There is also a soluble inhibitor of pathway #2 present in the system. The end result of the IL6 signalling is the production of an intracellular molecule J, inducing differentiation of the AHPC.

To build a system of ODEs for this mechanism, three scales of densities must be considered: cell densities, (soluble) chemical concentrations, and (surface) receptor densities. The soluble proteins and cell surface receptors involved in this model have similar masses of 20-50 kD and 80-250 kD, respectively, while the cells are much larger, comprised of millions of proteins. The difference in scale can be visualized easily by comparing a grain of rice to a standard room in a house. The length of the rice is roughly one-thousandth the length of the room. A eukaryotic cell is about one-thousandth the length of the last joint of a finger, and a protein is about one-thousandth the length of a cell ([21]).

The cell culture system under consideration consists of three cell types: progenitor cells (AHPC), differentiated cells (TUJ1-expressing cells, early neurites), and astrocytes. Cells move from the progenitor population into the differentiated population in response to cytokines secreted by the astrocytes. The species included in this model are listed in Table 3.1. The mechanism of action is illustrated by the wiring diagram in Figure 3.1.

Table 3.1 Variables and their definitions

Species	Chemical Abbreviation	Concentration/Density
interleukin-6	IL6	$[A_i]$
soluble IL6 receptor	sIL6Rα	$[R_{il}]$
IL6 ligand-soluble receptor complex	{IL6:sIL6Rα}	$[A_a]$
soluble glycoprotein-130	sgp130	$[G_p]$
IL6, sIL6Rα, sgp130 trimeric complex	{IL6:sIL6α:sgp130}	$[A_o]$
surface IL6 receptor on AHPC	IL6R	$[R^p_{il}]$
IL6 ligand-surface receptor complex	{IL6:IL6R}	$[A_s]$
transmembrane glycoprotein-130 on AHPC	gp130	$[R^p_{gp130}]$
IL6-induced signal transduction factor (a hypothesized intracellular protein)		$[J]$
progenitor cell	AHPC	N^p
TUJ1 expressing cell		N^d
astrocyte		N_a

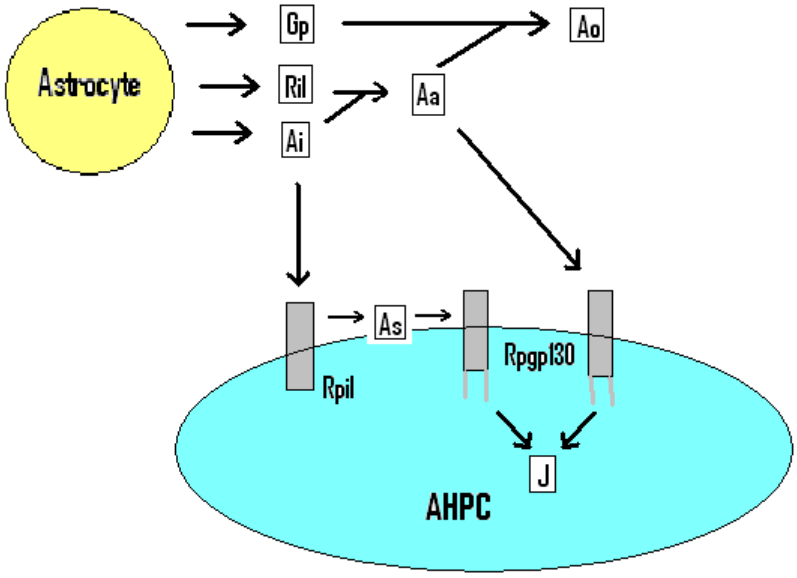

Figure 3.1 *Schematic of action for cellular communication through the IL6 mechanism.*

3.1 Building the Model

The steps in the hypothesized intercellular signal are modeled by the following reactions. We first consider pathway #1. Astrocyte-secreted IL6 (A_i) first binds to the IL6 receptor (R^p_{il}) on the surface of the AHPC, forming the complex A_s. This complex then binds to the surface gp130 homodimer (R^p_{gp130}), initiating a signal transduction cascade. This cascade leads to the production of the intracellular molecule J. In accordance with their biological activities, A_i can be termed "inactive IL6" and A_s "surface (activated) IL6". These reactions can be summarized as

$$A_i + R^p_{il} \underset{\widehat{k}_{-1}}{\overset{\widehat{k}_1}{\rightleftharpoons}} A_s,$$

$$A_s + R^p_{gp130} \underset{\widehat{l}_{-1}}{\overset{\widehat{l}_1}{\rightleftharpoons}} \{A_s : R^p_{gp130}\} \overset{\widehat{l}_2}{\rightarrow} \; J + R^p_{gp130} + R^p_{il}.$$

We now consider pathway #2. Astrocyte-secreted IL6 (A_i) first binds to the astrocyte-secreted soluble IL6 receptor (R_{il}), forming the soluble complex A_a. This complex can be referred to as "activated IL6", since it can bind directly to R^p_{gp130}, initiating the signal transduction cascade, producing J. These reactions can be summarized as

$$A_i + R_{il} \underset{l_{-1}}{\overset{l_1}{\rightleftharpoons}} A_a,$$

$$A_a + R^p_{gp130} \underset{\nu_{-1}}{\overset{\nu_1}{\rightleftharpoons}} \{A_a : R^p_{gp130}\} \overset{\nu_2}{\rightarrow} \; J + R^p_{gp130}.$$

Competitive inhibition of pathway #2 can occur through the reaction

$$A_a + G_p \underset{k_{-1}}{\overset{k_1}{\rightleftharpoons}} A_o$$

in which the activated IL6 (A_a) binds to the astrocyte-secreted soluble gp130 receptor (G_p), forming the complex A_o. A_o can be termed "inhibited IL6" since it is not bound to the cell membrane and hence cannot initiate an intracellular signal transduction cascade.

The kinetics of these reactions are given by the following system of ordinary differential

equations, formed through simple mass action considerations:

$$\begin{aligned}
\frac{d[A_i]}{dt} &= -l_1[A_i][R_{il}] + l_{-1}[A_a] - \widehat{k}_1[A_i][R^p_{il}]N^p + \widehat{k}_{-1}[A_s]N^p,\\
\frac{d[R_{il}]}{dt} &= -l_1[A_i][R_{il}] + l_{-1}[A_a],\\
\frac{d[A_a]}{dt} &= l_1[A_i][R_{il}] - l_{-1}[A_a] - k_1[A_a][G_p] + k_{-1}[A_o]\\
&\quad - \nu_1[A_a][R^p_{gp130}]N^p + \nu_{-1}[\{A_a : R^p_{gp130}\}]N^p,\\
\frac{d[G_p]}{dt} &= -k_1[A_a][G_p] + k_{-1}[A_o],\\
\frac{d[A_o]}{dt} &= k_1[A_a][G_p] - k_{-1}[A_o],\\
\frac{d[R^p_{il}]}{dt} &= -\widehat{k}_1[A_i][R^p_{il}] + \widehat{k}_{-1}[A_s] + \widehat{l}_2[\{A_s : R^p_{gp130}\}],\\
\frac{d[A_s]}{dt} &= \widehat{k}_1[A_i][R^p_{il}] - \widehat{k}_{-1}[A_s] - \widehat{l}_1[A_s][R^p_{gp130}] + \widehat{l}_{-1}[\{A_s : R^p_{gp130}\}],\\
\frac{d[\{A_s : R^p_{gp130}\}]}{dt} &= \widehat{l}_1[A_s][R^p_{gp130}] - (\widehat{l}_{-1} + \widehat{l}_2)[\{A_s : R^p_{gp130}\}],\\
\frac{d[R^p_{gp130}]}{dt} &= -\widehat{l}_1[A_s][R^p_{gp130}] + (\widehat{l}_{-1} + \widehat{l}_2)[\{A_s : R^p_{gp130}\}]\\
&\quad - \nu_1[A_a][R^p_{gp130}] + (\nu_{-1} + \nu_2)[\{A_a : R^p_{gp130}\}],\\
\frac{d[\{A_a : R^p_{gp130}\}]}{dt} &= \nu_1[A_a][R^p_{gp130}] - (\nu_{-1} + \nu_2)[\{A_a : R^p_{gp130}\}],\\
\frac{d[J]}{dt} &= \widehat{l}_2[\{A_s : R^p_{gp130}\}] + \nu_2[\{A_a : R^p_{gp130}\}].
\end{aligned}$$

In these equations, the cytokine concentrations $[A_i]$, $[R_{il}]$, $[A_a]$, $[G_p]$, and $[A_o]$ are measured in $nmol/mL$ and the surface receptor concentrations $[R^p_{il}]$, $[A_s]$, $[\{A_s : R^p_{gp130}\}]$, $[R^p_{gp130}]$, and $[\{A_a : R^p_{gp130}\}]$ are measured in $nmol/cell$. The concentration of the intracellular molecule $[J]$ is also measured in $nmol/cell$. N^p denotes the density of progenitor cells, and is included in the differential equations for A_i and A_a due to the different units used for soluble molecules and surface receptors.

Hippocampal astrocytes have been shown experimentally to secrete IL6 ([5]). In this model it is hypothesized that astrocytes also secrete the two soluble receptors sIL6Rα and sgp130. Thus the production and degradation of the soluble proteins, along with the degradation of

the soluble intracellular molecule J, satisfy the rate laws

$$\begin{aligned}
\frac{d[A_i]}{dt} &= S_{ai}(t) + a_1 N_a - \mu_{ai}[A_i], \\
\frac{d[R_{il}]}{dt} &= S_{il}(t) + b_a N_a - \mu_{il}[R_{il}], \\
\frac{d[A_a]}{dt} &= S_{aa}(t) - \mu_{aa}[A_a], \\
\frac{d[G_p]}{dt} &= S_{gp}(t) + s_a N_a - \mu_{gp}[G_p], \\
\frac{d[A_o]}{dt} &= S_{ao}(t) - \mu_{ao}[A_o], \\
\frac{d[J]}{dt} &= -\mu_j[J],
\end{aligned}$$

where N_a denotes the density of astrocytes and $S_{ai}(t)$, $S_{il}(t)$, $S_{aa}(t)$, $S_{gp}(t)$, and $S_{ao}(t)$ are possible source terms. The astrocyte density N_a and the source functions $S_z(t)$ are chosen according to experimental conditions. For example, if there are no astrocytes present (as in the experiments with AHPCs alone or in the conditioned media experiments), then $N_a = 0$. In the latter of these two cases, the source functions would be used to model the daily treatment of astrocyte conditioned medium. For example, they could be written as

$$S_z(t) = \sum_{i=1}^{N} Z_0 \delta(t - t_i)$$

where t_i, $i \in \{1, 2, ..., N\}$, are the times at which the astrocyte-conditioned medium is introduced to the culture, with Z_0 being the concentration of the protein Z present in the conditioned medium. This is the only experiment in which the source functions $S_{ai}(t)$, $S_{il}(t)$, $S_{aa}(t)$, $S_{gp}(t)$, and $S_{ao}(t)$ are taken to be not identically zero.

The last step in the IL6 mechanism is the production of the intracellular molecule J, and it is hypothesized within this simplified mechanism that the differentiation of the AHPC is a direct response to the concentration of J. However, since J is produced through the IL6 mechanism alone in this mathematical model, but differentiation is occuring during the control experiment where there are no astrocytes present to produce IL6, a certain level of background differentiation must be included. In the model, the differentiation of AHPCs into neurons can be expressed as the "chemical" equation

$$N^p \xrightarrow{K_1(N^p, N^d) + K_2([J])} N^d.$$

The background differentiation occurs via some unknown mechanism. For the simulations in this dissertation the function governing this rate of differentiation is taken to be

$$K_1(N^p, N^d) = \theta_1\Big(\theta_2 + (\frac{N^d}{N^p + N^d})^2\Big)^{-1}$$

for some empirical constants θ_1 and θ_2. These constants are obtained through data from the controlled experiment. When IL6 is present, we can assume that the process causing differentiation via the background mechanism is still active. However, the differentiation due to this mechanism cannot be distinguished from that due to the IL6 mechanism. The form for the function K_1 is chosen because it results in a consistent low level of differentiation during the other experiments ($\sim 10\%$). The function governing the rate of IL6-induced differentiation is taken here to be sigmoidal, under the assumption that a certain threshold of J must be reached to have any appreciable level of differentiation occuring. Thus $K_2([J])$ is taken to be

$$K_2([J]) = \frac{\kappa_1[J]^2}{{\kappa_2}^2 + [J]^2}$$

for some constants κ_1 and κ_2. N^p will decrease as cells differentiate. However, since $[J]$ is measured in $nmol/cell$, it will not decrease as the cells differentiate.

Finally, we include simple logistic growth for the proliferation of the progenitor cells. When a cell divides, it is assumed here that division is symmetric so that the molecules of J are divided equally among the daughter cells. Since $[J]$ is measured in $nmol/cell$, proliferation results in a decrease in J. During proliferation only the unbound receptors R^p_{il} and R^p_{gp130} are synthesized, and the receptors are divided equally among the daughter cells. Therefore $nmol/cell$ of bound surface receptors also decreases during proliferation. To see how the receptor concentrations are changing, note that the total $nmol$ of Z is given by $[Z] \cdot N^p$, where Z is a surface receptor or bound surface receptor complex. Differentiating, we have that

$$\frac{d([Z]N^p)}{dt} = \frac{d[Z]}{dt}N^p + [Z]\frac{dN^p}{dt} = 0,$$

which implies that

$$\begin{aligned}\frac{d[Z]}{dt} &= -\frac{[Z]}{N^p}\frac{dN^p}{dt}\\ &= -\frac{[Z]}{N^p}\cdot M_1 N^p\Big(1-\frac{N^p+N^d}{N_{max}}\Big)\\ &= -[Z]M_1\Big(1-\frac{N^p+N^d}{N_{max}}\Big).\end{aligned}$$

Denoting the total concentration of R^p_{il} (R^p_{gp130}) in both bound and unbound states by $[R^p_{il}]_0$ ($[R^p_{gp130}]_0$) $nmol/cell$, and letting $\eta = M_1\Big(1-\frac{N^p+N^d}{N_{max}}\Big)$, yields the equations

$$\begin{aligned}\frac{d[R^p_{il}]}{dt} &= ([R^p_{il}]_0 - [R^p_{il}])\eta,\\ \frac{d[A_s]}{dt} &= -[J]\eta,\\ \frac{d[\{A_s : R^p_{gp130}\}]}{dt} &= -[\{A_s : R^p_{gp130}\}]\eta,\\ \frac{d[R^p_{gp130}]}{dt} &= ([R^p_{gp130}]_0 - [R^p_{gp130}])\eta,\\ \frac{d[\{A_a : R^p_{gp130}\}]}{dt} &= -[\{A_a : R^p_{gp130}\}]\eta,\\ \frac{d[J]}{dt} &= -[J]\eta,\\ \frac{dN^p}{dt} &= -\Big\{K_1(N^p,N^d)+K_2([J])\Big\}N^p + N^p\eta,\\ \frac{dN^d}{dt} &= \Big\{K_1(N^p,N^d)+K_2([J])\Big\}N^p.\end{aligned}$$

Superimposing the above effects yields the system

$$\begin{aligned}\frac{d[A_i]}{dt} &= S_{ai}(t) + a_1N_a - l_1[A_i][R_{il}] + l_{-1}[A_a] - \widehat{k}_1[A_i][R^p_{il}]N^p\\ &\quad + \widehat{k}_{-1}[A_s]N^p - \mu_{ai}[A_i],\\ \frac{d[R_{il}]}{dt} &= S_{il}(t) + b_aN_a - l_1[A_i][R_{il}] + l_{-1}[A_a] - \mu_{Il}[R_{il}],\\ \frac{d[A_a]}{dt} &= S_{aa}(t) + l_1[A_i][R_{il}] - l_{-1}[A_a] - k_1[A_a][G_p] + k_{-1}[A_o]\\ &\quad - \nu_1[A_a][R^p_{gp130}]N^p + \nu_{-1}[\{A_a : R^p_{gp130}\}]N^p - \mu_{aa}[A_a],\\ \frac{d[G_p]}{dt} &= S_{gp}(t) + s_aN_a - k_1[A_a][G_p] + k_{-1}[A_o] - \mu_{gp}[G_p],\\ \frac{d[A_o]}{dt} &= S_{ao}(t) + k_1[A_a][G_p] - k_{-1}[A_o] - \mu_{ao}[A_o],\end{aligned}$$

$$
\begin{aligned}
\frac{d[R^p_{il}]}{dt} &= -\widehat{k}_1[A_i][R^p_{il}] + \widehat{k}_{-1}[A_s] + \widehat{l}_2[\{A_s : R^p_{gp130}\}] + ([R^p_{il}]_0 - [R^p_{il}])\eta, \\
\frac{d[A_s]}{dt} &= \widehat{k}_1[A_i][R^p_{il}] - \widehat{k}_{-1}[A_s] - \widehat{l}_1[A_s][R^p_{gp130}] + \widehat{l}_{-1}[\{A_s : R^p_{gp130}\}] - [A_s]\eta, \\
\frac{d[\{A_s : R^p_{gp130}\}]}{dt} &= \widehat{l}_1[A_s][R^p_{gp130}] - (\widehat{l}_{-1} + \widehat{l}_2)[\{A_s : R^p_{gp130}\}] - [\{A_s : R^p_{gp130}\}]\eta, \\
\frac{d[R^p_{gp130}]}{dt} &= -\widehat{l}_1[A_s][R^p_{gp130}] + (\widehat{l}_{-1} + \widehat{l}_2)[\{A_s : R^p_{gp130}\}] - \nu_1[A_a][R^p_{gp130}] \\
&\quad + (\nu_{-1} + \nu_2)[\{A_a : R^p_{gp130}\}] + ([R^p_{gp130}]_0 - [R^p_{gp130}])\eta, \\
\frac{d[\{A_a : R^p_{gp130}\}]}{dt} &= \nu_1[A_a][R^p_{gp130}] - (\nu_{-1} + \nu_2)[\{A_a : R^p_{gp130}\}] - [\{A_a : R^p_{gp130}\}]\eta, \\
\frac{d[J]}{dt} &= \widehat{l}_2[\{A_s : R^p_{gp130}\}] + \nu_2[\{A_a : R^p_{gp130}\}] - \mu_j[J] - [J]\eta, \\
\frac{dN^p}{dt} &= -\Big\{K_1(N^p, N^d) + K_2([J])\Big\}N^p + N^p\eta, \\
\frac{dN^d}{dt} &= \Big\{K_1(N^p, N^d) + K_2([J])\Big\}N^p.
\end{aligned}
$$

Two conservation laws exist for this system:

$$
\begin{aligned}
[R^p_{il}]_0 &= [R^p_{il}] + [A_s] + [\{A_s : R^p_{gp130}\}], \\
[R^p_{gp130}]_0 &= [R^p_{gp130}] + [\{A_s : R^p_{gp130}\}] + [\{A_a : R^p_{gp130}\}].
\end{aligned}
$$

The surface receptors act in a fashion similar to enzymes, in that they take a substrate (IL6) and convert it to product (J). Numerical simulations show that the concentrations of the surface receptor complexes $[A_s]$, $[\{A_s : R^p_{gp130}\}]$, and $[\{A_a : R^p_{gp130}\}]$ quickly come to equilibrium with the other species in the system. In accordance with the Michaelis-Menten hypothesis, we assume that the time rate of change of these complexes are small,

$$
\frac{d[A_s]}{dt} \approx 0, \qquad \frac{d[\{A_s : R^p_{gp130}\}]}{dt} \approx 0, \qquad \frac{d[\{A_a : R^p_{gp130}\}]}{dt} \approx 0.
$$

This will lead to a simplification of the above system. (A nondimensionalization will be performed as a part of future work, explicitly showing the existence of the different time scales and hence providing a mathematical justification for this approximation.) The population model

(3.1) for AHPC differentiation becomes:

$$\begin{aligned}
\frac{d[A_i]}{dt} &= S_{ai}(t) + a_1 N_a - l_1[A_i][R_{il}] + l_{-1}[A_a] - \widehat{k}_1[A_i][R^p_{il}]N^p + \widehat{k}_{-1}[A_s]N^p - \mu_{ai}[A_i],\\
\frac{d[R_{il}]}{dt} &= S_{il}(t) + b_a N_a - l_1[A_i][R_{il}] + l_{-1}[A_a] - \mu_{il}[R_{il}],\\
\frac{d[A_a]}{dt} &= S_{aa}(t) + l_1[A_i][R_{il}] - l_{-1}[A_a] - k_1[A_a][G_p] + k_{-1}[A_o]\\
&\quad - \nu_1[A_a][R^p_{gp130}]N^p + \nu_{-1}[\{A_a : R^p_{gp130}\}]N^p - \mu_{aa}[A_a],\\
\frac{d[G_p]}{dt} &= S_{gp}(t) + s_a N_a - k_1[A_a][G_p] + k_{-1}[A_o] - \mu_{gp}[G_p],\\
\frac{d[A_o]}{dt} &= S_{ao}(t) + k_1[A_a][G_p] - k_{-1}[A_o] - \mu_{ao}[A_o],\\
\frac{d[J]}{dt} &= \widehat{l}_2[\{A_s : R^p_{gp130}\}] + \nu_2[\{A_a : R^p_{gp130}\}] - \mu_j[J] - [J]\eta,\\
\frac{dN^p}{dt} &= -\Big\{K_1(N^p, N^d) + K_2([J])\Big\}N^p + N^p\eta,\\
\frac{dN^d}{dt} &= \Big\{K_1(N^p, N^d) + K_2([J])\Big\}N^p,
\end{aligned}$$

with AHPC receptor concentrations

$$\begin{aligned}
b &= \frac{L[R^p_{gp130}]_0 + ([R^p_{gp130}]_0 - [R^p_{il}]_0)[A_i]}{\widehat{K} + [A_i]} + \frac{\widehat{L}(V + [A_a])}{V},\\
c &= \frac{-\widehat{L}(V + [A_a])[A_i][R^p_{il}]_0}{V(\widehat{K} + [A_i])},\\
[A_s] &= (-b + \sqrt{b^2 - 4c})/2,\\
[\{A_a : R^p_{gp130}\}] &= \frac{L[R^p_{gp130}]_0 + [A_i]([R^p_{gp130}]_0 - [R^p_{il}]_0) + (\widehat{K} + [A_i])[A_s]}{(L + [A_i])(V + [A_a])}[A_a],\\
[\{A_s : R^p_{gp130}\}] &= \frac{[A_i][R^p_{il}]_0 - (\widehat{K} + [A_i])[A_s]}{L + [A_i]},\\
[R^p_{il}] &= [R^p_{il}]_0 - [A_s] - [\{A_s : R^p_{gp130}\}],\\
[R^p_{gp130}] &= [R^p_{gp130}]_0 - [\{A_a : R^p_{gp130}\}] - [\{A_s : R^p_{gp130}\}],
\end{aligned}$$

where $L = \frac{\widehat{l}_2 + \eta}{\widehat{k}_1}$, $\widehat{L} = \widehat{L_m} + \frac{\eta}{\widehat{l}_1}$, $V = V_m + \frac{\eta}{\nu_1}$, and $\widehat{K} = \widehat{K_d} + \frac{\eta}{\widehat{k}_1}$. Initial conditions must accompany this system. Under the assumption that there are no cytokines present initially, and that the only cell population present are the undifferentiated AHPCs (and possibly astrocytes),

the initial conditions are

$$
\begin{aligned}
&[A_i]_0 = [A_a]_0 = [A_o]_0 = 0 \\
&[R_{il}]_0 = [G_p]_0 = 0 \\
&[R^p_{il}]_0 = n_1, \qquad [R^p_{gp130}]_0 = n_2 \\
&[A_s]_0 = [\{A_a : R^p_{gp130}\}]_0 = [\{A_s : R^p_{gp130}\}]_0 = 0 \\
&N^p(0) = N^p_0, \qquad N^d(0) = 0.
\end{aligned}
$$

3.2 Numerical Results

The biological experiments occur on two different substrates. One set of experiments is performed on a smooth substrate, and the other set is performed on a plate that has parallel grooves etched into it. The first set can be simulated numerically on a two-dimensional surface. The second set can be simulated numerically on a three-dimensional surface, using grooves of finite thickness. However, it is claimed here that analysis of the population model will suffice for simulating most of the experiments. First, during the course of the experiments, the astrocytes are observed to be stationary, and little to no movement of cell bodies has been observed for the AHPCs or the TUJ1-expressing cells. Secondly, in all experiments, the AHPCs are plated with a uniform density. Finally, in all experiments except the contact coculture on the patterned substrate, all cytokines are being added to the system in a uniform manner. Due to the assumptions of homogeneity of all species, the homogeneous addition of all chemicals to the system, and the experimental observation of little to no movement of the cells of interest, the population model should suffice for simulating the following experiments: control (both substrates), IL6-pulse (which are only performed on smooth substrates), noncontact coculture (both substrates), conditioned media (both substrates), and contact coculture (smooth substrate only). Spatial considerations must be taken into account when simulating the contact coculture on the patterned substrate, since the astrocyte density is not uniform and hence cytokines are not added in a uniform fashion to the system. This case will be considered in Chapter 6.

All population models are simulated using the classical 4th order Runge-Kutta method. Simulations are executed in Fortran 90, with the resultant data illustrated graphically with Matlab. The values of the parameters used are given in Tables 3.4-5 at the end of the chapter.

3.2.1 Control

In this experiment, a uniform layer of AHPCs is applied to the laminin at a density of 1.5×10^4 cells/cm^2. No astrocytes are added to the system. There is no IL6 entering this system, so the only differentiation occuring is due to the background mechanism. The system of ODEs reduces to

$$\begin{aligned}
\frac{dN^p}{dt} &= -\theta_1 N^p \left(\theta_2 + (\frac{N^d}{N^p + N^d})^2\right)^{-1} + M_1 N^p \left(1 - \frac{N^p + N^d}{N_{max}}\right), \\
\frac{dN^d}{dt} &= \theta_1 N^p \left(\theta_2 + (\frac{N^d}{N^p + N^d})^2\right)^{-1}, \\
N_0^p &= 1.5 \times 10^4, \qquad N_0^d = 0.
\end{aligned}$$

The constants θ_1 and θ_2 were chosen with the aid of the ODE modeling program Berkeley Madonna. Values for these two parameters were found that yielded approximately 20% differentiation after six days, a rate similar to the level found experimentally, namely 16-19% after six days. The time course simulation is shown in Figure 3.2. This mechanism of simulating the background differentiation is discussed further in Appendix A.

3.2.2 IL6-pulse Experiments

The next task is to find κ_1 and κ_2, the constants controlling the cell's response to J. This can be accomplished using the data in Table 1.2. In these experiments, AHPCs were cultured on laminin and in the absence of astrocytes. However, fresh media containing various concentrations of IL6 was added every other day until the end of the experiment. A significant increase in the percentage of AHPCs expressing TUJ1 was observed for IL6 added at concentration at or greater than 0.1 ng/mL.

Notice that the entries in each of the last three columns in Table 1.2 are nearly equal. This cannot be due to a maximum response to J, since then the model will be unable to surpass

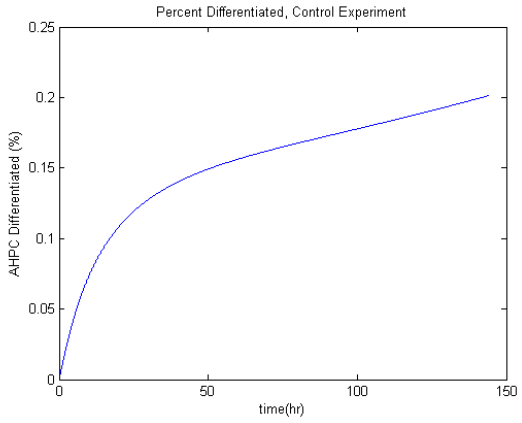

Figure 3.2 *Percentage of cells expressing TUJ1 over a six day period. The differentiation expressed in this figure is due solely to the background mechanism.*

35-40% differentiation, and hence it will not recreate noncontact coculture results. Therefore it is assumed that this "leveling off" is acheived through saturation of the R^p_{il} receptor. This receptor is chosen since, if R^p_{gp130} were saturating, we would again be unable to surpass 35-40% differentiation since both pathways utilize this receptor.

In these experiments, differentiation is only occuring via Pathway 1 and the background mechanism, not Pathway 2. The system of ODEs describing this situation is given by

$$\begin{aligned}
\frac{d[A_i]}{dt} &= S_{ai}(t) - \widehat{k_1}[A_i][R^p_{il}]N^p + \widehat{k_{-1}}[A_s]N^p - \mu_{ai}[A_i], \\
\frac{d[J]}{dt} &= \widehat{l_2}[\{A_s : R^p_{gp130}\}] - \mu_j[J] - [J]\eta, \\
\frac{dN^p}{dt} &= -\Big\{K_1(N^p, N^d) + K_2([J])\Big\}N^p + N^p\eta, \\
\frac{dN^d}{dt} &= \Big\{K_1(N^p, N^d) + K_2([J])\Big\}N^p, \\
[A_i]_0 &= [J]_0 = 0 \\
N^p_0 &= 1.5 \times 10^4, \quad N^d_0 = 0
\end{aligned}$$

with receptor concentrations

$$b = \frac{L[R^p_{gp130}]_0 + ([R^p_{gp130}]_0 - [R^p_{il}]_0)[A_i]}{\widehat{K} + [A_i]} + \widehat{L},$$

$$c = \frac{-\widehat{L}[A_i][R^p_{il}]_0}{\widehat{K} + [A_i]},$$

$$[A_s] = (-b + \sqrt{b^2 - 4c})/2,$$

$$[\{A_s : R^p_{gp130}\}] = \frac{[A_i][R^p_{il}]_0 - (\widehat{K} + [A_i])[A_s]}{L + [A_i]},$$

$$[R^p_{il}] = [R^p_{il}]_0 - [A_s] - [\{A_s : R^p_{gp130}\}],$$

$$[R^p_{gp130}] = [R^p_{gp130}]_0 - [\{A_s : R^p_{gp130}\}],$$

where L, $\widehat{L}$, and $\widehat{K}$ defined as before. The constants κ_1 and κ_2 were estimated via the Metropolis algorithm ([46]). These parameters are defined as

$$(\kappa_1, \kappa_2) = argmin_{(\widehat{\kappa_1}, \widehat{\kappa_2}) \in \Omega_\kappa} \Big(\sum_{i=1}^{8} ||P_i^{sim}(144) - P_i^{exp}||^2 \Big),$$

where P_i^{exp} is the percent differentiated after six days during the experiment with treatment of 10^{-6+i} ng/mL in Table 1.2, $P_i^{sim}(144)$ is the percent differentiated found through the corresponding simulation, and Ω_κ is an appropriate space of values for κ_1 and κ_2. An initial position in Ω_κ yielding similar values to Table 1.2 was found by using the program Berkeley Madonna. This choice was then refined by generating a random walk through Ω_κ. The direction of movement, corresponding to new combinations of κ_1 and κ_2, is chosen randomly. Define the energy at step j of the random walk by

$$E(j) = \sum_{i=1}^{8} ||P_i^j(144) - P_i^{exp}||^2.$$

If $E(j+1) \leq E(j)$, the step is accepted. If $E(j+1) > E(j)$, the step is accepted with probability $x^{E(j+1)-E(j)}$, for some $x \in (0, 1)$. These "bad" moves during the random walk are occasionally permitted in order to prevent the random walk from becoming "trapped" at a local minimum. This minimization process yielded values κ_1 and κ_2 producing the simulation results in Table 3.2. Time course simulations are shown in Figure 3.3. The percentage of differentiation due to the function simulating the background mechanism is shown in Figure 3.4. The time course of

Table 3.2 Percent observed differentiation (TUJ1 expression level)

IL6 added (ng/mL)	0	.00001	.0001	.001	.01	.1	1	10	100
Experimental(%)	19	20	20	27	25	31	37	35	36
Simulation(%)	20.1	20.12	20.14	20.72	23.47	28.67	35.11	37.06	37.26

$[A_s] + [\{A_s : R^p_{gp130}\}]$ in comparison to $[R^p_{il}]_0$ is shown in Figure 3.5, illustrating that the R^p_{il} receptors are saturating as the concentration of available IL6 increases.

3.2.3 Noncontact Coculture

In this experiment, a uniform layer of AHPCs is applied to the laminin at a density of 1.5×10^4 cells/cm^2. A uniform layer of astrocytes, also at a density of 1.5×10^4 cells/cm^2, is held above the AHPCs in an insert that allows diffusion of molecules but prevents direct contact between AHPCs and astrocytes. IL6 signalling can now occur through both pathways. Pathway 1 was seen earlier to be limited by $[R^p_{il}]$. However, pathway 2 does not use R^p_{il}. The time course simulation is shown in Figure 3.6. The percentage of cells that have differentiated after six days is found to be 66.3% from the simulation. This is a similar increase from the control as is seen experimentally, where 73-75% of cells differentiate. The time course of differentiation due to the function simulating the background mechanism is shown in Figure 3.7.

3.2.4 Conditioned Media

In this experiment, a uniform layer of AHPCs is applied to the laminin at a density of $1.5 \times 10^4 \frac{cells}{cm^2}$. Astrocytes, also at a density of $1.5 \times 10^4 \frac{cells}{cm^2}$, are cultured separately. Every 24 hours, the media from the astrocyte culture, now containing astrocyte-secreted factors, is removed and added to the AHPC culture. The concentrations of factors in this astrocyte-

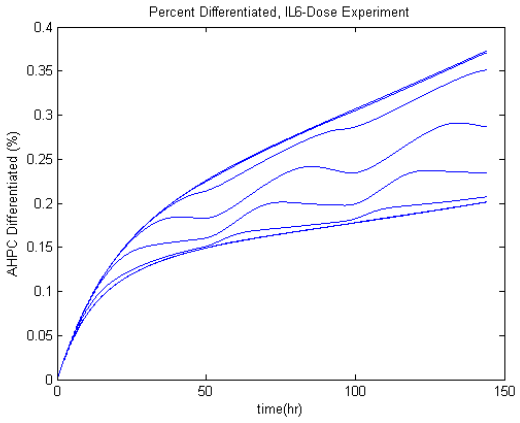

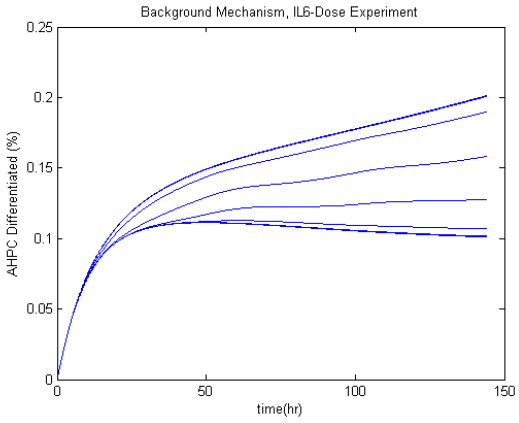

Figure 3.3 *(left) Percentage of cells expressing TUJ1 over a six day period. The differentiation expressed in this figure includes both IL6-induced differentiation and that due to the background mechanism. Eight experiments are illustrated. The bottom curve represents the time course for a treatment of media containing* 10^{-5} *ng/mL IL6 added every 48 hours. The top curve represents the time course for a treatment of media containing* 10^{2} *ng/mL IL6 added every 48 hours. Some curves overlap.*

Figure 3.4 *(right) Percentage of cells expressing TUJ1 over a six day period. The differentiation expressed in this figure is due solely to the background mechanism. Eight experiments are illustrated. The top curve represents the time course for a treatment of media containing* 10^{-5} *ng/mL IL6 added every 48 hours. The bottom curve represents the time course for a treatment of media containing* 10^{2} *ng/mL IL6 added every 48 hours. Some curves overlap. As higher concentrations of IL6 are added, the contribution to the percent differentiated due to the function* $K_1(N^p, N^d)$ *decreases until it reaches a minimum of around 10%. The increases in differentiation that result in the simulation of Table 1.2 can therefore be attributed to the IL6 mechanism.*

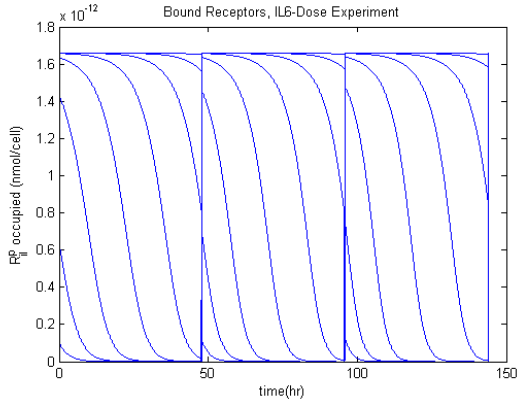

Figure 3.5 *Time course of the concentration of bound R^p_{il} receptors. The bottom curves represents the time course for a treatment of media containing 10^{-5} ng/mL IL6 added every 48 hours. The top curve represents the time course for a treatment of media containing 10^2 nmol/mL IL6 added every 48 hours. Saturation of R^p_{il} receptors is clear from the graph.*

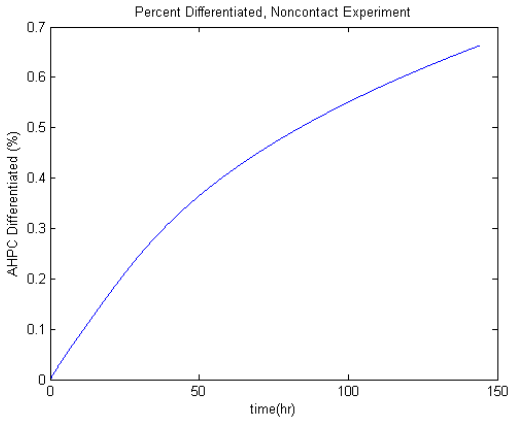

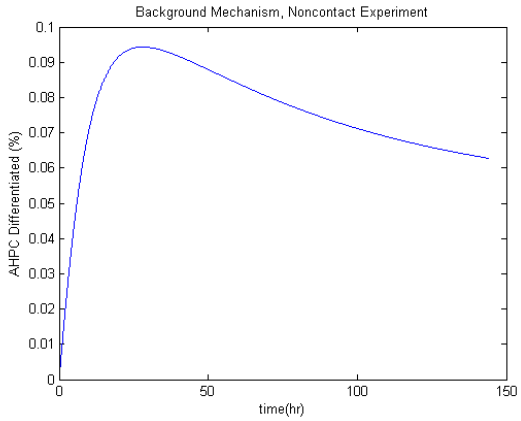

Figure 3.6 *Percentage of cells expressing TUJ1 over a six day period. The differentiation expressed in this figure includes both IL6-induced differentiation and that due to the background mechanism.*

Figure 3.7 *Percentage of cells expressing TUJ1 over a six day period. The differentiation expressed in this figure is due solely to the background mechanism.*

conditioned media are given by the solution of

$$\begin{aligned}
\frac{d[A_i]}{dt} &= a_1 N_a - l_1[A_i][R_{il}] + l_{-1}[A_a] - \mu_{ai}[A_i] \\
\frac{d[R_{il}]}{dt} &= b_a N_a - l_1[A_i][R_{il}] + l_{-1}[A_a] - \mu_{il}[R_{il}] \\
\frac{d[A_a]}{dt} &= -(l_2 + l_{-1})[A_a] + l_1[A_i][R_{il}] - k_1[A_a][G_p] + k_{-1}[A_o] \\
\frac{d[G_p]}{dt} &= s_a N_a - k_1[A_a][G_p] + k_{-1}[A_o] - \mu_{gp}[G_p] \\
\frac{d[A_o]}{dt} &= k_1[A_a][G_p] - (k_{-1} + k_2)[A_o] - \mu_{ao}[A_o]
\end{aligned}$$

with initial conditions

$$[A_i]_0 = [A_a]_0 = [A_o]_0 = [R_{il}]_0 = [G_p]_0 = 0.$$

Using the same secretion rates as for the noncontact coculture, the simulation yields 38.83% of cells differentiated. This is a similar decrease from the noncontact coculture as is seen experimentally, where 38-41% of cells differentiate. One explanation for this result is that contact between AHPCs and astrocytes is required to alter the secretion rates for the active proteins A_i, R_{il}, and G_p from astrocytes. The time course simulation is shown in Figure 3.8. The time course of differentiation due to the function simulating the background mechanism is shown in Figure 3.9.

3.2.5 Contact Coculture

Only the experiment on the smooth substrate is considered here. Spatial nonhomogeneities exist on the patterned substrate for the contact coculture experiment, so this situation is considered in Chapter 6. A uniform layer of astrocytes is applied to the laminin on the smooth substrate at a density of 1.5×10^4 cells/cm^2 and cultured for two days. A uniform layer of AHPCs is then applied to the astrocytes at a density of 1.5×10^4 cells/cm^2. The only difference between this experiment and the noncontact coculture experiment is that the AHPCs and astrocytes are in direct contact. This direct cell-cell contact may include binding by cadherins or other cell adhesion molecules (CAM) on the surface of these cells. It is hypothesized here that this binding alters the secretion rates of the soluble proteins.

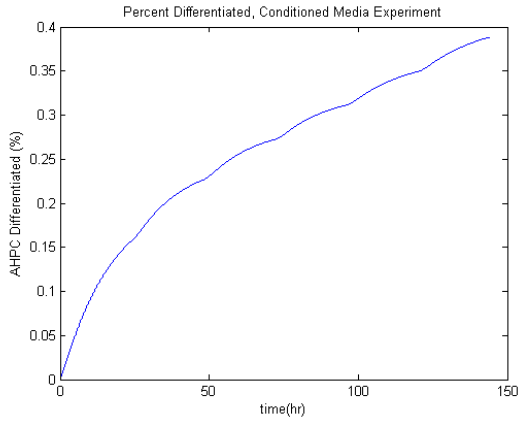

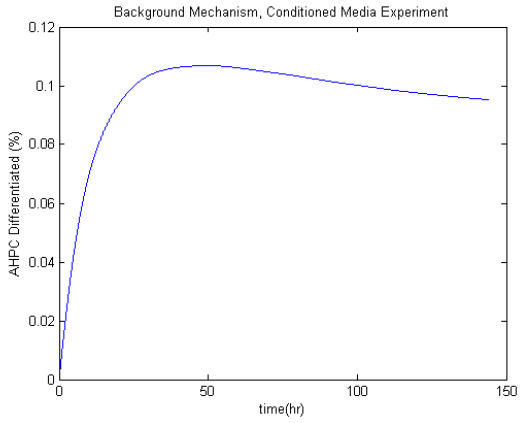

Figure 3.8 *Percentage of cells expressing TUJ1 over a six day period. The differentiation expressed in this figure includes both IL6-induced differentiation and that due to the background mechanism.*

Figure 3.9 *Percentage of cells expressing TUJ1 over a six day period. The differentiation expressed in this figure is due solely to the background mechanism.*

It will be shown in Chapter 4 that varying the secretion rate of the inhibitor G_p within biologically reasonable ranges does not affect the level of differentiation. To determine how to vary the other two secretion rates, it is important to understand the biological behavior of this system. The values for differentiation on smooth and patterned substrates are 20% and 35% respectively. These are approximately the same values as the minimum and maximum achieved during the IL6-pulse experiments. During those experiments, only the first pathway was active. Hence it is reasonable to assume that contact initiates a signal transduction cascade whose end result is to stop the secretion of the soluble IL6 receptor R_{il}. However, the extracellular concentration of IL6 is still similar to that achieved through the pulse experiments with greater than 0.1 ng/mL IL6 added to the system every other day. To achieve less than 23% differentiation on the smooth substrate, the parameter a_1 must be set to less than 5×10^{-14} nmol/cell·hr. This is (1/200)th of its rate when astrocytes are not in contact with AHPCs. The time course simulations are shown in Figure 3.10. The time course of differentiation due to the function simulating the background mechanism is shown in Figure 3.11.

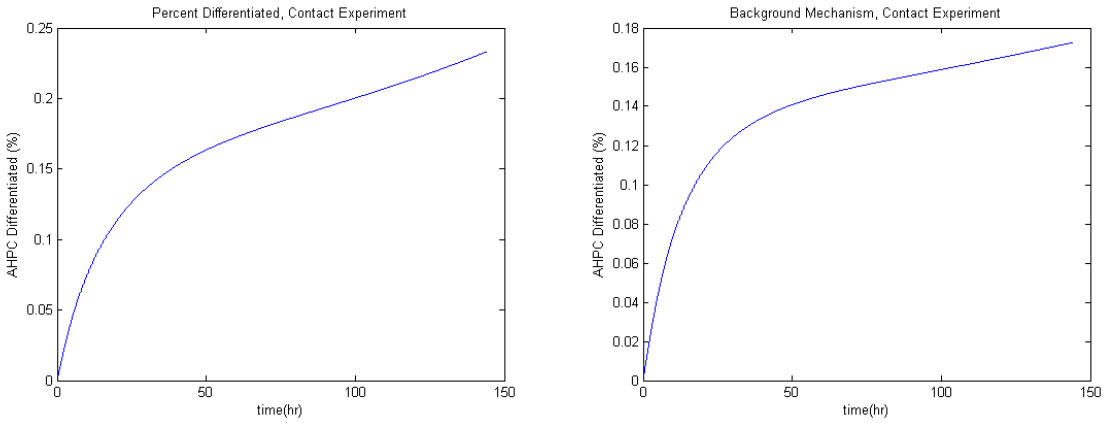

Figure 3.10 *Percentage of cells expressing TUJ1 over a six day period. The differentiation expressed in this figure includes both IL6-induced differentiation and that due to the background mechanism.*

Figure 3.11 *Percentage of cells expressing TUJ1 over a six day period. The differentiation expressed in this figure is due solely to the background mechanism. When A_i is secreted at these low values, the function simulating the background mechanism becomes more prominent, and the differences in the two graphs show that little differentiation is due to IL6.*

Table 3.3 Percent observed differentiation (TUJ1 expression level)

Experiment	% diff. observed	% diff. from model	% due to $K1(N^p, N^d)$
IL6 pulse, 10^{-5}ng/mL	20%(S)	20.12%	20.116%
IL6 pulse, 10^{-4}ng/mL	20%(S)	20.14%	20.06%
IL6 pulse, 10^{-3}ng/mL	27%(S)	20.72%	18.97%%
IL6 pulse, 10^{-2}ng/mL	25%(S)	23.47%	15.82%
IL6 pulse, 10^{-1}ng/mL	31%(S)	28.67%	12.78%
IL6 pulse, 10^{0}ng/mL	37%(S)	35.11%	10.68%
IL6 pulse, 10^{1}ng/mL	35%(S)	37.06%	10.16%
IL6 pulse, 10^{2}ng/mL	36%(S)	37.26%	10.11%
Control	17%,/19%(S) 16%(P)	20.12%	20.12%
Noncontact	73%(S) 75%(P)	66.3%	6.28%
Conditioned Media	41%(S) 38%(P)	38.83%	9.53%
Contact	20%(S)	23.30%	17.25%

3.3 Discussion

The results from the numerical simulations are shown in Tables 3.3. They show that the experimental behavior can be matched by an IL6-mediated mechanism alone. The background differentiation remains low and fairly constant, so the differences in percent of differentiation shown in column 3 of Table 3.3 are due to the IL6 mechanism. Unfortunately, the background mechanism is unknown, and its results cannot be distinguished from that due to IL6 through the available biological experiments. These results suggest that:

(1) AHPCs do not affect the secretion rates of IL6 and sIL6Rα when not in direct contact.

(2) When in direct contact, CAM binding inhibits the secretion of sIL6Rα and decreases the secretion of IL6. This could be due to alterring rates of transcription.

Table 3.4 Table of Kinetic Constants

Parameter	Description	Value	Comments
L_d, ℓ_{-1}, ℓ_1	Binding of		
L_d	inactivated IL6 A_i	30 nM	[49]
ℓ_{-1}	to soluble	5 hr^{-1}	[23]
ℓ_1	IL6 receptor R_{il}	$167(\frac{nmol}{mL})^{-1}hr^{-1}$	calc.
K_d, k_{-1}, k_1	Binding of		
K_d	active IL6 A_a	3 nM	[49]
k_{-1}	to soluble	5 hr^{-1}	sim.
k_1	gp130 receptor G_p	$1667(\frac{nmol}{mL})^{-1}hr^{-1}$	calc.
$\widehat{K_d}$, $\widehat{k_{-1}}$, $\widehat{k_1}$	Binding of		
$\widehat{K_d}$	inactivated IL6 A_i	100 pM	[49]
$\widehat{k_{-1}}$	to surface	500 hr^{-1}	sim.
$\widehat{k_1}$	IL6 receptor R^p_{il}	$1.67 \times 10^6(\frac{nmol}{mL})^{-1}hr^{-1}$	cal.
$\widehat{L_d}$, $\widehat{\ell_{-1}}$, $\widehat{\ell_1}$, $\widehat{\ell_2}$	Binding of		
$\widehat{L_d}$	surface complex	10 pM	[49]
$\widehat{\ell_{-1}}$	$A_s = \{A_i : R^p_{il}\}$	5 hr^{-1}	sim.
$\widehat{\ell_1}$	to surface	$5 \times 10^5(\frac{nmol}{mL})^{-1}hr^{-1}$	calc.
$\widehat{\ell_2}$	gp130 receptor R^p_{gp130}	.002 hr^{-1}	sim.
V_d, ν_{-1}, ν_1, ν_2	Binding of		
V_d	active IL6 A_a	60 pM	[49]
ν_{-1}	to surface	5 hr^{-1}	sim.
ν_1	gp130 receptor R^p_{gp130}	$8.33 \times 10^4(\frac{nmol}{mL})^{-1}hr^{-1}$	calc.
ν_2		.5 hr^{-1}	sim.

Table 3.5 Table of Constants

Parameter	Description	Value	Comments
μ_{ai}	decay of IL6	.173 hr^{-1}	[32]
μ_{il}	decay of sIL6Rα	.173 hr^{-1}	sim.
μ_{aa}	decay of activated IL6	.173 hr^{-1}	sim.
μ_{gp}	decay of sgp130	.173 hr^{-1}	sim.
μ_{ao}	decay of inhibited IL6	.173 hr^{-1}	sim.
μ_j	decay of differentiation factor	.173 hr^{-1}	sim.
a_1	IL6 secretion rate	$1 \times 10^{-11} \frac{nmol}{cell \cdot hr}$	[41]
b_a	sIL6Rα secretion rate	$2 \times 10^{-10} \frac{nmol}{cell \cdot hr}$	sim.
s_a	sgp130 secretion rate	$1 \times 10^{-11} \frac{nmol}{cell \cdot hr}$	sim.
$R^p_{il,0}$	density of IL6 receptors on AHPC	$1.66 \times 10^{-12} \frac{nmol}{cell}$	sim.
$R^p_{gp130,0}$	density of gp130 receptors on AHPC	$1.66 \times 10^{-10} \frac{nmol}{cell}$	sim.
M_1	cell growth parameter	$.0213 hr^{-1}$	[37]
N_{max}	carrying capacity	$1 \times 10^5 \frac{cells}{cm^2}$	calc.
D_{ai}	diffusion of inactive IL6	$4.86 \times 10^{-4} \frac{cm^2}{hr}$	calc.
D_{il}	diffusion of sIL6Rα	$3.9 \times 10^{-4} \frac{cm^2}{hr}$	calc.
D_{aa}	diffusion of activated IL6	$3.38 \times 10^{-4} \frac{cm^2}{hr}$	calc.
D_{gp}	diffusion of sgp130	$2.84 \times 10^{-4} \frac{cm^2}{hr}$	calc.
D_{ao}	diffusion of inhibited IL6	$2.44 \times 10^{-4} \frac{cm^2}{hr}$	calc.
D_p	random movement of AHPCs	$3.6 \times 10^{-8} \frac{cm^2}{hr}$	calc.
D_d	random movement of neurons	$3.6 \times 10^{-8} \frac{cm^2}{hr}$	calc.
θ_1	differentiation parameter	$10^{-4} hr^{-1}$	
θ_2	differentiation parameter	10^{-2}	
κ_1	differentiation parameter	$3.9 hr^{-1}$	
κ_2	differentiation parameter	$5.3 \times 10^{-13} \frac{nmol}{cell}$	

CHAPTER 4. Sensitivity Analysis of Population Model

Sensitivity analysis is an important component of the analysis of any mathematical model. This is especially true in mathematical biology, where there typically is much uncertainty in parameters for kinetic rates, dissociation constants, and secretion rates. For example, consider the dissociation constant for the reaction

$$A_i + R_{il}^p \underset{\widehat{k_{-1}}}{\overset{\widehat{k_1}}{\rightleftharpoons}} A_s.$$

The parameter $\widehat{K_d} = \frac{\widehat{k_{-1}}}{\widehat{k_1}}$ has been measured experimentally to be in the range of 500-750 pM ([49]). Due to this uncertainty, it may be informative to view it as a random variable with a certain probability distribution rather than as a fixed value. In this example this parameter could possibly be viewed as $\widehat{K_d} \sim U(500, 750)$ or $\widehat{K_d} \sim N(625, 75)$, where $U(\alpha, \beta)$ is the uniform distribution with endpoints α and β and $N(\mu, \sigma)$ is the normal distribution with mean μ and standard deviation σ. Representing a parameter as a random variable over a certain probability distribution results in uncertainty in the output of the model. The purpose of sensitivity analysis is to look at how variations in the input parameters affect variations in the output of the system. If there is a strong effect, the system is said to be sensitive to that parameter, and further experimental work may need to be done to lower the uncertainty in that parameter. Conversely, if there is little to no correlation, the system is insensitive to that parameter. These results may be used to simplify mathematical models while still retaining reasonable accuracy of the simulation.

There are two types of sensitivity analysis (SA): local sensitivity and global sensitivity. With local sensitivity analysis, one calculates the parametric gradient at a specific point in the parameter space. These values can be normalized, providing sensitivity coefficients that can be compared directly. They estimate which parameters are most influential on a specific output

at that particular point in the parameter space. However, these coefficients only measure sensitivity at a particular set of parameter values. In a dynamical system such as system (3.1) on p.18, there is much uncertainty in many parameters. Therefore one would like to have a measure of which parameters are most influential over the entire space of uncertainty, not just at the set of nominal values from Tables 3.4-5. With global sensitivity analysis, one varies all parameters of interest simultaneously over the entire range of each individual parameter. However, the sensitivity coefficients are then dependent on the range over which each parameter is varied. Therefore it is wise to choose a biologically relevant range for each parameter before calculating sensitivity coefficients.

There are two main classes of global SA techniques: sampling-based methods and variance-based methods (ANOVA - analysis of variance). The most reliable sampling-based method is to calculate Partial Rank Correlation Coefficients (PRCC) and the most reliable, albeit computationally expensive, ANOVA technique is the Extended Fourier Amplitude Sensitivity Test (eFAST) ([28]). Reliability in this context is defined as reproducibility of the results over multiple trials. In short, PRCC calculates how strong of a monotone relationship exists between a parameter and the output over the entire space of uncertainty, and whether it is a positive or negative correlation. eFAST calculates the percentage of the variance of the output that is attributable to each parameter, and whether it is due to that parameter solely or through its interactions with other parameters.

In this chapter, multiple sensitivity analyses are discussed with various probability distributions for both PRCC and eFAST. These will show three main results. First, although the system is sensitive to variations in input, many of the parameters that cause the highest amount of uncertainty are recorded in the literature. However, some of the most influential unknown parameters are involved with the production or decay of the intracellular differentiation factor J, and as such the intracellular mechanism leading to differentiation should be studied in more detail. Secondly, the biological inhibitor G_p does not seem to have a measurable effect on the percentage of cells that have differentiated after six days. As such, it can be removed from the mathematical model without altering simulation results. Finally, the sensitivity analyses show

that the system is more sensitive to parameters in the second pathway (via soluble receptors) than in the surface receptor pathway. Hence it may be hypothesized that the second pathway is more influential with respect to differentiation than the surface receptor pathway.

4.1 Partial Rank Correlation Coefficients (PRCC)

There are many parameters in this model. One of the aspects that is most important to understand is the relationships between increases or decreases in a parameter's value and corresponding changes in the output of interest. This is the idea of *correlation*. To measure the strength of the relationship, and whether it is a positive or negative correlation, one uses a *correlation coefficient*. For two random variables X and Y, it is calculated as

$$\rho_{xy} = \frac{Cov(X,Y)}{\sqrt{Var(X)}\sqrt{Var(Y)}}$$

where $Var(X)$ is the variance of X and $Cov(X,Y)$ is the covariance of X and Y. Given a sample of n data points $\{(x_i, y_i)\}_{i=1}^n$, this can be calculated via the sample variances and sample covariance. The sample variance (s_x) of X is a measure of the average deviation from the mean $\overline{x}$ of the set $\{x_i\}_{i=1}^n$ and is defined by $s_x^2 = \dfrac{\sum_{i=1}^{n}(x_i - \overline{x})^2}{n-1}$. (The factor $n-1$ is used instead of n so that the expected value of the sample variance equals the (population) variance, $E(s_x) = \sigma_x$. ([4])) The sample covariance is a natural extension of this idea, $c_{xy} = \dfrac{\sum_{i=1}^{n}(x_i - \overline{x})(y_i - \overline{y})}{n-1}$. The Correlation Coefficient for the data set $\{(x_i, y_i)\}_{i=1}^n$ is then given by

$$r_{xy} = \frac{\sum_{i=1}^{n}(x_i - \overline{x})(y_i - \overline{y})}{\sqrt{\sum_{i=1}^{n}(x_i - \overline{x})^2}\sqrt{\sum_{i=1}^{n}(y_i - \overline{y})^2}} = \frac{c_{xy}}{s_x s_y}.$$

Note that $r_{xy} = \dfrac{< v_1, v_2 >}{||v_1||||v_2||}$, where $v_1 = (x_1 - \overline{x}, ..., x_n - \overline{x})$, $v_2 = (y_1 - \overline{y}, ..., y_n - \overline{y})$, and $< \cdot, \cdot >$ is the standard inner product on R^n. By applying the Cauchy-Schwarz inequality, one gets that $|r_{xy}| \leq 1$.

Correlations between two variables x and y based on two sets of data can be viewed graphically through a *scatterplot* by plotting the data set $\{x_i\}$ on the x-axis and the corresponding data set $\{y_i\}$ on the y-axis, such that (x_i, y_i) are measurements from the same experiment. A scatterplot can reveal whether increases in x correspond to increases in y (positive correlation) or decreases in y (negative correlation). Moreover, linear or other trends may be revealed. A positive linear correlation between two data sets is illustrated in the scatterplot in Figure 4.1. Although not all data points are on a straight line, there is a definite correlation between increasing x and increasing y in Figure 4.1. A weaker correlation exists between x and y in Figure 4.2. An example where increases in x does not correspond to any discernible changes in y appears in Figure 4.3.

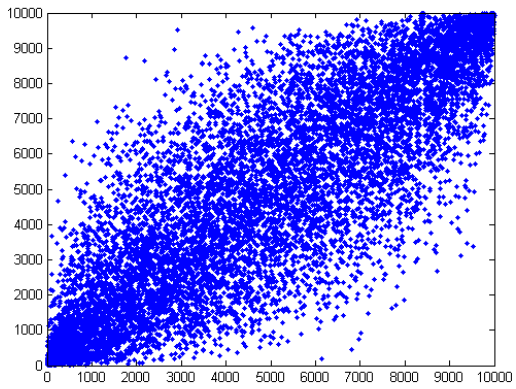

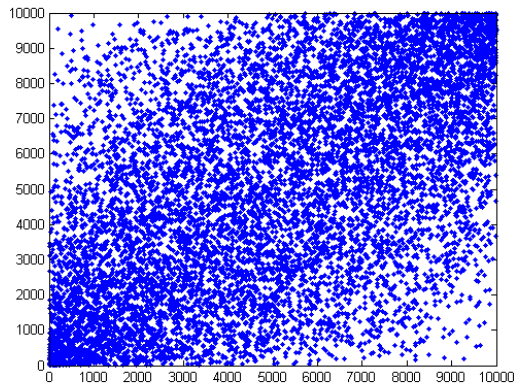

Figure 4.1 *(left) Data set showing a correlation between increasing the input variable x and a corresponding increase in the output variable y.*

Figure 4.2 *(right) Data set showing a correlation between increasing the input variable x and a corresponding increase in the output variable y. However, the correlation is weaker than Figure 4.1 as there is much more deviation from the mean at any point x.*

The Correlation Coefficient measures the strength of the linear relationship between the two data sets $\{x_i\}_{i=1}^n$ and $\{y_i\}_{i=1}^n$ from the n experiments. The coordinate set $\{(x_i, y_i)\}_{i=1}^n$ can be analyzed by forming a best-fit line through the set of points (x_i, y_i) through the use of the Method of Least Squares. The regression line $\widehat{y} = b_0 + b_1 x$ is formed by finding b_0 and b_1 such

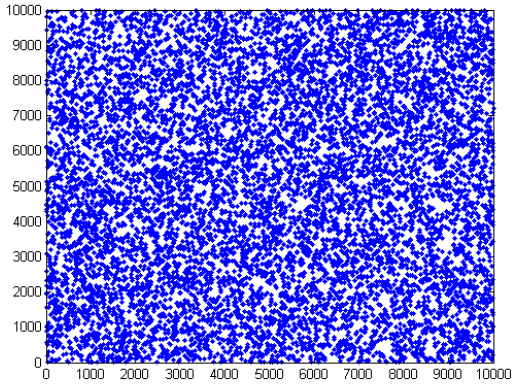

Figure 4.3 *Data set showing no correlation between increasing the input variable x and corresponding changes in the output variable y.*

that the function $H(b_0, b_1) = \sum_{i=1}^{n}(y_i - b_0 - b_1 x_i)^2$ is minimized. Standard calculus can show that $r_{xy} = \dfrac{b_1 s_x}{s_y}$. Rearranging this equation to solve for b_1 shows that if x is increased by 1% of its standard deviation, then y will change by r_{xy}% of its standard deviation. Hence strong linear correlations will occur with $|r_{xy}|$ close to 1, and weak linear correlations will occur with $|r_{xy}|$ close to 0.

Often, more than one parameter is varied simultaneously, and the corresponding values of the output are recorded. If there are p variables, and data sets of n trials are generated, this results in a coordinate set $\{x_{i1}, x_{i2}, ..., x_{ip}, y_i\}_{i=1}^{n}$. To see the correlation between the individual data sets $\{x_j\}$ and $\{y\}$, the linear effect of the other parameters on the output y must first be removed. This is done by forming the regressions:

$$\widehat{x_j} = c_0 + \sum_{k=1,k\neq j}^{p} c_k x_k$$

$$\widehat{y} = b_0 + \sum_{k=1,k\neq j}^{p} b_k x_k.$$

The components of the vectors $\widehat{x_j}$ and $\widehat{y}$ can both be written in the form $\widehat{z}_i = \beta_0 + \sum_{k=1,k\neq j}^{p} \beta_k x_{ik} +$

ε_i, for $\widehat{z} = \widehat{x_j}$ or $\widehat{z} = \widehat{y}$, so that $\widehat{z} = \widetilde{X}\beta + \varepsilon$ where

$$\widetilde{X} = \begin{bmatrix} 1 & x_{11} & \cdots & x_{1,j-1} & x_{1,j+1} & \cdots & x_{1p} \\ \vdots & \vdots & & \vdots & \vdots & & \vdots \\ 1 & x_{j-1,1} & \cdots & x_{j-1,j-1} & x_{j-1,j+1} & \cdots & x_{j-1,p} \\ 1 & x_{j+1,1} & \cdots & x_{j+1,j-1} & x_{j+1,j+1} & \cdots & x_{j+1,p} \\ \vdots & \vdots & & \vdots & \vdots & & \vdots \\ 1 & x_{n,1} & \cdots & x_{n,j-1} & x_{n,j+1} & \cdots & x_{n,p} \end{bmatrix},$$

$\widehat{z}$ and ε are $n \times 1$ column vectors, and β is a $p \times 1$ column vector. We need to minimize the sum

$$S(\beta) = \sum_{i=1}^{n} \left(z_i - \beta_0 - \sum_{k=1, k\neq j}^{p} \beta_i x_{ki} \right)^2 = (z - \widetilde{X}\beta)^T (z - \widetilde{X}\beta).$$

Standard calculus shows that the minimum occurs when $\beta = (\widetilde{X}^T \widetilde{X})^{-1} \widetilde{X} z$. Finally, $\widehat{z} = \beta_0 + \sum_{k=1, k\neq j}^{p} \beta_k x_k$. This is performed for both $z = y$ and $z = x_j$. The parial correlation coefficient (PCC) between x_j and y is then given by the correlation coefficient between $x_j - \widehat{x_j}$ and $y - \widehat{y}$. Hence the PCC is a measure of the linear relationship between x_j and y, with the linear effects of the other parameters removed. A more thorough discussion of correlation coefficients and partial correlation coefficients is provided in Kendall's "The Advanced Theory of Statistics, Vol. 2" ([27]).

Correlation coefficients provide a measure of the linear relationship between a model's input and output. However, this idea can be generalized to provide a measure of the nonlinear but monotonic relationships between the input parameter x and the output y through a rank transformation. For a rank transform, the data points $\{x_i\}_{i=1}^n$ and $\{y_i\}_{i=1}^n$ are assigned natural numbers corresponding to their position if all data points are written in ascending order. A correlation coefficient is then calculated for this rank transformed data. For example, for data $(1, 1)$, $(4, 16)$, $(5, 25)$, and $(10, 100)$, there is a nonlinear but monotonic relationship between $\{x_i\}_{i=1}^4$ and $\{y_i\}_{i=1}^4$. However, if the data are rank transformed as $(1, 1)$, $(2, 2)$, $(3, 3)$, and $(4, 4)$, a linear relationship now exists among the transformed data. The correlation coefficient formed for the rank transformed data is referred to as the rank correlation coefficient. This idea can also be extended to PCC, allowing one to calculate partial rank correlation coefficients

(PRCC), which measure the monotonic relationships existing between an input parameter and the output with the monotonic effects of the other parameters removed.

The PRCC analysis presented in this paper begins by choosing appropriate sample points within the parameter space. This is done through the method of Latin Hypercube Sampling (LHS). For each of the k parameters of interest, the domains of the corresponding probability density functions (pdf) are divided into N subintervals of equal probability. A sample point in the parameter space is then found by choosing one of these subintervals for each parameter, followed by choosing one random point from within each of these subintervals. A second point is then chosen by repeating this process using only the remaining subintervals for each parameter. A total of N sample points are chosen from the parameter space. The points are chosen as specified above through the algorithm presented in [53]. Once the sample points have been chosen, the model is evaluated at each of the points, and the percentage of cells that have differentiated after six days is recorded. PRCC's are then calculated using the corresponding Matlab command within the statistical toolbox. Finally, p-values are computed using the statistical toolbox in order to determine if the PRCC's are significantly different from 0. Discussions of the statistics used to generate the p-value for PRCC are provided by Kirschner ([28]) and Anderson ([3]).

4.2 Extended Fourier Amplitude Sensitivity Test (eFAST)

Fourier Amplitude Sensitivity Test (FAST) is a variance decomposition method initially developed by Cukier et.al. and published in 1973 ([13]). A review of this method including some modifications was published in 1978 ([14]). The extended version (eFAST) was later published by Saltelli in 1998 ([47]). It is a global sensitivity analysis, in that all parameters are varied simultaneously throughout the parameter space. The variance of the output of interest is then partitioned among the input factors, quantifying how much variance is due to variation in each parameter within their respective pdf's. This decomposition quantifies both the percentage of variance due to the *main effect* of a parameter and the percentage due to the *total effect* of a parameter. The main effect is given by the first-order sensitivity coefficient.

This is due solely to variation in the parameter. The total effect is the sum of both the first-order sensitivity coefficient and the higher-order sensitivity coefficients. These include effects due to interactions between the parameter of interest and other parameters. An interaction effect can be identified as occurring when the effect due to one parameter differs for different values of another parameter.

A mathematical derivation of the FAST method following the presentations provided in [14] and [47] is given in Appendix B. The method begins by assigning each parameter a unique integer frequency. A search curve is formed through the parameter space by way of a variable transformation $x_i(t) = g_i(\sin(\omega_i t))$ for each parameter x_i. Through a proper choice of g_i, each parameter will oscillate within its range, sampling points in accordance with its pdf. This results in corresponding oscillations in the output. The variance of the output is represented as a Fourier Series, separating the oscillations into the components occurring at different frequencies. Under appropriate assumptions on the frequencies, the effect due solely to parameter i (assigned frequency ω_i) is given by the Fourier coefficients at ω_i and its harmonics. The other terms represent higher-order effects. It is shown in Appendix B that the variance can be written as

$$D = 2\sum_{i=1}^{\infty}(A_i^2 + B_i^2)$$

where A_i and B_i are the coefficients of the Fourier expansion. Defining $D_i = 2\sum_{p=1}^{\infty}(A_{p\omega_i}^2 + B_{p\omega_i}^2)$, the percentage of variance due solely to parameter i, i.e. the main effect, is given by $S_i = \frac{D_i}{D}$.

The eFAST method extends this idea, allowing one to compute a parameter's total effect. It is based on the idea that the Fourier coefficients of the harmonics of the chosen frequencies rapidly converge to zero. Assign the parameter of interest a high frequency ω_i, and the complementary set of parameters low frequencies, denoted by $\{\omega_{\sim i}\}$. Repetition is allowed within $\{\omega_{\sim i}\}$. These frequencies are chosen so that $\max\{\omega_{\sim i}\} = \frac{\omega_i}{2M}$ where M is an *interference* parameter discussed in Appendix B, and is usually taken to be 4 or 6. The coefficients of Fourier series whose frequencies are below $\frac{\omega_i}{2}$ will not include any effect due to ω_i, and due to

the rapidity with which the harmonics converge to zero,

$$\frac{D_{\sim i}}{D} = \frac{\sum_{j=1}^{\omega_i/2}(A_j^2 + B_j^2)}{\sum_{j=1}^{\infty}(A_j^2 + B_j^2)}$$

approximates the main effect due to the complementary set. That is, the effect due solely to the parameters that are not i. This includes all interactions among themselves, but not with i. The total effect of parameter i can then be given by $S_{Ti} = 1 - \frac{D_{\sim i}}{D}$.

Multiple search curves can be generated within the parameter space by introducing a random phase-shift into the transformation functions, $x_i(t) = g_i(\sin(\omega_i t + \phi_i))$. Since different combinations of parameters are tested along each curve, the sensitivity indices will be slightly different. Those recorded in this chapter are the means of these samples.

To determine the significance of these sensitivity indices, a dummy parameter is introduced. This parameter is not included in the system of ODEs, and therefore should have $S_{dummy} = 0$ and $S_{Tot,dummy} = 0$. However, the eFAST algorithm assigns small but nonzero sensitivity indices to it. Kirschner ([28]) suggests that the nonzero first-order index can be attributed to interference and aliasing effects (Appendix B), while the total effect index is due to the simplifying assumptions used in its calculation. A two-sample t-test is performed with the data from the dummy parameter and the parameter of interest, using the statistical toolbox within Matlab. Those that are significantly higher than the dummy parameter are given in the following tables.

4.3 Results of Local Sensitivity Analysis

The parametric gradient was evaluated at the nominal values from Tables 3.4-5, in order to rank the variables according to how influential they are at the point of interest within the parameter space. Each parameter is varied one at a time by 1% of its nominal value. An approximation to $\frac{\partial y}{\partial k_j}$ is found, where y represents the percentage of cells differentiated after six days, and k_j is the $j-th$ parameter. These coefficients are normalized to make them

comparable to each other by forming the quantities

$$S_j = \frac{k_j}{y}\frac{\partial y}{\partial k_j} \approx \frac{k_j}{y}\frac{y(k_j + .01k_j) - y(k_j)}{(k_j + .01k_j) - k_j} = \frac{y(k_j + .01k_j) - y(k_j)}{.01y(k_j)}.$$

The quantity S_j approximates the percent change in y due to a 1% change in parameter k_j. The results of this local sensitivity analysis are present in Table 4.1. Note that the parameters involved with the inhibitor sgp130 possess five of the six lowest sensitivities.

Table 4.1 Sensitivity Coefficients from the Parametric Gradient:

Parameter	S_j	Parameter	S_j
μ_j	-.9593	ν_{-1}	3.97×10^{-2}
N_a	.8737	ℓ_{-1}	1.82×10^{-2}
$\widehat{\ell_2}$	.6083	μ_{aa}	-1.47×10^{-2}
$R^p_{il,0}$	.6030	$\widehat{K_d}$	-2.13×10^{-3}
a_1	.4373	$\widehat{L_d}$	-1.09×10^{-3}
$R^p_{gp130,0}$	.4352	$\widehat{k_{-1}}$	1.04×10^{-3}
b_a	.4333	s_a	-8.35×10^{-6}
L_d	-.4301	K_d	8.27×10^{-6}
μ_{ai}	-.4293	μ_{gp}	8.24×10^{-6}
μ_{il}	-.4272	μ_{ao}	-8.01×10^{-6}
V_d	-.4267	$\widehat{\ell_{-1}}$	3.23×10^{-6}
ν_2	.3906	k_{-1}	-2.77×10^{-7}

4.4 Results of Global Sensitivity Analysis

For the remainder of this chapter, *output* refers to the percentage of cells differentiated after six days. The *nominal* values are those found in Tables 3.4-5. For each group of parameters varied, three parameter spaces are explored. The first can be considered the "full" parameter space. It consists of wide ranges for each parameter, using either uniform or log uniform distributions, depending on the size of the interval. The second is a more local parameter space. It consists of varying each parameter with a normal distribution whose mean is it's nominal value. The standard deviation of this normal distribution is equal to one-sixth of it's mean. The third parameter space is similar to the second one, in that it is also a more local parameter space. It also consists of varying each parameter with a normal distribution with

it's nominal value as the mean. However, the standard deviation depends on which group the parameter belongs to: decay rate, secretion rate, dissociation constant, kinetic rate, or receptor/cell density. In this space, each parameter within a group has the same standard deviation regardless of its mean, so that each distribution within a group is "equal", just shifted around different means. The standard deviation is set at one-sixth of the smallest nominal value within a group. Significant eFAST results are written in the form X/Y, where X is S_i (the main effect), the percentage of variance due solely to the parameter, and Y is S_{Ti} (the total effect), the percentage of variance attributable to the parameter due to both its sole action and its interactions with other parameters. For the eFAST plots, the cross-hatched bar represents the main effect, and the dotted bar represents higher-order effects, so that the total height of the bar is S_{Ti}.

One observation of the eFAST plots is that, for the third type of parameter space tested, there is usually one parameter with most of the variance attributed to it. This is due to the distribution of each parameter relative to its mean. In this space, each parameter within a group is varied by the same amount. However, say for example one dissociation constant A_d has a mean of 10 nM, and another B_d has a mean of 10 μM. We vary them using normal distributions around their means, both with standard deviations of 1 nM. Then 68% of the values for A_d are within $\pm 10\%$ of its mean, 10 nM. However, 68% of the values for B_d are within $\pm .01\%$ of it's mean, 10 μM. In this case, variation of A_d should have a stronger effect than variation of B_d. Hence the second parameter space may be more informative, since in this space all parameters are varied by the same proportional amounts relative to their means.

4.4.1 Decay Rates

In this section, the decay rates are varied simultaneously while all other parameters are kept constant at their nominal values. Two sets of simulations are given. In the first set of simulations, all decay rates are assigned a uniform pdf, with $\mu_i \in [.1155, .6931]\ hr^{-1}$ for $i \in \{ai, il, aa, gp, ao, j\}$. This corresponds to varying the half-lives between values of 1 hour and 6 hours. In the other set of experiments, the decay rates are varied according to normal

distributions with mean values of .173, corresponding to a half-life of 4 hours. Standard deviations used for both of the parameter spaces are the same in this case, since the nominal values are equal. The standard deviation is taken to be $\frac{1}{6}(.173)$. Partial Rank Correlation Coefficients and eFAST sensitivity coefficients are presented in Table 4.2 and illustrated graphically in Figures 4.4-7.

Three decay rates have a significant influence on the output: $\mu_{ai}, \mu_{il}, \mu_j$. For all three rates, a negative correlation exists between them and changes in the output. This is expected, since if A_i and R_{il} decay at a faster rate, there will be less A_i and A_a available to initiate signal transduction. The parameter μ_{aa} could be hypothesized to have the same effect, however it appears to be negligible.

The most influential of these parameters is μ_j, the decay rate of the intracellular molecule that results in the differentiation of AHPCs. Most of the variance in the output can be attributed to this parameter. This is reasonable considering this molecule is directly involved with differentiation. The parameters associated with the inhibitor sgp130, μ_{gp} and μ_{ao}, do not appear to have a significant influence on the output.

Table 4.2 Distributions for sensitivity plots, varying decay rates:

Parameter	Code	Uni. Dist.	PRCC	eFAST (1st/Tot.)
dummy	1	U(.1155,.6931)	—	—
μ_{ai}	17	U(.1155,.6931)	-.7470	2.40/7.26
μ_{il}	18	U(.1155,.6931)	-.7354	2.06/6.24
μ_{aa}	19	U(.1155,.6931)	-.0751	—
μ_{gp}	20	U(.1155,.6931)	—	—
μ_{ao}	21	U(.1155,.6931)	—	—
μ_j	22	U(.1155,.6931)	-.9885	89.52/95.22
Parameter	Code	Norm. Dist.	PRCC	eFAST (1st/Tot.)
dummy	1	N(.173,.0288)	—	—
μ_{ai}	17	N(.173,.0288)	-.8334	14.83/17.37
μ_{il}	18	N(.173,.0288)	-.8298	14.60/17.15
μ_{aa}	19	N(.173,.0288)	-.0567	—/2.15
μ_{gp}	20	N(.173,.0288)	—	—
μ_{ao}	21	N(.173,.0288)	—	—
μ_j	22	N(.173,.0288)	-.9579	67.49/69.91

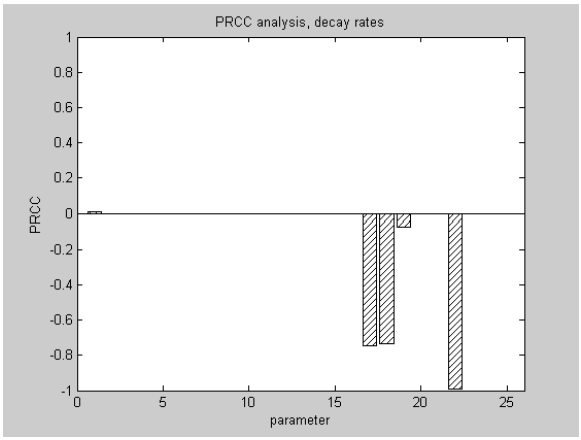

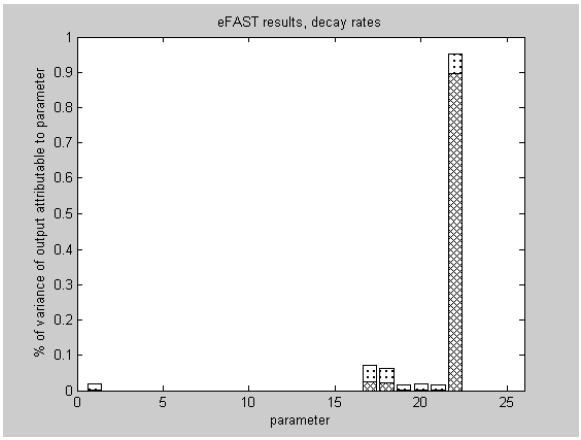

Figure 4.4 *(left) PRCC results, varying decay rates over entire parameter space.*

Figure 4.5 *(right) eFAST results, varying decay rates over entire parameter space.*

4.4.2 Production Constants

In this section, the secretion rates are varied simultaneously. These are the rates at which astrocytes secrete IL6 (a_1), sIL6Rα (b_a), and sgp130 (s_a). All other parameters are kept constant at their nominal values. Three sets of simulations are shown. In the first set of simulations, all secretion rates are assigned a log uniform pdf, with $z \in [1 \times 10^{-12}, 1 \times 10^{-9}]$ $\frac{nmol}{cell \cdot hr}$ for $z \in \{a_1, b_a, s_a\}$. A log uniform distribution is chosen to prevent undersampling of the region $[1 \times 10^{-12}, 1 \times 10^{-11}]$, which is an area with a significant effect when tested around the nominal values. This range corresponds biologically to astrocytes secreting between 600 and 600,000 of each of these molecules per cell per hour. In the second set of simulations, the secretion rates are varied according to normal distributions centered around their nominal values, and with standard deviations of $\frac{1}{6}$ of the mean. The third set of simulations show the results when this standard deviation is held constant for all three rates, at $\frac{1}{6}(1 \times 10^{-11})$. Partial Rank Correlation Coefficients and eFAST sensitivity coefficients are presented in Table 4.3 and illustrated graphically in Figures 4.8-13.

Two secretion rates have a significant effect on output: a_1 and b_a. Both of these parameters

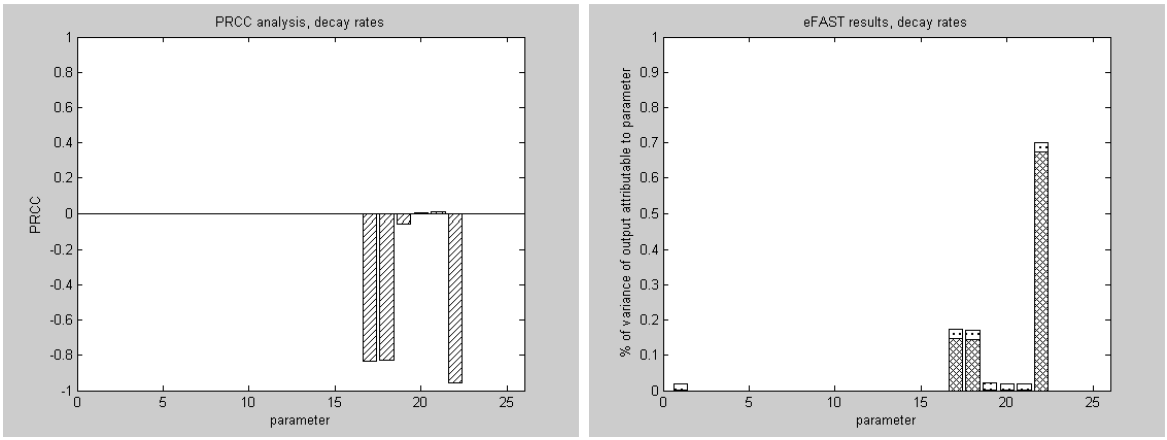

Figure 4.6 *(left) PRCC results, varying decay rates with normal distributions.*

Figure 4.7 *(right) eFAST results, varying decay rates with normal distributions.*

exhibit a positive monotonic relationship between changes in the parameter and changes in the output. This is expected, since if A_i and R_{il} are produced at a faster rate, more active molecules are available to initiate signal transduction cascades. Both of these parameters appear to be equally influential, since equal percentages of the variance in output can be attributed to each parameter. The parameter for the secretion rate of the inhibitor sgp130, s_a, does not appear to have a significant effect on the output.

The first two sets of simulations exhibit a roughly equal sensitivity to a_1 and b_a. However, the third set of simulations show an exaggerated effect of varying a_1 compared to b_a, since it is being varied by a higher percentage relative to its mean. However, s_a is changed by the same proportion and still exhibits no significant sensitivity.

4.4.3 Dissociation Constants

In this section, the dissociation constants are varied simultaneously. These parameters each determine the binding affinity between ligands and their respective receptors. It is a measure of how tightly they bind. The dissociation constant is equal to the concentration of ligand at which half of the receptors are bound to the ligand and the other half remains unbound. Low

Table 4.3 Distributions for sensitivity plots, varying secretion rates:

Parameter	Code	Uni. Dist.	PRCC	eFAST
dummy	1	LU(1e-12,1e-9)	—	—
a_1	14	LU(1e-12,1e-9)	.9558	41.49/59.78
b_a	15	LU(1e-12,1e-9)	.9509	40.24/58.53
s_a	16	LU(1e-12,1e-9)	—	—
Parameter	Code	Norm. Dist.	PRCC	eFAST (1st/Tot.)
dummy	1	N(1)	—	—
a_1	14	N(1e-11)	.9442	48.44/51.93
b_a	15	N(2e-10)	.9423	47.24/50.48
s_a	16	N(1e-11)	—	—
Parameter	Code	Norm. Dist.	PRCC	eFAST (1st/Tot.)
dummy	1	N(1e-11,1.7e-12)	—	—
a_1	14	N(1e-11,1.7e-12)	.9990	96.53/99.69
b_a	15	N(2e-10,1.7e-12)	.7259	.23/1.69
s_a	16	N(1e-11,1.7e-12)	—	—

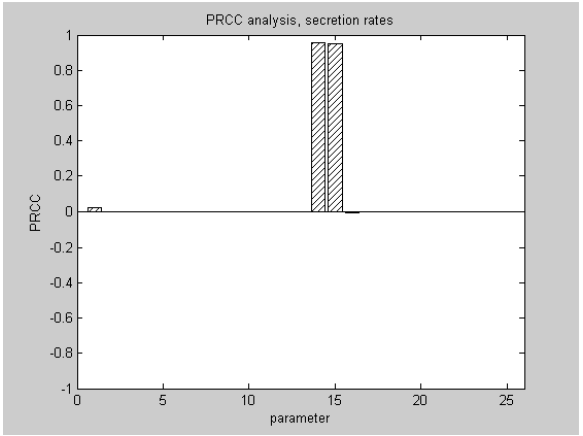

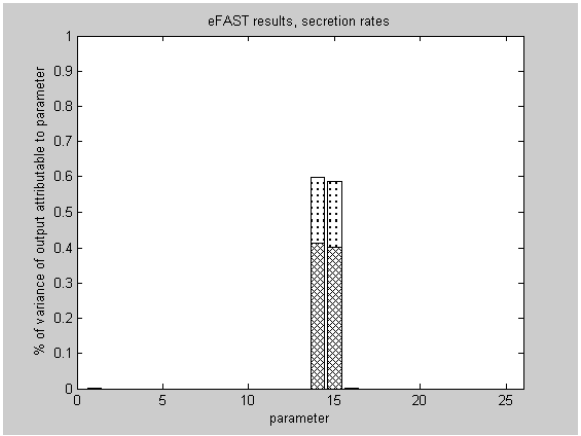

Figure 4.8 *(left) PRCC results, varying secretion rates rates over entire parameter space.*

Figure 4.9 *(right) eFAST results, varying secretion rates over entire parameter space.*

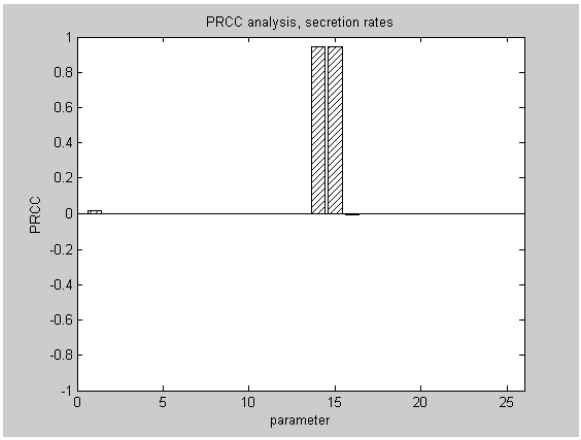

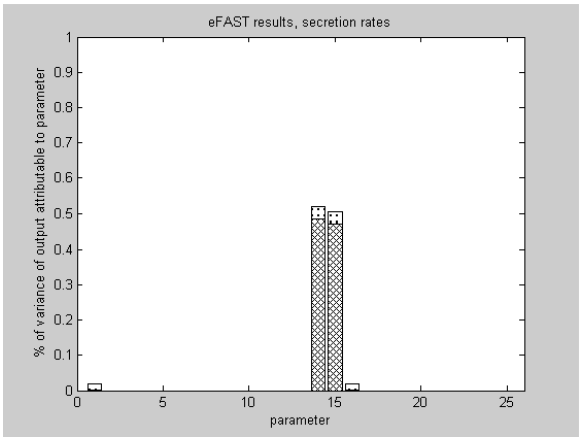

Figure 4.10 *(left) PRCC results, varying secretion rates with normal distributions, $\sigma_i = \frac{1}{6}\mu_i$.*

Figure 4.11 *(right) eFAST results, varying secretion rates with normal distributions, $\sigma_i = \frac{1}{6}\mu_i$.*

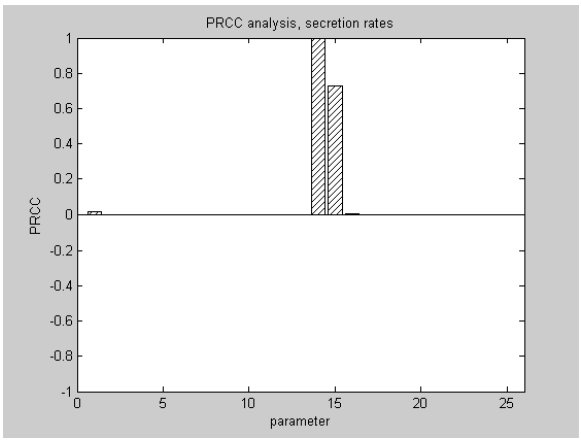

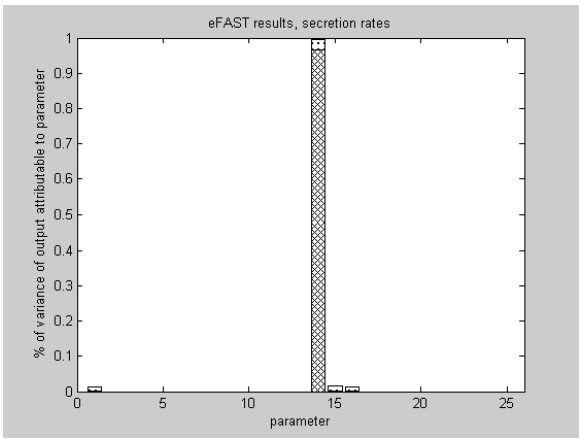

Figure 4.12 *(left) PRCC results, varying secretion rates with normal distributions, with equal standard deviations.*

Figure 4.13 *(right) eFAST results, varying secretion rates with normal distributions, with equal standard deviations.*

values for the dissociation constant signify a tight binding, while higher values indicate that the ligand can more easily dissociate from its receptor. All other parameters are kept constant at their nominal values. Three sets of simulations are shown. In the first set of simulations, all dissociation constants are assigned a log uniform pdf, with $z \in [1 \times 10^{-6}, 1 \times 10^{-1}]$ μM for $z \in \{L_d, K_d, \widehat{K_d}, \widehat{L_d}, V_d\}$. A log uniform distribution is chosen to get an even sampling of all orders within this range since some of the dissociation constants have been found experimentally to act in the range of 10-100 pM, while others have been found to act at 10-100 nM. In the other two sets of simulations, the dissociation constants are varied according to normal distributions centered around their nominal values. The second set uses standard deviations of $\frac{1}{6}$ of the mean. The third set of simulations use a common standard deviation of $\frac{1}{6}(1 \times 10^{-6})$. Partial Rank Correlation Coefficients and eFAST sensitivity coefficients are presented in Table 4.4 and illustrated graphically in Figures 4.14-19.

Two dissociation constants were found to have a significant effect on output in the first two simulations: L_d and V_d. L_d governs the binding of IL6 to its soluble receptor sIL6Rα to form activated IL6. This activated IL6 binds to the gp130 receptor dimer on the AHPC to initiate signal transduction via the second pathway, with this binding governed by the dissociation constant V_d. Both of these parameters exhibit a negative monotonic relationship between changes in the parameter and changes in the output. This is expected, since if A_i binds less tightly to R_{il}, less activated IL6 will be available to initiate the signal transduction cascade. Likewise, if activated IL6 binds less tightly to R^p_{gp130}, A_a will be less effective at initiating the signal transduction cascade. When varied with a normal distribution around their nominal values with standard deviations chosen relative to their means, both of these parameters appear to be equally influential, since equal percentages of the variance in output can be attributed to each parameter. However, when varied over the wider log-uniform distribution, V_d appears to be more influential. In addition, over the log-uniform distribution $\widehat{K_d}$ and $\widehat{L_d}$, the dissociation coefficients involved with the first pathway, appear to have a slightly significant effect on the output. However, much less of the variance in the output can be attributed to these parameters in comparison to L_d and V_d. When using normal distributions with equal standard deviations,

most of the variance is attributable to V_d. However, V_d is being varied by a higher percentage relative to its mean than the other parameters in this case.

Alterring binding strength for the second pathway causes much more variability in differentiation than alterring binding strength for the first pathway. These results suggest that the second pathway, utilizing soluble receptors, has a much stronger effect on the differentiation of AHPCs than the first pathway. The dissociation constant K_d, governing the binding of activated IL6 (A_a) to its inhibitor (sgp130), does not appear to have a significant effect on the output.

Table 4.4 Distributions for sensitivity plots, varying dissociation constants:

Parameter	Code	Uni. Dist.	PRCC	eFAST (1st/Tot.)
dummy	1	LU(1e-6,1e-1)	—	—
L_d	3	LU(1e-6,1e-1)	-.6160	23.49/48.42
K_d	5	LU(1e-6,1e-1)	—	.04/1.18
$\widehat{K_d}$	7	LU(1e-6,1e-1)	-.1508	.99/4.02
$\widehat{L_d}$	10	LU(1e-6,1e-1)	-.1354	.77/3.51
V_d	13	LU(1e-6,1e-1)	-.7626	49.75/75.48
Parameter	Code	Norm. Dist.	PRCC	eFAST (1st/Tot.)
dummy	1	N(1)	—	—
L_d	3	N(30e-3)	-.9457	47.65/51.47
K_d	5	N(3e-3)	—	—
$\widehat{K_d}$	7	N(100e-6)	—	—
$\widehat{L_d}$	10	N(10e-6)	—	—
V_d	13	N(60e-6)	-.9437	47.27/50.25
Parameter	Code	Norm. Dist.	PRCC	eFAST (1st/Tot.)
dummy	1	N(1e-3,1.7e-6)	—	—
L_d	3	N(30e-3,1.7e-6)	-.0500	—
K_d	5	N(3e-3,1.7e-6)	—	—
$\widehat{K_d}$	7	N(100e-6,1.7e-6)	-.0553	—
$\widehat{L_d}$	10	N(10e-6,1.7e-6)	-.3361	—/.04
V_d	13	N(60e-6,1.7e-6)	-.9992	96.66/99.91

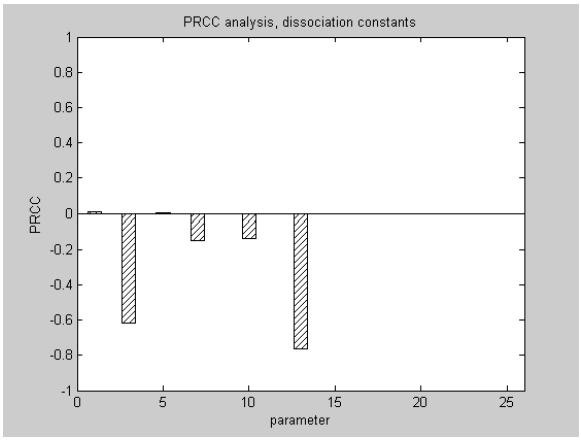

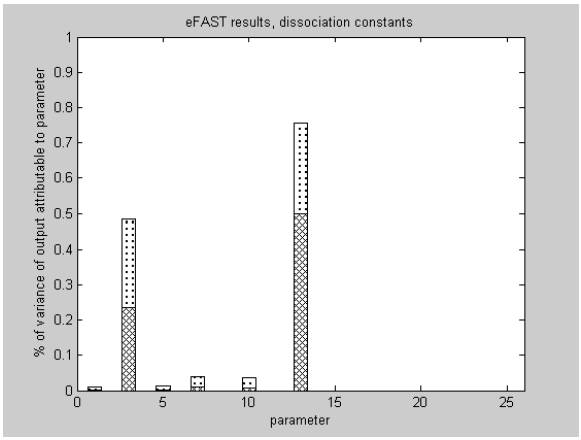

Figure 4.14 *(left) PRCC results, varying dissociation constants over entire parameter space.*

Figure 4.15 *(right) eFAST results, varying dissociation constants over entire parameter space.*

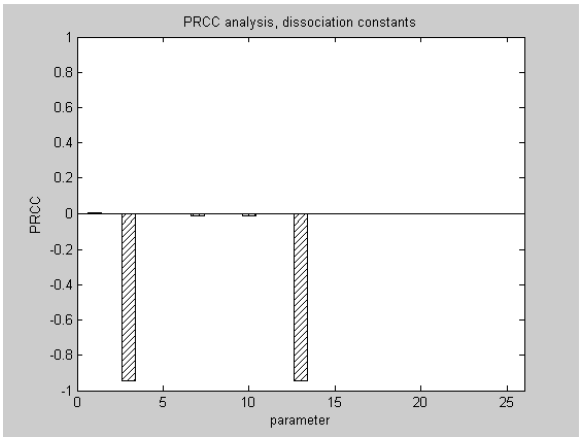

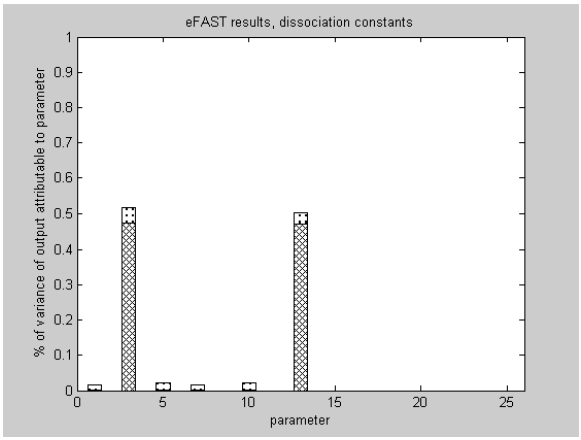

Figure 4.16 *(left) PRCC results, varying dissociation constants with normal distributions,* $\sigma_i = \frac{1}{6}\mu_i$.

Figure 4.17 *(right) eFAST results, varying dissociation constants with normal distributions,* $\sigma_i = \frac{1}{6}\mu_i$.

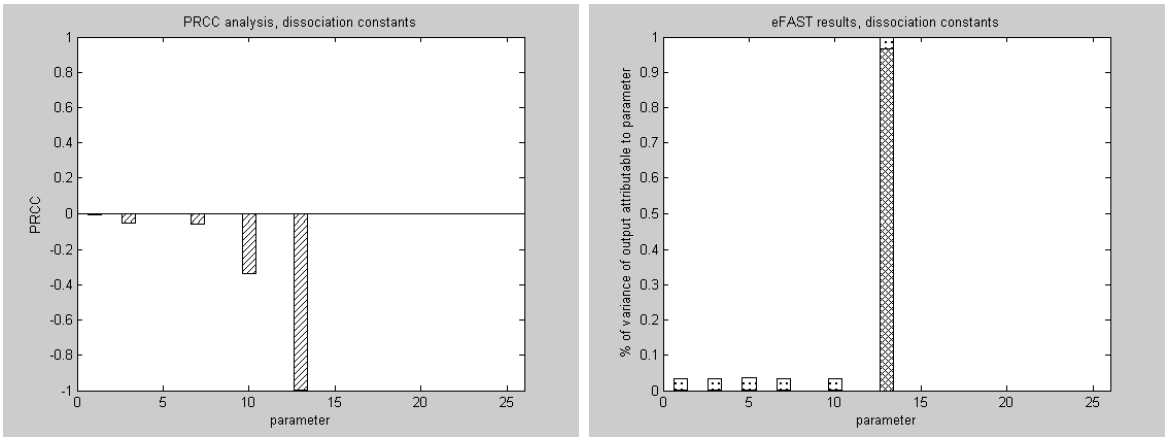

Figure 4.18 *(left) PRCC results, varying dissociation constants with normal distributions, with equal standard deviations.*

Figure 4.19 *(right) eFAST results, varying dissociation constants with normal distributions, with equal standard deviations.*

4.4.4 Kinetic Rates

In this section, the kinetic rates are varied simultaneously. These rates are measurements of how fast the reactions occur. For reversible reactions, kinetic rates appear in pairs; for example, ℓ_1 is the rate for A_i binding to R_{il} to form the complex A_a, while ℓ_{-1} is the rate for the dissociation of A_a back into its constituent parts A_i and R_{il}. They are related through the dissociation constant; for example, $L_d = \frac{\ell_{-1}}{\ell_1}$, or equivalently, $\ell_{-1} = L_d\ell_1$. Experimentally it is much easier to measure the dissociation constant than it is to measure these rates separately.

Since all other parameters are held constant at their nominal values, including the dissociation constants, only one rate constant from each pair is varied explicitly for the sensitivity analysis. Changing this one parameter has the effect of simultaneously changing the rate constant for the alternate direction because of the fixed dissociation constants. Therefore, in reality, these sensitivity coefficients are not necessarily measures of the sensitivity solely to those parameters in the table (ex. ℓ_{-1}). Instead, it is a measure of the sensitivity to the pair of rate constants (ex. ℓ_{-1} and ℓ_1). However, note that $\widehat{\ell_2}$ and ν_2 are rates from irreversible reactions, and as such the sensitivity to each of these parameters is due solely to these

parameters.

In the first set of simulations, all kinetic rates are assigned a log uniform pdf, with $z \in [1 \times 10^{-3}, 1 \times 10^{+3}]\ hr^{-1}$ for $z \in \{\ell_{-1}, k_{-1}, \widehat{k}_{-1}, \widehat{\ell}_{-1}, \widehat{\ell}_2, \nu_{-1}, \nu_2\}$. A log uniform distribution is chosen to get an even sampling of all orders within this range. In the other two sets of simulations, the kinetic rates are varied according to normal distributions centered around their nominal values. The second set uses standard deviations of $\frac{1}{6}$ of the mean. The third set of simulations use a common standard deviation of $\frac{1}{6}(.002)$. Partial Rank Correlation Coefficients and eFAST sensitivity coefficients are presented in Table 4.5 and illustrated graphically in Figures 4.20-25.

When varying the parameters locally around their nominal values using normal distributions, two parameters appear to be the most important: ν_2 and $\widehat{\ell}_2$. These are the two parameters governing the rates of the final reactions in the two pathways. They both govern the rate of production of the differentiation factor J. When using normal distributions with equal standard deviations, the most influential parameter is $\widehat{\ell}_2$, accounting for nearly all of the variance in the output. However, this is the parameter being varied by the largest amount relative to its mean in this case.

An interesting situation occurs when considering the larger parameter space. The parameter $\widehat{k}_{-1}$, which governs the binding of soluble activated IL6 to the surface R^p_{gp130} receptor, accounts for a majority of the variance in the output. When local distributions are considered, the system does not show sensitivity to this parameter. This indicates that there is a range of high sensitivity to this parameter, although it is farther from the mean than the areas the normal distributions sample heavily. This result makes sense since this parameter governs the rate of the A_a binding to the cell. If it becomes too low, the second pathway is essentially shut off. This result indicates that this parameter should be studied more to try to reduce the uncertainty in it's value. Finally, note that in all cases, the parameter k_{-1}, governing the rate of binding of activated IL6 to its inhibitor sgp130, does not appear to be significant. It does appear in the table under the PRCC column for the large parameter set, however the p-value associated with it is .0451. (Parameters with p-values less than .05 are included here.)

Table 4.5 Distributions for sensitivity plots, varying kinetic rates:

Parameter	Code	Uni. Dist.	PRCC	eFAST (1st/Tot.)
dummy	1	LU(1e-3,1e+3)	—	—
ℓ_{-1}	2	LU(1e-3,1e+3)	.1538	1.83/12.77
k_{-1}	4	LU(1e-3,1e+3)	-.0200*	—
$\widehat{k_{-1}}$	6	LU(1e-3,1e+3)	.7337	62.58/79.46
$\widehat{\ell_{-1}}$	8	LU(1e-3,1e+3)	—	—
$\widehat{\ell_2}$	9	LU(1e-3,1e+3)	.3178	8.55/17.43
ν_{-1}	11	LU(1e-3,1e+3)	.2249	2.58/14.78
ν_2	12	LU(1e-3,1e+3)	.2276	2.18/13.38

Parameter	Code	Norm. Dist.	PRCC	eFAST (1st/Tot.)
dummy	1	N(1)	—	—
ℓ_{-1}	2	N(5)	.1276	0.19/2.37
k_{-1}	4	N(5)	—	—
$\widehat{k_{-1}}$	6	N(500)	—	—
$\widehat{\ell_{-1}}$	8	N(5)	—	—
$\widehat{\ell_2}$	9	N(.002)	.9692	68.32/71.13
ν_{-1}	11	N(5)	.2618	0.46/2.70
ν_2	12	N(.5)	.9266	27.87/30.28

Parameter	Code	Norm. Dist.	PRCC	eFAST (1st/Tot.)
dummy	1	N(1,3.3e-4)	—	—
ℓ_{-1}	2	N(5,3.3e-4)	—	—
k_{-1}	4	N(5,3.3e-4)	—	—
$\widehat{k_{-1}}$	6	N(500,3.3e-4)	—	—
$\widehat{\ell_{-1}}$	8	N(5,3.3e-4)	—	—
$\widehat{\ell_2}$	9	N(.002,3.3e-4)	.9992	97.07/99.95
ν_{-1}	11	N(5,3.3e-4)	—	—
ν_2	12	N(.5,3.3e-4)	.0539	—

				*: p-value is .0451

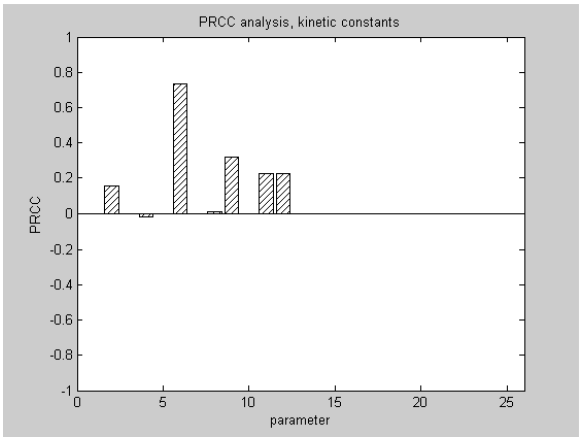

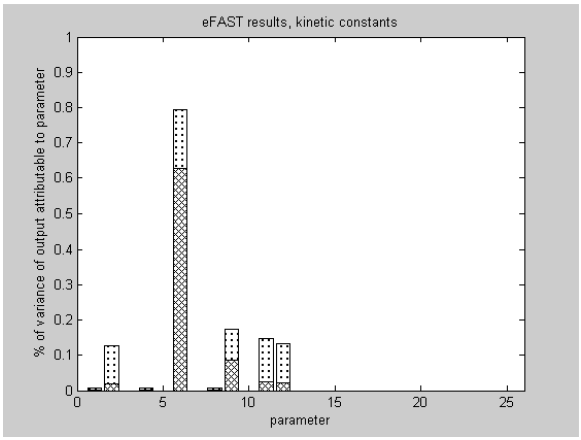

Figure 4.20 *(left) PRCC results, varying kinetic rates over entire parameter space.*

Figure 4.21 *(right) eFAST results, varying kinetic rates over entire parameter space.*

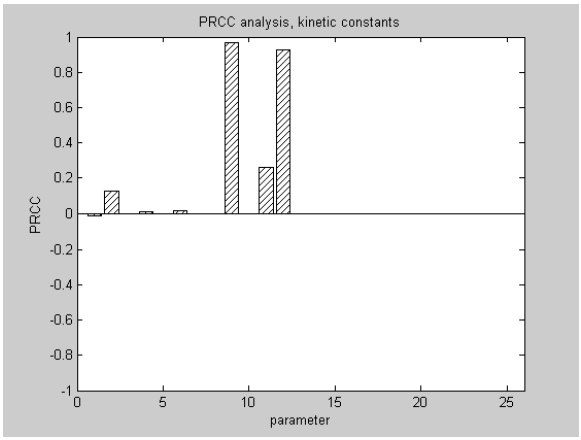

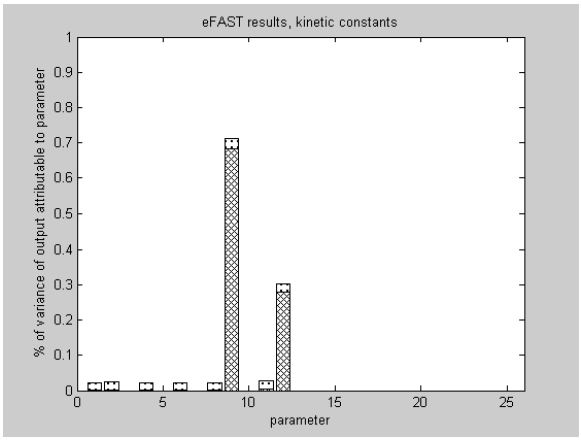

Figure 4.22 *(left) PRCC results, varying kinetic rates with normal distributions,* $\sigma_i = \frac{1}{6}\mu_i$.

Figure 4.23 *(right) eFAST results, varying kinetic rates with normal distributions,* $\sigma_i = \frac{1}{6}\mu_i$.

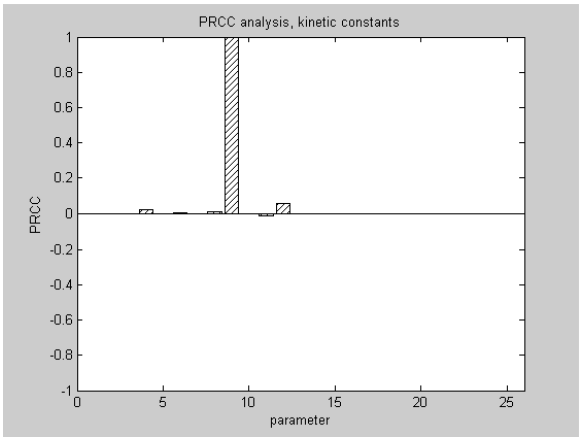

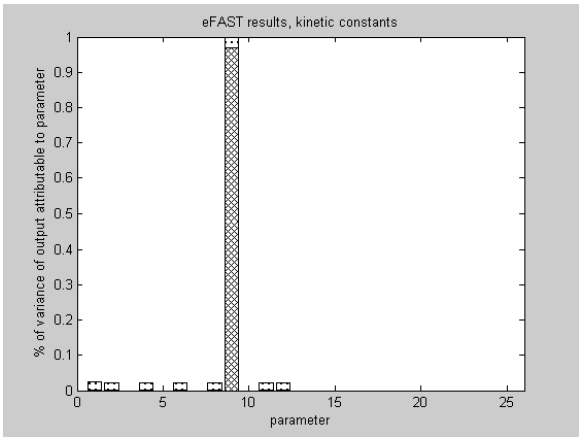

Figure 4.24 *(left) PRCC results, varying kinetic rates with normal distributions, with equal standard deviations.*

Figure 4.25 *(right) eFAST results, varying kinetic rates with normal distributions, with equal standard deviations.*

4.4.5 Densities of Cell Receptors and Astrocytes

In this section, the densities of astrocytes and the AHPC surface receptors are varied simultaneously. The astrocytes produce the molecule IL6 and the soluble receptors sIL6Rα and sgp130, and binding to the surface receptors must occur for the cells to communicate. The communication via binding and the resultant signal transduction induces the AHPC to produce the differentiation factor J.

In the first set of simulations, the cell surface receptor densities are assigned a log uniform pdf, with $z \in [1 \times 10^{+2}, 1 \times 10^{+5}]$ receptors per cell. The astrocyte density is varied with a uniform distribution with $N_a \in [1 \times 10^{+4}, 1 \times 10^{+5}]$ cells per cm^2. The reason for the smaller distribution for N_a has to do with the consequences of lowering this parameter too much. N_a produces IL6, the basis of all of the activity. If N_a has a log uniform pdf of $[1 \times 10^{+2}, 1 \times 10^{+5}]$, then for N_a in the lower regions, it does not produce enough IL6 for any substantial amount of differentiation to occur. Most parameters will appear to be insensitive, while N_a will have a strong effect on the output. For the experiments being considered in this thesis, N_a is a known quantity, within the range $[1 \times 10^{+4}, 1 \times 10^{+5}]$ cells per cm^2. Hence we will restrict

the distribution of this parameter in order to have an effective study of the sensitivity of the model to the other parameters. In the other two sets of simulations, the densities are varied according to normal distributions centered around their nominal values. The second set uses standard deviations of $\frac{1}{6}$ of the mean. The third set of simulations use a common standard deviation of $\frac{1}{6}(1 \times 10^{+3})$. Partial Correlation Coefficients and eFAST sensitivity coefficients are presented in Table 4.6 and illustrated graphically in Figures 4.26-31.

The results show sensitivity to all three parameters. Over the large parameter space, $R^p_{gp130,0}$ appears to be the most important, which makes sense since this receptor is utilized by both pathways. When considered more locally, N_a is the most important when the standard deviations of the normal distributions are relative to their nominal values. However, when varied with an equal standard deviation, $R^p_{il,0}$ is the most important. This parameter is being varied by the largest percentage of its mean in this case.

Table 4.6 Distributions for sensitivity plots, varying receptor and astrocyte densities:

Parameter	Code	Uni. Dist.	PRCC	eFAST (1st/Tot.)
dummy	1	LU(1e+2,1e+5)	—	—
$R^p_{il,0}$	23	LU(1e+2,1e+5)	.7711	24.22/42.01
$R^p_{gp130,0}$	24	LU(1e+2,1e+5)	.8972	57.38/75.17
N_a	25	U(1e+4,1e+5)	.2627	.92/5.77
Parameter	Code	Norm. Dist.	PRCC	eFAST (1st/Tot.)
dummy	1	N(1)	—	—
$R^p_{il,0}$	23	N(1e+3)	.8951	27.36/30.30
$R^p_{gp130,0}$	24	N(1e+5)	.8198	14.11/17.04
N_a	25	N(3e+4)	.9450	54.69/58.23
Parameter	Code	Norm. Dist.	PRCC	eFAST (1st/Tot.)
dummy	1	N(1e+4,167)	—	—
$R^p_{il,0}$	23	N(1e+3,167)	.9990	96.83/99.72
$R^p_{gp130,0}$	24	N(1e+5,167)	.1360	—
N_a	25	N(3e+4,167)	.7080	.92/5.77

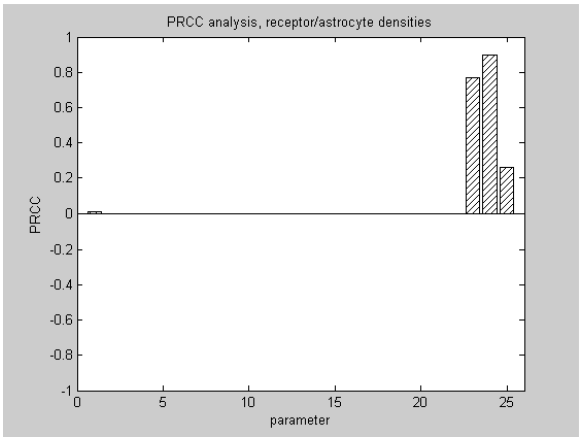

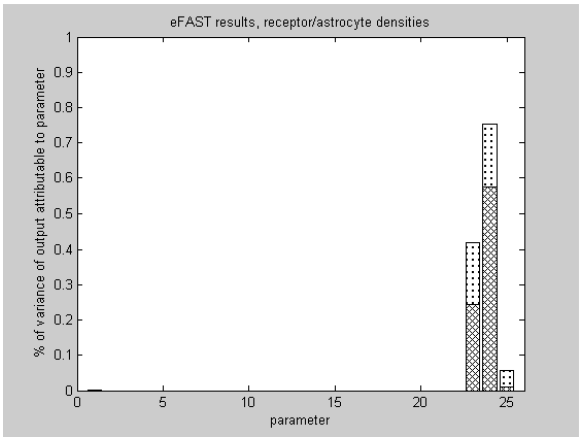

Figure 4.26 *(left) PRCC results, varying receptor/astrocyte densities over entire parameter space.*

Figure 4.27 *(right) eFAST results, varying receptor/astrocyte densities over entire parameter space.*

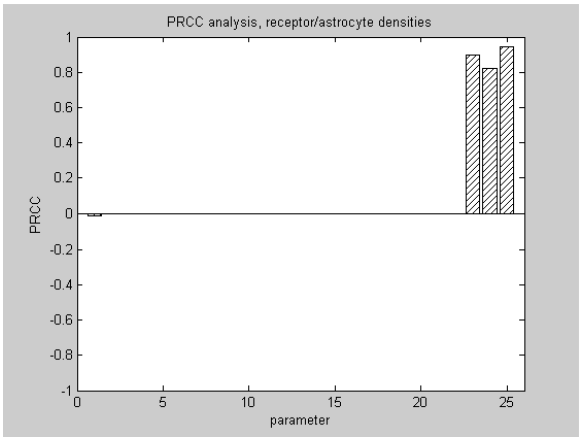

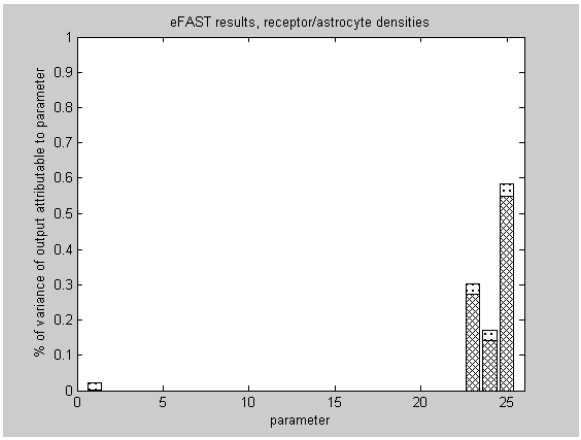

Figure 4.28 *(left) PRCC results, varying receptor/astrocyte densities with normal distributions,* $\sigma_i = \frac{1}{6}\mu_i$.

Figure 4.29 *(right) eFAST results, varying receptor/astrocyte densities with normal distributions,* $\sigma_i = \frac{1}{6}\mu_i$.

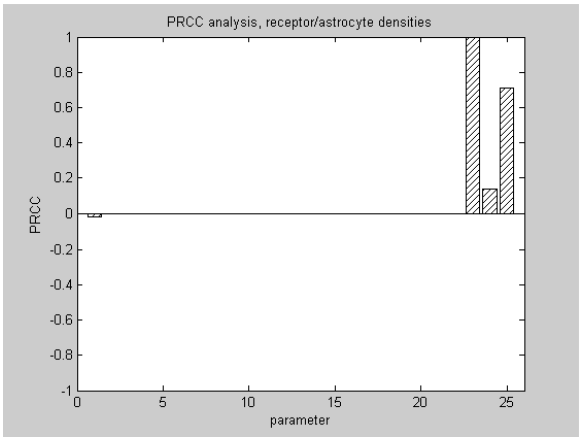

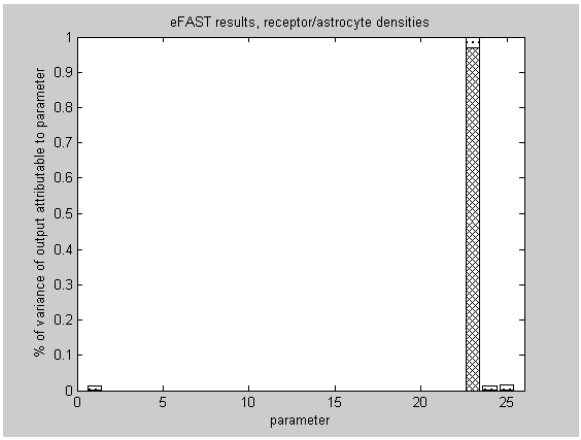

Figure 4.30 *(left) PRCC results, varying receptor/astrocyte densities with normal distributions, with equal standard deviations.*

Figure 4.31 *(right) eFAST results, varying receptor/astrocyte densities with normal distributions, with equal standard deviations.*

4.4.6 Parameters involved with sIL6Rα and sgp130

In this section, all parameters involved with the soluble receptors, excluding decay constants, are varied simultaneously. The main result here is that the parameters involving the inhibitor sgp130 ($k_{-1}, K_d,$ and s_a) do not have significantly different effect on the output than does the dummy parameter. The most important of the parameters that do show a significant effect are L_d, V_d, ν_2, and b_a. The parameter distributions and PRCC and eFAST coefficients are provided in Table 4.7. The results are illustrated graphically in Figures 4.32-37.

4.4.7 Unknown Parameters

In this section, the parameters for which no value was found recorded in the literature were varied. All other parameters are held at their nominal values, which are within the ranges reported in the literature. Three sets of simulations are shown. In the first set of simulations, parameters are varied over a wide range relative to their nominal values. These are sampled using either uniform or log-uniform distributions. In the other two sets of simulations, these parameters are varied more locally around their nominal values via normal distributions. The

Table 4.7 Distributions for sensitivity plots, varying parameters related to sIL6Rα and sgp130 activity:

Parameter	Code	Uni. Dist.	PRCC	eFAST (1st/Tot.)
dummy	1	LU(1e-3,1e+3)	—	—
ℓ_{-1}	2	LU(1e-3,1e+3)	.4126	4.13/15.65
L_d	3	LU(1e-6,1e-1)	-.7165	18.83/43.08
k_{-1}	4	LU(1e-3,1e+3)	-.0362	—
K_d	5	LU(1e-6,1e-1)	.0680	.04/—
ν_{-1}	11	LU(1e-3,1e+3)	.5850	9.29/27.54
ν_2	12	LU(1e-3,1e+3)	.5846	8.58/26.38
V_d	13	LU(1e-6,1e-1)	-.7718	20.31/44.43
b_a	15	LU(1e-12,1e-9)	.5045	4.94/18.01
s_a	16	LU(1e-12,1e-9)	-.0666	—
Parameter	Code	Norm. Dist.	PRCC	eFAST (1st/Tot.)
dummy	1	N(1)	—	—
ℓ_{-1}	2	N(5)	.0842	—
L_d	3	N(30e-3)	-.8583	25.94/29.94
k_{-1}	4	N(5)	—	—
K_d	5	N(3e-3)	—	—
ν_{-1}	11	N(5)	.1742	0.36/—
ν_2	12	N(.5)	.8274	20.32/23.47
V_d	13	N(60e-6)	-.8545	26.13/29.66
b_a	15	N(2e-10)	.8557	24.45/27.84
s_a	16	N(1e-11)	—	—
Parameter	Code	Norm. Dist.	PRCC	eFAST (1st/Tot.)
dummy	1	N(1,3.3e-4)	—	—
ℓ_{-1}	2	N(5,3.3e-4)	—	—
L_d	3	N(30e-3,1.7e-6)	—	—
k_{-1}	4	N(5,3.3e-4)	—	—
K_d	5	N(3e-3,1.7e-6)	—	—
ν_{-1}	11	N(5,3.3e-4)	—	—
ν_2	12	N(.5,3.3e-4)	.1580	—
V_d	13	N(60e-6,1.7e-6)	-.9905	88.57/91.85
b_a	15	N(2e-10,1.7e-12)	.9019	8.18/10.99
s_a	16	N(1e-11,1.7e-12)	—	—

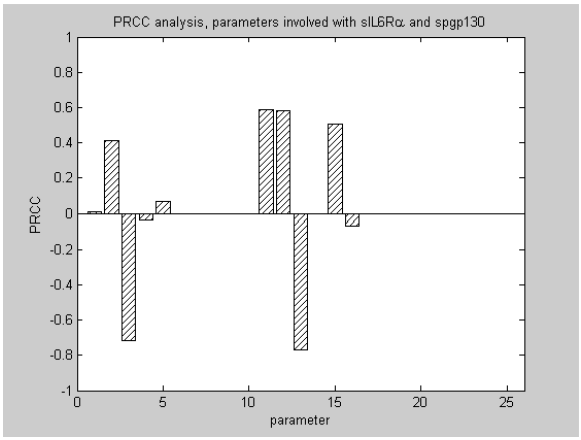

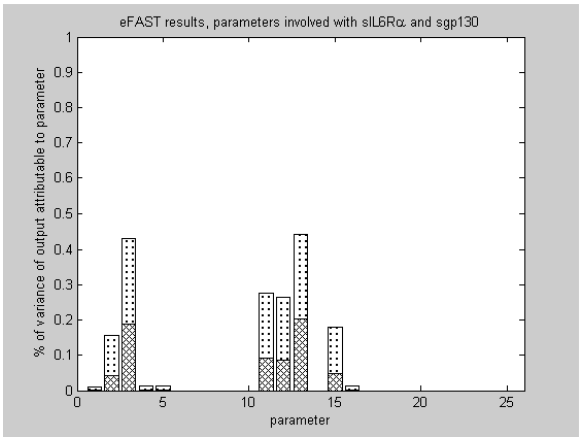

Figure 4.32 *(left) PRCC results, varying parameters involved with sIL6Rα and sgp130 activity over entire parameter space.*

Figure 4.33 *(right) eFAST results, varying parameters involved with sIL6Rα and sgp130 activity over entire parameter space.*

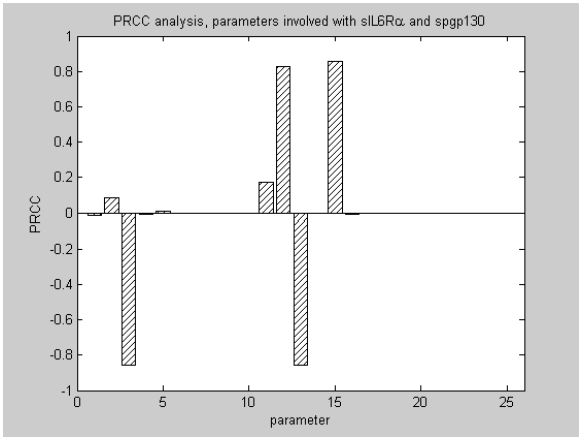

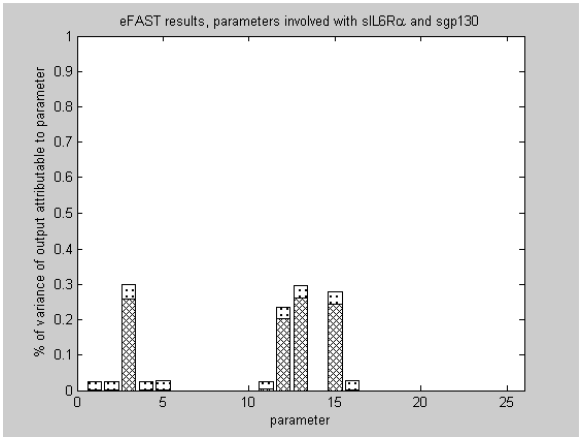

Figure 4.34 *(left) PRCC results, varying parameters involved with sIL6Rα and sgp130 activity with normal distributions,* $\sigma_i = \frac{1}{6}\mu_i$.

Figure 4.35 *(right) eFAST results, varying parameters involved with sIL6Rα and sgp130 activity with normal distributions,* $\sigma_i = \frac{1}{6}\mu_i$.

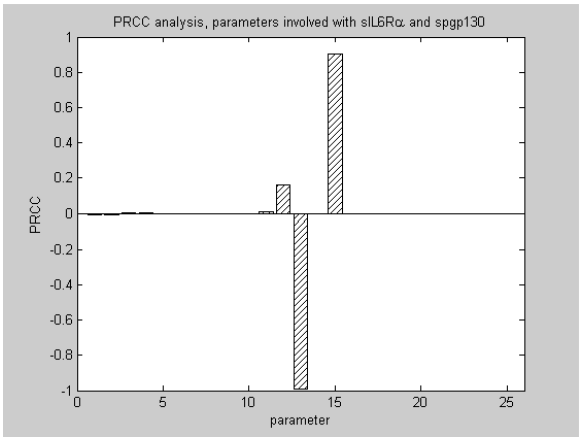

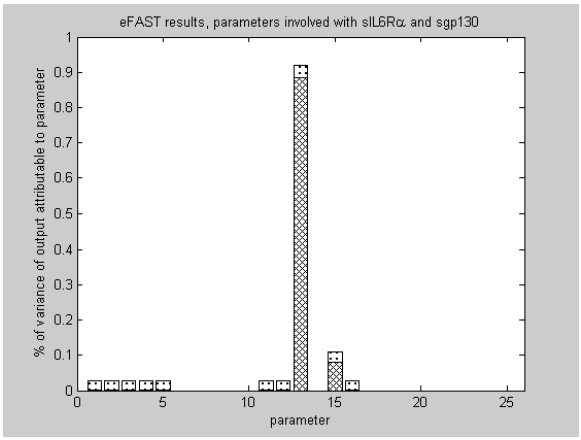

Figure 4.36 *(left) PRCC results, varying parameters involved with sIL6Rα and sgp130 activity with normal distributions, with equal standard deviations (see Table 4.11).*

Figure 4.37 *(right) eFAST results, varying parameters involved with sIL6Rα and sgp130 activity with normal distributions, with equal standard deviations (see Table 4.11).*

parameters that are the most influential, and as such should be studied biologically in more detail, are as follows: $\widehat{k}_{-1}$, $\widehat{\ell}_2$, ν_2, b_a, $R^p_{il,0}$, and $R^p_{gp130,0}$. Note that in order to study ν_2 and $\widehat{\ell}_2$, the intracellular mechanism leading to differentiation needs to be studied in more detail. In particular, the intracellular mechanism producing the differentiation factor J would need to be explored. Partial Rank Correlation Coefficients and eFAST sensitivity coefficients are presented in Table 4.8 and illustrated graphically in Figures 4.38-43.

4.4.8 All Parameters

In this section, all parameters are varied simultaneously. Each parameter can be considered as belonging to one of the following groups: decay rates, secretion rates, dissociation constants, kinetic rates, or receptor/cell densities. Three sets of simulations are shown. In the first set of simulations, each parameter is assigned either a uniform or log uniform pdf, whose range depends on which group it belongs to. In the other two sets of simulations, the parameters are varied according to normal distributions centered around their nominal values. The second set

Table 4.8 Distributions for sensitivity plots, varying unknown parameters:

Parameter	Code	Uni. Dist.	PRCC	eFAST (1st/Tot.)
dummy	1	LU(1e-3,1e+3)	—	—
ℓ_{-1}	2	LU(1e-3,1e+3)	.0266	—
k_{-1}	4	LU(1e-3,1e+3)	—	—
$\widehat{k_{-1}}$	6	LU(1e-3,1e+3)	.7038	44.93/67.49
$\widehat{\ell_{-1}}$	8	LU(1e-3,1e+3)	.0653	.12/1.69
$\widehat{\ell_2}$	9	U(1e-3,1e+3)	.3790	11.29/24.38
ν_{-1}	11	LU(1e-3,1e+3)	.0303	.08/2.25
ν_2	12	LU(1e-3,1e+3)	.0450	.08/2.14
b_a	15	LU(1e-12,1e-9)	.0603	—
s_a	16	LU(1e-12,1e-9)	—	—
$R^p_{il,0}$	23	U(1e+2,1e+5)	.5198	14.45/36.84
$R^p_{gp130,0}$	24	U(1e+2,1e+5)	.1909	2.18/12.55

Parameter	Code	Norm. Dist.	PRCC	eFAST (1st/Tot.)
dummy	1	N(1)	—	—
ℓ_{-1}	2	N(5)	.0424	—
k_{-1}	4	N(5)	—	—
$\widehat{k_{-1}}$	6	N(500)	—	—
$\widehat{\ell_{-1}}$	8	N(5)	—	—
$\widehat{\ell_2}$	9	N(.002)	.8700	28.21/31.08
ν_{-1}	11	N(5)	.1248	—
ν_2	12	N(.5)	.7475	11.21/13.33
b_a	15	N(2e-10)	.7779	14.25/16.67
s_a	16	N(1e-11)	—	—
$R^p_{il,0}$	23	N(1e+3)	.8689	29.28/32.07
$R^p_{gp130,0}$	24	N(1e+5)	.7822	14.53/17.15

Parameter	Code	Norm. Dist.	PRCC	eFAST (1st/Tot.)
dummy	1	N(1,3.3e-4)	—	—
ℓ_{-1}	2	N(5,3.3e-4)	—	—
k_{-1}	4	N(5,3.3e-4)	—	—
$\widehat{k_{-1}}$	6	N(500,3.3e-4)	—	—
$\widehat{\ell_{-1}}$	8	N(5,3.3e-4)	—	—
$\widehat{\ell_2}$	9	N(.002,3.3e-4)	.9426	48.55/51.33
ν_{-1}	11	N(5,3.3e-4)	—	—
ν_2	12	N(.5,3.3e-4)	—	—
b_a	15	N(2e-10,1.7e-12)	.1043	.06/—
s_a	16	N(1e-11,1.7e-12)	—	—
$R^p_{il,0}$	23	N(1e+3,167)	.9418	48.37/51.17
$R^p_{gp130,0}$	24	N(1e+5,167)	.0198*	—
				*: p-value is .0480

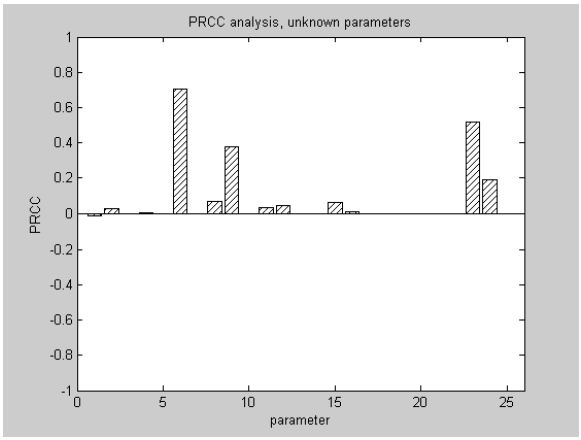

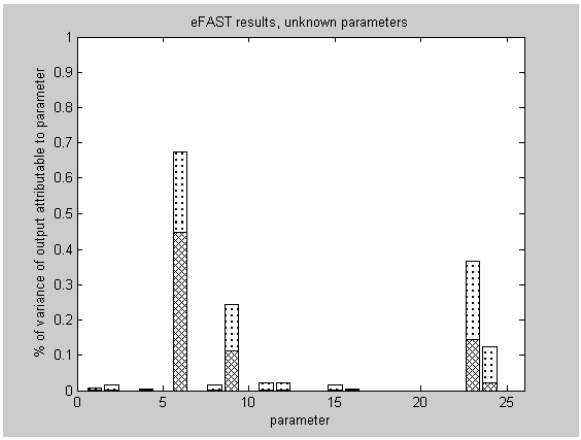

Figure 4.38 *(left) PRCC results, varying unknown parameters over entire parameter space.*

Figure 4.39 *(right) eFAST results, varying unknown parameters over entire parameter space.*

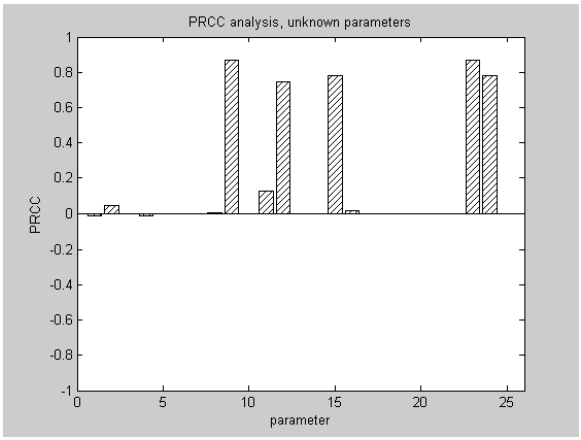

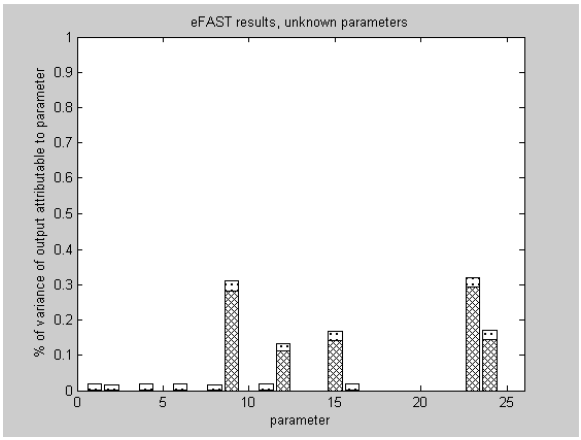

Figure 4.40 *(left) PRCC results, varying unknown parameters with normal distributions,* $\sigma_i = \frac{1}{6}\mu_i$.

Figure 4.41 *(right) eFAST results, varying unknown parameters with normal distributions,* $\sigma_i = \frac{1}{6}\mu_i$.

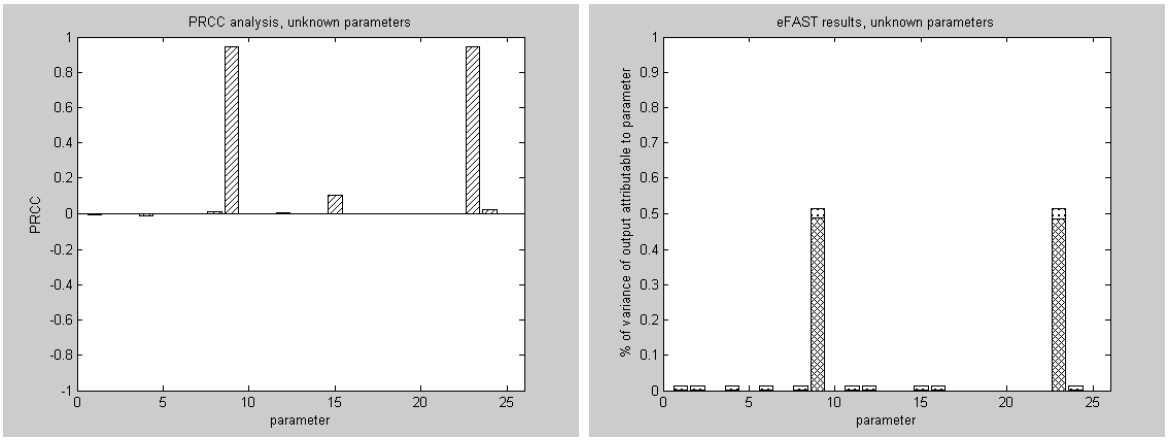

Figure 4.42 *(left) PRCC results, varying unknown parameters with normal distributions, with equal standard deviations (see Table 4.13).*

Figure 4.43 *(right) eFAST results, varying unknown parameters with normal distributions, with equal standard deviations (see Table 4.13).*

uses standard deviations of $\frac{1}{6}$ of the mean. The third set of simulations use a standard deviation common to all members of the particular group to which the parameter belongs. Partial Rank Correlation Coefficients and eFAST sensitivity coefficients are presented in Tables 4.9-11 and illustrated graphically in Figures 4.44-49.

When varied throughout the "large" parameter space, utilizing uniform/log-uniform distributions, the output does not appear to be very sensitive to the variations in the decay rates. The other groups, however, do appear to have significant effects on the output. Many of the eFAST sensitivities are very similar, and there is apparently much variance occurring due to interactions among the parameters. When the distributions are considered more locally, then the decay rates appear to be influential on the output. The most influential parameter in this local space is μ_j, the decay rate of the intracellular differentiation factor. Other important parameters in this space are: $\widehat{\ell}_2$, L_d, ν_2, V_d, $R^p_{il,0}$, $R^p_{gp130,0}$, a_1, and b_a. Many of these parameters are known. However, $\widehat{\ell}_2$, ν_2, and μ_j are all involved with the intracellular differentiation molecule, and since the model exhibits sensitivity to these parameters, a goal of future work should be to better understand the intracellular mechanism leading to AHPC differentiation.

Table 4.9 Distributions for sensitivity plots, varying all parameters:

Parameter	Code	Uni. Dist.	PRCC	eFAST (1st/Tot.)
dummy	1	U(1,10)	—	—
ℓ_{-1}	2	LU(1e-3,1e+3)	.0609	—/6.47
L_d	3	LU(1e-6,1e-1)	-.1535	.86/12.72
k_{-1}	4	LU(1e-3,1e+3)	—	—/1.76
K_d	5	LU(1e-6,1e-1)	—	—
$\widehat{k_{-1}}$	6	LU(1e-3,1e+3)	.4276	7.43/27.55
$\widehat{K_d}$	7	LU(1e-6,1e-1)	-.5450	13.59/37.58
$\widehat{\ell_{-1}}$	8	LU(1e-3,1e+3)	.1934	1.41/10.61
$\widehat{\ell_2}$	9	LU(1e-3,1e+3)	.3344	7.43/22.43
$\widehat{L_d}$	10	LU(1e-6,1e-1)	-.2795	3.39/16.96
ν_{-1}	11	LU(1e-3,1e+3)	.1670	.81/9.84
ν_2	12	LU(1e-3,1e+3)	.1768	.92/9.30
V_d	13	LU(1e-6,1e-1)	-.2322	—/12.49
a_1	14	LU(1e-12,1e-9)	.4455	7.01/24.20
b_a	15	LU(1e-12,1e-9)	.0970	—/7.23
s_a	16	LU(1e-12,1e-9)	—	—
μ_{ai}	17	U(.1155,.6931)	-.1066	.32/3.56
μ_{il}	18	U(.1155,.6931)	-.0278	—/2.35
μ_{aa}	19	U(.1155,.6931)	—	—/1.98
μ_{gp}	20	U(.1155,.6931)	—	—
μ_{ao}	21	U(.1155,.6931)	—	—
μ_j	22	U(.1155,.6931)	-.1449	.47/4.10
$R^p_{il,0}$	23	U(1e+2,1e+5)	.4003	9.31/28.40
$R^p_{gp130,0}$	24	U(1e+2,1e+5)	.3504	7.65/25.65
N_a	25	U(1e+4,1e+5)	.1745	1.35/7.50

Table 4.10 Distributions for sensitivity plots, varying all parameters:

Parameter	Code	Norm. Dist.	PRCC	eFAST (1st/Tot.)
dummy	1	N(1)	—	—
ℓ_{-1}	2	N(5)	.0290	—
L_d	3	N(30e-3)	-.5175	5.72/8.91
k_{-1}	4	N(5)	—	—
K_d	5	N(3e-3)	—	—
$\widehat{k_{-1}}$	6	N(500)	—	—
$\widehat{K_d}$	7	N(100e-6)	—	—
$\widehat{\ell_{-1}}$	8	N(5)	—	—
$\widehat{\ell_2}$	9	N(.002)	.6546	9.99/12.94
$\widehat{L_d}$	10	N(10e-6)	—	—
ν_{-1}	11	N(5)	.0337	0.07/—
ν_2	12	N(.5)	.4799	3.56/6.14
V_d	13	N(60e-6)	-.5155	4.28/6.66
a_1	14	N(1e-11)	.5246	4.81/7.64
b_a	15	N(2e-10)	.5196	4.15/6.57
s_a	16	N(1e-11)	—	—
μ_{ai}	17	N(.173)	-.5170	5.61/8.62
μ_{il}	18	N(.173)	-.5112	5.93/9.00
μ_{aa}	19	N(.173)	-.0246	—
μ_{gp}	20	N(.173)	—	—
μ_{ao}	21	N(.173)	—	—
μ_j	22	N(.173)	-.8096	22.27/26.12
$R^p_{il,0}$	23	N(1e+3)	.6456	9.18/12.41
$R^p_{gp130,0}$	24	N(1e+5)	.5137	5.42/8.42
N_a	25	N(3e+4)	.7703	20.28/25.36

Table 4.11 Distributions for sensitivity plots, varying all parameters:

Parameter	Code	Norm. Dist.	PRCC	eFAST (1st/Tot.)
dummy	1	N(1,3.3e-4)	—	—
ℓ_{-1}	2	N(5,3.3e-4)	—	—
L_d	3	N(30e-3,1.7e-6)	—	—
k_{-1}	4	N(5,3.3e-4)	—	—
K_d	5	N(3e-3,1.7e-6)	—	—
$\widehat{k_{-1}}$	6	N(500,3.3e-4)	—	—
$\widehat{K_d}$	7	N(100e-6,1.7e-6)	—	—
$\widehat{\ell_{-1}}$	8	N(5,3.3e-4)	—	—
$\widehat{\ell_2}$	9	N(.002,3.3e-4)	.7801	15.33/17.86
$\widehat{L_d}$	10	N(10e-6,1.7e-6)	—	—
ν_{-1}	11	N(5,3.3e-4)	—	—
ν_2	12	N(.5,3.3e-4)	.0215*	—
V_d	13	N(60e-6,1.7e-6)	-.1342	.22/—
a_1	14	N(1e-11,1.7e-12)	.6800	8.07/10.24
b_a	15	N(2e-10,1.7e-12)	.0478	—
s_a	16	N(1e-11,1.7e-12)	—	—
μ_{ai}	17	N(.173,.0288)	-.6811	9.04/11.51
μ_{il}	18	N(.173,.0288)	-.6826	8.42/10.76
μ_{aa}	19	N(.173,.0288)	-.0287	—
μ_{gp}	20	N(.173,.0288)	—	—
μ_{ao}	21	N(.173,.0288)	-.0287**	—
μ_j	22	N(.173,.0288)	-.8986	40.64/43.75
$R^p_{il,0}$	23	N(1e+3,167)	.7765	14.76/17.56
$R^p_{gp130,0}$	24	N(1e+5,167)	—	—
N_a	25	N(3e+4,167)	.0582	.07/—
		*: p-value is .0319		**: p-value is .0172

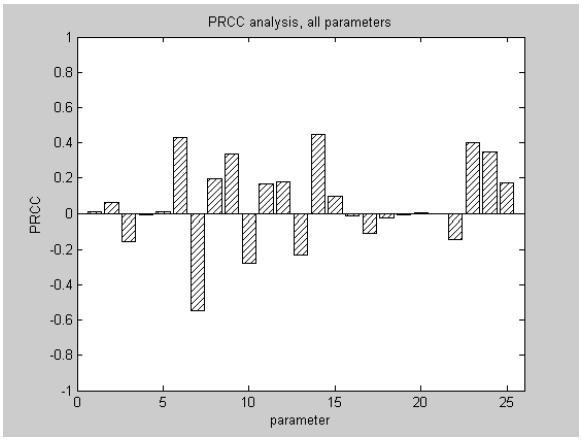

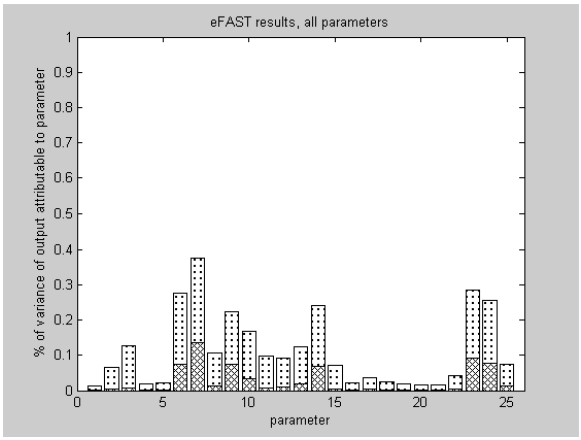

Figure 4.44 *(left) PRCC results, varying all parameters over entire parameter space.*

Figure 4.45 *(right) eFAST results, varying all parameters over entire parameter space.*

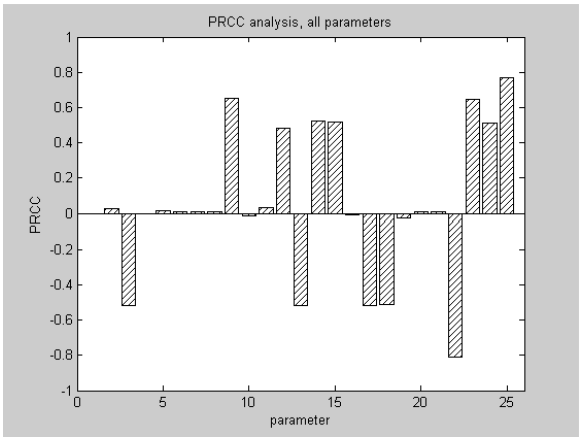

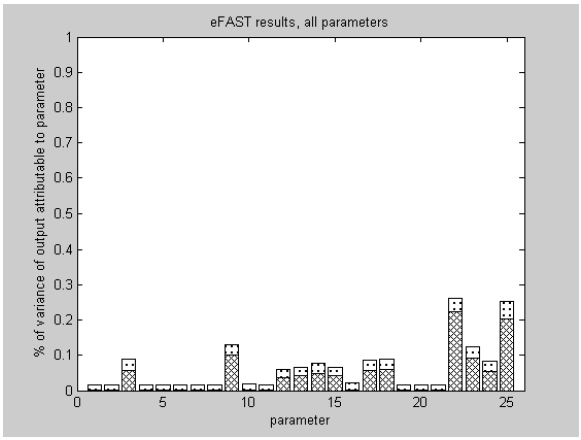

Figure 4.46 *(left) PRCC results, varying all parameters with normal distributions, $\sigma_i = \frac{1}{6}\mu_i$.*

Figure 4.47 *(right) eFAST results, varying all parameters with normal distributions, $\sigma_i = \frac{1}{6}\mu_i$.*

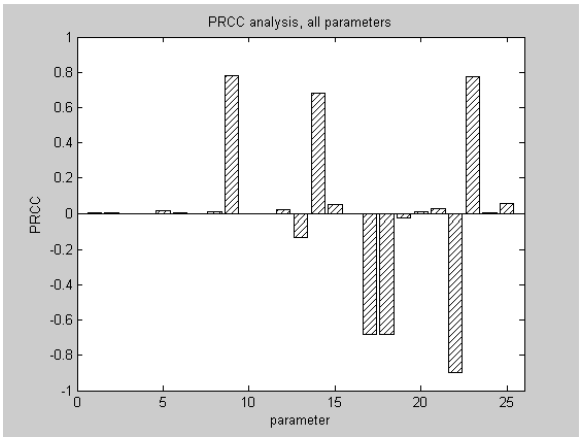

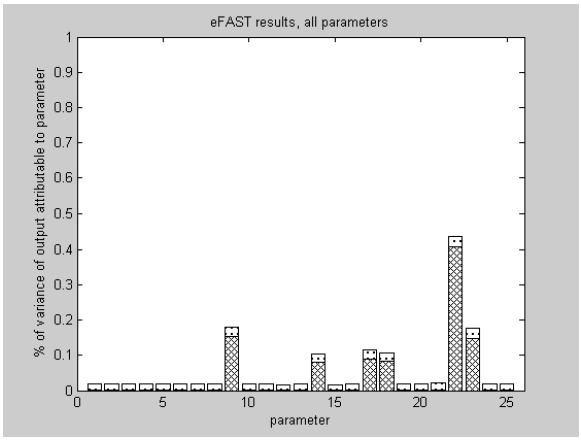

Figure 4.48 *(left) PRCC results, varying all parameters with normal distributions, with equal standard deviations within subgroups of parameters (see Table 4.15).*

Figure 4.49 *(right) eFAST results, varying all parameters with normal distributions, with equal standard deviations within subgroups of parameters (see Table 4.15).*

CHAPTER 5. Steady State Analysis of the Population Model

In this chapter, steady-state solutions are calculated for the population model, and linearized stability results are established. These results are performed both for the full system and for a simplified system comprised solely of the cellular equations, where the rate of differentiation is assumed constant. The phase plane of the simplified system is analyzed in this chapter, and in Appendix C a solution of this system is derived in the form of a formal power series. However, the first step in studying ODEs is to verify that there is a unique solution. The following theorem can be used to establish existence and uniqueness. Proofs of this and many other similar theorems can be found in any standard text on Ordinary Differential Equations. The following is from [8].

Theorem 5.1. *Let* $\mathbf{f}$ *be a vector function (with* n *components) defined in a region* D *of* $(n+1)$*-dimensional Euclidean space. Let the vectors* $\mathbf{f}$, $\partial\mathbf{f}/\partial y_k$ $(k = 1, ..., n)$ *be continuous in* D*. Then given any point* (t_0, ξ) *in* D *there exists a unique solution* ϕ *of the system*

$$\mathbf{y}' = \mathbf{f}(t, \mathbf{y})$$

satisfying the initial condition $\phi(t_0) = \xi$*. The solution* ϕ *exists on any interval* I *containing* t_0 *for which the points* $(t, \phi(t))$*, with* t *in* I*, lie in* D*. Furthermore, the solution* ϕ *is a continuous function of the "triple"* (t, t_0, ξ)*.*

The *biological region* mentioned in this chapter refers to the space where the concentrations of all species are nonnegative and cells are present with total density at or below the carrying capacity,

$$\Omega_+ = \{v \in R^{11} : [Z] \geq 0 \text{ and } N^p + N^d \in (0, N_{max}]\}$$

for

$$Z \in \{A_i, R_{il}, A_a, R^p_{il}, A_s, R^p_{gp130}, \{A_s : R^p_{gp130}\}, \{A_a : R^p_{gp130}\}, J, N^p, N^d\}.$$

Theorem 5.1 can be used to establish the existence and uniqueness of a solution of system (3.1) on p.18. It also says that the solution can be extended for all time $t > 0$ provided the concentrations of the species remain nonnegative and bounded above by some constant M.

Theorem 5.2: *A unique solution to system (3.1) with initial conditions in the biological region exists and can be extended from time $t = 0$ to any positive time $t > 0$.*

Proof. $\mathbf{f}$ is clearly continuous in Ω_+, as each component of the vector is comprised of sums of continuous functions. Define $g([J], N^p, N^d) = \dfrac{\kappa_1[J]^2}{\kappa_2^2 + [J]^2} N^p + \theta_1 \left(\theta_2 + (\frac{N^p}{N^p + N^d})^2 \right)^{-1} N^p$. The partial derivatives of g are given by

$$\begin{aligned}
\frac{\partial g}{\partial [J]} &= \frac{2\kappa_1 \kappa_2^2 [J]}{(\kappa_2^2 + [J]^2)^2} N^p \\
\frac{\partial g}{\partial N^p} &= \frac{\kappa_1 [J]^2}{\kappa_2^2 + [J]^2} + \frac{\theta_2 \left[\theta_2 (N^p + N^d)^2 + (N^p)^2 - 2N^d (\frac{(N^p)^2}{N^p + N^d}) \right]}{\left[(N^p + N^d)(\theta_2 + (\frac{N^p}{N^p + N^d})^2) \right]^2} \\
\frac{\partial g}{\partial N^d} &= \frac{2\theta_1 (N^p)^3}{(N^p + N^d) \left[\theta_2 (N^p + N^d) + (N^p)^2 \right]^2}.
\end{aligned}$$

These functions are all continuous in Ω_+. All other terms in $\mathbf{f}$ are polynomials and as such are infinitely continuously differentiable. Hence $\partial \mathbf{f} / \partial y_k$ $(k = 1, ..., n)$ are all continuous in Ω_+, and therefore a unique solution exists for all sets of initial conditions in Ω_+.

All species are bounded below by 0, since $\dfrac{d[Z]}{dt}(\eta') \geq 0$ for each species Z, where the component for $[Z]$ in $\eta' \in \Omega_+$ is zero. It remains to be shown that the concentrations of all species are bounded above by some constant M for all time $t > 0$. This can be accomplished by looking at relationships among the species and employing Gronwall's inequality. Let $\mu =$

$\min\{\mu_{ai}, \mu_{il}, \mu_{aa}, \mu_{gp}, \mu_{ao}\}$.

$$\frac{dN^p}{dt} + \frac{dN^d}{dt} = M_1 N^p \left(1 - \frac{N^p + N^d}{N_{max}}\right) \quad \begin{cases} = 0, & \text{if} \quad N^p + N^d = N_{max} \\ \geq 0, & \text{if} \quad 0 < N^p + N^d < N_{max} \end{cases}$$

$$\implies \text{Whenever the initial vector } \xi \in \Omega_+, \text{ then for all } t > 0,\ N^p, N^d \leq N_{max} = B_1.$$

$$\frac{d[R^p_{il}]}{dt} + \frac{d[A_s]}{dt} + \frac{d[\{A_s : R^p_{gp130}\}]}{dt} = 0$$

$$\implies [R^p_{il}] + [A_s] + [\{A_s : R^p_{gp130}\}] = [R^p_{il}]_0 + [A_s]_0 + [\{A_s : R^p_{gp130}\}]_0$$

$$\implies \max\left\{[R^p_{il}], [A_s], [\{A_s : R^p_{gp130}\}]\right\} \leq [R^p_{il}]_0 + [A_s]_0 + [\{A_s : R^p_{gp130}\}]_0 = B_2$$

$$\frac{d[R^p_{gp130}]}{dt} + \frac{d[\{A_s : R^p_{gp130}\}]}{dt} + \frac{d[\{A_a : R^p_{gp130}\}]}{dt} = 0$$

$$\implies [R^p_{gp130}] + [\{A_s : R^p_{gp130}\}] + [\{A_a : R^p_{gp130}\}]$$

$$= [R^p_{gp130}]_0 + [\{A_s : R^p_{gp130}\}]_0 + [\{A_a : R^p_{gp130}\}]_0$$

$$\implies \max\left\{[R^p_{gp130}], [\{A_a : R^p_{gp130}\}]\right\}$$

$$\leq [R^p_{gp130}]_0 + [\{A_s : R^p_{gp130}\}]_0 + [\{A_a : R^p_{gp130}\}]_0 = B_3$$

$$\frac{d[J]}{dt} = \widehat{l_2}[\{A_s : R^p_{gp130}\}] + \nu_2[\{A_a : R^p_{gp130}\}] - \mu_j[J] - M_1[J]\left(1 - \frac{N^p + N^d}{N_{max}}\right)$$

$$\leq \widehat{l_2} B_2 + \nu_2 B_3 - \mu_j[J]$$

$$\implies [J] \leq \left([J]_0 - \frac{\widehat{l_2} B_2 + \nu_2 B_3}{\mu_j}\right) e^{-\mu_j t} + \frac{\widehat{l_2} B_2 + \nu_2 B_3}{\mu_j}$$

$$\implies [J] \leq \max\left\{([J]_0, \frac{\widehat{l_2} B_2 + \nu_2 B_3}{\mu_j})\right\} = B_4$$

$$\begin{aligned}
\frac{d[G_p]}{dt} + \frac{d[A_o]}{dt} &= s_a N_a - \mu_{gp}[G_p] - \mu_{ao}[A_o] \\
&\leq s_a N_a - \mu([G_p] + [A_o]) \\
&\Longrightarrow [G_p] + [A_o] \leq \left([G_p]_0 + [A_o]_0 - \frac{s_a N_a}{\mu}\right) e^{-\mu t} + \frac{s_a N_a}{\mu} \\
&\Longrightarrow \max\{[G_p], [A_o]\} \leq \max\left\{[G_p]_0 + [A_o]_0, \frac{s_a N_a}{\mu}\right\} = B_5
\end{aligned}$$

$$\begin{aligned}
\frac{d[A_i]}{dt} + \frac{d[A_a]}{dt} &= a_1 N_a - \widehat{k_1}[A_i][R^p_{il}]N^p + \widehat{k_{-1}}[A_s]N^p - k_1[A_a][G_p] + k_{-1}[A_o] \\
&\qquad - \nu_1[A_a][R^p_{gp130}]N^p + \nu_{-1}[\{A_a : R^p_{gp130}\}]N^p - \mu_{ai}[A_i] - \mu_{aa}[A_a] \\
&\leq a_1 N_a + \widehat{k_{-1}} B_2 B_1 + k_{-1} B_5 + \nu_{-1} B_3 B_1 - \mu([A_i] + [A_a]) \\
&\Longrightarrow [A_i] + [A_a] \leq \left([A_i]_0 + [A_a]_0 - \frac{(a_1 N_a + \widehat{k_{-1}} B_2 B_1 + k_{-1} B_5 + \nu_{-1} B_3 B_1)}{\mu}\right) e^{-\mu t} \\
&\qquad + \frac{(a_1 N_a + \widehat{k_{-1}} B_2 B_1 + k_{-1} B_5 + \nu_{-1} B_3 B_1)}{\mu} \\
&\Longrightarrow \max\{[A_i], [A_a]\} \leq \\
&\qquad \max\left\{[A_i]_0 + [A_a]_0, \frac{(a_1 N_a + \widehat{k_{-1}} B_2 B_1 + k_{-1} B_5 + \nu_{-1} B_3 B_1)}{\mu}\right\} = B_6
\end{aligned}$$

$$\begin{aligned}
\frac{d[R_{il}]}{dt} + \frac{d[A_a]}{dt} &= b_a N_a - k_1[A_a][G_p] + k_{-1}[A_o] - \nu_1[A_a][R^p_{gp130}]N^p \\
&\qquad + \nu_{-1}[\{A_a : R^p_{gp130}\}]N^p - \mu_{il}[R_{il}] - \mu_{aa}[A_a] \\
&\leq b_a N_a + k_{-1} B_5 + \nu_{-1} B_3 B_1 - \mu([R_{il}] + [A_a]) \\
&\Longrightarrow [R_{il}] + [A_a] \leq \left([R_{il}]_0 + [A_a]_0 - \frac{(b_a N_a + k_{-1} B_5 + \nu_{-1} B_3 B_1)}{\mu}\right) e^{-\mu t} \\
&\qquad + \frac{(b_a N_a + k_{-1} B_5 + \nu_{-1} B_3 B_1)}{\mu} \\
&\Longrightarrow [R_{il}] \leq \max\left\{[R_{il}]_0 + [A_a]_0, \frac{(b_a N_a + k_{-1} B_5 + \nu_{-1} B_3 B_1)}{\mu}\right\} = B_7
\end{aligned}$$

Letting $B = \max\{B_1, ..., B_7\}$, we see that for all species Z, $0 \leq [Z] \leq B$. These bounds were found independent of t, hence the solution curves can be extended for all $t > 0$.

□

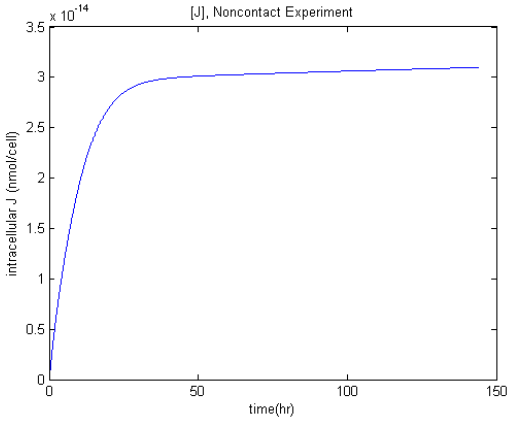

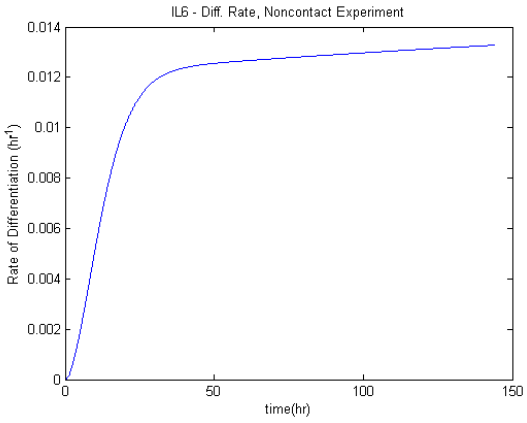

Figure 5.1 *Time course of $[J]$ (left) over a six day period for the noncontact experiment. Parameters are given in Tables 3.4-5.*

Figure 5.2 *Corresponding time course of $\frac{\kappa_1[J]^2}{\kappa_2^2+[J]^2}$ (right). Note that both $[J]$ and $\frac{\kappa_1[J]^2}{\kappa_2^2+[J]^2}$ are increasing very slowly after about 24 hours.*

5.1 Analysis of a Simplified System

Consider the cellular equations in the ODE system:

$$\frac{dN^p}{dt} = -\frac{\kappa_1[J]^2}{\kappa_2^2+[J]^2}N^p + M_1\left(1-\frac{N^p+N^d}{N_{max}}\right),$$
$$\frac{dN^d}{dt} = \frac{\kappa_1[J]^2}{\kappa_2^2+[J]^2}N^p,$$
$$N^p(0) = N_0^p, \qquad N^d(0) = 0.$$

Although $[J]$ depends on the other molecular species in the system, it is possible for it's concentration to become approximately constant after a short period of time. Figure 5.1 shows the time course of $[J]$ for the noncontact coculture experiment based on the parameters in Tables 3.4-5, and Figure 5.2 shows the corresponding time-course of $\frac{\kappa_1[J]^2}{\kappa_2^2+[J]^2}$. Provided

$[J]$ is approximately constant, the above system can be written as

$$\begin{aligned}\frac{dx}{dt} &= \beta x\big(1-(x+y)\big)-\gamma x\\ \frac{dy}{dt} &= \gamma x\\ x(0) = x_0, &\qquad y(0)=0\end{aligned}$$

where $x=\dfrac{N^p}{N_{max}}$, $y=\dfrac{N^d}{N_{max}}$, $\gamma=\dfrac{\kappa_1[J]^2}{\kappa_2^2+[J]^2}$, and $\beta=\dfrac{M_1}{N_{max}}$. It is possible to find a solution for this system in the form of a formal power series. However, the phase plane will be analyzed first.

Because x is a scaled population density, it can be assumed that $x_0 \geq 0$. However, since $(x,y)=(0,y)$ is a steady state solution for this system for all y, we consider the case where $x_0>0$. First note that positivity holds for both $x(t)$ and $y(t)$ for all t. To see this, note that if $x(t_0)=0$ for some $t_0>0$, then $x(t)=0$ for all $t>t_0$. Therefore, if $x_0>0$ then $x(t)\geq 0$ for all t. As for y, we have that $y(t)$ is strictly increasing for $x(t)>0$, and constant for $x(t)=0$. Since $x(t)\geq 0$, $y(t)$ is necessarily nonnegative, and in fact is a strictly monotone increasing function of t for all $t\leq t_0$. Denote the solutions by $x=\phi(t)$, $y=\psi(t)$, with $\phi(0)=x_0$ and $\psi(0)=0$. Since $\psi(t)$ is strictly increasing, ψ can be inverted, so $t=\psi^{-1}(y)$. It follows that $x=\phi(\psi^{-1}(y))$. Applying the chain rule,

$$\frac{dx}{dy}=\frac{dx}{dt}\frac{dt}{dy}=\frac{dx}{dt}\frac{1}{dy/dt}$$

since differentiating $y=\psi(t)$ with respect to y yields $1=\psi'(t)\dfrac{dt}{dy}=\dfrac{dy}{dt}\dfrac{dt}{dy}$. Letting $\mu=\frac{\beta}{\gamma}$, and denoting $\widehat{x}(y)=\phi(\psi(y))$,

$$\begin{aligned}\frac{d\widehat{x}}{dy} &= \frac{\beta\widehat{x}\big(1-(\widehat{x}+y)\big)-\gamma\widehat{x}}{\gamma\widehat{x}}\\ &= \mu\big(1-(\widehat{x}+y)\big)-1\\ &= -\mu(\widehat{x}+y)+(\mu-1)\\ \frac{d\widehat{x}}{dy}+\mu\widehat{x} &= -\mu y+(\mu-1)\\ [e^{\mu y}\widehat{x}]' &= [-\mu y+(\mu-1)]e^{\mu y}\end{aligned}$$

$$e^{\mu y}\widehat{x} = \widehat{x}(0) + \int_0^y (-\mu s e^{\mu s} + (\mu - 1)e^{\mu s})ds$$
$$\widehat{x}(y) = e^{-\mu y}\widehat{x}(0) + e^{-\mu y}\int_0^y (-\mu s e^{\mu s} + (\mu - 1)e^{\mu s})ds$$

which upon integrating yields

$$\widehat{x}(y) = e^{-\mu y}\big(\widehat{x}(0) - 1\big) + (1 - y)$$

where $\widehat{x}(0)$ denotes the value of x when $y = 0$. Since y is strictly increasing when $x \neq 0$, and $x_0 > 0$, we have that the only time t when $y(t) = 0$ is when $t = 0$. Hence $\widehat{x}(0) = x(0) = x_0$, and so

$$\widehat{x}(y) = e^{-\mu y}\big(x_0 - 1\big) + (1 - y).$$

This is the equation that describes the curves in the phase plane. However, more information can be found by analyzing the ODEs. The nullcline satisfying $\dfrac{dy}{dt} = 0$ is the line $x = 0$, and the nullclines satisfying $\dfrac{dx}{dt} = 0$ are the lines $x = 0$ and $x = -y + (1 - \frac{1}{\mu})$. Hence there exists a line of nonisolated critical points

$$(0, y^*) = \{(x, y) \in R_+^2 : x = 0\}$$

where $R_+^2 = \{(x, y) \in R^2 : x \geq 0, y \geq 0\}$. To determine the stability properties of these critical points, consider the Jacobian of $f(x, y)$, where $f(x, y) = \begin{pmatrix} \beta x(1 - (x + y)) - \gamma x \\ \gamma x \end{pmatrix}$. The Jacobian is given by $J(x, y) = \begin{pmatrix} \beta(1 - 2x - y) - \gamma & -\beta x \\ \gamma & 0 \end{pmatrix}$. The eigenvalues of $J(0, y^*)$ are

$$\lambda_1 = 0,$$
$$\lambda_2 = \beta\bigg((1 - \frac{1}{\mu}) - y^*\bigg).$$

First note that both eigenvalues are real numbers. λ_1 corresponds to the neutrally stable direction along the line of critical points. Hence any of these critical points can be stable, but not asymptotically stable. If $y^* < 1 - \frac{1}{\mu}$, then $\lambda_2 > 0$, therefore the critical point $(0, y^*)$ is unstable. If $y^* > 1 - \frac{1}{\mu}$, then $\lambda_2 < 0$, therefore the critical point is stable.

Two different phase planes are possible, depending on the relation between β and γ. If $\beta < \gamma$, then the nullcline $x = -y + (1 - \frac{1}{\mu})$ does not intersect R^2_+. In this case, all critical points (x, y) on the line $x = 0$ with $y > 0$ are stable. The phase plane for this case is illustrated in Figure 5.3. Moreover, the largest population of AHPCs present at any time would correspond to x_0, since in this case $\dfrac{dx}{dt} \leq 0$ for all $(x, y) \in R^2_+$. This is the case where the differentiation constant is larger than the proliferation constant.

If $\gamma < \beta$, then the nullcline $x = -y + (1 - \frac{1}{\mu})$ intersects R^2_+. In this case, if $y^* < 1 - \frac{1}{\mu}$ then $(0, y^*)$ is unstable, but if $y^* > 1 - \frac{1}{\mu}$ then $(0, y^*)$ is stable. The phase plane for this case is illustrated in Figure 5.4. If $x_0 < 1 - \frac{1}{\mu}$ the AHPC density will increase for a short time before it starts to decrease, eventually resulting in all cells differentiating into neurons, since $\dfrac{dx}{dt} > 0$ for (x, y) satisfying $x < -y + (1 - \frac{1}{\mu})$. However, since $\dfrac{dx}{dt} < 0$ for (x, y) satisfying $x > -y + (1 - \frac{1}{\mu})$, it can be seen that the largest population of AHPCs possible corresponds to $\max\{x_0, (1 - \frac{1}{\mu}) - \frac{1}{\mu}\ln(\mu(1 - x_0))\}$. Moreover, due to the stability properties of $(0, y^*)$, at least $(1 - \frac{1}{\mu})N_{max}$ neurons will be produced, regardless of the initial AHPC population. This is the case where the proliferation constant is greater than the differentiation constant.

The final density (of differentiated cells) y_s can be determined by using the equation $\widehat{x}(y)$. When reaching the steady state, $x = 0$, the corresponding y_s is the solution of the equation $e^{-\mu y_s}(x_0 - 1) - y_s + 1 = 0$. Note that, as should be expected, $0 < y_s \leq 1$, since $\widehat{x}(0) > 0$ and $\widehat{x}(1) \leq 0$, with equality holding only in the case $x_0 = 1$.

The equation relating the initial condition to a steady state along the line $(0, y^*)$ also shows that there is a one-to-one correspondence between x_0 and y_s. To see this, the equation $e^{-\mu y_s}(x_0 - 1) - y_s + 1 = 0$ must be differentiated implicitly. Note that

$$\begin{aligned}
\frac{dy_s}{dx_0} &= \frac{e^{-\mu y_s}}{\mu e^{-\mu y_s}(x_0 - 1) + 1} \\
&= \frac{e^{-\mu y_s}}{\mu y_s + (1 - \mu)} \qquad \text{since } \mu e^{-\mu y_s}(x_0 - 1) = \mu(y_s - 1) \\
&= \frac{\frac{1}{\mu} e^{-\mu y_s}}{y_s - (1 - \frac{1}{\mu})} > 0
\end{aligned}$$

for all stable steady states, i.e. $y_s > 1 - \frac{1}{\mu}$. Hence, if $x_1 < x_2$, then $y_s(x_1) < y_s(x_2)$; every initial condition results in a unique final density of neurons.

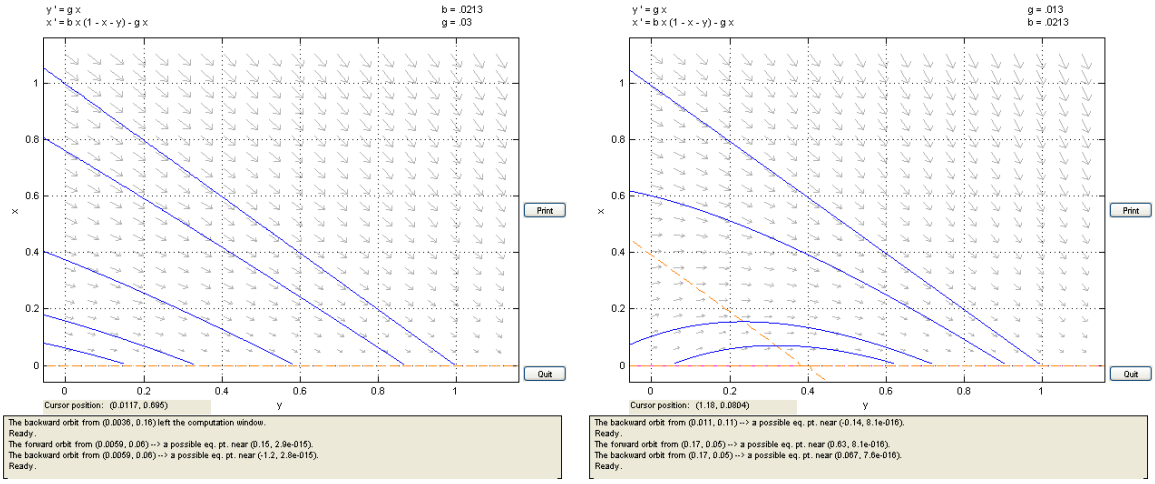

Figure 5.3 *(left) Representative phase plane for the case $\gamma > \beta$, using $\gamma = .03$ and $\beta = .0213$. The only nullcline in R^2_+ corresponds to the line of nonisolated critical points, $x = 0$. All solution curves exhibit x strictly decreasing and y strictly increasing. Any number of neurons can be produced, up to the carrying capacity, depending on the relation between β and γ.*

Figure 5.4 *(right) Representative phase plane for the case $\gamma < \beta$, using $\gamma = .013$ and $\beta = .0213$. Nullclines in R^2_+ are $x = 0$ and $x = -y + (1 - \frac{1}{\mu})$. A line of nonisolated steady states exists, $x = 0$. $(0, y^*)$ is unstable for $y^* < 1 - \frac{1}{\mu}$ and stable for $y^* > 1 - \frac{1}{\mu}$. Hence at least $(1 - \frac{1}{\mu})N_{max}$ neurons will be produced.*

5.2 Steady-State Solutions of the Full System

The above analysis gives a general idea of the behavior of the system. However, some questions still remain. What are the steady state concentrations of the cytokines and surface receptors? How does the behavior of the system depend on astrocyte density? How will the steady state concentrations of the other species depend on $(N^d)^*$, if at all?

The sensitivity analysis presented in Chapter 4 showed that the species G_p and A_o do not have any appreciable affect on the percentage of cells differentiated after six days. The biological system under observation could instead reasonably be modelled by a system of ODEs that do not take these two proteins into consideration. Eliminating these proteins from the ODE system is acceptable from a biological standpoint, considering the ODE system is itself just a simplified representation of the biology. Astrocytes likely secrete many other proteins, but the ODE system only considered IL6, sIL6Rα, and sgp130.

Of interest here are the steady state solutions related to IL6-induced differentiation. The background mechanism is unknown, and was simulated with a function of N^p and N^d. The function

$$K_1(N^p, N^d) = \theta_1\Big(\theta_2 + (\frac{N^d}{N^p + N^d})^2\Big)^{-1}$$

was chosen as the rate of background differentiation to model a small amount of differentiation due to another mechanism, not to infer that this is the rate that is occuring in nature. It is only meant to apply for short periods of time. As $t \to \infty$, this modeling function will cause all cells to differentiate, masking the effects due to IL6. We are only concerned with the IL6 mechanism here, so we remove $K_1(N^p, N^d)$ and instead consider steady state solutions for the system

$$\begin{aligned}
\frac{d[A_i]}{dt} &= a_1 N_a - l_1[A_i][R_{il}] + l_{-1}[A_a] - \widehat{k}_1[A_i][R^p_{il}]N^p + \widehat{k}_{-1}[A_s]N^p - \mu_{ai}[A_i], \\
\frac{d[R_{il}]}{dt} &= b_a N_a - l_1[A_i][R_{il}] + l_{-1}[A_a] - \mu_{il}[R_{il}], \\
\frac{d[A_a]}{dt} &= l_1[A_i][R_{il}] - (l_{-1} + \mu_{aa})[A_a] - \nu_1[A_a][R^p_{gp130}]N^p + \nu_{-1}[\{A_a : R^p_{gp130}\}]N^p,
\end{aligned}$$

$$
\begin{aligned}
\frac{d[R^p_{il}]}{dt} &= -\widehat{k}_1[A_i][R^p_{il}] + \widehat{k}_{-1}[A_s] + \widehat{l}_2[\{A_s : R^p_{gp130}\}] + \eta([R^p_{il}]_{tot} - [R^p_{il}]),\\
\frac{d[A_s]}{dt} &= \widehat{k}_1[A_i][R^p_{il}] - \widehat{k}_{-1}[A_s] - \widehat{l}_1[A_s][R^p_{gp130}] + \widehat{l}_{-1}[\{A_s : R^p_{gp130}\}] - \eta[A_s],\\
\frac{d[R^p_{gp130}]}{dt} &= -\widehat{l}_1[A_s][R^p_{gp130}] + (\widehat{l}_{-1} + \widehat{l}_2)[\{A_s : R^p_{gp130}\}] - \nu_1[A_a][R^p_{gp130}]\\
&\quad + (\nu_{-1} + \nu_2)[\{A_a : R^p_{gp130}\}] + \eta([R^p_{gp130}]_{tot} - [R^p_{gp130}]),\\
\frac{d[\{A_s : R^p_{gp130}\}]}{dt} &= \widehat{l}_1[A_s][R^p_{gp130}] - (\widehat{l}_{-1} + \widehat{l}_2)[\{A_s : R^p_{gp130}\}] - \eta[\{A_s : R^p_{gp130}\}],\\
\frac{d[\{A_a : R^p_{gp130}\}]}{dt} &= \nu_1[A_a][R^p_{gp130}] - (\nu_{-1} + \nu_2)[\{A_a : R^p_{gp130}\}] - \eta[\{A_a : R^p_{gp130}\}],\\
\frac{d[J]}{dt} &= \widehat{l}_2[\{A_s : R^p_{gp130}\}] + \nu_2[\{A_a : R^p_{gp130}\}] - \mu_j[J] - \eta[J],\\
\frac{dN^p}{dt} &= -\frac{\kappa_1[J]^2}{\kappa_2^2 + [J]^2}N^p + \eta N^p,\\
\frac{dN^d}{dt} &= \frac{\kappa_1[J]^2}{\kappa_2^2 + [J]^2}N^p
\end{aligned}
$$

where $[R^p_{il}]_{tot} = [R^p_{il}]_0 + [A_s]_0 + [\{A_s : R^p_{gp130}\}]_0$, $[R^p_{gp130}]_{tot} = [R^p_{gp130}]_0 + [\{A_a : R^p_{gp130}\}]_0 + [\{A_s : R^p_{gp130}\}]_0$, and $\eta = M_1\left(1 - \frac{N^p + N^d}{N_{max}}\right)$. The steady states depend on whether or not astrocytes are present. If the fixed value $N_a > 0$, there is one curve of steady states in the biological region Ω_+, parameterized by $(N^d)^*$. It is given by

$$S_1 = (A_i^*, R_{il}^*, A_a^*, R_{il}^{p\,*}, A_s^*, R_{gp130}^{p\ \ *}, \{A_s : R^p_{gp130}\}^*, \{A_a : R^p_{gp130}\}^*, J^*, (N^p)^*, (N^d)^*),$$

where

$$
\begin{aligned}
A_i^* &= \frac{a_1 N_a - \mu_{aa} x}{\mu_{ai}},\\
R_{il}^* &= \frac{b_a N_a - \mu_{aa} x}{\mu_{il}},\\
A_a^* &= x,\\
R_{il}^{p\,*} &= [R^p_{il}]_{tot} - A_s^* - \{A_s : R^p_{gp130}\}^*,\\
A_s^* &= \frac{(-b + \sqrt{b^2 - 4c})}{2},\\
R_{gp130}^{p\ \ *} &= [R^p_{gp130}]_{tot} - \{A_a : R^p_{gp130}\}^* - \{A_s : R^p_{gp130}\}^*,\\
\{A_s : R^p_{gp130}\}^* &= \frac{A_i^*[R^p_{il}]_{tot} - (\widehat{K} + A_i^*)A_s^*}{L + A_i^*},
\end{aligned}
$$

$$\{A_a : R^p_{gp130}\}^* = \frac{L[R^p_{gp130}]_{tot} + A_i^*([R^p_{gp130}]_{tot} - [R^p_{Il}]_{tot}) + (\widehat{K} + A_i^*)A_s^*}{(L + A_i^*)(V + A_a^*)} A_a^*,$$

$$J^* = \frac{\widehat{l_2}\{A_s : R^p_{gp130}\}^* + \nu_2\{A_a : R^p_{gp130}\}^*}{\mu_j + \eta},$$

$$(N^p)^* = 0,$$

$$(N^d)^* \text{arbitrary},$$

with the following quantities abbreviated:

$$x = \frac{\widetilde{L}\frac{\mu_{ai}\mu_{il}}{\mu_{aa}} + (a_1 + b_a)N_a - \sqrt{\left[\widetilde{L}\frac{\mu_{ai}\mu_{il}}{\mu_{aa}}\right]^2 + \left[(a_1 - b_a)N_a\right]^2 + 2(a_1 + b_a)N_a\widetilde{L}\frac{\mu_{ai}\mu_{il}}{\mu_{aa}}}}{2\mu_{aa}},$$

$$b = \frac{L[R^p_{gp130}]_{tot} + ([R^p_{gp130}]_{tot} - [R^p_{il}]_{tot})A_i^*}{\widehat{K} + A_i^*} + \frac{\widehat{L}(V + A_a^*)}{V},$$

$$c = \frac{-\widehat{L}(V + A_a^*)A_i^*[R^p_{il}]_{tot}}{V(\widehat{K} + A_i^*)}, \qquad \eta = M_1(1 - \frac{(N^d)^*}{N_{max}}), \qquad \widetilde{L} = \frac{l_{-1} + \mu_{aa}}{l_1},$$

$$\widehat{K} = \widehat{K_d} + \frac{\eta}{\widehat{k_1}}, \qquad L = \frac{\widehat{l_2} + \eta}{\widehat{k_1}}, \qquad \widehat{L} = \widehat{L_m} + \frac{\eta}{\widehat{l_1}}, \qquad V = V_m + \frac{\eta}{\nu_1}.$$

A second curve of steady states (S_2) exists where the square root is added instead of subtracted within the equation for x, but the other species satisfy the same relationships as in S_1. However, S_2 is not in the biological region Ω_+. To see this, suppose $a_1 \geq b_a$. Then $A_i^* < 0$, since then

$$a_1N_a - \mu_{aa}x < a_1N_a - \frac{(a_1 + b_a)N_a}{2} - \frac{(a_1 - b_a)N_a}{2} = 0.$$

Similarly, assuming $a_1 < b_a$ results in $R_{il}^* < 0$.

There are two more curves of steady states (S_3, S_4), that correspond to (S_1, S_2), which are not in Ω_+. These are formed by setting $A_s^* = \frac{-b - \sqrt{b^2 - c}}{2}$ with all other terms unchanged from S_1 and S_2. A_s^* is found by considering the roots of $(A_s^*)^2 + b(A_s^*) + c = 0$. Since $c < 0$, the roots $(A_s^*)_+$ and $(A_s^*)_-$ satisfy $(A_s^*)_+(A_s^*)_- < 0$, so that only one root is positive. Since $(A_s^*)_+$ is the component in (S_1, S_2), $S_3 \notin \Omega_+$ and $S_4 \notin \Omega_+$.

When $N_a = 0$, there are two curves of steady states, parameterized by $(N^d)^*$, existing within the biological region:

$$T_1 = (0, 0, 0, [R^p_{il}]_0, 0, [R^p_{gp130}]_0, 0, 0, 0, 0, (N^d)^*),$$

$$T_2 = (0, 0, 0, [R^p_{il}]_0, 0, [R^p_{gp130}]_0, 0, 0, 0, N_{max} - (N^d)^*, (N^d)^*),$$

again with $(N^d)^*$ arbitrary. Two more curves of steady states exist outside of this region,

$$T_{3,4} = \Big(\frac{\mu_{il}}{\mu_{ai}}z, z, -\frac{\mu_{il}}{\mu_{aa}}z, R_{il}^{p\,*}, A_s^*, {R_{gp130}^p}^*, \{A_s : R_{gp130}^p\}^*, \{A_a : R_{gp130}^p\}^*, J^*, 0, (N^d)^*\Big),$$

with $(N^d)^*$ again arbitrary, $z = -\dfrac{\mu_{ai}}{\mu_{aa}}\widetilde{L}$, $A_s^* = (A_s^*)_+$ for T_3, $A_s^* = (A_s^*)_-$ for T_4, and the other species given by the corresponding equations in S_1. T_3 and T_4 are clearly not in Ω_+ since $R_{il}^* = z < 0$. Finally note that the steady states S_2, S_3, S_4, T_3, and T_4 could have non-real components since $A_i^* < 0$ or $A_a^* < 0$ may cause $b^2 - 4c < 0$.

The critical points S_1, T_1, T_2 are what one would expect from the biology. If astrocytes are present, they will be producing cytokines that lead to the production of J. Hence the only way differentiation will stop is if there are no AHPCs left to differentiate (S_1). If astrocytes are not present, then no differentiation will occur (via the IL6 pathway). So if there are no progenitor cells, nothing happens (T_1). If progenitor cells are present, they will proliferate until the total cell density reaches the carrying capacity (T_2). In both cases T_1 and T_2, $(N^d)^* = N^d(0)$ provided that $[Z](0) = 0$ for all chemical densities so that no differentiation can occur. Also note that $\lim\limits_{N_a \to 0^+} S_1 = T_1$ and $\lim\limits_{N_a \to 0^+} S_2 = T_3$.

5.3 Stability of the Biologically Relevant Steady-State Solutions of the Full System

To determine the stability of the critical points in Ω_+, we first consider the Jacobian, $J(\vec{x})$, of $f(\vec{x})$, where $\dfrac{d\vec{x}}{dt} = f(\vec{x})$ is the above system of differential equations. Defining $\eta = M_1(1 - \frac{(N^p)^* + (N^d)^*}{N_{max}})$, we can write $J(\vec{x}) = \begin{pmatrix} J_1 & J_2 & J_3 \\ J_4 & J_5 & J_6 \end{pmatrix}$ where the blocks J_1, J_2, J_3, J_4, J_5, and J_6 are given by:

$$J_1(\vec{x}) = \begin{pmatrix} -(l_1 R_{il}^* + \widehat{k_1} R_{il}^{p*} N^{p*} + \mu_{ai}) & -l_1 A_i^* & l_{-1} & -\widehat{k_1} A_i^* N^{p*} \\ -l_1 R_{il}^* & -(l_1 A_i^* + \mu_{il}) & l_{-1} & 0 \\ l_1 R_{il}^* & l_1 A_i^* & -(l_{-1} + \nu_1 R_{gp130}^{p*} N^{p*} + \mu_{aa}) & 0 \\ -\widehat{k_1} R_{il}^{p*} & 0 & 0 & -(\widehat{k_1} A_i^* + \eta) \\ \widehat{k_1} R_{il}^{p*} & 0 & 0 & \widehat{k_1} A_i^* \end{pmatrix}$$

$$J_2(\vec{x}) = \begin{pmatrix} \widehat{k_{-1}} N^{p*} & 0 & 0 & 0 \\ 0 & 0 & 0 & 0 \\ 0 & 0 & -\nu_1 A_a^* N^{p*} & \nu_{-1} N^{p*} \\ \widehat{k_{-1}} & \widehat{l_2} & 0 & 0 \\ -(\widehat{k_{-1}} + \widehat{l_1} R_{gp130}^{p*} + \eta) & \widehat{l_{-1}} & \widehat{l_1} A_s^* & 0 \end{pmatrix}$$

$$J_3(\vec{x}) = \begin{pmatrix} 0 & -\widehat{k_1} A_i^* R_{il}^{p*} + \widehat{k_{-1}} A_s^* & 0 \\ 0 & 0 & 0 \\ 0 & -\nu_1 A_a^* R_{gp130}^{p*} + \nu_{-1}\{Aa : R_{gp130}^{p}\}^* & 0 \\ 0 & -([R_{il}^{p}]_{tot} - R_{il}^{p*})(\frac{M_1}{N_{max}}) & -([R_{il}^{p}]_{tot} - R_{il}^{p*})(\frac{M_1}{N_{max}}) \\ 0 & A_s^*(\frac{M_1}{N_{max}}) & A_s^*(\frac{M_1}{N_{max}}) \end{pmatrix}$$

$$J_4(\vec{x}) = \begin{pmatrix} 0 & 0 & 0 & 0 \\ 0 & 0 & -\nu_1 R_{gp130}^{p*} & 0 \\ 0 & 0 & \nu_1 R_{gp130}^{p*} & 0 \\ 0 & 0 & 0 & 0 \\ 0 & 0 & 0 & 0 \\ 0 & 0 & 0 & 0 \end{pmatrix}$$

$$J_5(\vec{x}) = \begin{pmatrix} \widehat{l_1} R_{gp130}^{p*} & -(\widehat{l_{-1}} + \widehat{l_2} + \eta) & \widehat{l_1} A_s^* & 0 \\ -\widehat{l_1} R_{gp130}^{p*} & \widehat{l_{-1}} + \widehat{l_2} & -(\widehat{l_1} A_s^* + \nu_1 A_a^* + \eta) & \nu_{-1} + \nu_2 \\ 0 & 0 & \nu_1 A_a^* & -(\nu_{-1} + \nu_2 + \eta) \\ 0 & \widehat{l_2} & 0 & \nu_2 \\ 0 & 0 & 0 & 0 \\ 0 & 0 & 0 & 0 \end{pmatrix}$$

$$J_6(\vec{x}) = \begin{pmatrix} 0 & \{A_s : R_{gp130}^{p}\}^*(\frac{M_1}{N_{max}}) & \{A_s : R_{gp130}^{p}\}^*(\frac{M_1}{N_{max}}) \\ 0 & -([R_{gp130}^{p}]_{tot} - R_{gp130}^{p*})(\frac{M_1}{N_{max}}) & -([R_{gp130}^{p}]_{tot} - R_{gp130}^{p*})(\frac{M_1}{N_{max}}) \\ 0 & \{A_a : R_{gp130}^{p}\}^*(\frac{M_1}{N_{max}}) & \{A_a : R_{gp130}^{p}\}^*(\frac{M_1}{N_{max}}) \\ -(\mu_j + \eta) & J^*(\frac{M_1}{N_{max}}) & J^*(\frac{M_1}{N_{max}}) \\ -\frac{-2\kappa_1\kappa_2^2 J^*}{(\kappa_2^2 + (J^*)^2)^2} N^{p*} & -\big(\frac{\kappa_1 (J^*)^2}{\kappa_2^2 + (J^*)^2} - \eta\big) - N^{p*}(\frac{M_1}{N_{max}}) & -N^{p*}(\frac{M_1}{N_{max}}) \\ \frac{2\kappa_1\kappa_2^2 J^*}{(\kappa_2^2 + (J^*)^2)^2} N^{p*} & \frac{\kappa_1 (J^*)^2}{\kappa_2^2 + (J^*)^2} & 0 \end{pmatrix}$$

To determine the stability properties of the critical points, the Jacobian will be evaluated at each critical point, and the eigenvalues of the resultant matrix will be calculated. For each

steady state, either three or six eigenvalues will be left as the roots of cubic polynomials ($p_i(\xi)$) with real positive coefficients. These roots can be evaluated explicitly using available formulas. However, these expressions will be quite complicated, and of little use, since all that is needed is the sign of the real parts of these eigenvalues. All real roots of these polynomials must be negative, since $p_i(\xi) > 0$ for all $\xi > 0$. However, it is possible for a cubic polynomial to have two complex conjugate roots. Since some eigenvalues will be represented as roots of cubic polynomials, the following theorem is needed.

Theorem 5.5: *Consider the cubic polynomial $p(x) = x^3 + bx^2 + cx + d$. If b, c, d are all positive and two of the zeros of $p(x)$ are complex conjugates, their real components satisfy the conditions:*

(i) *positive if* $bc < d$

(ii) *negative if* $bc > d$

(iii) *zero if* $bc = d$.

Proof. Assume that $p(x)$ has two complex conjugate roots. To locate these roots, consider the modulus of $p(x)$,

$$q(z) = |p(z)|^2 = [\alpha^3 - 3\alpha\beta^2 + b(\alpha^2 - \beta^2) + c\alpha + d]^2 + (3\alpha^2\beta - \beta^3 + 2b\alpha\beta + c\beta)^2,$$

where $z = \alpha + i\beta$ for $\alpha, \beta \in R$. The equation $p(z) = 0$ is equivalent to $q(z) = 0$. To find the solutions of $q(z) = 0$, one must solve the system of equations

$$\alpha^3 - 3\alpha\beta^2 + b(\alpha^2 - \beta^2) + c\alpha + d = 0$$
$$3\alpha^2\beta - \beta^3 + 2b\alpha\beta + c\beta = 0.$$

Since we are concerned with the complex roots of p, we can assume $\beta \neq 0$. Dividing the second equation by β, we have $\beta^2 = 3\alpha^2 + 2b\alpha + c$. Substituting this for β^2 in the first equation, we get

$$\alpha^3 + (\frac{7}{8}b)\alpha^2 + \frac{1}{4}(c + b^2)\alpha + \frac{1}{8}(bc - d) = 0.$$

Hence the real parts of the complex roots of $p(x)$ must be the real roots of

$$\widehat{q}(x) = x^3 + (\frac{7}{8}b)x^2 + \frac{1}{4}(c + b^2)x + \frac{1}{8}(bc - d)$$

that satisfy the condition

$$m = 3x^2 + 2bx + c > 0.$$

Denote one of these roots by α. Note that $\widehat{q}\,'(x) = 3x^2 + \frac{7}{4}bx + \frac{1}{4}(c + b^2) > 0$ for all $x > 0$.

If $bc - d < 0$, then $\widehat{q}(0) < 0$. Since $\lim_{x\to\infty} \widehat{q}(x) = \infty$, there exists an $\alpha > 0$ with $\widehat{q}(\alpha) = 0$. Moreover, the condition $3\alpha^2 + 2b\alpha + c > 0$ is satisfied at this α. Hence the real part of the the complex solutions of $p(x)$ is positive. If $bc = d$, then $\widehat{q}(0) = 0$. At this α, $m = c > 0$, so the real part of the complex solutions of $p(x)$ is zero.

If $bc - d > 0$, then $\widehat{q}(0) > 0$. Since $\widehat{q}\,'(x) > 0$ for all $x > 0$, there can be no $\alpha \geq 0$ such that $\widehat{q}(\alpha) = 0$. Hence in this case the real part of the complex solutions of $p(x)$ must be negative. □

First consider the case where $N_a \neq 0$. The only set of critical points in the biological range is the curve S_1. At S_1, $(N^p)^* = 0$, and as a result, $\eta = M_1(1 - \frac{(N^d)^*}{N_{max}})$. The eigenvalues of $J(S_1)$ are:

$$\begin{aligned}
\lambda_1 &= 0 \\
\lambda_2 &= \eta - \frac{\kappa_1 (J^*)^2}{\kappa_2^2 + (J^*)^2} \\
\lambda_3 &= -(\eta + \mu_j) \\
\lambda_4 &= \lambda_5 = -\eta \\
\lambda_{6-8} &: \text{ Roots of } p_1(\lambda) = \lambda^3 + b_1\lambda^2 + c_1\lambda + d_1 \\
\lambda_{9-11} &: \text{ Roots of } p_2(\lambda) = \lambda^3 + b_2\lambda^2 + c_2\lambda + d_2
\end{aligned}$$

where

$$\begin{aligned}
b_1 &= \mu_{ai} + \mu_{il} + \mu_{aa} + l_{-1} + l_1(A_i^* + R_{il}^*) \\
c_1 &= \mu_{ai}\mu_{il} + (l_{-1} + \mu_{aa})(\mu_{ai} + \mu_{il}) + l_1(A_i^*\mu_{ai} + R_{il}^*\mu_{il} + \mu_{aa}(A_i^* + R_{il}^*)) \\
d_1 &= \mu_{ai}\mu_{il}(\mu_{aa} + l_{-1}) + l_1\mu_{aa}(A_i^*\mu_{ai} + R_{il}^*\mu_{il})
\end{aligned}$$

$$b_2 = (\widehat{k}_1 A_i^* + \widehat{k}_{-1} + \eta) + (\widehat{l}_1(A_s^* + R_{gp130}^{p*}) + \widehat{l}_{-1} + \widehat{l}_2 + \eta + \nu_1 A_a^* + \nu_{-1} + \nu_2 + \eta)$$

$$c_2 = b_2 + (\widehat{l}_1(A_s^* + R_{gp130}^{p*}) + \widehat{l}_{-1} + \widehat{l}_2 + \eta)(\nu_1 A_a^* + \nu_{-1} + \nu_2 + \eta) - \nu_1 \widehat{l}_1 A_a^* A_s^* + \widehat{l}_1 R_{gp130}^{p*}(\widehat{l}_2 - \widehat{k}_{-1})$$

$$d_2 = (\widehat{k}_1 A_i^* + \widehat{k}_{-1}\eta)\Big((\widehat{l}_1(A_s^* + R_{gp130}^{p*}) + \widehat{l}_{-1} + \widehat{l}_2 + \eta)(\nu_1 A_a^* + \nu_{-1} + \nu_2 + \eta) - \nu_1 \widehat{l}_1 A_a^* A_s^*\Big)$$
$$+ \widehat{l}_1 R_{gp130}^{p*}(\widehat{l}_2 - \widehat{k}_{-1})(\nu_1 A_a^* + \nu_{-1} + \nu_2 + \eta).$$

The coefficients b_1, c_1, and d_1 are all clearly positive along S_1. Moreover, $b_1 c_1 > d_1$ since

$$\begin{aligned}
b_1 c_1 = &\Big[\mu_{ai}\mu_{il}(\mu_{aa} + l_{-1}) + l_1\mu_{aa}(A_i^*\mu_{ai} + R_{il}^*\mu_{il})\Big] \\
&+ \mu_{ai}\mu_{il}(\mu_{ai} + \mu_{il} + l_1(A_i^* + R_{il}^*) \\
&+ l_1(A_i^*\mu_{ai} + R_{il}^*\mu_{il})(\mu_{ai} + \mu_{il} + l_{-1} + l_1(A_i^* + R_{il}^*)) \\
&+ \Big((l_{-1} + \mu_{aa})(\mu_{ai} + \mu_{il}) + l_1\mu_{aa}(A_i^* + R_{il}^*)\Big) \cdot \Big(\mu_{ai} + \mu_{il} + \mu_{aa} + l_{-1} + l_1(A_i^* + R_{il}^*)\Big) \\
&> \Big[\mu_{ai}\mu_{il}(\mu_{aa} + l_{-1}) + l_1\mu_{aa}(A_i^*\mu_{ai} + R_{il}^*\mu_{il})\Big] \\
&= d_1.
\end{aligned}$$

Applying Theorem 5.5 to the polynomial p_1 proves that $Re(\lambda_i) < 0$ for $i = 6, 7, 8$.

The coefficient b_2 is clearly positive along S_1. c_2 and d_2 are also positive, since they contain positive terms identical to their negative terms. Moreover, $b_2 c_2 > d_2$ since

$$\begin{aligned}
b_2 c_2 = &(\widehat{k}_1 A_i^* + \widehat{k}_{-1} + \eta)\Big((\widehat{l}_1(A_s^* + R_{gp130}^{p*}) + \widehat{l}_{-1} + \widehat{l}_2 + \eta)(\nu_1 A_a^* + \nu_{-1} + \nu_2 + \eta) - \nu_1 \widehat{l}_1 A_a^* A_s^*\Big) \\
&+ (\widehat{k}_1 A_i^* + \widehat{k}_{-1} + \eta)\Big(\widehat{l}_1 R_{gp130}^{p*}(\widehat{l}_2 - \widehat{k}_{-1}) + (\widehat{k}_1 A_i^* + \widehat{k}_{-1} + \eta)(\widehat{l}_1(A_s^* + R_{gp130}^{p*}) \\
&\qquad + \widehat{l}_{-1} + \widehat{l}_2 + \eta + \nu_1 A_a^* + \nu_{-1} + \nu_2 + \eta)\Big) \\
&+ \widehat{l}_1 R_{gp130}^{p*}(\widehat{l}_2 - \widehat{k}_{-1})(\nu_1 A_a^* + \nu_{-1} + \nu_2 + \eta) \\
&+ \widehat{l}_1 R_{gp130}^{p*}(\widehat{l}_2 - \widehat{k}_{-1})(\widehat{l}_1(A_s^* + R_{gp130}^{p*}) + \widehat{l}_{-1} + \widehat{l}_2 + \eta) \\
&+ \Big(\widehat{l}_1(A_s^* + R_{gp130}^{p*}) + \widehat{l}_{-1} + \widehat{l}_2 + \eta + \nu_1 A_a^* + \nu_{-1} + \nu_2 + \eta\Big) \\
&\qquad \cdot \Big((\widehat{k}_1 A_i^* + \widehat{k}_{-1} + \eta)(\widehat{l}_1(A_s^* + R_{gp130}^{p*}) + \widehat{l}_{-1} + \widehat{l}_2 + \eta + \nu_1 A_a^* + \nu_{-1} + \nu_2 + \eta) \\
&\qquad\quad + (\widehat{l}_1(A_s^* + R_{gp130}^{p*}) + \widehat{l}_{-1} + \widehat{l}_2 + \eta)(\nu_1 A_a^* + \nu_{-1} + \nu_2 + \eta) - \nu_1 \widehat{l}_1 A_a^* A_s^*\Big)
\end{aligned}$$

$$> (\widehat{k}_1 A_i^* + \widehat{k}_{-1} + \eta)\Big((\widehat{l}_1(A_s^* + R_{gp130}^{p*}) + \widehat{l}_{-1} + \widehat{l}_2 + \eta)(\nu_1 A_a^* + \nu_{-1} + \nu_2 + \eta) - \nu_1 \widehat{l}_1 A_a^* A_s^* \Big)$$
$$+ \widehat{l}_1 R_{gp130}^{p*}(\widehat{l}_2 - \widehat{k}_{-1})(\nu_1 A_a^* + \nu_{-1} + \nu_2 + \eta)$$
$$= d_2$$

where the last inequality again holds due to the presence of postive terms identical to the negative terms. Applying Theorem 5.5 to the polynomial p_2 proves that $Re(\lambda_i) < 0$ for $i = 9, 10, 11$.

Note that λ_1 and λ_2 correspond to the eigenvalues of the simplified system discussed earlier. If $\gamma = \dfrac{\kappa_1 (J^*)^2}{\kappa_2^2 + (J^*)^2}$, $\beta = M_1$, and $\mu = \dfrac{\beta}{\gamma}$, then $\lambda_2 = \beta[1 - \frac{(N^d)^*}{N_{max}} - \frac{1}{\mu}]$. If $(N^d)^* < N_{max}(1 - \frac{1}{\mu})$, then $\lambda_2 > 0$, while if $(N^d)^* > N_{max}(1 - \frac{1}{\mu})$, then $\lambda_2 < 0$. It is also assumed that $(N^d)^* \in (0, N_{max}]$ in the biological region, so clearly $\lambda_{3-4} \leq 0$ with $\lambda_{3-4} < 0$ for $(N^d)^* < N_{max}$. All other eigenvalues are either negative real numbers or are complex numbers with negative real components. To determine local stability of the steady state, we make use of the following claim.

Claim 5.6: *Let L be a one-dimensional curve of nonisolated steady states, and let $J(x^*)$ be the Jacobian matrix of the system evaluated at one of these steady states (x^*). If all but one of the eigenvalues of this matrix have negative real components and the remaining eigenvalue is 0, then the steady state x^* is locally stable but not asymptotically stable.*

Remarks on Claim 5.6: The key statement of this claim is that we are considering the local linearlization around a point on a curve of *nonisolated* steady states. If this point were isolated, the claim would clearly be false, (see any text on qualitative theory of differential equations, [8] for example). In the case of a linear system of differential equations, the statement is true. The zero eigenvalue corresponds to the neutrally stable direction along the line of steady states ([45]), with the line corresponding to the eigenvector for $\lambda = 0$. However, I have been unable to find a proof of this statement in the literature in the case of a nonlinear system with nonisolated steady states. The result itself was applied in the analysis provided in [7].

In our case, it should be true for S_1, if not in general. This can be seen by considering the biology. As long as AHPCs are present and astrocytes continue supplying the cells with IL6, the AHPCs will continue to differentiate. The only way that differentiation will cease is if either (1) all cells have differentiated, or (2) there are no more differtiation factors available to the system. Since the astrocytes are secreting factors at a constant rate, the mechanism must continue until all AHPCs have differentiated. The proteins being produced by the astrocytes are not being used; they are just being produced and decaying. It is a "simple" mechanism (as opposed to a chemical oscillator), and as such the concentrations of these proteins should approach equilibrium values.

When an eigenvalue of the linearization of a nonlinear ODE has a zero real component, one often employs center manifold theory to investigate stability. In this case, it would correspond to generating a one-dimensional invariant manifold. Stability of the critical point on the manifold is equivalent to local stability of the critical point. However, calculating a center manifold for this system is a very involved calculation (which is as yet uncompleted), and determining stability on this center manifold may not be possible due to the complexity of the reduced system. See [11], [33], and [43] for discussions of Center Manifold Theory. □

The critical points along the curve S_1 where $(N^d)^* < N_{max}(1-\frac{1}{\mu})$ are clearly unstable due to the positivity of one of the eigenvalues. However, due to $\lambda_1 = 0$ we cannot simply apply the principle of linearized stability when $(N^d)^* > N_{max}(1-\frac{1}{\mu})$. Since we have a curve of nonisolated steady states we instead apply Claim 5.6. The other ten eigenvalues are negative, so the critical points along the curve S_1 where $(N^d)^* > N_{max}(1-\frac{1}{\mu})$ are stable, but not asymptotically stable. Biological reasoning also leads to the conclusion that these steady states should be stable, and was discussed both during the analysis of the steady states for the simplified system provided earlier in this chapter, and in the remarks for Claim 5.6.

Now consider the case where $N_a = 0$. There are two curves of critical points in the biological range: T_1 and T_2. We first look at T_1. Along this curve, $(N^p)^* = 0$ and $\eta = M_1(1 - \frac{(N^d)^*}{N_{max}})$.

The eigenvalues of $J(T_1)$ are:

$$\begin{aligned} \lambda_1 &= 0, & \lambda_5 &= -(l_{-1} + \mu_{aa}) \\ \lambda_2 &= -\mu_{ai}, & \lambda_6 &= -(\nu_{-1} + \nu_2 + \eta) \\ \lambda_3 &= -\mu_{il}, & \lambda_7 &= \lambda_8 = -\eta \\ \lambda_4 &= -(\mu_j + \eta), & \lambda_9 &= \eta \end{aligned}$$

$$\lambda_{10-11} = \frac{1}{2}\left(-[\gamma + \widehat{l}_2 + \widehat{l}_{-1} + \eta] \pm \sqrt{(\gamma + \widehat{l}_2 + \widehat{l}_{-1} + \eta)^2 - 4(\widehat{l}_{-1}(\eta + \widehat{k}_{-1}) + \gamma(\widehat{l}_2 + \eta))} \right)$$

where

$$\gamma = \widehat{k}_{-1} + \widehat{l}_1 [R^p_{gp130}]_{tot} + \eta.$$

All points along T_1 are unstable due to the presence of the positive eigenvalue λ_9. This is a logical result when considered from a biological standpoint. In the absence of astrocytes, this critical point is only attainable if there are no AHPCs present initially. If any AHPCs are introduced, they will then proliferate until the total cell population reaches the carrying capacity. No astrocytes are present to produce the proteins needed for these AHPCs to differentiate. If some proteins are introduced to the system at time $t = 0$ some differentiation will occur provided $N^p(0) > 0$, but the proteins decay, and the remaining cells will be still be capable of proliferation. This reasoning also hints to points along the curve T_2 being stable.

We now consider T_2. Along this curve, $(N^p)^* = N_{max} - (N^d)^*$ and $\eta = 0$. The eigenvalues of $J(T_2)$ are:

$$\lambda_1 = \lambda_2 = \lambda_3 = 0, \quad \lambda_4 = -\mu_{il}, \quad \lambda_5 = -\mu_j, \quad \lambda_6 = -(N^p)^* \frac{M_1}{N_{max}}$$

$$\lambda_{7-8} = \frac{1}{2}\left(-[\nu_{-1} + \nu_2 + \gamma_1] \pm \sqrt{(\nu_{-1} + \nu_2 + \gamma_1)^2 - 4(\nu_{-1}(l_{-1} + \mu_{aa}) + \nu_2\gamma_1)} \right)$$

$$\lambda_{9-11}: \text{ Roots of } p(\lambda) = \lambda^3 + b\lambda^2 + c\lambda + d$$

where

$$\gamma_1 = l_{-1} + \mu_{aa} + \nu_1 [R^p_{gp130}]_{tot} (N^p)^*$$

$$\gamma_2 = \mu_{ai} + \widehat{k}_1 [R^p_{il}]_{tot} (N^p)^*$$

$$b = \gamma_2 + \widehat{l}_{-1} + \widehat{l}_2 + \widehat{k}_{-1} + \widehat{l}_1[R^p_{gp130}]_{tot}$$
$$c = \gamma_2 \cdot (\widehat{l}_{-1} + \widehat{l}_2 + \widehat{l}_1[R^p_{gp130}]_{tot}) + \widehat{l}_2(\widehat{k}_{-1} + \widehat{l}_1[R^p_{gp130}]_{tot}) + \widehat{k}_{-1}(\mu_{ai} + \widehat{l}_{-1})$$
$$d = \gamma_2\widehat{l}_2\widehat{l}_1[R^p_{gp130}]_{tot} + \widehat{k}_{-1}\mu_{ai}(\widehat{l}_{-1} + \widehat{l}_2).$$

The coefficients b, c, and d are all clearly positive along T_2. Moreover, $bc > d$ since

$$\begin{aligned} bc &= \gamma\widehat{l}_2\widehat{l}_1[R^p_{gp130}]_{tot} + \gamma \cdot \left(\gamma_2(\widehat{l}_{-1} + \widehat{l}_2 + \widehat{l}_1[R^p_{gp130}]_{tot}) + \widehat{l}_2\widehat{k}_{-1} + \widehat{k}_{-1}(\mu_{ai} + \widehat{l}_{-1})\right) \\ &+ \widehat{k}_{-1}\mu_{ai}(\widehat{l}_{-1} + \widehat{l}_2) + \widehat{k}_{-1}\mu_{ai} \cdot \left(\widehat{l}_1[R^p_{gp130}]_{tot} + \widehat{k}_{-1}\right) \\ &+ \left(\widehat{l}_{-1} + \widehat{l}_2 + \widehat{l}_1[R^p_{gp130}]_{tot} + \widehat{k}_{-1}\right) \\ &\qquad \cdot \left(\gamma(\widehat{l}_{-1} + \widehat{l}_2 + \widehat{l}_1[R^p_{gp130}]_{tot}) + \widehat{l}_2(\widehat{k}_{-1} + \widehat{l}_1[R^p_{gp130}]_{tot}) + \widehat{k}_{-1}\widehat{l}_{-1}\right) \\ &> \gamma\widehat{l}_2\widehat{l}_1[R^p_{gp130}]_{tot} + \widehat{k}_{-1}\mu_{ai}(\widehat{l}_{-1} + \widehat{l}_2) \\ &= d. \end{aligned}$$

Applying Theorem 5.5 again proves that $Re(\lambda_i) < 0$ for $i = 9, 10, 11$. However, there is a problem due to the existence of three zero eigenvalues. Only one of these would correspond to the neutrally stable direction along the one-dimensional curve of steady states, therefore we cannot apply Claim 5.6. Hence we cannot conclude that points along T_2 are stable just by considering the local linearization around T_2. However, the curve T_2 is likely stable due to the biological reasoning presented after the analysis of T_1.

Since we are attempting to establish stability of points along the curve T_2, for which $(N^p)^* \neq 0$, we assume N^p does not approach 0 as $t \to \infty$. Then, since $N^p(t_0) = 0$ implies $N^p(t) = 0$ for all $t > t_0$, there exists $\varepsilon > 0$ such that $N^p(t) > \varepsilon$ for all $t > 0$. Recall that for any solution $\phi(t)$ of the ODE system with $\phi(0) = \xi \in \Omega_+$, $\phi(t) \in \Omega_+$ for all $t > 0$. Define the function

$$\begin{aligned} V(\vec{x}) &= 2[A_i] + [R_{il}] + 3[A_a] + N^p\left(2[A_s] + 3[\{A_a : R^p_{gp130}\}] + 2[\{A_s : R^p_{gp130}\}] + J\right) \\ &+ \frac{1}{2}\left(N_{max} - (N^p + N^d)\right)^2 \end{aligned}$$

where $\vec{x} = ([A_i], [R_{il}], [A_a], [A_s], [\{A_a : R^p_{gp130}\}], [\{A_s : R^p_{gp130}\}], [J], N^p, N^d)^T$. This function is positive definite in Ω_+ since $V(\xi) = 0$ for all $\xi \in T_2$ and $V(\xi) > 0$ for all $\xi \in \Omega_+ \backslash \{T_2\}$. Moreover, it can be interpreted as the distance of $\phi(t)$ to the curve of steady states T_2. $[R^p_{il}]$ and $[R^p_{gp130}]$ are not included in this function, because if $[A_s] \to 0$, $[\{A_a : R^p_{gp130}\}] \to 0$, and $[\{A_s : R^p_{gp130}\}] \to 0$, conservation laws show that $[R^p_{il}] \to [R^p_{il}]_{tot}$ and $[R^p_{gp130}] \to [R^p_{gp130}]_{tot}$. Taking the derivative of $V(\vec{x})$ with respect to time along the solution curve,

$$\begin{aligned}
\frac{dV}{dt} &= \sum \frac{\partial V}{\partial x_i}\frac{\partial x_i}{\partial t} = \nabla V \cdot f(\vec{x}) \\
&= -\Big[N^p\bigg(2\nu_2[\{A_a : R^p_{gp130}\}] + \widehat{l}_2[\{A_s : R^p_{gp130}\}] + \mu_j J\bigg) + 2\mu_{ai}[A_i] + \mu_{il}[R_{il}] + 3\mu_{aa}[A_a] \\
&\quad + \frac{\kappa_1[J]^2}{\kappa_2^2 + [J]^2} N^p(2[A_s] + 3[\{A_a : R^p_{gp130}\}] + 2[\{A_s : R^p_{gp130}\}] + [J]) \\
&\quad + \bigg(N_{max} - (N^p + N^d)\bigg)\bigg(M_1 N^p(1 - \frac{N^p + N^d}{N_{max}})\bigg)\Big] \\
&< -\Big[\varepsilon\bigg(2\nu_2[\{A_a : R^p_{gp130}\}] + \widehat{l}_2[\{A_s : R^p_{gp130}\}] + \mu_j J\bigg) + 2\mu_{ai}[A_i] + \mu_{il}[R_{il}] + 3\mu_{aa}[A_a] \\
&\quad + \varepsilon\frac{\kappa_1[J]^2}{\kappa_2^2 + [J]^2}(2[A_s] + 3[\{A_a : R^p_{gp130}\}] + 2[\{A_s : R^p_{gp130}\}] + [J]) \\
&\quad + \bigg(N_{max} - (N^p + N^d)\bigg)\bigg(M_1 N^p(1 - \frac{N^p + N^d}{N_{max}})\bigg)\Big] \\
&\leq 0 \quad \text{in} \quad \Omega_+.
\end{aligned}$$

Define the subspace $\omega_\ell = (0, 0, 0, [R^p_{il}]_{tot} - [A_s]^*, [A_s]^*, [R^p_{gp130}]_{tot}, 0, 0, 0, N_{max} - (N^d)^*, (N^d)^*)$, where $[A_s]^* > 0$ and $(N^d)^* \in (0, N_{max})$ are both arbitrary. The above calculation shows that $\dfrac{dV}{dt} < 0$ for all $\xi \in \Omega_+ \backslash \omega_\ell$, but $\dfrac{dV}{dt} = 0$ for all $\xi \in \omega_\ell$. This shows that the curve of steady states T_2 is stable. Any solution curve $\phi(t)$ with initial condition $\xi \in \Omega_+$ will remain "near" T_2 as $t \to \infty$, in the sense that the distance between the two curves, measured by $V(\vec{x})$, does not increase. This is provided $\phi(t)$ is such that N^p does not converge to 0.

However, we can claim that T_2 is asymptotically stable. First note that $\dfrac{dV}{dt} < 0$ for all $\xi \in \Omega_+ \backslash \omega_\ell$. Choose any number $N^d_\infty \in (0, N_{max})$ and consider the line

$$\vec{L} = (0, 0, 0, [R^p_{il}]_{tot} - [A_s]^*, [A_s]^*, [R^p_{gp130}]_{tot}, 0, 0, 0, N_{max} - N^d_\infty, N^d_\infty),$$

so that $\vec{L} \subset \omega_\ell$. Evaluating the vector field $f(\vec{x})$ at any point along the line $\vec{L}$ shows that $\frac{d[A_i]}{dt} > 0$, $\frac{d[A_s]}{dt} < 0$, $\frac{d[R^p_{il}]}{dt} > 0$, $\frac{d[R^p_{gp130}]}{dt} < 0$, and $\frac{d[\{A_s : R^p_{gp130}\}]}{dt} > 0$. In other words, if the solution curve intersects the line $\vec{L}$, it does not remain on the line; the vector field drives the curve back into $\Omega_+ \backslash \{\omega_\ell\}$, where $\frac{dV}{dt} < 0$. Hence the curve of steady states T_2 is asymptotically stable. Note however that nothing has been said about the stability of individual steady states along T_2; we have only shown here that

$$[A_i] \to 0, \qquad [R_{il}] \to 0, \qquad [A_a] \to 0, \qquad [R^p_{il}] \to [R^p_{il}]_{tot}, \qquad [A_s] \to 0, \qquad [J] \to 0$$

$$[R^p_{gp130}] \to [R^p_{gp130}]_{tot}, \qquad [\{A_a : R^p_{gp130}\}] \to 0, \qquad [\{A_s : R^p_{gp130}\}] \to 0, \qquad N^p + N^d \to N_{max}.$$

A derivation of the Lyapunov function $V(\vec{x})$, and a more detailed computation showing $\frac{dV}{dt} \leq 0$ along the solution curve $\phi(t)$, are provided in Appendix D.

CHAPTER 6. Spatial Variation and Chemotaxis

This dissertation has thus far been solely concerned with a population model for the experiments discussed in Chapter 1. However, there is a spatial element that must be addressed. Experiments are performed on one of two types of substrates. One type is smooth, consisting of a uniform layer of laminin coating a nonpatterned polystyrene substrate. The other type of substrate can be referred to as the *patterned* substrate. The polystyrene substrate is microetched to introduce multiple evenly-spaced parallel grooves. The grooves may be termed *troughs*, and they are separated by *mesas*. The groove width is 16 μm, the mesa width is 13 μm, and the mesa height (groove depth) is 4 μm. A uniform layer of laminin is then applied to the substrate.

First consider the simulations on the nonpatterned substrate. A spatial model would consider activity over a two-dimensional region $[0, L_x] \times [0, L_y]$. However, it can be claimed that analysis of the population model will suffice due to the spatial homogeneity of all species involved. In each experiment, AHPCs are plated uniformly, and astrocyte density is either uniform or nonexistent. It has been observed that there is little to no movement of the cell bodies of either the AHPCs or the astrocytes during these experiments. All molecules present on the nonpatterned substrate are therefore either added uniformly by adding homogeneous cultured media to the system, or they are secreted by the astrocytes which are present in a uniform density, again causing the addition of chemicals to be uniform.

Now consider the simulations on the patterned substrate. When astrocytes are not present on the plate (i.e. all but the contact coculture experiment), all chemicals are again added to the system uniformly as described above. Moreover, there is little to no cell movement occuring. Hence the uniform layer of AHPCs plated on the substrate remains uniform. By

the same reasoning as the smooth substrate experiments, it can be argued that the population model will suffice for the analysis. Note also that for the experimental data in Table 1.1, the same percentage of cells differentiated regardless of whether the experiments occurred on the patterned or nonpatterned substrate. This is another argument for considering the population model in this instance.

This reasoning no longer holds for the contact coculture on the patterned substrate. In this experiment, a uniform layer of astrocytes is applied to the laminin at a density of $1.5 \times 10^4 \frac{cells}{cm^2}$ and cultured for two days. After this period of time, it is found that the astrocytes have aggregated in the grooved regions. The AHPCs are then plated above the astrocytes, in direct contact with them. Since astrocytes are secreting active molecules in this system, we no longer can use the assumption that all molecules are being added to the system uniformly. Hence AHPCs in some regions may be exposed to different concentrations of active molecules than AHPCs in other regions. Thus we must consider a spatial model. However, instead of modeling this environment as a three-dimensional region, we may consider cellular differentiation on a representative two-dimensional region. When the astrocytes arrange themselves in the grooves, they roughly form a striped monolayer. AHPCs are then plated onto these astrocytes. Thus their action is occurring on a two-dimensional region. The grooves then correspond to regions of high astrocyte density, and the mesas correspond to regions of low astrocyte density. The astrocyte density of the representative portion of the plate used in the numerical simulations is illustrated in Figure 6.1.

To understand how to modify the population model to take into account spatial considerations, it is important to understand the mathematical aspects of random motion (i.e. diffusion) and directed motion (i.e. chemotaxis).

6.1 Spatial Movement of Molecular/Cellular Species

The model under consideration in this chapter involves spatial variations existing in only two dimensions, corresponding to those of the flat surface AHPCs are placed on. Concentrations of species are considered to be homogeneous with respect to the height dimension. Let A

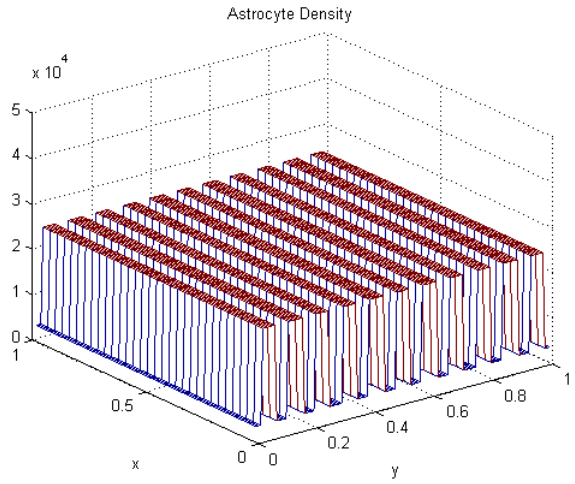

Figure 6.1 *Astrocyte density for numerical simulations. Regions of high density correspond to troughs and regions of low density correspond to mesas.*

be an arbitrary rectangle of this two-dimensional surface, and let S denote its boundary. The rate of change of the quantity of Z within A is equal to the net inflow of Z through through S plus the net change in Z within A due to production and degradation. The net inflow through S is the negative of the net outflow, so

$$\frac{\partial}{\partial t}\iint_A [Z]dxdy = \iint_A Q^{(z)}dxdy - \int_S J^{(z)} \cdot ndS.$$

$Q^{(z)}$ is the net change in Z due to production and degradation per unit area per unit time. It has units of $\frac{cells}{cm^2 \cdot hr}$. $J^{(z)}$ is the flux of Z, the net amount leaving A through a unit length segment of S per unit time, and n is the outward unit vector normal to S. It has units of mass per length per time, in our case $\frac{cells}{cm \cdot hr}$. Applying the divergence theorem, and assuming $[Z](x, y)$ is continuous, yields

$$\iint_A \Big(\frac{\partial [Z]}{\partial t} + \nabla \cdot J^{(z)} - Q^{(z)}\Big)dxdy = 0.$$

This is true for all regions A, therefore the integrand must be zero,

$$\frac{\partial [Z]}{\partial t} = -\nabla \cdot J^{(z)} + Q^{(z)}.$$

The function $Q^{(z)}$ is given by the kinetic terms of the population model. The term we must study is $J^{(z)}$, the flux of species Z. This term describes the net movement of Z.

To examine the flux of Z, we consider a system where there is no production or degradation of Z, that is $Q^{(z)} = 0$. Then $\dfrac{\partial [Z]}{\partial t} = -\nabla \cdot J$. We first examine the case where there are no attractive or repelling forces present and movement is in one dimension only. Due to the bombardment of a molecule of Z by other molecules of Z, we assume that after a time Δt, a molecule at x moves to either $x - \Delta x$ or $x + \Delta x$. Since there are no attractive or repelling forces, and the bombardment of other molecules is random, the probability of moving in either direction is equal, both being 1/2.

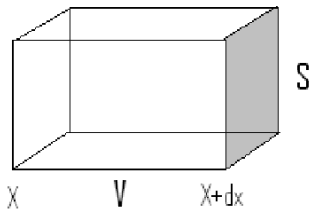

Figure 6.2 *Diagram for the derivation of the flux terms. The box is labelled V, and the surface the molecules pass through is S.*

Consider this one dimensional movement within a small box V, a portion of the environment where the molecules reside. Half of the molecules in the box V will leave the box through S, and let A be the area of S. Half of the molecules in an identical box between $x + \Delta x$ and $x + 2\Delta x$ will enter V through S. Hence the net outflow through S is

$$\frac{1}{2}\int_{x}^{x+\Delta x} [Z](s)Ads - \frac{1}{2}\int_{x+\Delta x}^{x+2\Delta x} [Z](s)Ads$$

every Δt hours. Therefore

$$J^{(z)} = \frac{1}{2\Delta t}\Big[\int_{x}^{x+\Delta x} [Z](s)ds - \int_{x+\Delta x}^{x+2\Delta x} [Z](s)ds\Big]$$

molecules exit through S per unit area per unit time. Define $G(x) = \displaystyle\int_{0}^{x} [Z](s)ds$ and $F(x) =$

$\int_x^{x+\Delta x}[Z](s)ds$. Expanding G with a Taylor series to the second order, we get

$$\begin{aligned}
G(x+\Delta x) &= G(x) + G'(x)\Delta x + G''(x)\Big(\frac{\Delta x^2}{2}\Big) + O(\Delta x^3) \\
&= \int_0^x [Z](s)ds + [Z](x)\Delta x + \frac{d[Z]}{dx}\Big(\frac{\Delta x^2}{2}\Big) + O(\Delta x^3) \\
G(x+2\Delta x) &= G(x+\Delta x) + G'(x+\Delta x)\Delta x + G''(x+\Delta x)\Big(\frac{\Delta x^2}{2}\Big) + O(\Delta x^3) \\
&= \int_0^{x+\Delta x} [Z](s)ds + [Z](x+\Delta x)\Delta x + \frac{d[Z]}{dx}\Big(\frac{\Delta x^2}{2}\Big) + O(\Delta x^3).
\end{aligned}$$

Note that

$$\begin{aligned}
J^{(z)} &= \frac{-1}{2\Delta t}\Big[F(x+\Delta x) - F(x)\Big] \\
&= \frac{-1}{2\Delta t}\Big[\int_{x+\Delta x}^{x+2\Delta x}[Z](s)ds - \int_x^{x+\Delta x}[Z](s)ds\Big] \\
&= \frac{-1}{2\Delta t}\Big[\int_0^{x+2\Delta x}[Z](s)ds - 2\int_0^{x+\Delta x}[Z](s)ds + \int_0^x [Z](s)ds\Big] \\
&= \frac{-1}{2\Delta t}\Big[G(x+2\Delta x) - 2G(x+\Delta x) + G(x)\Big] \\
&= \frac{-1}{2\Delta t}\Big[G(x+\Delta x) + G'(x+\Delta x)\Delta x + G''(x+\Delta x)\Big(\frac{\Delta x^2}{2}\Big) - G(x+\Delta x) \\
&\qquad - G(x) - G'(x)\Delta x - G''(x)\Big(\frac{\Delta x^2}{2}\Big) + G(x) + O(\Delta x^3)\Big] \\
&= \frac{-1}{2\Delta t}\Big[G(x+\Delta x) + G'(x+\Delta x)\Delta x + G''(x)\Big(\frac{\Delta x^2}{2}\Big) + O(\Delta x^3) - G(x+\Delta x) \\
&\qquad - G(x) - G'(x)\Delta x - G''(x)\Big(\frac{\Delta x^2}{2}\Big) + G(x) + O(\Delta x^3)\Big] \\
&= -\frac{\Delta x}{2\Delta t}\Big[G'(x+\Delta x) - G'(x)\Big] + O\Big(\frac{\Delta x^3}{\Delta t}\Big) \\
&= -\frac{\Delta x^2}{2\Delta t}\Big[\frac{[Z](x+\Delta x) - [Z](x)}{\Delta x}\Big] + O\Big(\frac{\Delta x^3}{\Delta t}\Big).
\end{aligned}$$

Taking the limit as $\Delta x \to 0$ and $\Delta t \to 0$ such that $\lim_{\Delta x, \Delta t \to 0}\Big[\frac{\Delta x^2}{2\Delta t}\Big] = D$, we get $J^{(z)} = -D\frac{\partial [Z]}{\partial x}$, the flux of Z. This can be repeated along the y-axis (and also the z-axis) to show that in the absence of attractive and repulsive forces, the flux is $J^{(z)} = -D\nabla[Z]$. That is, molecules flow down their gradient, from regions of high density to regions of lower density.

Now consider the case where cells undergo chemotaxis, so that the movement of Z is influenced by another chemical C. Suppose that the decision of when the cells move is independent of the decision of where to move ([42]). We can then assume as above that after a time Δt, a

molecule at x moves to either $x-\Delta x$ or $x+\Delta x$. This movement is governed by a continuously differentiable function $f(C)$, which is related to the *chemotactic sensitivity*, a measure of how strong of an influence C has on Z. For simplicity we use $f\Big(C(x\pm\frac{\Delta x}{2})\Big)$ to determine if a molecule of Z moves right or left. (At the end of the derivation, we take the limit as $\Delta x\to 0$ and this becomes a reading of C in the immediate neighborhood of the cell. Long-range sampling is not included in this derivation; that situation is discussed in [39]). All cells take one step of length Δx every Δt period of time, so the probability that Z moves right/left from x is $T_{\pm}(x)=\dfrac{f\Big(C(x\pm\frac{\Delta x}{2})\Big)}{f\Big(C(x-\frac{\Delta x}{2})\Big)+f\Big(C(x+\frac{\Delta x}{2})\Big)}$. The flux of cells through S out of V is then given by

$$J^{(z)}=\frac{-1}{\Delta t}\Big[\int_{x+\Delta x}^{x+2\Delta x}T_{-}(s)[Z](s)ds-\int_{x}^{x+\Delta x}T_{+}(s)[Z](s)ds\Big].$$

Defining

$$g(x)=f\Big(C(x)\Big)$$
$$G_{\pm}(x)=\int_0^x\frac{g(s\pm\frac{\Delta x}{2})}{g(s-\frac{\Delta x}{2})+g(s+\frac{\Delta x}{2})}[Z](s)ds$$

and proceeding as above, we get

$$\begin{aligned}
J^{(z)}&=-\frac{1}{\Delta t}\Big[G_{-}(x+2\Delta x)-G_{-}(x+\Delta x)-G_{+}(x+\Delta x)+G_{+}(x)\Big]\\
&=-\frac{1}{\Delta t}\Big[G_{-}(x+\Delta x)+G'_{-}(x+\Delta x)\Delta x+G''_{-}(x+\Delta x)\Big(\frac{\Delta x^2}{2}\Big)+O(\Delta x^3)\\
&\qquad -G_{-}(x+\Delta x)-G_{+}(x)-G'_{+}(x)\Delta x-G''_{+}(x)\Big(\frac{\Delta x^2}{2}\Big)+O(\Delta x^3)+G_{+}(x)\Big]\\
&=-\frac{1}{\Delta t}\Big[G_{-}(x+\Delta x)+G'_{-}(x+\Delta x)\Delta x+G''_{-}(x)\Big(\frac{\Delta x^2}{2}\Big)+O(\Delta x^3)+O(\Delta x^3)\\
&\qquad -G_{-}(x+\Delta x)-G_{+}(x)-G'_{+}(x)\Delta x-G''_{+}(x)\Big(\frac{\Delta x^2}{2}\Big)+O(\Delta x^3)+G_{+}(x)\Big]\\
&=-\frac{\Delta x}{\Delta t}\Big[G'_{-}(x+\Delta x)-G'_{+}(x)\Big]+\Big(\frac{\Delta x^2}{2\Delta t}\Big)\Big[G''_{-}(x)-G''_{+}(x)+O(\Delta x)\Big]\\
&=-\frac{\Delta x^2}{\Delta t}\Big[\frac{1}{\Delta x}\Big(G'_{-}(x+\Delta x)-G'_{+}(x)\Big)\Big]+\Big(\frac{\Delta x^2}{2\Delta t}\Big)\Big[G''_{-}(x)-G''_{+}(x)+O(\Delta x)\Big]\\
&=-\frac{\Delta x^2}{\Delta t}g(x+\frac{\Delta x}{2})\Big[\frac{1}{\Delta x}\Big(\frac{1}{g(x+\frac{\Delta x}{2})+g(x+\frac{3\Delta x}{2})}[Z](x+\Delta x)\\
&\qquad -\frac{1}{g(x+\frac{\Delta x}{2})+g(x+\frac{3\Delta x}{2})}[Z](x)+\frac{1}{g(x+\frac{\Delta x}{2})+g(x+\frac{3\Delta x}{2})}[Z](x)\\
&\qquad -\frac{1}{g(x-\frac{\Delta x}{2})+g(x+\frac{\Delta x}{2})}[Z](x)\Big)\Big]+\Big(\frac{\Delta x^2}{2\Delta t}\Big)\Big[G''_{-}(x)-G''_{+}(x)+O(\Delta x)\Big]
\end{aligned}$$

Finally, since

$$\begin{aligned}
&\lim_{h\to 0}\frac{\Big(g(x+\frac{3h}{2})+g(x+\frac{h}{2})\Big)^{-1}-\Big(g(x+\frac{h}{2})+g(x-\frac{h}{2})\Big)^{-1}}{h}\\
&\quad=\lim_{h\to 0}\Big[\frac{g(x+\frac{h}{2})+g(x-\frac{h}{2})-g(x+\frac{3h}{2})-g(x+\frac{h}{2})}{\Big(g(x+\frac{h}{2})+g(x-\frac{h}{2})\Big)\Big(g(x+\frac{3h}{2})+g(x+\frac{h}{2})\Big)h}\Big]\\
&\quad=\lim_{h\to 0}\Big[\frac{g(x+\frac{3h}{2})-g(x-\frac{h}{2})}{h}\cdot\frac{-1}{\Big(g(x+\frac{h}{2})+g(x-\frac{h}{2})\Big)\Big(g(x+\frac{3h}{2})+g(x+\frac{h}{2})\Big)}\Big]\\
&\quad=\frac{-2g'(x)}{4g^2(x)}
\end{aligned}$$

we get that in the limit as $\Delta x\to 0$ and $\Delta t\to 0$ such that $\lim_{\Delta x,\Delta t\to 0}\dfrac{\Delta x^2}{2\Delta t}=D$,

$$\begin{aligned}
J^{(z)}&=-D\frac{g(x)}{g(x)}\frac{\partial[Z]}{\partial x}+D\frac{g'(x)g(x)}{g^2(x)}[Z](x)\\
&=-D\frac{\partial[Z]}{\partial x}+D\frac{g'(x)}{g(x)}[Z](x)\\
&=-D\frac{\partial[Z]}{\partial x}+D\frac{f'(C)}{f(C)}[Z](x)\frac{\partial C}{\partial x}\\
&=-D\frac{\partial[Z]}{\partial x}+\chi(C)[Z]\frac{\partial C}{\partial x}.
\end{aligned}$$

This can be repeated along the y-axis (and also the z-axis) to show that in the presence of an attractive and repulsive force, the flux is $J^{(z)}=-D\nabla[Z]+\chi(C)[Z]\nabla[C]$. The first term represents random motion, while the second term represents directed motion. The function $\chi(C)=D\Big(\ln\big(f(C)\big)\Big)'$ is referred to as the *chemotactic sensitivity*. If $\chi(C)>0$, then positive taxis occurs; $[Z]$ tends to move up the gradient of C to regions of higher concentration. If $\chi(C)<0$, then negative taxis occurs; $[Z]$ tends to move down the gradient of C to regions of lower concentration. This motion can either work in concert with, or in opposition to, the tendency to move down the gradient of $[Z]$ to regions of lower concentration of the moving species Z. This interplay can have interesting consequences; see [31] and [42] for details.

If $[Z]$ responds to multiple attractive and repulsive forces, the flux term can be generalized to one of the form

$$J^{(z)}=-D\nabla[Z]+[Z]\sum_{i=1}^{N}\chi_i(C_i)\nabla C_i.$$

One may also extend this idea to a quorom-sensing mechanism, where the rate of random motion of $[Z]$ depends on its population density, so that $J(z)=-D([Z])\nabla[Z]$. This can occur

in models for insect dispersal, where population pressures can influence the rate of dispersal. A typical forms for $D([Z])$ are $D([Z]) = D_0\Big(\frac{[Z]}{[Z]_0}\Big)^m$ or $D([Z]) = D_0\Big[1+\varepsilon\Big(\frac{[Z]}{[Z]_0}\Big)^m\Big]$, for $m > 0$, and D_0, ε, and $[Z]_0$ positive constants. This situation is discussed more in [39]. Responses to long-range stimuli are also presented in [39]. Many aspects of diffusion, from both the microscopic and macroscopic viewpoint are presented in [6]. Finally, these same equations for the flux terms can be derived through a reinforced random walk, where one considers how the probability density changes according to the chemical master equation. This approach is studied in [42]. The presentation provided here is based on the work in [25].

6.2 Spatial Model for the Contact Coculture

Movement of the cell types N^p and N^d occur in two-dimensions, and the mathematical derivations of their flux terms are given above. It has been observed that little cell movement is occuring in the experiments of interest, so we let the corresponding flux terms be comprised solely of random motion,

$$J^{(np)} = -D_p \nabla N^p, \qquad J^{(nd)} = -D_d \nabla N^d.$$

No chemotaxis is occurring with these flux terms. The soluble chemicals are of a much smaller scale with respect to size than the cells, and are moving in three dimensions within the media. However, we assume their concentrations are homogeneous with respect to their height within the fluid so that we only consider movement in two dimensions. The relevant relationship is that 0.5 mL of media covers 1 cm^2 plate with a uniform thickness. Molecules are much simpler than cells, so we assume that those of interest do not undergo significant attractive or repulsive influences from other chemicals. They then move solely under diffusion, so $J^{(z)} = -D_z \nabla [Z]$ for $Z \in \{A_i, R_{il}, A_a, G_p, A_o\}$.

The movement of J presents some difficulty. J is an intracellular molecule measured in $\frac{nmol}{cell}$, so its movement is coupled to the movement of N^p. Let $\eta = [J] \cdot N^p$, so that the units of η are $\frac{nmol}{cm^2}$. The change in η with respect to time is given by

$$\frac{\partial \eta}{\partial t} = -\nabla \cdot J^{(\eta)} + Q^{(\eta)}.$$

The mechanisms producing J increase η at the rate

$$(\widehat{\ell}_2[\{As : R^p_{gp130}\}] + \nu_2[\{A_a : R^p_{gp130}\}])N^p.$$

It decays at the rate $-\mu_j\eta$. Proliferation of N^p does not alter η since no J is being created or destroyed during this process, however differentiation decreases η at the rate

$$-\Big(\frac{\kappa_1[J]^2}{\kappa_2^2+[J]^2}N^p + \frac{\theta_1}{\theta_2 + \Big(\frac{N^d}{N^p+N^d}\Big)^2}N^p\Big)[J].$$

For every AHPC that moves, $[J]$ nmol of J move, so the flux of η is $J^{(\eta)} = [J]J^{(np)}$. Recall that if ϕ is a scalar function and F is a vector field,

$$\nabla\cdot(\phi F) = \nabla\phi\cdot F + \phi\nabla\cdot F.$$

Applying this identity, we have

$$\begin{aligned}\nabla\cdot J^{(\eta)} &= \nabla\cdot([J]J^{(np)})\\ &= \big(\nabla[J]\big)\cdot J^{(np)} + [J]\nabla\cdot J^{(np)}\end{aligned}$$

which, after rearranging and dividing by N^p, yields the relation

$$-\big(\nabla[J]\big)\cdot\Big(\frac{J^{(np)}}{N^p}\Big) = \frac{-1}{N^p}\nabla\cdot J^{(\eta)} + \frac{[J]}{N^p}\nabla\cdot J^{(np)}.$$

Finally,

$$\begin{aligned}\frac{\partial[J]}{\partial t} = \frac{\partial}{\partial t}\Big(\frac{\eta}{N^p}\Big) &= \frac{1}{N^p}\frac{\partial\eta}{\partial t} - \frac{\eta}{(N^p)^2}\frac{\partial N^p}{\partial t} = \frac{1}{N^p}\frac{\partial\eta}{\partial t} - \frac{[J]}{N^p}\frac{\partial N^p}{\partial t}\\ &= \frac{-1}{N^p}\nabla\cdot J^{(\eta)} + \widehat{\ell}_2[\{A_s : R^p_{gp130}\}] + \nu_2[\{A_a : R^p_{gp130}\}] - \mu_j[J]\\ &\quad - \frac{\kappa_1[J]^2}{\kappa_2^2+[J]^2}[J] - \frac{\theta_1}{\theta_2 + \Big(\frac{N^d}{N^p+N^d}\Big)^2}[J] + \frac{[J]}{N^p}\nabla\cdot J^{(np)}\\ &\quad - M_1[J]\Big(1-\frac{N^p+N^d}{N_{max}}\Big) + \frac{\kappa_1[J]^2}{\kappa_2^2+[J]^2}[J] + \frac{\theta_1}{\theta_2 + \Big(\frac{N^d}{N^p+N^d}\Big)^2}[J]\\ &= \frac{-1}{N^p}\nabla\cdot J^{(\eta)} + \frac{[J]}{N^p}\nabla\cdot J^{(np)} + \widehat{\ell}_2[\{A_s : R^p_{gp130}\}] + \nu_2[\{A_a : R^p_{gp130}\}]\\ &\quad - \mu_j[J] - M_1[J]\Big(1-\frac{N^p+N^d}{N_{max}}\Big)\end{aligned}$$

so that we finally get the equation for $[J]$:

$$\frac{\partial[J]}{\partial t} = -\big(\nabla[J]\big)\cdot\Big(\frac{J^{(np)}}{N^p}\Big)+\widehat{\ell}_2[\{A_s : R^p_{gp130}\}]+\nu_2[\{A_a : R^p_{gp130}\}]-\mu_j[J]-M_1[J]\Big(1-\frac{N^p+N^d}{N_{max}}\Big).$$

By defining $\gamma = M_1\Big(1-\dfrac{N^p+N^d}{N_{max}}\Big)$ we get the following system of reaction-diffusion equations for our model:

$$\begin{aligned}
\frac{\partial[A_i]}{d\partial t} &= D_{ai}\Delta[A_i] + S_{ai}(t) + a_1N_a - l_1[A_i][R_{Il}] + l_{-1}[A_a] - \widehat{k}_1[A_i][R^p_{Il}]N^p + \widehat{k}_{-1}[A_s]N^p - \mu_{ai}[A_i],\\
\frac{\partial[R_{Il}]}{\partial t} &= D_{il}\Delta[R_{Il}] + S_{Il}(t) + b_aN_a - l_1[A_i][R_{Il}] + l_{-1}[A_a] - \mu_{Il}[R_{Il}],\\
\frac{\partial[A_a]}{\partial t} &= D_{aa}\Delta[A_a] + S_{aa}(t) + l_1[A_i][R_{Il}] - l_{-1}[A_a] - k_1[A_a][G_p] + k_{-1}[A_o]\\
&\quad - \nu_1[A_a][R^p_{gp130}]N^p + \nu_{-1}[\{A_a : R^p_{gp130}\}]N^p - \mu_{aa}[A_a],\\
\frac{\partial[G_p]}{\partial t} &= D_{gp}\Delta[G_p] + S_{gp}(t) + s_aN_a - k_1[A_a][G_p] + k_{-1}[A_o] - \mu_{gp}[G_p],\\
\frac{\partial[A_o]}{\partial t} &= D_{ao}\Delta[A_o] + S_{ao}(t) + k_1[A_a][G_p] - k_{-1}[A_o] - \mu_{ao}[A_o],\\
\frac{\partial[J]}{\partial t} &= -\big(\nabla[J]\big)\cdot\Big(\frac{-D_p\nabla N^p}{N^p}\Big) + \widehat{l}_2[\{A_s : R^p_{gp130}\}] + \nu_2[\{A_a : R^p_{gp130}\}] - \mu_j[J] - \gamma[J],\\
\frac{\partial N^p}{\partial t} &= D_p\Delta N^p - \frac{\kappa_1[J]^2}{\kappa_2^2+[J]^2}N^p - \frac{\theta_1}{\theta_2+\Big(\dfrac{N^d}{N^p+N^d}\Big)^2}N^p + \gamma N^p,\\
\frac{\partial N^d}{\partial t} &= D_d\Delta N^d + \frac{\kappa_1[J]^2}{\kappa_2^2+[J]^2}N^p + \frac{\theta_1}{\theta_2+\Big(\dfrac{N^d}{N^p+N^d}\Big)^2}N^p,
\end{aligned}$$

with AHPC receptor concentrations

$$\begin{aligned}
b &= \frac{L[R^p_{gp130}]_0 + ([R^p_{gp130}]_0 - [R^p_{il}]_0)[A_i]}{\widehat{K}+[A_i]} + \frac{\widehat{L}(V+[A_a])}{V},\\
c &= \frac{-\widehat{L}(V+[A_a])[A_i][R^p_{il}]_0}{V(\widehat{K}+[A_i])},\\
[A_s] &= (-b+\sqrt{b^2-4c})/2,\\
[\{A_a : R^p_{gp130}\}] &= \frac{L[R^p_{gp130}]_0 + [A_i]([R^p_{gp130}]_0 - [R^p_{Il}]_0) + (\widehat{K}+[A_i])[A_s]}{(L+[A_i])(V+[A_a])}[A_a],\\
[\{A_s : R^p_{gp130}\}] &= \frac{[A_i][R^p_{il}]_0 - (\widehat{K}+[A_i])[A_s]}{L+[A_i]},\\
[R^p_{il}] &= [R^p_{il}]_0 - [A_s] - [\{A_s : R^p_{gp130}\}],\\
[R^p_{gp130}] &= [R^p_{gp130}]_0 - [\{A_a : R^p_{gp130}\}] - [\{A_s : R^p_{gp130}\}],
\end{aligned}$$

where $L = \frac{\widehat{\ell_2}+\gamma}{\widehat{k_1}}$, $\widehat{L} = \widehat{L_m} + \frac{\gamma}{\widehat{\ell_1}}$, $V = V_m + \frac{\gamma}{\nu_1}$, and $\widehat{K} = \widehat{K_d} + \frac{\gamma}{\widehat{k_1}}$.

To aid in the numerical simulations, it is useful to consider the evolution of η instead of $[J]$, so we can instead use

$$\frac{\partial \eta}{\partial t} = -\nabla \cdot \Big(\eta \frac{J^{(np)}}{N^p}\Big) + (\widehat{\ell_2}[\{A_s : R^p_{gp130}\}] + \nu_2[\{A_a : R^p_{gp130}\}])N^p$$
$$- \Big(\frac{\kappa_1 \eta^2}{\kappa_2^2 (N^p)^2 + \eta^2} + \frac{\theta_1}{\theta_2 + \Big(\frac{N^d}{N^p + N^d}\Big)^2}\Big)\eta - \mu_j \eta.$$

Note that the movement of η due to the random motion of N^p can be viewed as a chemotactic repulsion of η down the gradient of N^p:

$$J^{(np)} = -D \nabla N^p$$
$$\Rightarrow \eta \frac{J^{(np)}}{N^p} = -\frac{D\eta}{N^p} \nabla N^p = -D\eta \nabla \ln(N^p).$$

Initial conditions for the spatial model are identical to the population model:

$$[A_i](x,y,0) = [A_a](x,y,0) = [A_o](x,y,0) = [R_{Il}](x,y,0) = [G_p](x,y,0) = 0$$
$$[R^p_{Il}](x,y,0) = [R^p_{il}]_0, \qquad [R^p_{gp130}](x,y,0) = [R^p_{gp130}]_0$$
$$[A_s](x,y,0) = [\{A_a : R^p_{gp130}\}](x,y,0) = [\{A_s : R^p_{gp130}\}](x,y,0) = 0$$
$$N^p(x,y,0) = N^p_0, \qquad N^d(x,y,0) = 0.$$

We must also specify the distribution of astrocytes since it is nonuniform. We simulate a $319\mu m \times 319\mu m$ section of the plate and normalize lengths, so that $L_x = L_y = 1$. Since the groove width is $16\mu m$ and the mesa width is $13\mu m$, this magnification corresponds to a region with 11 grooves and 10 full mesas, with an additional half-mesa on each end. This particular area for the simulation then has 55.2% of its area in the grooved regions and 44.8% on the mesas. It has been observed that approximately 90% of astrocyte density is in the grooved regions and 10% of astrocyte density is on the mesas. Hence the density in the grooved region is given by

$$\Big[\Big(\frac{1.5 \times 10^4 cells}{cm^2}\Big) \cdot (\text{total area of plate}) \cdot (90\%)\Big] \cdot \Big(\frac{1}{\text{total area of grooves}}\Big)$$
$$= \Big(\frac{1.5 \times 10^4 cells}{cm^2}\Big) \cdot (90\%) \cdot \Big(\%\text{ of area in grooves}\Big)^{-1}$$
$$= 2.44565 \times 10^4 \frac{cells}{cm^2}.$$

The density on the mesas is calculated similarly, yielding a density of $0.3343 \times 10^4 \frac{cells}{cm^2}$.

Finally, this model must also include boundary conditions. To derive these, consider the pattern of the substrate, which is the inverse of that illustrated in Figure 6.1. Note that the substrate, and hence the astrocyte density, is constant in the direction along the grooves and mesas, $N_a(x, y_1) = N_a(x, y_2)$ for all $y_1, y_2 \in [0, L_y]$. Since this $319\mu m \times 319\mu m$ subplate is one of many identical subplates comprising the $1cm \times 1cm$ plate, it is natural to assume no-flux boundary conditions in this direction. This boundary condition is valid under the asssumption that identical concentrations of species Z leave the subplate through this boundary as enter the subplate through this boundary from an adacent subplate. The B.C.'s are then given by $\frac{\partial [Z]}{\partial y} = 0$ for $Z \in \{A_i, R_{il}, A_a, G_p, A_o\}$ and $J^{(z)} \cdot \nu = 0$ for $z \in \{np, nd\}$ where ν is the outward unit normal vector, along the boundaries $(x, 0)$ and (x, L_y) for $x \in [0, L_x]$. Note that $[J]$ automatically satisfies the no-flux B.C.'s when N^p satisfies them. The other direction along the subplate can be considered to have periodic boundary conditions, again due to this subplate being one of many repeating identical subplates. The B.C.'s are then given by $[Z](0, y, t) = [Z](L_x, y, t)$ for all $y \in [0, L_x]$ and $Z \in \{A_i, R_{il}, A_a, G_p, A_o, J\}$, and with N^p or N^d in place of $[Z]$.

6.3 Results

All of the surfaces generated by the simulations have the property that they are constant along the grooves/mesas. This is due to the homogeneity of all species in this direction. Therefore, rather than presenting three-dimensional surfaces of the entire plate, a profile is taken of the surface. Two graphs will be shown. A two-dimensional graph is formed by superimposing profiles taken at twelve hour intervals in the same plot. A three-dimensional surface is formed by taking profiles at six hour intervals and plotting them against time.

6.3.1 Random Motion of Progenitor Cells

Experimentally it has been shown that approximately 35% of the cells on the patterned substrate differentiate after six days in the contact coculture experiment. Meanwhile, on the

smooth substrate, only about 20% of the cells differentiate. During the noncontact coculture experiment, both on the smooth substrate and the patterned substrate, approximately 70% of the cells differentiate. The only difference between the contact coculture and the noncontact coculture is the direct contact between the astrocytes and AHPCs. In Chapter 3 it was discussed that the second pathway of the IL6 mechanism (via soluble receptors) is likely being inactivated by the direct contact. This would occur by inhibiting the secretion of R_{il} from the astrocytes. However, to reduce differentiation to 20%, we also needed to reduce the secretion of A_i to (1/200)th of its normal rate. Since this behavior occurs during direct contact, it could possibly be mediated by cadherin binding. On the patterned substrate, much of the astrocyte density is in the grooves. The area of the astrocytes accessible to the AHPCs is decreased relative to that available on the smooth substrate. Therefore there would be less cadherin binding, so it would be reasonable to assume that the secretion of A_i is not reduced as drastically on the patterned substrate. Figure 6.3 shows that if a_1 is lowered to (1/25)th of its noncontact rate, then we can achieve approximately 35% differentiation after six days.

6.3.2 Exploration of Other Flux Terms

Although little to no cell movement has been observed in this system, it is interesting to see numerically what effects chemotactic movement may have. In this section, we start with the above system using $a_1 = (1 \times 10^{-11})/200 \frac{nmol}{cell \cdot hr}$ and $b_a = 0$ as the basal case, and add various chemotactic terms to see the effects. Without chemotaxis, this system yields 23.47% differentiation. When all species are homogeneous and no movement occurs (which is simulated with the population model), the maximum level of differentiation possible over a six day period with only the first IL6 pathway is approximately 35%, due to the saturation of R_{il}^p. We will explore this case by allowing chemotactic movement of AHPCs up the gradient of IL6. However, there is a slight problem with this. The diffusion rate of A_i can be approximated from its radius to be $4.86 \times 10^{-4} \frac{cm^2}{hr}$. With this rate, A_i diffuses quickly over the substrate, so that its concentration is roughly uniform, and hence there is little to no gradient for the cells to follow. Therefore we reduce the diffusion coefficient to $4.86 \times 10^{-8} \frac{nmol}{cm^2 \cdot hr}$, which is of

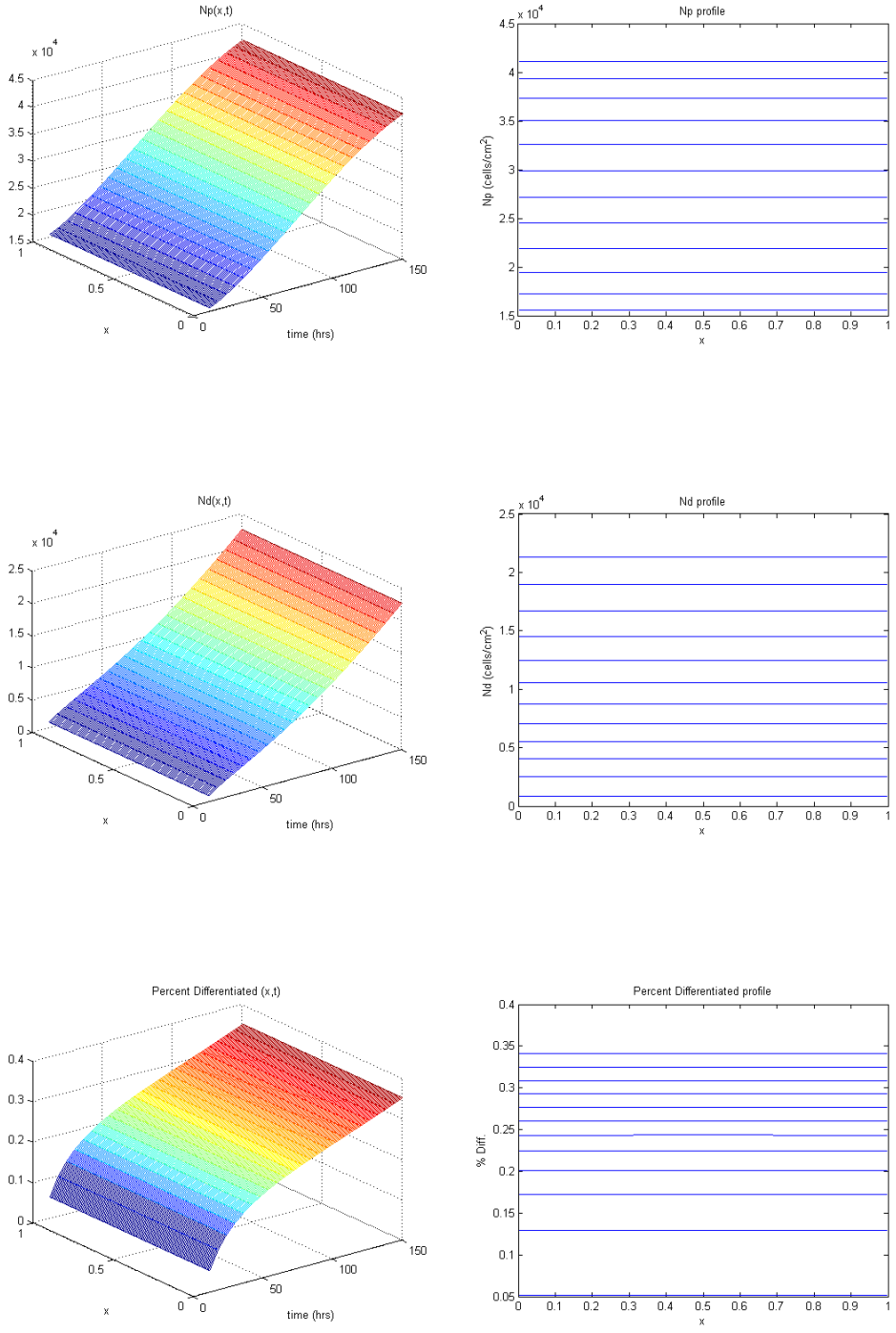

Figure 6.3 *(left) Time evolution of profile, every 6 hours, no taxis. (right) Proflies taken every 12 hours to show densities in different regions.*

the same order as the rates calculated for the cells. This allows gradients of A_i to exist, and allows chemotaxis to occur.

Since we are allowing chemotaxis of N^p to gradients of A_i, we now have a flux term of the form

$$J^{(np)} = -D_p \nabla N^p + \chi(A_i) N^p \nabla [A_i].$$

We first take $\chi(A_i)$ to be constant, and then we take it to be a saturable function. Since IL6 is an active differentiation factor for AHPCs, we assume that it is an attracting molecule, so that we have positive taxis. First let $\chi(A_i) = \chi_0$. Three cases are presented in Figure 6.4, Figure 6.5, and Figure 6.6. We have $\chi_0 = 1 \times 10^3 \frac{cm^2}{\mu M \cdot hr}$ for Figures 6.4, $\chi_0 = 1 \times 10^4 \frac{cm^2}{\mu M \cdot hr}$ for Figure 6.5, and $\chi_0 = 1 \times 10^5 \frac{cm^2}{\mu M \cdot hr}$ for Figure 6.6. In each case, cells are being driven up the gradient of $[A_i]$ onto the areas of high astrocyte density. The attraction is progressively greater as one moves through these graphs. The case where $\chi_0 = 1 \times 10^3 \frac{cm^2}{\mu M \cdot hr}$ does not yield a significantly different result from the non-taxis case, with 23.55% of cells differentiating. The case where $\chi_0 = 1 \times 10^4 \frac{cm^2}{\mu M \cdot hr}$ also yields similar results to the non-taxis case, with 25.87% of cells differentiating. The number of differentiated cells on the mesas is similar to the number of differentiated cells in the troughs. However, there is a noticable difference between the percentages of cells that have differentiated in the two regions. Close to 40% of the cells on the mesas have differentiated and only about 20% of cells in the troughs have differentiated. This situation will occur in most of the taxis systems presented here. Only N^p is being driven up the gradient of A_i. Therefore, the differentiated cells remain on the mesas, while the undifferentiated cells are leaving this area. The regions of highest A_i concentration are the centers of the grooves. Most undifferentiated cells are being attracted to this area, so there will be a lower portion of cells in this area that have differentiated. This result is much more pronounced when $\chi_0 = 1 \times 10^5 \frac{cm^2}{\mu M \cdot hr}$. In this case, 44.39% of cells differentiate, with almost 100% differentiation on the areas of lowest astrocyte density and near background levels in areas of highest astrocyte density. This result is suprising considering the population model only permits about 35% differentiation when only the first pathway is utilized, due to the saturation of the R_{il}^p receptor. When experimenting more with the population model, it can

be seen that the level of differentiation can be increased to 45% by restricting proliferation. The AHPCs are being strongly driven up the gradient of $[A_i]$, and their density surpasses the carrying capacity in these regions. Hence proliferation ceases here, and in fact the cells start to die due to the logistic term. It is only N^p being driven up this gradient, so this results in a higher proportion of those that remain being in the differentiated state.

The next type of chemotactic response simulated uses a sigmoidal function, $\chi(A_i) = \frac{\chi_0[A_i]^2}{\alpha^2 + [A_i]^2}$. It exhibits a saturable response. For high concentrations of IL6, $\chi(A_i) \approx \chi_0$. For $[A_i] = \alpha$, $\chi(A_i) = \chi_0/2$. For low concentrations of IL6, there is little to no chemotactic sensitivity, so cells in this environment do not move in response to gradients in $[A_i]$. Three cases are presented in Figure 6.7, Figure 6.8, and Figure 6.9. We have $\chi_0 = 1 \times 10^3 \frac{cm^2}{\mu M \cdot hr}$ and $\alpha = 1 \times 10^{-9} \frac{nmol}{mL}$ for Figure 6.7, $\chi_0 = 1 \times 10^5 \frac{cm^2}{\mu M \cdot hr}$ and $\alpha = 1 \times 10^{-9} \frac{nmol}{mL}$ for Figure 6.8, and $\chi_0 = 1 \times 10^5 \frac{cm^2}{\mu M \cdot hr}$ and $\alpha = 4 \times 10^{-9} \frac{nmol}{mL}$ for Figure 6.9. The results in Figure 6.7 (23.54% differentiation) and Figure 6.8 (46.99% differentiation) are nearly identical to the results in Figure 6.4 (23.55%) and Figure 6.6 (46.86%), respectively. However, the results in Figure 6.9 (43.84%) differ from Figure 6.8 due to the higher concentration of IL6 needed for a measurable response, caused by to the increase in α.

One final mechanism of taxis was simulated. This case is an alteration of those presented in Figure 6.5 and Figure 6.6. We still have cells moving up the gradient in $[A_i]$ with $\chi_0 = 1 \times 10^4 \frac{cm^2}{\mu M \cdot hr}$ (or 10^5, respectively). However, we now introduce a quorum-sensing mechanism where AHPCs undergo random motion down the gradient of N^p as before when the total cell density is low relative to the carrying capacity. But when $N^p + N^d \approx N_{max}$, the diffusion down the gradient of N^p increases. The flux of N^p is now

$$J^{(np)} = -D_p\Big[1 + 3\Big(\frac{N^p + N^d}{N_{max}}\Big)^3\Big]\nabla N^p + \chi_0 N^p \nabla[A_i].$$

Hence we have two competing forces. N^p moves up the gradient of $[A_i]$, but as $N^p + N^d$ approaches N_{max}, N^p has a much stronger incentive to move down the gradient in N^p and as a result N^p is also being driven down the gradient of $[A_i]$. In the case where $\chi_0 = 1 \times 10^4 \frac{cm^2}{\mu M \cdot hr}$, we have 24.07% of cells differentiating, slightly less than when the quorum-sensing mechanism was absent. However, note that cell densities are more uniformly distributed across the plate

than they previously were. These results are illustrated in Figure 6.10. In the case where $\chi_0 = 1 \times 10^5 \frac{cm^2}{\mu M \cdot hr}$, we have 32.67% of cells differentiating, much less than when the quorum-sensing mechanism was absent, and instead near the value of maximum differentiation available in the population model when only the first pathway is used. In this case, the quorum-sensing mechanism is preventing the cell density from accumulating at carrying-capacity levels, or as in the case without this mechanism, 2.5 times greater than the carrying capacity. Since the cell density is under the carrying capacity, the logistic term is not leading to death of the cells. As a result, the percentage of cells that are in the differentiated state is not artificially inflated due to the death of nondifferentiated cells.

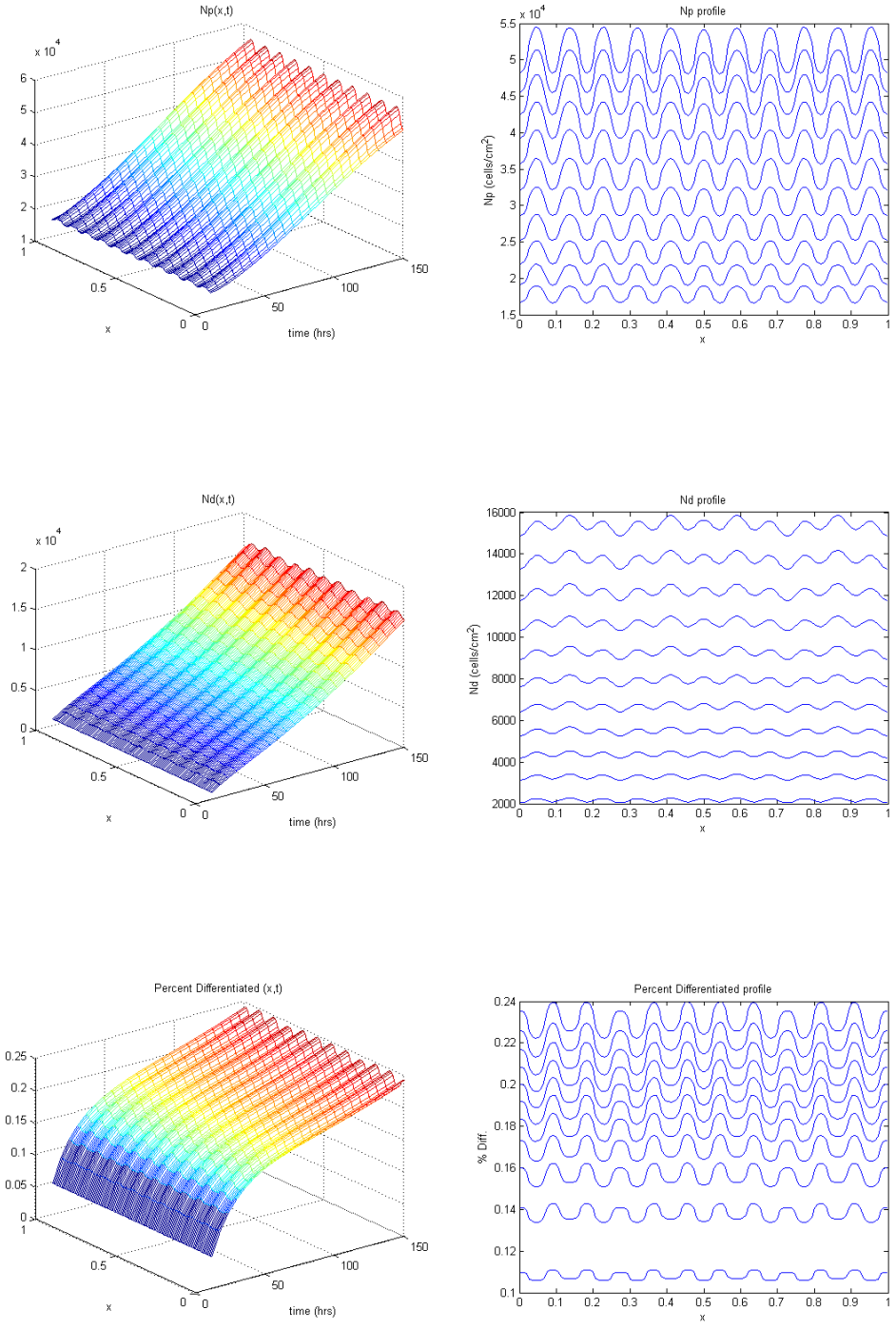

Figure 6.4 *(left) Time evolution of profile, every 6 hours, weak constant chemotaxis ($\chi_0 = 1e+3$) up IL6 gradients. (right) Profiles taken every 12 hours to show densities in different regions.*

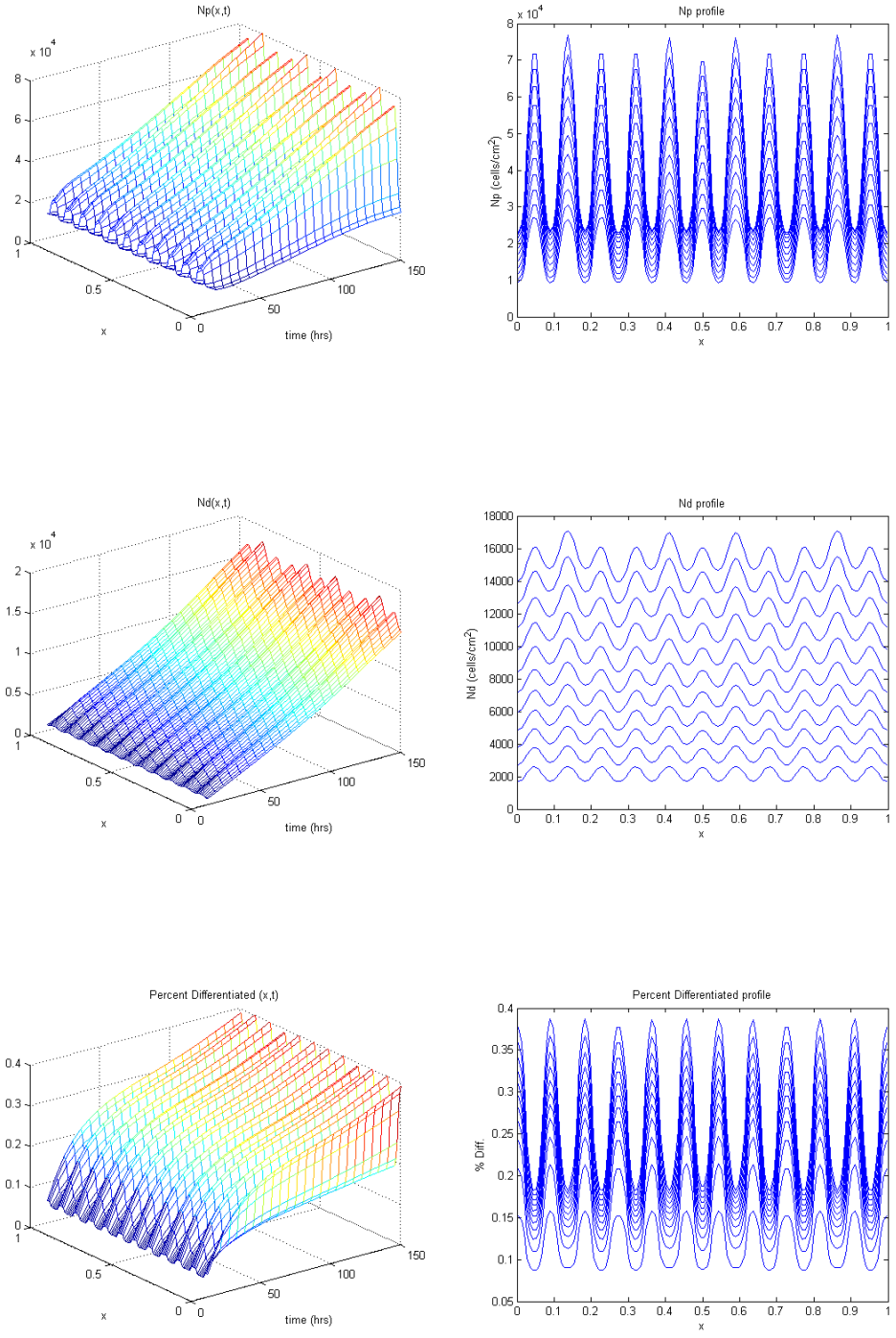

Figure 6.5 *(left) Time evolution of profile, every 6 hours, moderate constant chemotaxis ($\chi_0 = 1e{+}4$) up IL6 gradients. (right) Profiles taken every 12 hours to show densities in different regions.*

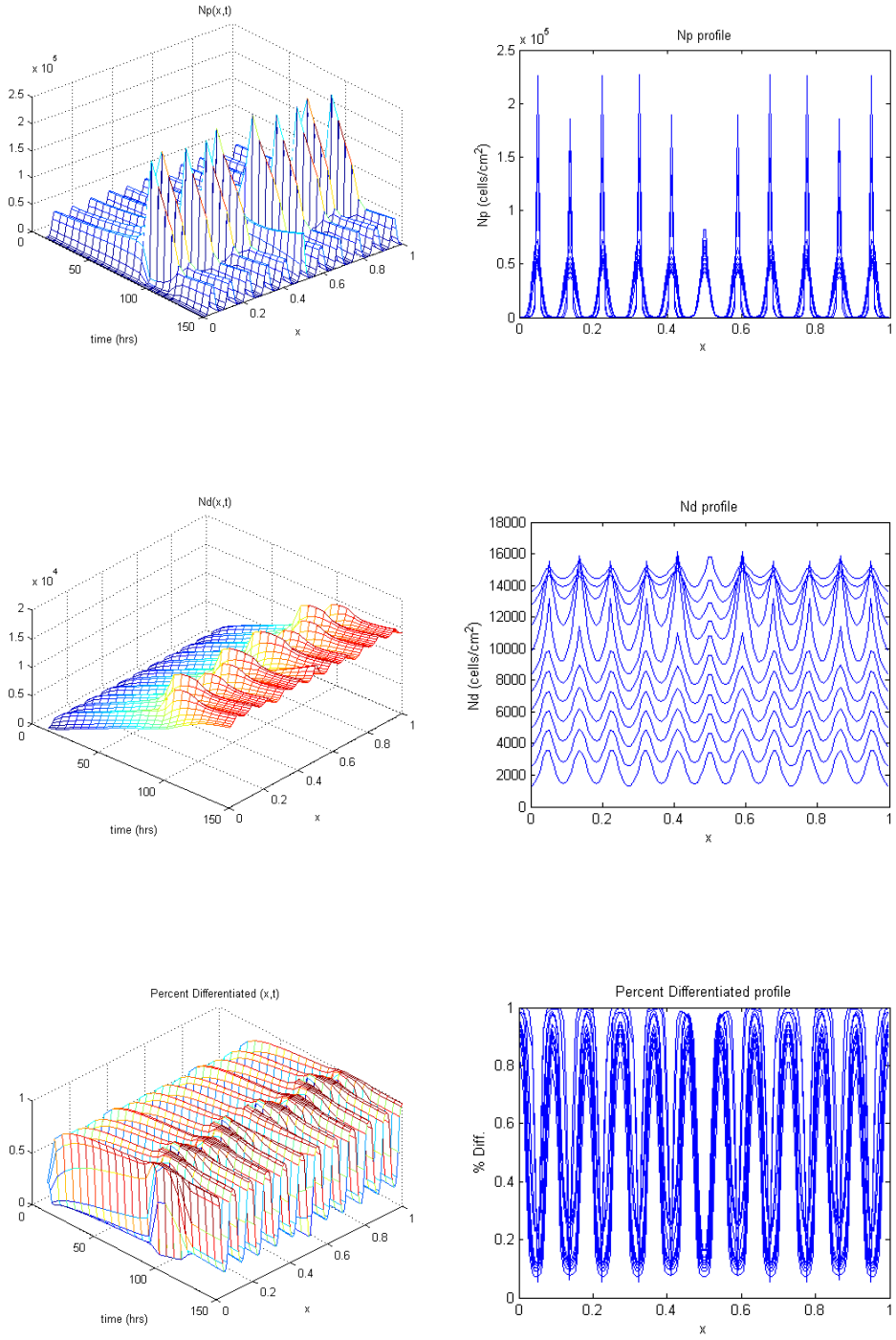

Figure 6.6 *(left) Time evolution of profile, every 6 hrs, strong constant chemotaxis ($\chi_0 = 1e+5$). (right) Profiles taken every 12 hrs to show densities in different regions.*

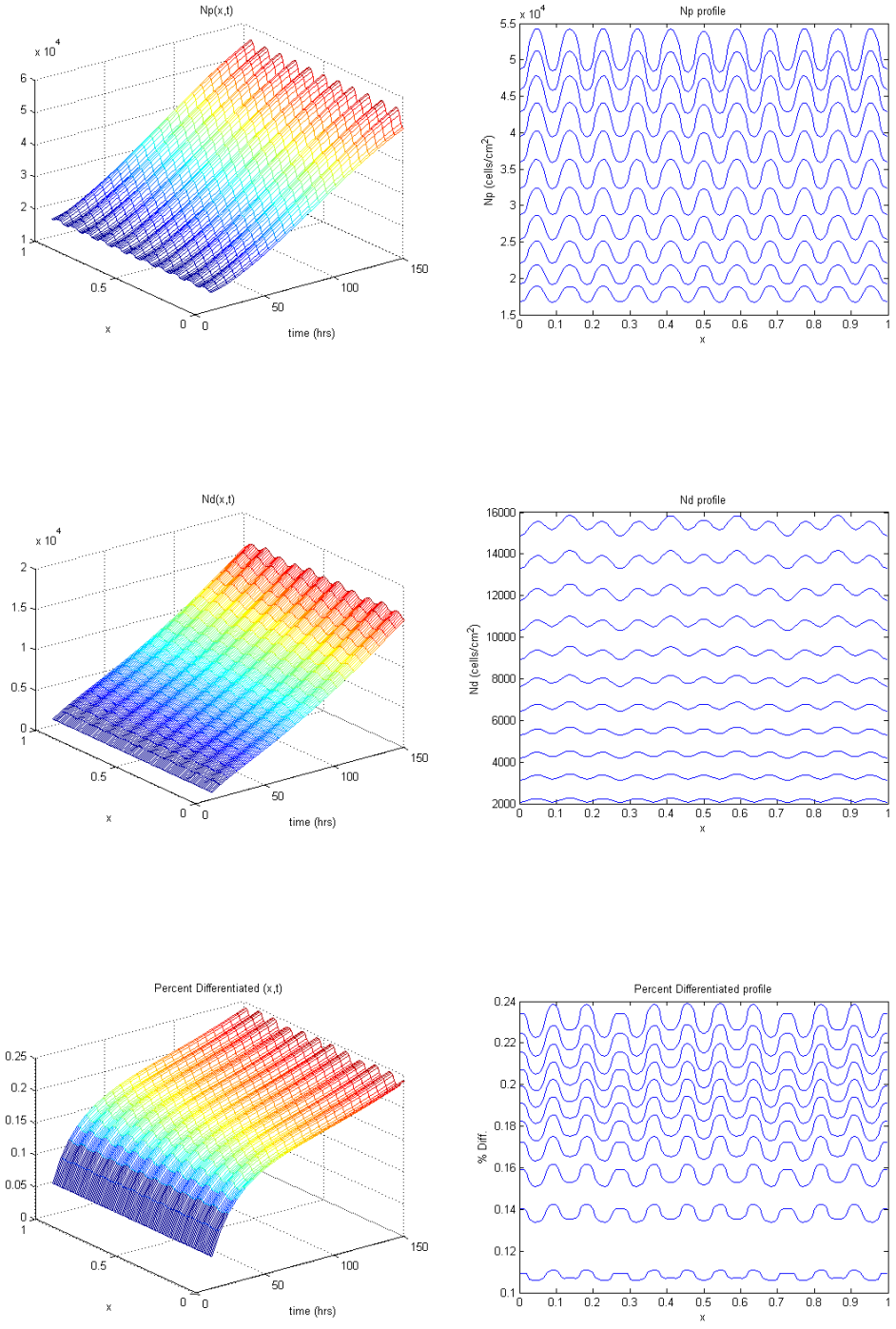

Figure 6.7 *(left) Time evolution of profile, every 6 hours, weak saturable chemotaxis ($\chi_0 = 1e+3$) up IL6 gradients. (right) Proflies taken every 12 hours to show densities in different regions.*

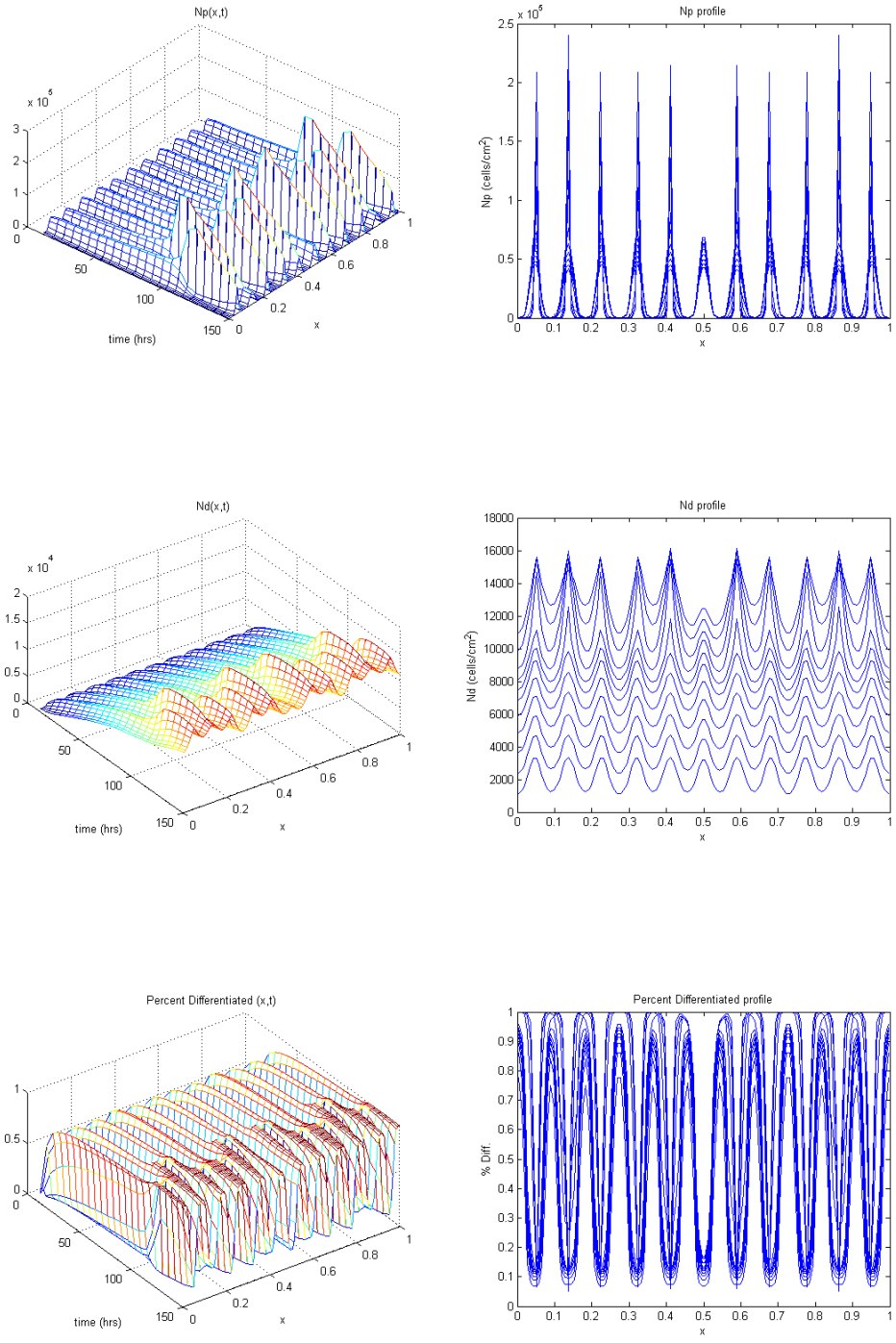

Figure 6.8 *(left) Time evolution of profile, every 6 hours, strong saturable chemotaxis ($\chi_0 = 1e+5$) up IL6 gradients. (right) Proflies taken every 12 hours to show densities in different regions.*

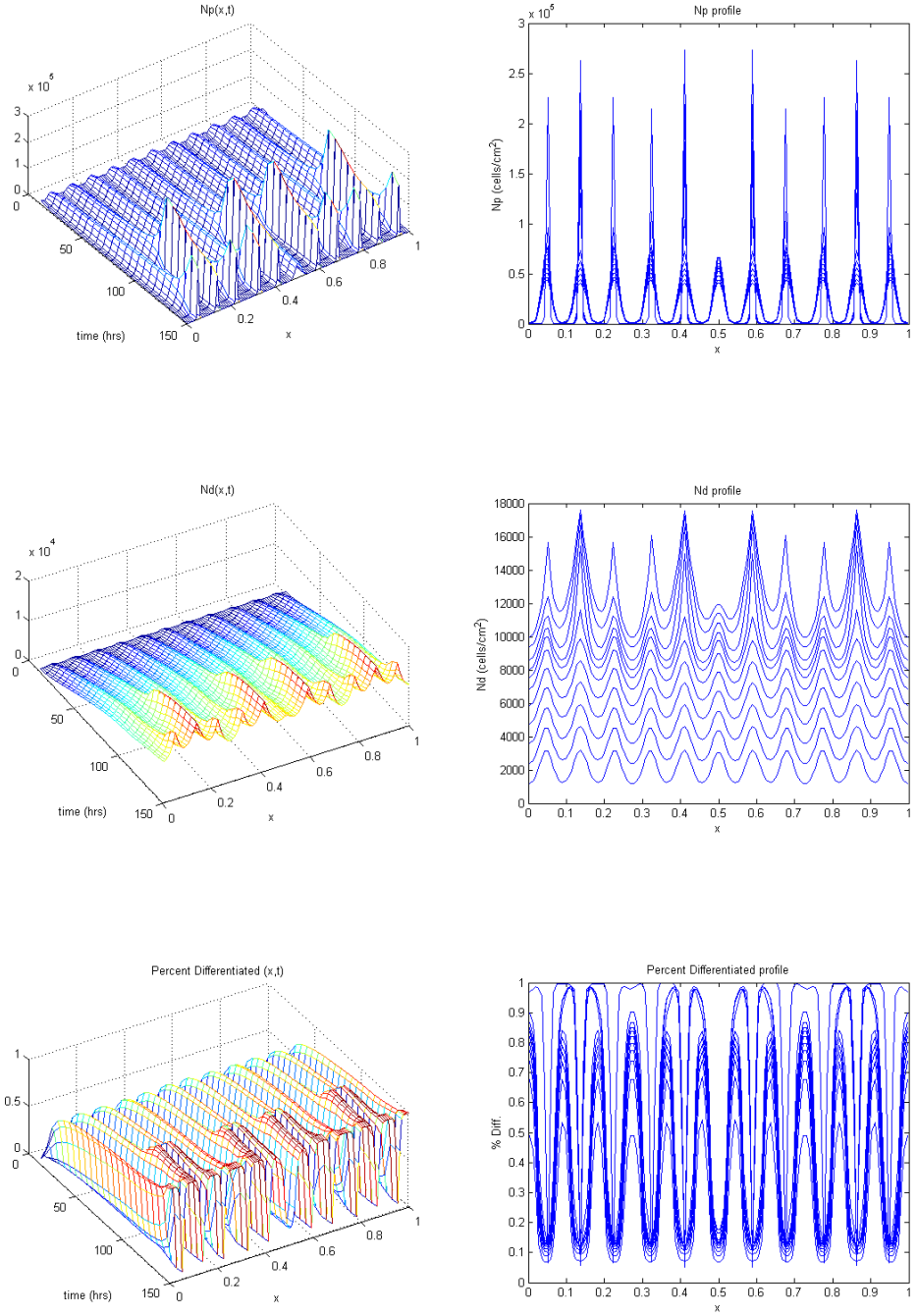

Figure 6.9 *(left) Time evolution of profile, every 6 hours, strong saturable chemotaxis ($\chi_0 = 1e+5$) up IL6 gradients, but higher concentrations of IL6 needed for strong effect to become apparent. (right) Proflies taken every 12 hours to show densities in different regions.*

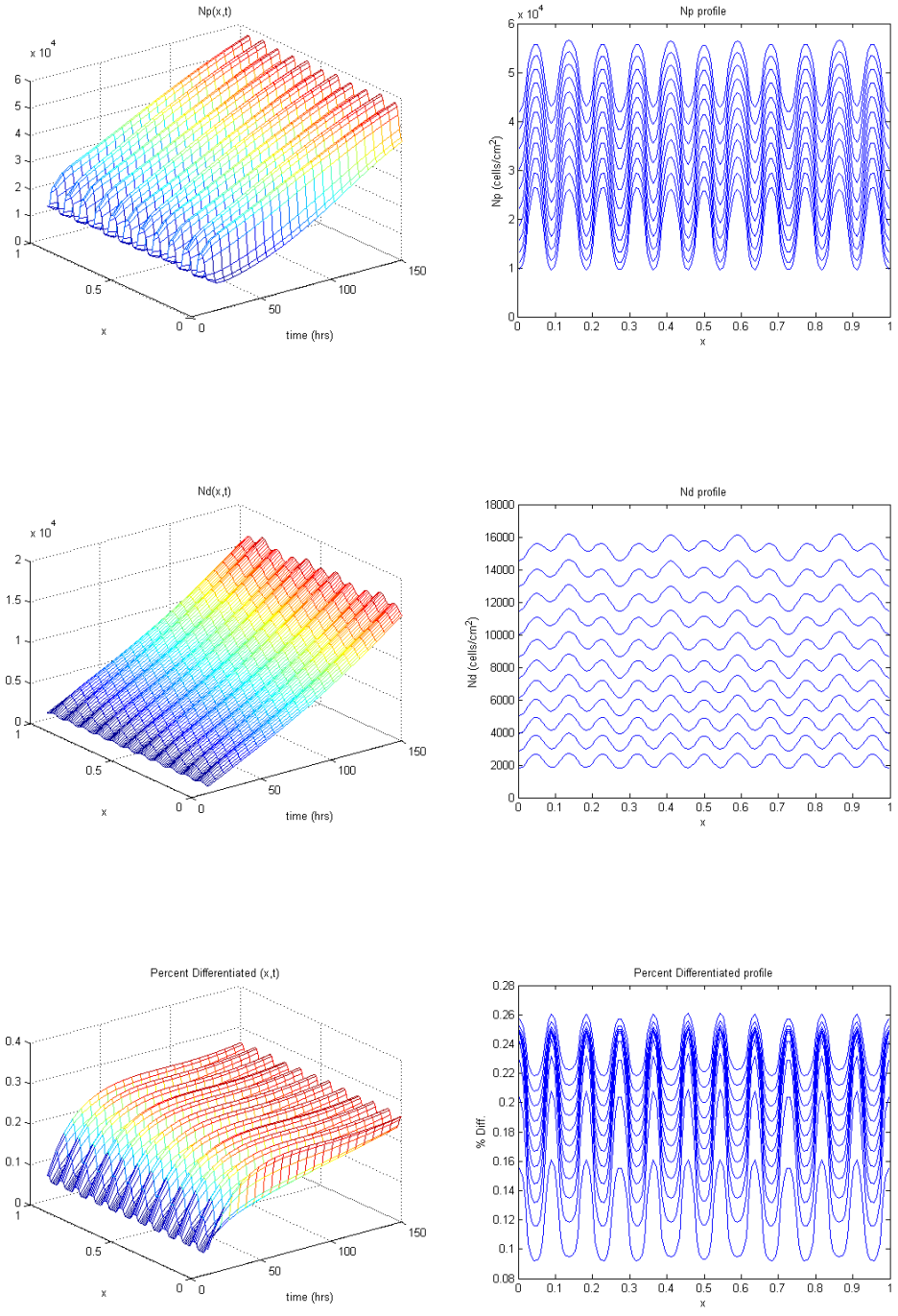

Figure 6.10 *(left) Time evolution of profile, every 6 hours, variable diffusion with moderate constant chemotaxis ($\chi_0 = 1e+4$) up IL6 gradients. (right) Proflies taken every 12 hours to show densities in different regions.*

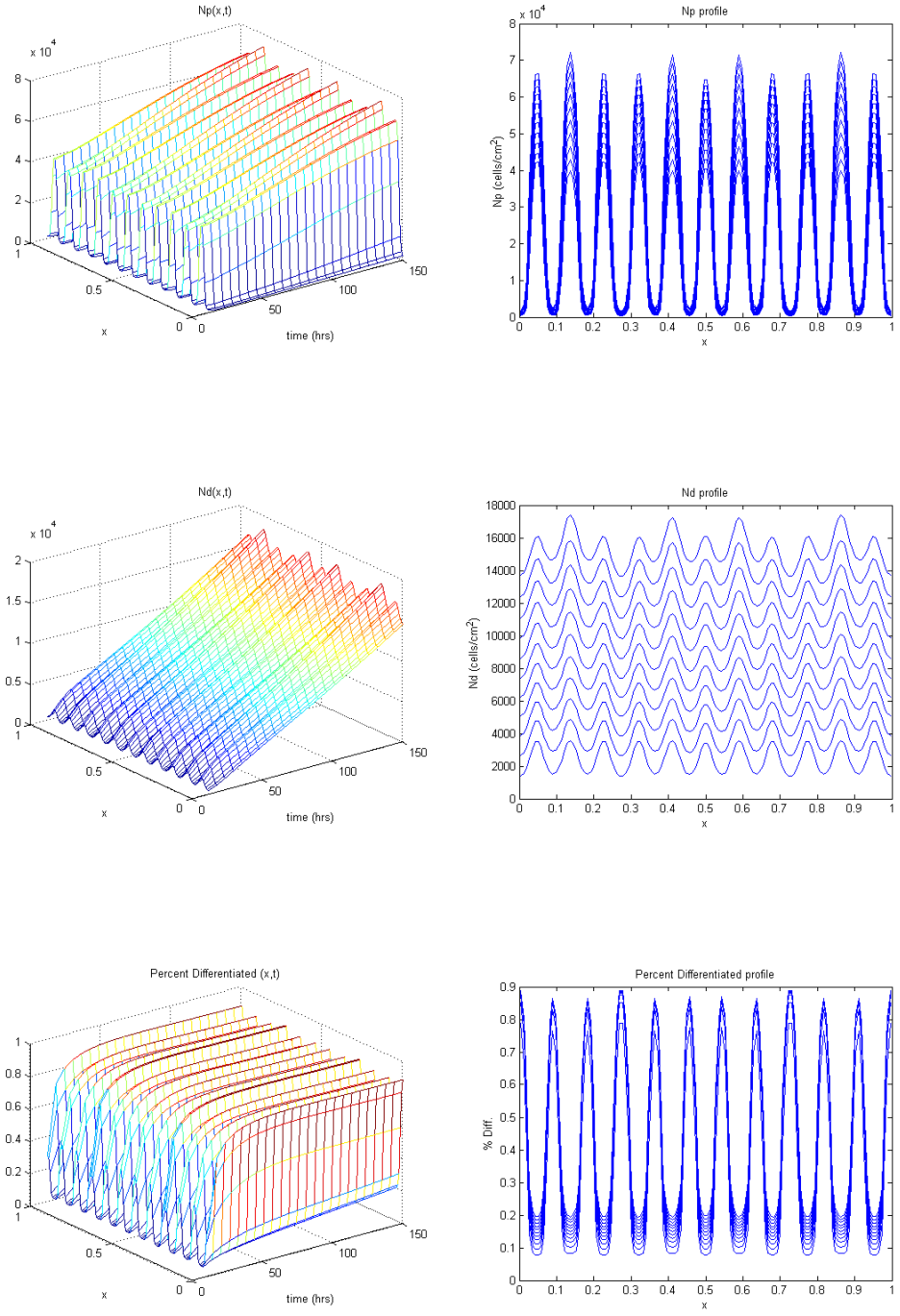

Figure 6.11 *(left) Time evolution of profile, every 6 hours, variable diffusion with strong constant chemotaxis ($\chi_0 = 1e+5$) up IL6 gradients. (right) Proflies taken every 12 hours to show densities in different regions.*

CHAPTER 7. Numerical Methods for the Spatial Model

This chapter includes brief descriptions of the numerical methods used for performing the simulations for the PDE system presented in Chapter 6. The solution to the PDE system was numerically approximated by using a Finite Volume approach as discussed in [50]. In the case where the diffusion coefficients were constant, the resultant system was solved using an efficient Fast Fourier Transform (FFT) method as discussed in [51]-[52]. In the case where the diffusion coefficients were variable, exhibiting a dependence on the species that is diffusing (a quorum-sensing mechanism), the PDE was numerically approximated using an Iterative Alternating Direction Implicit (ADI) Method discussed below. Issues such as stability and convergence are not discussed here; the reader is referred to the original publications for details. All PDE simulations were performed with Fortran 90.

7.1 Characteristics and Transport

Partial differential equations involving advection can usually be studied by looking at their *characteristic* curves. In physical applications, the characteristic curves correspond to the curves along which "material" flows or is transported. To see this, consider the first-order PDE $a(x,t)u_x + b(x,t)u_t + c(x,t)u = 0$. The characteristic curves satisfy

$$\frac{dx}{ds} = a(x,t)$$
$$\frac{dt}{ds} = b(x,t).$$

Solving this system yields the parametrically-defined curve $\{(x(s), t(s)) : 0 < s < \infty\}$. Along this curve,

$$\begin{aligned}\frac{du}{ds} &= \frac{\partial u}{\partial x}\frac{dx}{ds} + \frac{\partial u}{\partial t}\frac{dt}{ds} \\ &= a(x,t)u_x + b(x,t)u_t \\ &= -c(x,t)u.\end{aligned}$$

Letting $v(s) = u(x(s), t(s))$, we see that this is equivalent to the ODE $\dfrac{dv}{ds} = -c(s)v$. That is, the PDE is simplified to an ODE along the characteristic curve. Hence along this curve we are only looking at how $u(x(0), t(0))$ changes; this "material" is being transported along the curve. For a concrete example, consider the PDE $u_t + Vu_x = 0$ with initial condition $u(x, 0) = \phi(x)$. The characteristics are defined by

$$\begin{aligned}\frac{dt}{d\tau} &= 1, \qquad t(0) = 0 \\ \frac{dx}{d\tau} &= V, \qquad x(0) = \xi\end{aligned}$$

which has solutions $t = \tau$ and $x = v\tau + \xi$. Our new coordinates are $\xi = x - Vt$ and $\tau = t$. Letting $w(\tau) = u(x(\tau), t(\tau))$, we get

$$\begin{aligned}\frac{dw}{d\tau} &= 0 \\ w(0) &= \phi(\xi)\end{aligned}$$

which has the solution $w(\tau) = \phi(\xi)$, or equivalently, $u(x, t) = \phi(x - Vt)$. Hence $\phi(x)$ is a profile that remains constant as it travels along the characteristics.

The characteristic variables can be interpreted as a new coordinate system that varies with time. One analogy is to think of a chemical being dumped in a river. It's concentration $u(x, t)$ could be measured with a fixed coordinate system relating to the river bank. Alternatively, we could let the coordinate system "flow" along with the river and measure the concentration of the chemical with respect to this system. Consider the reaction-convection equation $u_t = Du_{xx} - Vu_x$ for constant V. The characteristics associated with $u_t + Vu_x$ are provided above. The change of variable $\xi = x - Vt$, $\tau = t$ transforms $u_t = Du_{xx} - Vu_x$ into $u_\tau = Du_{\xi\xi}$. With

respect to the river example, this says that the chemical is diffusing (in new coordinates) as it is moving downstream (along the characteristics, the new coordinate system).

In summary, mathematically the characteristics are simply a change of variables. Within the new coordinate system the PDE takes a simpler form, and the new coordinates themselves have an important physical interpretation relating to transport of material along specific curves. This presentation is based on material in [18]. For a more thorough discussion of charactersitics and their applications to partial differential equations, see [19].

7.2 Finite Volume Methods

We would like to approximate the solution $u(x, y, t)$ of a PDE over a specific spatial domain, in our case a square section of the experimental plate. To accomplish this, we first cover the domain with a uniform grid, so that the distance between consecutive grid points in the horizontal direction is Δx and the distance between consecutive grid points in the vertical direction is Δy. This grid can now be viewed in two (related) ways. First, one could approximate $u(x, y, t)$ by discretizing the derivatives in the PDE and using these to approximate the values of u at the lattice points at discrete times. For example, the PDE $u_t = D\Delta u$ could be discretized as

$$\frac{u_{i,j}^{n+1} - u_{i,j}^{n}}{\Delta t} = D\Big[\frac{u_{i+1,j}^{n} - 2u_{i,j}^{n} + u_{i-1,j}^{n}}{\Delta x^2} + \frac{u_{i,j+1}^{n} - 2u_{i,j}^{n} + u_{i,j-1}^{n}}{\Delta y^2}\Big]$$

where $u_{i,j}^{n} \approx u(x_i, y_j, t_n) = u(x_0 + i\Delta x, y_0 + j\Delta y, n\Delta t)$, with (x_0, y_0) being the lower left corner point of the above grid. These approximations are typically classified as *Finite Difference Methods*.

The other viewpoint considers the rectangular regions formed by the grid (*cells*) and approximates the average value of $u(x, y, t)$ within each cell at discrete times. These methods are referred to as *Finite Volume Methods*. The average value of $u(x, y, t)$ within the cell $[x_i, x_{i+1}] \times [y_j, y_{j+1}]$ at time t_n is $U_{i,j}^{n} = \dfrac{1}{\Delta x \Delta y}\displaystyle\int_{y_j}^{y_{j+1}}\int_{x_i}^{x_{i+1}} u(x, y, t_n)dxdy$. This quantity is also an approximation to the value of $u(x, y, t_n)$ at the midpoint of the cell. Finite Volume Methods are useful for PDEs involving advection through application of the divergence theorem. For example, consider the PDE $u_t = \nabla \cdot f(u)$, and let $R_{i,j} = [x_i, x_{i+1}] \times [y_j, y_{j+1}]$. We

can first integrate the PDE with respect to time to get

$$u(x,y,t_{n+1}) = u(x,y,t_n) + \int_{t_n}^{t_{n+1}} \nabla \cdot f(u) dt.$$

We now integrate both sides of the equation over the region $R_{i,j}$ and divide by the area of $R_{i,j}$, to get

$$\frac{1}{\Delta x \Delta y} \iint_{R_{i,j}} u(x,y,t_{n+1}) dA = \frac{1}{\Delta x \Delta y} \iint_{R_{i,j}} u(x,y,t_n) dA + \frac{1}{\Delta x \Delta y} \iint_{R_{i,j}} \int_{t_n}^{t_{n+1}} \nabla \cdot f(u) dt dA,$$

or equivalently,

$$U_{i,j}^{n+1} = U_{i,j}^n + \frac{1}{\Delta x \Delta y} \iint_{R_{i,j}} \int_{t_n}^{t_{n+1}} \nabla \cdot f(u) dt dA.$$

In our applications, f will be continuous with respect to x, y, and t within $R_{i,j}$, allowing us to interchange the order of integration in the final integral. Applying the divergence theorem,

$$U_{i,j}^{n+1} = U_{i,j}^n + \int_{t_n}^{t_{n+1}} \Big[\frac{1}{\Delta x \Delta y} \int_{\partial R_{i,j}} f(u) \cdot \nu dS \Big] dt$$

where ν is the outward unit normal vector on the boundary of $R_{i,j}$ ($\partial R_{i,j}$). We can then use any number of methods to approximate the final integral, completing the derivation of the finite volume scheme.

7.3 A Finite Volume Scheme for the PDE System

The cellular equations in our model may include advection and are of the form

$$u_t + \nabla \cdot (u \nabla \xi(v)) = \nabla \cdot (\kappa \nabla u) + g(u,v,x,y,t).$$

For now we assume κ is constant. This equation is a good candidate for a finite volume approximation due to the presence of the term $\nabla \cdot (u \nabla \xi(v))$. A finite volume scheme has been derived in [50] for this type of equation, using properties of the characteristics to approximate the left-hand side of the PDE. The following is simply a restatement of this method's derivation, and is provided in [50].

First form a mesh over the rectangular domain $[0,1] \times [0,1]$ as specified above, with M_x subintervals in the x direction and M_y subintervals in the y direction. There are then $M_x \times M_y$

cells covering the domain. Choose the mesh so that each cell has dimensions $\Delta x \times \Delta y = \frac{1}{M_x} \times \frac{1}{M_y}$. The sides of each cell are given by the coordinates $x_i = i\Delta x$ and $y_j = j\Delta y$ for $i = 0, 1, ..., M_x$ and $j = 0, 1, ..., M_y$. Label each cell $R_{i,j} = [x_{i-1}, x_i] \times [y_{j-1}, y_j]$, and denote the midpoints of these cells by $(\bar{x_i}, \bar{y_j})$ for $i = 1, 2, ..., M_x$ and $j = 1, 2, ..., M_y$. We are interested in advective transport to $(\alpha, \beta) \in R_{i,j}$ at time t_{n+1} for some i, j. The characteristic curves associated with the left side of the equation are defined by

$$\frac{dx}{dt} = \xi_x(x, y, t), \quad x(t_{n+1}) = \alpha, \qquad \frac{dy}{dt} = \xi_y(x, y, t), \quad y(t_{n+1}) = \beta.$$

These characteristics can be found for any $(\alpha, \beta) \in R_{i,j}$, yielding a characteristic preimage $\widehat{R}_{i,j}(t_n)$ that gets mapped to $R_{i,j}$ in Δt under the flow of this ODE system.

Noting that $u_t + \nabla \cdot (u\nabla\xi(v)) =< \partial_x, \partial_y, \partial_t > \cdot < u\xi_x, u_{\xi y}, u >$, we integrate the PDE over the solid volume $Q_{i,j}^{n+1} = \{(x, y, t) : (x, y) \in \widehat{R}_{i,j}(t), t \in [t_n, t_{n+1}]\}$ to derive our scheme.

$$\begin{aligned}
\iiint_{Q_{i,j}^{n+1}} (\nabla \cdot (\kappa\nabla u) + g)dV &= \iiint_{Q_{i,j}^{n+1}} < \partial_x, \partial_y, \partial_t > \cdot < u\xi_x, u_{\xi y}, u > dV \\
&= \iint_{\partial Q_{i,j}^{n+1}} u < \xi_x, \xi_y, 1 > \cdot \nu dS \\
&= \iint_{R_{i,j}} u(x, y, t_{n+1})dA - \iint_{\widehat{R}_{i,j}(t_n)} u(x, y, t_n)dA
\end{aligned}$$

Note that by using the characteristic curves to sweep out the region $Q_{i,j}^{n+1}$ we are integrating over, $< \xi_x, \xi_y, 1 > \cdot \nu = 0$ along the sides of $Q_{i,j}^{n+1}$. This is due to $< \xi_x, \xi_y, 1 >$ being tangent to these surfaces and $T \cdot n = 0$ for every tangent and normal vector along the surface. Meanwhile, the normal vector along $R_{i,j}$ is $< 0, 0, 1 >$ and the normal vector along $\widehat{R}_{i,j}(t_n)$ is $< 0, 0, -1 >$, leading to the final equality.

Note that $\iint_{R_{i,j}} u(x, y, t_{n+1})dA \approx U_{i,j}^{n+1}\Delta x\Delta y$. To calculate $\iint_{\widehat{R}_{i,j}(t_n)} u(x, y, t_n)dA$, we need to be able to approximate the location of the characteristic preimage. We assume for this method that $D_{k,m}^{i,j} = \widehat{R}_{i,j}(t, n) \cap R_{i+k,j+m} = \emptyset$ for $|k| > 1$ and $|m| > 1$; that is, all portions of $\widehat{R}_{i,j}(t_n)$ lie within either $R_{i,j}$ or cells adjacent to it. Denoting the area of $D_{k,m}^{i,j}$ by $|D_{k,m}^{i,j}|$, we have that $\iint_{\widehat{R}_{i,j}(t_n)} u(x, y, t_n)dA \approx \sum_{k,m=-1}^{1} U_{i+k,j+m}^{n} |D_{k,m}^{i,j}|$. This sum can be approximated using the following equations, appropriately modified for boundary cells when either no-flux

or periodic boundary conditions are present. The details of the derivation are provided in [50].

$$\theta^x_{i,j} = \frac{-\Delta t}{\Delta x}\Big(\frac{\xi(v^{n+1}_{i+1,j}) + \xi(v^{n+1}_{i,j})}{2}\Big)\Big(\frac{v^{n+1}_{i+1,j} - v^{n+1}_{i,j}}{\Delta x}\Big)$$
$$\theta^y_{i,j} = \frac{-\Delta t}{\Delta x}\Big(\frac{\xi(v^{n+1}_{i,j+1}) + \xi(v^{n+1}_{i,j})}{2}\Big)\Big(\frac{v^{n+1}_{i,j+1} - v^{n+1}_{i,j}}{\Delta y}\Big)$$

$$a_{i,j} = \min\{0, \theta^x_{i,j}\}, \qquad A_{i,j} = \max\{0, \theta^x_{i,j}\}$$

$$b_{i,j} = \min\{0, \theta^y_{i,j}\}, \qquad B_{i,j} = \max\{0, \theta^y_{i,j}\}$$

$$S^{ab}_{i,j} = a_{i,j}b_{i,j}, \qquad S^{aB}_{i,j} = a_{i,j}B_{i,j-1}, \qquad S^{Ab}_{i,j} = A_{i-1,j}b_{i,j}, \qquad S^{AB}_{i,j} = A_{i-1,j}B_{i,j-1}$$

$$E^{x,n}_{i,j} = a_{i,j}U^n_{i,j} + A_{i,j}U^n_{i+1,j}, \qquad E^{y,n}_{i,j} = b_{i,j}U^n_{i,j} + B^n_{i,j},$$

$$T^n_{i,j} = S^{ab}_{i,j}U^n_{i,j} + S^{aB}_{i,j+1}U^n_{i,j+1} + S^{Ab}_{i+1,j}U^n_{i+1,j} + S^{AB}_{i+1,j+1}U^n_{i+1,j+1}$$

With these definitions, we define $C_{i,j}(\{V^{n+1}\}, \{U^n\}) \approx \sum_{k,m=-1}^{1} U^n_{i+k,j+m}|D^{i,j}_{k,m}|$ by

$$\begin{aligned} C_{i,j}(\{V^{n+1}\}, \{U^n\}) &= \sum_{k,m=-1}^{1} M^{i,j}_{k,m}U^n_{i+k,j+m} \\ &= U^n_{i,j} + E^{x,n}_{i,j} - E^{x,n}_{i-1,j} + E^{y,n}_{i,j} - E^{y,n}_{i,j-1} + T^n_{i,j} - T^n_{i,j-1} - T^n_{i-1,j} + T^n_{i-1,j-1}. \end{aligned}$$

We still must approximate one more integral, $\iiint_{Q^{n+1}_{i,j}} (\nabla\cdot(\kappa\nabla u) + g)dV$. We can approximate the reaction term for the sinks and sources by $\iiint_{Q^{n+1}_{i,j}} g dV \approx g(U^{n+1}_{i,j}, V^{n+1}_{i,j}, \bar{x}_i, \bar{y}_j, t_{n+1})\Delta x\Delta y\Delta t$. The remaining integral can be approximated via the divergence theorem to get

$$\begin{aligned} \iiint_{Q^{n+1}_{i,j}} \nabla\cdot(\kappa\nabla u)dV &\approx \Delta t \iint_{R_{i,j}} \nabla\cdot(\kappa\nabla u)|_{t_{n+1}} dA \\ &= \Delta t \int_{\partial R_{i,j}} \kappa\nabla u|_{t_{n+1}} \cdot \nu dS \\ &\approx \kappa\Delta t\Big\{\Big[\frac{U^{n+1}_{i,j} - U^{n+1}_{i,j-1}}{\Delta y}\Big]\cdot(-1)\cdot\Delta x + \Big[\frac{U^{n+1}_{i+1,j} - U^{n+1}_{i,j}}{\Delta x}\Big]\cdot(1)\cdot\Delta y \\ &\quad + \Big[\frac{U^{n+1}_{i,j+1} - U^{n+1}_{i,j}}{\Delta y}\Big]\cdot(1)\cdot\Delta x + \Big[\frac{U^{n+1}_{i,j} - U^{n+1}_{i-1,j}}{\Delta x}\Big]\cdot(-1)\cdot\Delta y\Big\} \\ &= \frac{\kappa\Delta t\Delta x\Delta y}{\Delta y^2}(U^{n+1}_{i,j-1} - 2U^{n+1}_{i,j} + U^{n+1}_{i,j+1}) \\ &\quad + \frac{\kappa\Delta t\Delta x\Delta y}{\Delta x^2}(U^{n+1}_{i-1,j} - 2U^{n+1}_{i,j} + U^{n+1}_{i+1,j}). \end{aligned}$$

Letting $r_x = \dfrac{\kappa\Delta t}{(\Delta x)^2}$ and $r_y = \dfrac{\kappa\Delta t}{(\Delta y)^2}$, we define

$$\Delta^\kappa_{i,j}\{U^{n+1}\} = r_x(U^{n+1}_{i-1,j} - 2U^{n+1}_{i,j} + U^{n+1}_{i+1,j}) + r_y(U^{n+1}_{i,j-1} - 2U^{n+1}_{i,j} + U^{n+1}_{i,j+1}),$$

yielding the finite volume scheme

$$U_{i,j}^{n+1} = C_{i,j}(\{V^{n+1}\}, \{U^n\}) + \Delta t \Delta_{i,j}^{\kappa}\{U^{n+1}\} + \Delta t g_{i,j}^{n+1}(U_{i,j}^{n+1}, V_{i,j}^{n+1}, \bar{x}_i, \bar{y}_j, t_{n+1}).$$

7.4 FFT Method for Numerically Solving the Finite Volume Scheme for the PDE System

The system of PDEs we are dealing with is highly coupled. However, they fall into two classes:

$$u_t + \nabla \cdot (u\xi(v)\nabla v) = \nabla \cdot (\kappa \nabla u) + g(u, v, x, y, t)$$

$$v_t = \nabla \cdot (\sigma \nabla v) + f(u, v, x, y, t)$$

over a two-dimensional bounded rectangular domain Ω. All equations satisfy no-flux boundary conditions on two opposing sides and periodic boundary conditions on the other two opposing sides. The solution to this system can be approximated with the scheme

$$u_{i,j}^{n+1} = C_{i,j}(\{v^{n+1}\}, \{u^n\}) + \Delta t \Delta_{i,j}^{\kappa}\{u^{n+1}\} + \Delta t g_{i,j}^{n+1}(u_{i,j}^{n+1}, v_{i,j}^{n+1})$$

$$v_{i,j}^{n+1} = v_{i,j}^{n} + \Delta t \Delta_{i,j}^{\sigma}\{v^{n+1}\} + \Delta t f_{i,j}^{n+1}(u_{i,j}^{n+1}, v_{i,j}^{n+1}),$$

through the use of the finite volume method provided above. At the core of this implicit method lies the approximation of a two-dimensional Poisson equation $-\nabla \cdot (\kappa \nabla u) = g$, due to the diffusion term. (The advection portion of the PDE yielded an explicit quantity, based on the previous timestep, and therefore casues no additional difficulty.) An efficient method for approximating this system is provided in [51], with details on its implementation provided in [52] and [55]. The following is simply a restatement of this method's derivation as provided in [51], with slight alterations due to the differing boundary conditions.

Assuming κ is constant, $-\kappa \Delta u = g$. Using a five-point stencil, the equation $-\kappa \Delta u = g$ can be discretized as

$$-\Big[\frac{\kappa}{\Delta x^2}(u_{i+i,j} - 2u_{i,j} + u_{i-1,j}) + \frac{\kappa}{\Delta y^2}(u_{i,j+1} - 2u_{i,j} + u_{i,j-1})\Big] = g_{i,j}.$$

Note that this is just $\Delta_{i,j}^{\kappa}\{u\}$ as defined above. Column vectors u and g can be formed by evaluating $u(x, y)$ and $g(x, y)$ at the cell centers and then placing the entries corresponding

to $(\bar{x}_i, \bar{y}_j)$ at the $i + (j-1)M_\alpha$ position of the vector. Let $N = M_\alpha M_\beta$. The $N \times N$ matrix satisfying $Au = g$ is a tridiagonal block matrix derived from the discretization. The matrices associated with the stencil are

$$\widetilde{P}_\alpha = \frac{\kappa}{\Delta x^2} \begin{bmatrix} 2 & -1 & & & 1 \\ -1 & 2 & -1 & & \\ & \ddots & \ddots & \ddots & \\ & & -1 & 2 & -1 \\ 1 & & & -1 & 2 \end{bmatrix},$$

a $M_\alpha \times M_\alpha$ matrix corresponding to the periodic boundary conditions, and

$$\widetilde{N}_\beta = \frac{\kappa}{\Delta y^2} \begin{bmatrix} 1 & -1 & & & \\ -1 & 2 & -1 & & \\ & \ddots & \ddots & \ddots & \\ & & -1 & 2 & -1 \\ & & & -1 & 1 \end{bmatrix},$$

a $M_\beta \times M_\beta$ matrix corresponding to the no-flux boundary conditions. Define $\widetilde{r_x} = \dfrac{r_x}{\Delta t}$ and $\widetilde{r_y} = \dfrac{r_y}{\Delta t}$. The matrix A has the form

$$A = \begin{bmatrix} \widetilde{r_y} I_\alpha + \widetilde{P}_\alpha & -\widetilde{r_y} I_\alpha & & & \\ -\widetilde{r_y} I_\alpha & 2\widetilde{r_y} I_\alpha + \widetilde{P}_\alpha & -\widetilde{r_y} I_\alpha & & \\ & \ddots & \ddots & \ddots & \\ & & -\widetilde{r_y} I_\alpha & 2\widetilde{r_y} I_\alpha + \widetilde{P}_\alpha & -\widetilde{r_y} I_\alpha \\ & & & -\widetilde{r_y} I_\alpha & \widetilde{P}_\alpha \end{bmatrix}.$$

Using Kronecker Products (discussed in [16]), we can write

$$A = \left[\left(I_\beta \otimes \widetilde{P}_\alpha \right) + \left(N_\beta \otimes (\widetilde{r_y} I_\alpha) \right) \right]$$

or equivalently,

$$A = \left[\frac{\kappa}{\Delta x^2} (I_\beta \otimes P_\alpha) + \frac{\kappa}{\Delta y^2} (N_\beta \otimes I_\alpha) \right]$$

where $\widetilde{P}_\alpha = \dfrac{\kappa}{\Delta x^2} P_\alpha$, I_z is the identity matrix of dimensions $M_z \times M_z$, and $\widetilde{N}_\beta = \dfrac{\kappa}{\Delta y^2} N_\beta$. The properties of Kronecker products used above are

$$(A \otimes B) = \begin{bmatrix} a_{11}B & \cdots & a_{1n}B \\ \vdots & \ddots & \vdots \\ a_{n1}B & \cdots & a_{nn}B \end{bmatrix}$$

and

$$(kA) \otimes B = A \otimes (kB) = k(A \otimes B).$$

Define the components of the $n \times n$ FFT matrix by $[F_n]_{r,q} = \omega_n^{r,q} = exp(-2\pi(r-1)(q-1)i/n)$. Then $F_n^{-1} = \frac{1}{n}\bar{F}_n$ and $F_n^T = F_n$. In [4] it is shown that with this definition of F_n, $F_n P_n F_n^{-1} = \Lambda_n^{(P)}$ where $\Lambda_n^{(P)}$ is an $n \times n$ diagonal matrix with $[\Lambda_n^{(P)}]_{ii} = 4\sin^2\left(\dfrac{(i-1)\pi}{n}\right)$. It is shown in [2] that if the matrix V_n is defined with components $[V_n]_{r,q} = \cos\left(\dfrac{(r-\frac{1}{2})(q-1)\pi}{n}\right)$, then $V_n^T N_n V_n^{-T} = \Lambda_n^{(N)}$ where $\Lambda_n^{(N)}$ is an $n \times n$ diagonal matrix with $[\Lambda_n^{(N)}]_{ii} = 4\sin^2\left(\dfrac{(i-1)\pi}{2n}\right)$.

The method for solving the system $Au = g$ presented in [51] is derived under the assumption of no-flux boundary conditions on all sides of the rectangular region Ω. However, in our case we have two opposing sides with no-flux B.C.'s, while the other two opposing sides satisfy periodic B.C.'s. This method can be easily modified for our case. Above we have

$$\Big[\widetilde{r_x}(I_\beta \otimes P_\alpha) + \widetilde{r_y}(N_\beta \otimes I_\alpha)\Big]u = g.$$

Multiplying both sides by $[V_\beta^T \otimes F_\alpha^T]$, and using the properties $(A \otimes B)^{-1} = (A^{-1}) \otimes (B^{-1})$, $(A \otimes B)(C \otimes D) = (AC) \otimes (BD)$, and the fact that $F_n = F_n^T$, we get

$$[V_\beta^T \otimes F_\alpha^T]\Big[\widetilde{r_x}(I_\beta \otimes P_\alpha) + \widetilde{r_y}(N_\beta \otimes I_\alpha)\Big][(V_\beta^T)^{-1} \otimes (F_\alpha^T)^{-1}][V_\beta^T \otimes F_\alpha^T]u = [V_\beta^T \otimes F_\alpha^T]g$$

$$\Big[\widetilde{r_x}\Big((V_\beta^T I_\beta V_\beta^{-T}) \otimes (F_\alpha^T P_\alpha F_\alpha^{-T})\Big) + \widetilde{r_y}\Big((V_\beta^T N_\beta V_\beta^{-T}) \otimes (F_\alpha^T I_\alpha F_\alpha^{-T})\Big)\Big][V_\beta^T \otimes F_\alpha^T]u = [V_\beta^T \otimes F_\alpha^T]g$$

$$\Big[\widetilde{r_x}(I_\beta \otimes \Lambda_\alpha^{(P)}) + \widetilde{r_y}(\Lambda_\beta^{(N)} \otimes I_\alpha)\Big][V_\beta^T \otimes F_\alpha^T]u = [V_\beta^T \otimes F_\alpha^T]g$$

Defining $f = [V_\beta^T \otimes F_\alpha^T]g$ and $w = [V_\beta^T \otimes F_\alpha^T]u$, we get the diagonal system

$$\Big[\widetilde{r_x}(I_\beta \otimes \Lambda_\alpha^{(P)}) + \widetilde{r_y}(\Lambda_\beta^{(N)} \otimes I_\alpha)\Big]w = f.$$

Finally, it is shown in [51]-[52] that if the vectors are converted to matrices by the relation $z_{i+(j-1)M_\alpha} = [z_{\alpha\times\beta}]_{i,j}$, then this system is equivalent to $\widetilde{r_x}\Lambda_\alpha^{(P)} w_{\alpha\times\beta} + \widetilde{r_y} w_{\alpha\times\beta}\Lambda_\beta^{(N)} = f_{\alpha\times\beta}$, which can easily be solved to obtain

$$(w_{\alpha\times\beta})_{i,j} = \frac{(f_{\alpha\times\beta})_{i,j}}{\widetilde{r_x}\lambda_i^{(P)} + \widetilde{r_y}\lambda_j^{(N)}}.$$

Efficient algorithms for performing these computations are provided in [52] and [55].

To solve the full system, we need to advance from the values of the current time step, $\{u^n\}$ for each cell type and $\{v^n\}$ for each soluble molecule, to the next time step, $\{u^{n+1}\}$ and $\{v^{n+1}\}$. Due to the coupling of the equations within the implicit numerical scheme, it is most convenient to solve the system through iteration. For each time step, we have a system of the form $F(u,v) = 0$, $G(u,v) = 0$ where $F(u,v) = M^\sigma v - \Delta t f(u,f) - h$ and $G(u,v) = M^\kappa u - \Delta g(u,v) - C(v)$. Our matrices M^σ and M^κ are defined by

$$M^\sigma = I + \sigma\Delta t[\frac{1}{\Delta x^2}(I_\beta \otimes P_\alpha) + \frac{1}{\Delta y^2}(N_\beta \otimes I_\alpha)]$$
$$M^\kappa = I + \kappa\Delta t[\frac{1}{\Delta x^2}(I_\beta \otimes P_\alpha) + \frac{1}{\Delta y^2}(N_\beta \otimes I_\alpha)]$$

and have eigenvalues

$$\lambda_{i,j}^{(\sigma)} = 1 + \Delta t\Big(\frac{\sigma}{\Delta x^2}\lambda_i^{(P)} + \frac{\sigma}{\Delta y^2}\lambda_j^{(N)}\Big)$$
$$\lambda_{i,j}^{(\kappa)} = 1 + \Delta t\Big(\frac{\kappa}{\Delta x^2}\lambda_i^{(P)} + \frac{\kappa}{\Delta y^2}\lambda_j^{(N)}\Big).$$

In these equations, h depends on the known values of v from the previous time step, and $C(v)$ depends both on the known values of u from the previous time step and the current values of v from the new time step. We can solve this system through iteration with Newton's Method. Newton's Method in this case takes the form

$$x^{k+1} = x^k - [DF(x^k)]^{-1}F(x^k)$$

where $F(x^k)$ is a vector and $DF(x^k)$ is its Jacobian matrix, defined componentwise by $[DF]_{i,j} = \frac{\partial F_i}{\partial x_j}$. Note that this could also be written as $[DF(x^k)](\delta x^{k+1}) = -F(x^k)$, with $x^{k+1} = x^k +$

δx^{k+1}. To find u^{n+1} and v^{n+1}, we start with $u^{(0)} = u^n$ and sequentially solve the equations

$$F(u^{(n)}, v^{(n+1)}) = 0$$
$$G(u^{(n+1)}, v^{(n+1)}) = 0.$$

The equations for the Newton's iteration are given in [51]-[52] as

$$M^\sigma \delta v - \Delta t D^f(v^{(k)})\delta v = F(u^{(k)}, v^{(k)})$$
$$v^{(k+1)} = v^{(k)} - \delta v$$
$$M^\kappa \delta u - \Delta t D^g(u^{(k)})\delta u = G(u^{(k)}, v^{(k+1)})$$
$$u^{(k+1)} = u^{(k)} - \delta u,$$

where the Jacobian matrices $D^f(v)$ and $D^g(u)$ are diagonal $N \times N$ matrices with $[D^f(v)]_{k,k} = \dfrac{\partial f}{\partial v}(u_{i,j}^{(k)}, v_{i,j}, \bar{x}_i, \bar{y}_j, t_{n+1})$ where $k = i + (j-1)M_\alpha$ for $i = 1, ..., M_\alpha$ and $j = 1, ..., M_\beta$. $D^g(u)$ is defined analagously.

The problem now is to solve an equation of the form $Mx - Dx = Mw - b$ for unknown x, where w and b are known quantities defined explicitly through data from the previous iteration. The quantity x is the increment for one step of Newton's iteration above. To solve such a system via iteration, we consider it as $Mx^{(p+1)} - Dx^{(p)} = Mw - b$. If we let our initial approximation be $x^{(0)} = 0$, we get $x^{(1)} = w - M^{-1}b$. The next iterate can be found to be $Mx^{(2)} - Dx^{(1)} = Mw - b$, or equivalently, $Mx^{(2)} = Dx^{(1)} + Mx^{(1)}$. Since $x^{(0)} = 0$, this can be rearranged to $M(x^{(2)} - x^{(1)}) = D(x^{(1)} - x^{(0)})$. If we let $y^{(p)} = x^{(p)} - x^{(p-1)}$, this equation becomes $My^{(2)} = Dy^{(1)}$, where $y^{(1)} = x^{(1)}$ by choice of $x^{(0)}$. This is the idea behind our iterative method. To solve for the Newton iterates above, we iterate $My^{(p+1)} = Dy^{(p)}$, so that $x^{(p+1)} = x^{(p)} + y^{(p+1)}$ for $p = 1, 2, ...$ At each step, we can use the FFT method described above to solve for $y^{(p+1)}$.

7.5 An ADI Method for the Variable-Diffusion Problem

A method for discretizing the PDE

$$u_t + \nabla \cdot (u\nabla\xi) = \nabla \cdot (\kappa \nabla u) = g(u, x, y, t), \qquad (x, y) \in \Omega, \quad t > 0,$$

$$\frac{\partial u}{\partial \nu} = 0, \qquad (x,y) \in \partial\Omega, \quad t > 0,$$

utilizing a finite volume, cell-centered approach is outlined in [50]. It results in a system of the form

$$U_{i,j}^{n+1} = \sum_{k,m=-1}^{1} M_{k,m}^{i,j} U_{i+k,j+m}^{n} + \Delta_{i,j}\{U^{n+1}\} + \Delta t G_{i,j}^{n+1}$$

where

$$G_{i,j}^{n+1} = g(U_{i,j}^{n+1}, \overline{x}_i, \overline{y}_j)$$

and

$$\Delta_{i,j}\{U^{n+1}\} = r_x(U_{i-1,j}^{n+1} - 2U_{i,j}^{n+1} + U_{i+1,j}^{n+1}) + r_y(U_{i,j-1}^{n+1} - 2U_{i,j}^{n+1} + U_{i,j+1}^{n+1}),$$

with $r_x = \dfrac{\kappa\Delta t}{(\Delta x)^2}$ and $r_y = \dfrac{\kappa\Delta t}{(\Delta y)^2}$. At the core of solving this problem is a 2-dimensional Poisson equation $-\kappa\Delta u = f$ subject to Neumann boundary conditions $\frac{\partial u}{\partial \nu} = 0$ on $\partial\Omega$. The resultant $Au = \widetilde{f}$ system can be solved efficiently using the fast Fourier transform method in [51] since the matrix A has a special structure as described in [51].

We are now interested in the PDE

$$u_t + \nabla \cdot (u\nabla\xi) = \nabla \cdot (\kappa(u)\nabla u) = g(u,x,y,t), \qquad (x,y) \in \Omega, \quad t > 0,$$

$$\frac{\partial u}{\partial \nu} = 0, \qquad (x,y) \in \partial\Omega, \quad t > 0,$$

where $\kappa(u) \geq K_{min} > 0$ is an increasing, differentiable function. The finite volume approach discussed in [50] is still valid, except that we now need to approximate the integral

$$\iiint_{Q_{i,j}^{n+1}} \nabla \cdot (\kappa(u)\nabla u) dV.$$

Similarly to the constant κ case, by using implicit Euler and the divergence theorem, we get

$$\iiint_{Q_{i,j^{n+1}}} \nabla \cdot (\kappa(u)\nabla u) dV \approx \Delta t \iint_{R_{i,j}} \nabla \cdot (\kappa(u)\nabla u)|_{t_{n+1}} dA = \Delta t \int_{\partial R_{i,j}} \kappa(u)\nabla u|_{t_{n+1}} \cdot \vec{n} dS$$

$$\approx L_{i,j}\{U^{n+1}\}\Delta x \Delta y$$

where the operator $L_{i,j}\{U^{n+1}\}$ is defined by

$$L_{i,j}\{U^{n+1}\} = r_x\big[K_{i-1,j}^{n+1}U_{i-1,j}^{n+1} - (K_{i-1,j}^{n+1} + K_{i+1,j}^{n+1})U_{i,j}^{n+1} + K_{i+1,j}^{n+1}U_{i+1,j}^{n+1}\big]$$

$$+ r_y\big[K_{i,j-1}^{n+1}U_{i,j-1}^{n+1} - (K_{i,j-1}^{n+1} + K_{i,j+1}^{n+1})U_{i,j}^{n+1} + K_{i,j+1}^{n+1}U_{i,j+1}^{n+1}\big]$$

with $r_x = \dfrac{\Delta t}{(\Delta x)^2}$, $r_y = \dfrac{\Delta t}{(\Delta y)^2}$, and

$$K^{n+1}_{i-1,j} = \kappa\Big(\frac{U^{n+1}_{i-1,j} + U^{n+1}_{i,j}}{2}\Big), \qquad K^{n+1}_{i+1,j} = \kappa\Big(\frac{U^{n+1}_{i+1,j} + U^{n+1}_{i,j}}{2}\Big),$$

$$K^{n+1}_{i,j-1} = \kappa\Big(\frac{U^{n+1}_{i,j-1} + U^{n+1}_{i,j}}{2}\Big), \qquad K^{n+1}_{i,j+1} = \kappa\Big(\frac{U^{n+1}_{i,j+1} + U^{n+1}_{i,j}}{2}\Big).$$

This results in the system

$$(1) \qquad U^{n+1}_{i,j} = \sum_{k,m=-1}^{1} M^{i,j}_{k,m} U^{n}_{i+k,j+m} + L_{i,j}\{U^{n+1}\} + \Delta t G^{n+1}_{i,j}$$

where

$$G^{n+1}_{i,j} = g(U^{n+1}_{i,j}, \overline{x}_i, \overline{y}_j)$$

as before. This problem is no longer able to be solved as the constant κ case was, since the Poisson equation at the core of this problem would now be $-\nabla \cdot (\kappa(u)\nabla u) = f$ subject to Neumann boundary conditions $\frac{\partial u}{\partial \nu} = 0$ on $\partial\Omega$. The matrix A in the $Au = \widetilde{f}$ system has lost the special structure needed for an FFT method.

System (1) corresponds to a nonlinear equation of the form $A(v)v = b(v)$, where $A(v)$ denotes a pentadiagonal matrix dependent on v, and a vector $b(v)$ also dependent on v. More specifically, we have to solve the system $M(\kappa_{i,j}(v))v = \Delta t f(v) + h$, where
$h = \sum_{k,m=-1}^{1} M^{i,j}_{k,m} U^{n}_{i+k,j+m}$. $M(\kappa_{i,j}(v))$ is a $M_\alpha M_\beta \times M_\alpha M_\beta$ block triangular matrix,

$$M(\kappa_{i,j}(v)) = \begin{bmatrix} T_1 & D_1 & & & & \\ D_1 & T_2 & D_2 & & & \\ & \ddots & \ddots & \ddots & & \\ & & D_{M_\beta-2} & T_{M_\beta-1} & D_{M_\beta-1} & \\ & & & D_{M_\beta-1} & T_{M_\beta} & \end{bmatrix},$$

T_i is a triadiagonal $M_\alpha \times M_\alpha$ matrix where, with $k = (i-1)M_\alpha$.

$$T_i = \begin{bmatrix} 1+b_{k+1}+d_1 & -b_{k+1} & & & & \\ -b_{k+1} & 1+e^k_{1,2}+d_2 & -b_{k+2} & & & \\ & \ddots & \ddots & \ddots & & \\ & & -b_{k+M_\alpha-2} & 1+e^k_{M_\alpha-2,M_\alpha-1}+d_{M_\alpha-1} & -b_{k+M_\alpha-1} & \\ & & & -b_{k+M_\alpha-1} & 1+b_{k+M_\alpha-1}+d_{M_\alpha} \end{bmatrix},$$

$$b_i = r_x\kappa(\frac{v^{n+1}_{k+i}+v^{n+1}_{k+i+1}}{2}) \text{ for } i = 1, ..., M_\alpha \text{ and } k = (i-1)M_\alpha$$

$$e^k_{1,2} = b_{k+1} + b_{k+2}$$

$$c_j = r_y\kappa(\frac{v^{n+1}_j + v^{n+1}_{M_\alpha+j}}{2}) \text{ for } 1 \le j \le (M_\beta - 1)M_\alpha$$

$$c_j = 0 \text{ whenever } j < 1 \text{ or } j > (M_\beta - 1)M_\alpha$$

$$d_j = c_{k+M_\alpha+j} + c_{k-M_\alpha+j} \text{ for } j = 1, ..., M_\alpha$$

and D_i is a diagonal $M_\alpha \times M_\alpha$ matrix where

$$D_i = \begin{bmatrix} -c_{k+1} & & & & \\ & -c_{k+2} & & & \\ & & \ddots & & \\ & & & -c_{k+M_\alpha-1} & \\ & & & & -c_{k+M_\alpha} \end{bmatrix}.$$

To solve the equation $M(\kappa_{i,j}(v))v = \Delta t f(v) + h$ we will be using Newton's Method (since in the system being modelled, f will also depend on other species, all of which are being solved through Newton's Method). Define the function $F(v) = M(\kappa_{i,j}(v))v - \Delta t f(v) - h$. We are interested in finding v such that $F(v) = 0$. Newton's Method can be stated as: $v^{(k+1)} = v^{(k)} - [DF(v^{(k)})]^{-1}F(v^{(k)})$, or equivalently,

$$[DF(v^{(k)})](v^{(k+1)} - v^{(k)}) = -F(v^{(k)})$$

which is also equivalent to

$$[DF(v^{(k)})]\delta v = M(\kappa_{i,j}(v^{(k)}))v^{(k)} - \Delta t f(v^{(k)}) - h$$
$$v^{(k+1)} = v^{(k)} - \delta v$$
$$v^{(0)} = v^n$$

It is easy to see that $[DF(v^{(k)})] = M'(\kappa_{i,j}(v^{(k)}))v^{(k)} + M(\kappa_{i,j}(v^{(k)})) - \Delta t D(v^{(k)})$ where $D(v^{(k)})$ is the Jacobian matrix given in [51] and $M'(\kappa_{i,j}(v))$ is a tensor that can be viewed as a $1 \times M_\alpha M_\beta$ vector, where the i-th element is the $M_\alpha M_\beta \times M_\alpha M_\beta$ matrix

$$\frac{\partial M(\kappa_{i,j}(v^{(k)}))}{\partial v_i}.$$

Carrying out the calculations shows that

$$[DF(v^{(k)})] = M\Big(\kappa'_{i,j}(v^{(k)}) \cdot (\frac{v_i^{(k)} + v_j^{(k)}}{2})\Big) + M(\kappa_{i,j}(v^{(k)})) - I - \Delta t D(v^{(k)}).$$

Recall that a symmetric real-valued diagonally dominant matrix with nonnegative real diagonal entries is positive semi-definite. $[DF(v^{(k)})]$ is a pentadiagonal matrix that satisfies these hypotheses, provided that $\Delta t < 1/||f_v||_\infty$. We could use a preconditioned conjugate gradient method to solve this equation, or in fact any of a number of iterative methods, however we choose to solve this with an iterative ADI method. This method is chosen because the amount of work needed at each step up the iteration is only $O(n)$, and is easy to implement numerically. Each iteration involves solving a sequence of two diagonally dominant tridiagonal system of equations, which can easily be solved.

We need to solve the system

$$[M\Big(\kappa'_{i,j}(v) \cdot (\frac{v_i + v_j}{2})\Big) + M(\kappa_{i,j}(v)) - I - \Delta t D(v)]\delta v = b$$

where $b = M(\kappa_{i,j}(v))v - \Delta t f(v) - h$. Set $A = [M\Big(\kappa'_{i,j}(v) \cdot (\frac{v_i+v_j}{2})\Big) + M(\kappa_{i,j}(v)) - I - \Delta t D(v)]$. Note that A can be written as $A = M(\tilde{\kappa}_{i,j}(v)) - \Delta t D(v)$ where $\tilde{\kappa}_{i,j}(v) = v\kappa'_{i,j}(v) + \kappa_{i,j}(v)$. Split A so that $A = B + C$, where $B = \frac{1}{2}(I + D) + (\tilde{\kappa}\delta_x^2)$ and $C = \frac{1}{2}(I + D) + (\tilde{\kappa}\delta_y^2)$ where $D = -\Delta t D(v)$, $(\tilde{\kappa}\delta_x^2)$ denotes the matrix comprising only those terms of $M(\tilde{\kappa}_{i,j}(v))$ including

r_x, and $(\tilde{\kappa}\delta_y^2)$ denotes the corresponding matrix for r_y. The iterative ADI method ([22],[38]) then consists of:

$$\begin{aligned}(I+B)\delta v^{(m+1/2)} &= b + (I-C)\delta v^{(m)} \\ (I+C)\delta v^{(m+1)} &= b + (I-B)\delta v^{(m+1/2)}.\end{aligned}$$

Note that through a simple substitution this could also be written as:

$$\begin{aligned}(I+B)\delta v^{(m+1/2)} &= b + (I-C)\delta v^{(m)} \\ (I+C)\delta v^{(m+1)} &= 2\delta v^{(m+1/2)} - (I-C)\delta v^{(m)}.\end{aligned}$$

Assuming this method converges, we would like to see it converge to the solution of $A\delta v = b$.

$$\begin{aligned}(I+C)\delta v^{(m+1)} &= 2\delta v^{(m+1/2)} - (I-C)\delta v^{(m)} \\ &= 2[(I+B)^{-1}b + (I+B)^{-1}(I-C)\delta v^{(m)}] - (I-C)\delta v^{(m)} \\ (I+B)(I+C)\delta v^{(m+1)} &= 2b + 2(I-C)\delta v^{(m)} - (I+B)(I-C)\delta v^{(m)} \\ &= 2b + (I-B)(I-C)\delta v^{(m)}.\end{aligned}$$

Since the method converges by assumption, take $\delta v^{(m+1)} = \delta v^{(m)} = \delta v$.

$$\begin{aligned}(I+B)(I+C)\delta v &= 2b + (I-B)(I-C)\delta v \\ (I+B+C+BC-I+B+C-BC)\delta v &= 2b \\ (2B+2C)\delta v &= 2b \\ A\delta v &= b\end{aligned}$$

Hence provided that the method converges, it will converge to the solution. Note that the iterative method is the same as the iteration $\delta v^{(m+1)} = T\delta v^{(m)} + \tilde{b}$, where $T = (I+C)^{-1}(I+B)^{-1}(I-B)(I-C)$. For the iterative method to converge, we need the spectral radius ρ to satisfy $\rho(T) < 1$. To find conditions for T to converge, we need two results from linear algebra. Theorems 7.1 is from [22], theorem 7.2 is from [10], and some ideas in theorems 7.3 and 7.4 are based on proofs in [22].

Theorem 7.1: *The products AB and BA have the same spectrum, except possibly a zero eigenvalue:*

$$\sigma(AB) \setminus \{0\} = \sigma(BA) \setminus \{0\}.$$

Proof: Let the eigenvector $e \neq 0$ belong to the eigenvalue $\lambda \in \sigma(AB) \setminus \{0\}$; $ABe = \lambda e$. Since $\lambda e \neq 0$, $v := Be$ does not vanish. Multiplication by B yields $BABe = \lambda Be$, i.e., $BAv = \lambda v$, with $v \neq 0$. $\lambda \in \sigma(BA) \setminus \{0\}$ proves $\sigma(AB) \setminus \{0\} \subset \sigma(BA) \setminus \{0\}$. The reverse inclusion is analogous. □

Theorem 7.2: Gershgorin Circle Theorem. *Let A be an $n \times n$ matrix and R_i denote the circle in the complex plane with center a_{ii} and radius $\sum_{j=1,j\neq i}^{n} |a_{ij}|$; that is,*

$$R_i = \Big\{ z \in C \Big| |z - a_{ii}| \leq \sum_{j=1,j\neq i}^{n} |a_{ij}| \Big\},$$

where C denotes the complex plane. The eigenvalues of A are contained within $R = \bigcup_{i=1}^{n} R_i$. Moreover, the union of any k if these circles that do not intersect the remaining (n-k) contains precisely k (counting multiplicities) of the eigenvalues.

Theorem 7.3: *Define the rational function $R(x) = \dfrac{1-x}{1+x}$. Then $\sigma(R(B)) = R(\sigma(B))$ and $\sigma(R(C)) = R(\sigma(C))$.*

Proof: Consider B. The proof for C is identical. We will see below that if $\beta \in \sigma(B)$, then $\beta > 0$ under the condition that $\Delta t < \dfrac{1}{||f||_\infty}$. Hence $(I + B)$ is invertible.

Let $\mu \in R(\sigma(B))$. Then $\mu = \dfrac{1-\lambda}{1+\lambda}$ for some $\lambda \in \sigma(B)$. We want to show that $\mu I - R(B)$ is singular. Note first that $R(B)$ is well-defined, since $I + B$ is invertible.

$$\begin{aligned}
\mu I - (I+B)(I+B)^{-1} &= \frac{1-\lambda}{1+\lambda} I - (I-B)(I+B)^{-1} \\
&= \frac{1-\lambda}{1+\lambda}(I+B)(I+B)^{-1} - (I-B)(I+B)^{-1} \\
&= \Big[\frac{1-\lambda}{1+\lambda}(I+B) - (I-B)\Big](I+B)^{-1}
\end{aligned}$$

$$= \Big[\frac{1-\lambda}{1+\lambda}I + \frac{1-\lambda}{1+\lambda}B - I + B\Big](I+B)^{-1}$$
$$= \Big[\frac{1-\lambda-1-\lambda}{1+\lambda}I + \frac{1-\lambda+1+\lambda}{1+\lambda}B\Big](I+B)^{-1}$$
$$= \frac{-2}{1+\lambda}(\lambda I - B)(I+B)^{-1}.$$

Taking determinants of both sides we see that $\mu I - R(B)$ is singular since $\lambda \in \sigma(B)$. Therefore, $R(\sigma(B)) \subseteq \sigma(R(B))$.

Now let $\mu \in \sigma(R(B))$. We assume $\mu \neq -1$, since if $\mu = -1$ then $R(B)$ is not well-defined. We want to show that $\mu \in R(\sigma(B))$, i.e., show $\exists \lambda \in \sigma(B)$ such that $\mu = \frac{1-\lambda}{1+\lambda}$. Since $\mu I - (I-B)(I+B)^{-1}$ is singular, we see that all of the following are also singular:

$$\begin{aligned}[\mu(I+B) - (I-B)](I+B)^{-1} &= [\mu I + \mu B - I + B](I+B)^{-1} \\ &= [(\mu-1)I + (\mu+1)B](I+B)^{-1} \\ &= -(\mu+1)\Big[\frac{1-\mu}{\mu+1}I - B\Big](I+B)^{-1}\end{aligned}$$

Hence we have that $\lambda = \frac{1-\mu}{\mu+1} \in \sigma(B)$. A little algebra then shows that $\mu = \frac{1-\lambda}{1+\lambda}$, and therefore $\mu \in R(\sigma(B))$. Hence we have that $R(\sigma(B)) = \sigma(R(B))$. $\square$

Theorem 7.4: *If* $\Delta t < \frac{1}{||f||_\infty}$, *then the iterative ADI method described above will converge to* δv, *the solution of*

$$\Big[M\Big(\kappa'_{i,j}(v) \cdot (\frac{v_i + v_j}{2})\Big) + M(\kappa_{i,j}(v)) - I - \Delta t D(v)\Big]\delta v = M(\kappa_{i,j}(v))v - \Delta t f(v) - h.$$

Proof: We have that the method will converge provided that $\rho((I+C)^{-1}(I+B)^{-1}(I-B)(I-C)) < 1$, where ρ denotes spectral radius. By theorem 7.1, $\rho((I+C)^{-1}(I+B)^{-1}(I-B)(I-C)) = \rho((I+B)^{-1}(I-B)(I-C)(I+C)^{-1})$. Since B, C are real symmetric, they are Hermitian, and so too are $(I+B)^{-1}(I-B)$ and $(I-C)(I+C)^{-1}$. In particular, they are normal matrices, and so $\rho[(I+B)^{-1}(I-B)] = ||(I+B)^{-1}(I-B)||_2$ and $\rho[(I-C)(I+C)^{-1}] =$

$||(I-C)(I+C)^{-1}||_2$. By properties of norms and spectral radius,

$$\begin{aligned}\rho((I+B)^{-1}(I-B)(I-C)(I+C)^{-1}) &\leq ||(I+B)^{-1}(I-B)(I-C)(I+C)^{-1}||_2 \\ &\leq ||(I+B)^{-1}(I-B)||_2||(I-C)(I+C)^{-1}||_2 \\ &= \rho[(I+B)^{-1}(I-B)]\rho[(I-C)(I+C)^{-1}] \\ &= \rho[(I-B)(I+B)^{-1}]\rho[(I-C)(I+C)^{-1}].\end{aligned}$$

By theorem 7.3 we have that

$$\sigma[(I-B)(I+B)^{-1}] = \Big\{\frac{1-\beta}{1+\beta} : \beta \in \sigma(B)\Big\}$$

and

$$\sigma[(I-C)(I+C)^{-1}] = \Big\{\frac{1-\beta}{1+\beta} : \beta \in \sigma(C)\Big\}.$$

Thus we require all β to satisfy $|\frac{1-\beta}{1+\beta}| < 1$, or equivalently, $\beta > 0$.

Consider $B = \frac{1}{2}I - \frac{\Delta t}{2}D(v) + \tilde{\kappa}\delta_x^2$. Since $\kappa > 0$, $\kappa' \geq 0$, and $v \geq 0$ (see the remark below), we have that $(\tilde{\kappa}\delta_x^2)_{ii} > 0$ and $(\tilde{\kappa}\delta_x^2)_{ij} \leq 0, i \neq j$, with

$$(\tilde{\kappa}\delta_x^2)_{ii} = \sum_{j=1, j\neq i}^{n} |(\tilde{\kappa}\delta_x^2)_{ij}|.$$

By Gershgorin Circle Theorem, we have that if $\lambda \in \sigma(\tilde{\kappa}\delta_x^2)$, then $\lambda \geq 0$. We would like to guarantee the condition that if $\lambda \in \sigma(B)$, then $\lambda > 0$. Note that when adding $\frac{1}{2}I - \frac{\Delta t}{2}D(v)$ to $\tilde{\kappa}\delta_x^2$, we are only altering the diagonal element. This will shift the center of the circle for each row, but will not change its radius. If the circle is shifted to the left at all, then there is a possibility that an eigenvalue will be negative. Hence we need $\frac{1}{2} - \frac{\Delta t}{2}D(v)_{ii} > 0$ for all i, or equivalently, $\Delta t < \frac{1}{D(v)_{ii}}$ for all i. We can guarantee this if we introduce the restriction that $\Delta t < \frac{1}{||f||_\infty}$. The proof for C is identical. Hence, provided that

$$\Delta t < \frac{1}{||f||_\infty},$$

we will have that $\rho(T) < 1$, and therefore the iterative ADI method converges. □

Remark: In the proof of convergence we use that $v \geq 0$, where $v = v^{(k)}$, the k-th iterate of the

Newton's iteration. However, if for some component i of the vector v is less than 0, $v_i^{(k)} < 0$, we can still show convergence provided that the function $\kappa(x)$ satisfies $-x\kappa'(x) \leq \kappa(x)$. Note that this condtition is automatically satisfied if $v \geq 0$ since $\kappa'(x) \geq 0 \ \forall x > 0$ in a quorum-sensing mechanism. This condition can be weakened to where the method will converge provided $-\frac{v_i + v_j}{2}\kappa'(\frac{v_i + v_j}{2}) \leq \kappa(\frac{v_i + v_j}{2})$ holds for all nonzero elements on a diagonal of $(\tilde{\kappa}\delta_x^2)$ where v_i appears with $v_i < 0$. This should only be in 5 positions in the matrix when using the five point stencil. We should still consider the following question: if we assume $v^{(k)} \geq 0$, can we show that the Newton's method yields $v^{(k+1)} \geq 0$ for this particular problem? If the answer is yes, then we do not need the further restriction on $\kappa(u)$.

CHAPTER 8. Conclusions and Future Work

The goals of this project were to hypothesize a mechanism to explain the experimental results provided in Chapter 1, show that they were both biologically reasonable and could simulate the behaviors exhibited within these tables, and finally to study the mathematical model and see if we could form any hypotheses to help guide future work. Before the molecule IL6 was suggested, many other mechanisms were tested numerically against the results in Table 1.1. A few of these are presented in Appendix E. They were all biologically reasonable, but for various reasons were discarded. Once IL6 was suggested, and the results in Table 1.2 were found, we could use this data to form the differentiation parameters and thereby show that the experimental results can be simulated by the model. This finding lends more credence to the hypothesis that the IL6 mechanism is responsible for the variations within the table.

A sensitivity analysis was performed on the model to determine which parameters are the most influential on the output. This analysis shows three main results. First, although the system is sensitive to variations in input, many of the parameters that cause the highest amount of uncertainty are recorded in the literature. However, some of the most influential unknown parameters are involved with the production or decay of the intracellular differentiation factor J, and as such the intracellular mechanism leading to differentiation should be studied in more detail. Secondly, the biological inhibitor G_p does not seem to have a measurable effect on the percentage of cells that have differentiated after six days. As such, it can be removed from the mathematical model without altering simulation results. Finally, the sensitivity analyses show that the system is more sensitive to parameters in the second pathway (via soluble receptors) than in the surface receptor pathway. Hence it may be hypothesized that the second pathway is more influential with respect to differentiation than the surface receptor pathway.

Steady states were calculated for the population model in chapter 5, and their stability was explored. It was found that if $N_a > 0$ (astrocytes are present), then there is one curve (S_1) of nonisolated steady states in the biological region. This curve corresponds physically to the situation where all progenitor cells have differentiated. Steady states satisfying $(N^d)^* > (1 - \frac{1}{\mu})N_{max}$ were shown to be stable to small perturbations in the initial conditions, where $\mu = \dfrac{\beta}{\gamma}$, with $\beta = M_1$ (the proliferation constant) and $\lim_{t\to\infty} \dfrac{\kappa_1[J]^2}{\kappa_2^2 + [J]^2} = \gamma$ being considered as a differentiation constant. If $N_a = 0$, two curves (T_1, T_2) of steady states exist within the biological region. The curve T_1 is unstable, and corresponds physically to the case where no AHPCs are present initially. If any AHPCs are introduced to the system, they will proliferate until the carrying capacity is reached, due to the lack of a differentiation factor. This steady state is on the curve T_2 and was found to be stable to small perturbations in initial conditions.

Chapter 6 showed that the experimental results for the contact coculture can be recreated by blocking the second pathway ($b_a = 0$) and limiting the available IL6 (decrease a_1). It is hypothesized that this behavior is due to cadherins or CAM binding between astrocytes and AHPCs. Chemotaxis was also explored, showing that we can alter differentiation results by artificially forming gradients in IL6 concentration and attracting cells up these gradients. In the absence of an apoptotic component in the logistic growth term, blow-up of the solution may be possible, depending on the strength of the taxis. However, this behavior can be prevented by including a quorum-sensing mechanism, preventing uncontrolled aggregation.

The mechanism for IL6-induced differentiation of AHPCs has been analyzed in some detail throughout this dissertation. However, in addition to Claim 5.6 from Chapter 5, there are four other areas that need to be considered for future work.

(1) The results of the control experiment must be accounted for. This differentiation is occurring in the absence of IL6. What is causing this?

(2) The difference between the contact and noncontact cocultures must be studied. To generate the difference in levels of differentiation, we are currently alterring the rates of secretion

of IL6 and sIL6Rα. We hypothesized that this is occurring via cadherins or CAM binding. The coefficients in the model (a_1, b_a) may be replaced by contact-dependent functions. Is this occurring biologically? If not, how else may these differences arise?

(3) The intracellular mechanism leading to differentiation should be studied in more detail. For this model, we hypothesized the existence of an intracellular molecule J, created through a signal transduction cascade, that the leads to TUJ1 expression. How does the intracellular mechanism lead to increased TUJ1 expression? The protein J could be considered an important molecule within the cascade, possible a STAT protein. Is the mechanism used in the model an adequate depiction of this cascade, capturing its basic features, or does more complexity need to be introduced?

(4) Although not much cell movement is observed, the neuritic extensions appearing after differentiation are observed to be undergoing directed movement. We ignore this effect in our modelling as the volume of these extensions is small compared to the cell bodies during this early phase. However, we should account for why these processes exhibit the particular behaviors observed. This is currently being investigated using a hybrid model, where the neurite is divided into discrete compartments existing on a grid for a cellular automatan model. ODEs model the transmission of molecules between compartments, and the neurite itself elongates directionally depending on probabilities generated by available intracellular and extracellular proteins.

APPENDIX A. Discussion of the Background Function

When no atrocytes or IL6 are added to the AHPC culture, about 18% of the cells express the protein TUJ1 after six days. TUJ1 is an early neuronal marker, indicating that the cell has differentiated. This mechanism leading to the background level of differentiation has not yet been identified.

In order to simulate the other results properly, the background level should be accounted for. Since this mechanism is presently unknown, we introduce an artificial function into the ODE system meant to simulate this background differentiation. Since this is an artificial construction, the goal of the modelling becomes recreating differences between different experiments as opposed to recreating the specific levels of differentiation. The differences must be due to the IL6 mechanism, not different actions of this function. However, it needs to be mentioned that this function is only meant to be included for initial simulations, those covering the first six days of culture. It is an artificial construction, and any hypothesis of long-term behavior based on this funciton may not be valid.

The coefficient on N^p for the rate of differentiation due to the background mechanism is taken to be

$$f(N^p, N^d) = \frac{\theta_1}{\theta_2 + \left(\frac{N^d}{N^p+N^d}\right)^2}.$$

As the percentage of cells that have differentiated $\left(\dfrac{N^d}{N^p + N^d}\right)$ increases, this coefficient decreases. Hence it is most prevalent during the initial periods, when this ratio is approximately zero. The graph of $f(N^p, N^d)$ for $\dfrac{N^d}{N^p + N^d} \in [0, 1]$ is provided in Figure A.1.

In accordance with the above comments, we remove this term when studying long-term behavior of the IL6 mechanism. However, the function has been chosen so that the rate of

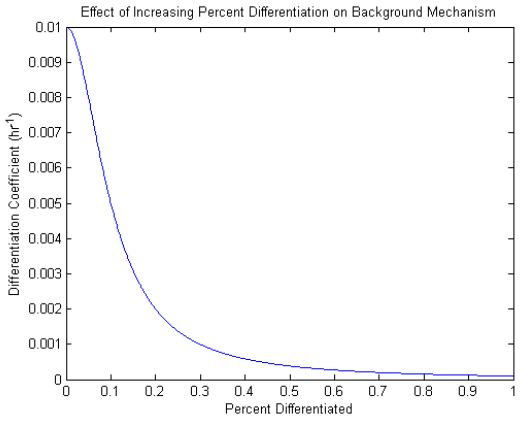

Figure A.1 *The value of the differentiation coefficient, $f(N^p, N^d)$, after the given percentage of cells has already differentiated.*

differentiation due to this function becomes negligible as $\frac{N^d}{N^p + N^d} \to 1$. This allows us to study differentiation for times above but near six days without much interference from this function. The results of the control experiment described in Chapter 3 are shown for 250 days in Figure A.2 to illustrate the negligible nature of this function as $\frac{N^d}{N^p + N^d} \to 1$.

The system

$$\frac{dN^p}{dt} = -\theta_1 N^p \left(\theta_2 + (\frac{N^d}{N^p + N^d})^2\right)^{-1} + M_1 N^p \left(1 - \frac{N^p + N^d}{N_{max}}\right),$$
$$\frac{dN^d}{dt} = \theta_1 N^p \left(\theta_2 + (\frac{N^d}{N^p + N^d})^2\right)^{-1},$$

admits an infinite number of steady states, with $(N^p)^* = 0$ and $(N^d)^*$ arbitrary. Stability of these steady states can be analyzed similarly to the steady states of the simplified system presented in Chapter 5. Note that this says that all cells would differentiate. This may not be biologically correct. However, as stated above, this function is only meant to be used for these initial time periods in this simulation as we do not understand what mechanism this differentiation is occurring by. A back term could be introduced into this system to control this effect, thereby yielding a single steady state. However, a back term would have the unwanted effect of reducing the level of differentiation due to the IL6 mechanism and causing the full system to also have a single steady state value even when IL6 is present. This value

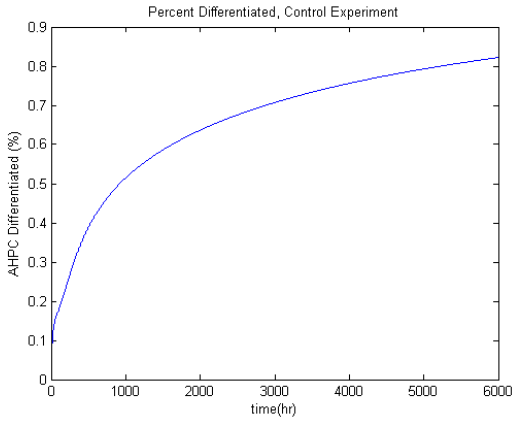

Figure A.2 *Control experiment, differentiation due solely to the background function, for 250 days. Notice how slowly the curve is increasing relative to the time axis.*

would depend on the parameters of the back term, and thus can be made to be any arbitrary value. A long-term analysis of the IL6 effect on this system would need to remove this back term. However, this is exactly what we are already doing with the background function when performing long-term analysis.

APPENDIX B. Mathematical Description of FAST

Cukier et.al. introduced the Fourier Amplitude Sensitivity Test (FAST) in a paper in 1973 ([13]). The method has since become widely used to perform global sensitivity analysis due to its reliability and its ability to assess the importance of various parameters in the presence of nonlinear and even non-monotonic relationships. The basic idea behind the method is to assign frequencies to each parameter of interest and vary these parameters simultaneously along search curves in the parameter space. The search curves oscillate in each dimension in accordance with the frequency of that parameter. The variance in the output is decomposed as a Fourier Series to explicitly show the contribution to the variance occurring at each frequency. These are used to derive partial variances attributable to each parameter, which are then interpreted as sensitivity measures.

The mathematical derivation of the FAST method is based on the presentations given in [14] and [47]. Some aspects of the derivation are further elaborated on in [12], [34], and [48]. Let $\mathbf{x} = (x_1, x_2, ..., x_n)$ be a random vector of input parameters with pdf $P(\mathbf{x})$. Suppose the components of $\mathbf{x}$ are each uncorrelated continuous random variables, where the pdf of x_i is given by $p_i(x_i)$. Then $P(\mathbf{x}) = \prod_{i=1}^{n} p_i(x_i)$. The output of interest from this model is the percentage of cells that have differentiated after six days. In this sensitivity analysis, we would like to decompose the variance of this output into partial variances attributable to each parameter. These can be separated into *main effects*, variance attributable solely to variation in a specific parameter, and *total effects*, variance attributable to both the main effect of a parameter and its interactions with other parameters. Hence we are concerned with the variance of an output function $y = f(\mathbf{x})$. The m-th moment of y can be defined by $< y^{(m)} >= \int_{\Omega} f^m(\mathbf{x}) P(\mathbf{x}) d\mathbf{x}$, where $\Omega \subset R^n$ is the input parameter space.

The idea behind the eFAST method is to use a transformation to express this n-dimensional integral by a one-dimensional integral, via a space-filling curve. This curve is referred to as the *search curve*. Parameterize each x_i by the parametric equation

$$x_i(t) = g_i\Big(\sin(\omega_i t)\Big)$$

for all $i \in \{1, 2, ..., n\}$, with $-\infty < t < \infty$. It was shown by Cukier et.al. ([14]) that if the functions g_i satisfy

$$\pi\sqrt{1-u^2}p_i(g_i(u))\frac{dg_i(u)}{du} = 1$$

then the total arc length of the portion of the search curve between x_i and $x_i + dx_i$ is $p_i(x_i)dx_i$. To solve this equation for g_i, first write the equation as $p_i(g_i)dg_i = \frac{1}{\pi}\frac{du}{\sqrt{1-u^2}}$. Integrating yields

$$F_i(g_i) = \int_{-\infty}^{g_i} p_i(t)dt = \frac{1}{\pi}\arcsin(u) + C$$

where F_i is the cumulative distribution function (CDF) of the pdf p_i. In [9], Saltelli suggests using $C = \frac{1}{2}$, as then $F_i(g_i) \in [0, 1]$. If F_i is continuous and strictly increasing, this can be solved to yield $g_i(u) = F_i^{-1}\Big(\frac{1}{\pi}\arcsin(u) + \frac{1}{2}\Big)$, where F_i^{-1} is the inverse cumulative distribution function (ICDF) for p_i. The ICDF for a uniform distribution is given by $F^{-1}(y) = a + (b-a)y$. The ICDF for a log uniform distribution is likewise given by $F^{-1}(y) = exp\{\log(a) + [\log(b) - \log(a)]y\}$. The ICDF for a normal distribution can be approximated with the statistical toolbox in Matlab. A list of ICDF's for many other distributions is provided in Appendix A of [34]. This list includes a rational function approximation to the ICDF of the normal distribution.

If the frequencies $\{\omega_i\}_{i=1}^n$ are chosen to be *incommensurate*, i.e. $\sum_{i=1}^{n} a_i\omega_i = 0$ does not hold for any set of integers $\{a_i\}_{i=1}^n$, the curve $\mathbf{x}(s)$ is space-filling in the sense that it comes arbitrarily close to any point in the parameter space for some s ([56]). Hence the search curve will explore the whole parameter space with density specified by the pdf $P(\mathbf{x})$. Moreover, if we define $\overline{y}^{(m)} = \lim_{T\to\infty}\frac{1}{2T}\int_{-T}^{T} f^m(\mathbf{x}(s))ds$, then by Weyl's ergodic theorem ([13]), $< y^{(m)} >= \overline{y}^{(m)}$, i.e. "the phase-space average equals the time average". The moments can then be expressed as one-dimensional integrals. The variance of the output function f is defined as $D =< y^{(2)} > - < y^{(1)} >^2 = \overline{y}^{(2)} - (\overline{y}^{(1)})^2$.

There are two problems encountered when using this formulation. First is the inability to achieve incommensurate frequencies due to the finite precision of computers, since to be incommensurate the frequencies would by necessity need to be irrational. Integer frequencies are used instead. Denoting $f(x_1(s), ..., x_n(s))$ by $f(s)$, it then holds that $f(s) = f(s + 2\pi)$. The search curve is now a closed path in the parameter space, and is no longer space-filling, so the ergodic hypothesis that $< y^{(m)} >= \overline{y}^{(m)}$ no longer holds. However, Cukier et.al. ([14]) showed that this error can be minimized through appropriate choices for the frequencies.

We now have that $\overline{y}^{(m)} = \dfrac{1}{2\pi}\displaystyle\int_{-\pi}^{\pi} f^m(s)ds$, and we define $\widehat{D} = \overline{y}^{(2)} - (\overline{y}^{(1)})^2 = \dfrac{1}{2\pi}\displaystyle\int_{-\pi}^{\pi} f^2(s)ds - \Big(\dfrac{1}{2\pi}\displaystyle\int_{-\pi}^{\pi} f(s)ds\Big)^2$. Since $f(s)$ is 2π-periodic, it can be expressed as a Fourier Series

$$f(s) = A_0 + \sum_{i=1}^{\infty}\{A_i \cos(is) + B_i \cos(is)\}$$

where $A_0 = \dfrac{1}{2\pi}\displaystyle\int_{-\pi}^{\pi} f(s)ds = \overline{y}^{(1)}$, and for $i = \{1, 2, ...\}$, $A_i = \dfrac{1}{\pi}\displaystyle\int_{-\pi}^{\pi} f(s)\cos(is)ds$ and $B_i = \dfrac{1}{\pi}\displaystyle\int_{-\pi}^{\pi} f(s)\sin(is)ds$. By Parseval's theorem,

$$\overline{y}^{(2)} = A_0^2 + 2\sum_{i=1}^{\infty}\{A_i^2 + B_i^2\},$$

and therefore $\widehat{D}$, which is an approximation to the variance D, is given by

$$\widehat{D} = 2\sum_{i=1}^{\infty}\{A_i^2 + B_i^2\}.$$

Each parameter is oscillating in its own parameter space with a specific frequency. This leads to corresponding oscillations in the output at linear combinations of all of these frequencies. If the coefficients are incommensurate, then $\widehat{D}_i = 2\displaystyle\sum_{k=1}^{\infty}\{A_{ki}^2 + B_{ki}^2\}$ is the variance due solely to variation in the parameter oscillating at frequency ω_i, as was shown by Cukier et.al. in [14]. Therefore, $S_i = \dfrac{\widehat{D}_i}{\widehat{D}}$ is the *main effect* of parameter i, the percentage of the variance due solely to parameter i.

However, we are using integer frequencies instead of incommensurate frequencies. Consider the following example: let there be two parameters, and assign frequencies $\omega_1 = 3$ and $\omega_2 = 4$. The coefficient $A_{12}^2 + B_{12}^2$ is a harmonic for both frequencies, so variation in the output at

frequency $\omega = 12$ contains contributions from both parameters, and the amount due to either parameter individually cannot be ascertained. This is the problem of *interference*. Although these interferences cannot be avoided, these effects can be "postponed" to the higher frequencies of the Fourier Series. Then, since the Fourier coefficients rapidly converge to zero for higher harmonics, we approximate the above series with 4-6 harmonics of the specified frequencies, avoiding the interference while retaining most of the information provided by the specified frequencies. Let M denote the number of harmonics considered. The frequencies are chosen such that

$$\sum_{i=1}^{n} a_i\omega_i \neq 0 \qquad \text{for } \sum_{i=1}^{n} |a_i| \leq M+1$$

for integers a_i. A set of frequencies that satisfies this property is said to be free of interference through order M. The higher that M is set, the "more incommensurate" the frequencies become, allowing them to search the parameter space more thoroughly. In the eFAST method, where one parameter is assigned a high frequency ω_i and the other parameters are assigned frequencies $\{\omega_{\sim i}\}$ with $\max\{\omega_{\sim i}\} = \dfrac{\omega_i}{2M}$, this limit on the maximum that the complementary set of frequencies can be assigned prevents interference between the complementary set and parameter i. Hence $\widehat{D}_{\sim i} = 2\sum_{i=1}^{\omega_i/2}(A_i^2 + B_i^2)$ measures the contributions to the variance due solely to the complementary set of parameters, so that the total effect of parameter i can be measured by $S_{Ti} = 1 - \dfrac{\widehat{D_{\sim i}}}{\widehat{D}}$.

Finally, there is one other effect that needs to be discussed. This is the process of *aliasing*. Aliasing is a result of using discrete sampling. If a sample of N_s equally spaced points is used over the interval $(-\pi, \pi)$, the Nyquist critical frequency is defined as one-half of the sampling frequency, $\omega_{Ny} = \dfrac{N_s}{2}$. It is a well-known phenomenon in information theory and in signal processing that any frequency components outside of the range $(-\omega_{Ny}, \omega_{Ny})$ are aliased to lower frequencies. To avoid this affect, ensuring that the coefficients of the Fourier Series belonging to ω_i and its harmonics do not contain any of this extra information, we need to ensure that the information outside of this range is negligible. This is done by taking the largest meaningful harmonic, $M\omega_i < \dfrac{N_s}{2}$. This equation can be rearranged to provide us with a lower limit for the number of sample points N_s that must be taken. If the largest frequency

assigned to a parameter is ω_{max}, then we need to sample at least $N_s = 2M\omega_{max} + 1$ points per search curve.

APPENDIX C. A Formal Power Series Solution of the Simplified System

Consider the cellular equations in the ODE system:

$$\begin{aligned}
\frac{dN^p}{dt} &= -\frac{\kappa_1[J]^2}{\kappa_2^2+[J]^2}N^p + M_1\left(1-\frac{N^p+N^d}{N_{max}}\right),\\
\frac{dN^d}{dt} &= \frac{\kappa_1[J]^2}{\kappa_2^2+[J]^2}N^p,\\
N^p(0) &= N_0^p, \qquad N^d(0) = 0.
\end{aligned}$$

Although $[J]$ depends on the other molecular species in the system, it is possible for it's concentration to become approximately constant after a short period of time. Given this assumption, this system can be written as

$$\begin{aligned}
\frac{dx}{dt} &= \beta x\big(1-(x+y)\big) - \gamma x\\
\frac{dy}{dt} &= \gamma x\\
x(0) &= x_0, \qquad y(0) = 0
\end{aligned}$$

where $x = \dfrac{N^p}{N_{max}}$, $y = \dfrac{N^d}{N_{max}}$, $\gamma = \dfrac{\kappa_1[J]^2}{\kappa_2^2+[J]^2}$, and $\beta = \dfrac{M_1}{N_{max}}$. Here we find a solution for this system in the form of a formal power series.

In chapter 5 we calculated the solution to $\dfrac{dx}{dy}$, finding that $\widehat{x}(y) = e^{-\mu}y(x_0-1)+(1-y)$, a curve that provides a relation between the solution curves $x(t)$ and $y(t)$. Using this relationship we can find a solution to this coupled system in the form of a formal power series. First $y(t)$ will be calculated, and then $x(t)$ can be found by substituting $y(t)$ into $\widehat{x}(y)$. If convergence of the series can be proven, it would provide a way to calculate the densities of AHPCs and neurons at any time t for the simplified system, which would then provide an approximation

to the solution of the full system. To solve for $y(t)$, first substitute $\widehat{x}(y)$ into $\dfrac{dy}{dt}$.

$$\frac{dy}{dt} = \lambda e^{-\mu y} - \gamma y + \gamma$$
$$y(0) = 0$$

where $\lambda = \gamma\big(x_0 - 1\big)$. Assume $y(t) = \sum_{n=0}^{\infty} a_n t^n$. Noting that

$$\sum_{n=0}^{\infty}(n+1)a_{n+1}t^n = \sum_{n=1}^{\infty} n a_n t^{n-1},$$

we find

$$\begin{aligned}
\sum_{n=0}^{\infty}(n+1)a_{n+1}t^n &= \lambda exp\Big(-\mu\sum_{n=0}^{\infty}a_n t^n\Big) - \gamma\Big(\sum_{n=0}^{\infty}a_n t^n\Big) + \gamma \\
&= \lambda\prod_{n=0}^{\infty} exp(-\mu a_n t^n) - \gamma\Big(\sum_{n=0}^{\infty}a_n t^n\Big) + \gamma \\
&= \lambda e^{-\mu a_0}\prod_{n=1}^{\infty} exp(-\mu a_n t^n) - \gamma\Big(\sum_{n=0}^{\infty}a_n t^n\Big) + \gamma \\
&= \lambda e^{-\mu a_0}\prod_{n=1}^{\infty}\Big(\sum_{m=0}^{\infty}\frac{(-\mu a_n t^n)^m}{m!}\Big) - \gamma\Big(\sum_{n=0}^{\infty}a_n t^n\Big) + \gamma \\
&= \lambda e^{-\mu a_0}\sum_{n=0}^{\infty}\Big[\sum_{\alpha\cdot N=n}\frac{(-\mu)^{|\alpha|}\prod_{j=1}^{\infty}a_j^{\alpha_j}}{\alpha!}\Big]t^n - \gamma\Big(\sum_{n=0}^{\infty}a_n t^n\Big) + \gamma
\end{aligned}$$

where α is an infinite multiindex of nonnegative integers and N is the vector $N = (1, 2, 3, ...)$. In other words, the inner sum is over all partitions of the positive integer n. Equating coefficients, and defining $\Lambda = \lambda e^{-\mu a_0}$ and $C_n = \sum_{\alpha\cdot N=n}\dfrac{(-\mu)^{|\alpha|}\prod_{j=1}^{\infty}a_j^{\alpha_j}}{\alpha!}$, we get a series $y(t) = \sum_{n=0}^{\infty} a_n t^n$ with recursively defined coefficients:

$$\begin{aligned}
a_0 &= y(0), \\
a_1 &= \Lambda - \gamma a_0 + \gamma, \\
a_n &= \frac{C_{n-1}\Lambda - \gamma a_{n-1}}{n}, \qquad n \geq 2.
\end{aligned}$$

Since $y(0) = 0$ and $\lambda = \gamma(x_0 - 1)$, we have that $a_0 = 0$, $a_1 = \gamma x_0$, and $\Lambda = \lambda$. In addition, since α is comprised of nonnegative integers, and $\alpha_j \cdot j > n$ for $j > n$ if $\alpha_j > 0$, we can truncate the infinite product so that $C_n = \sum_{\alpha\cdot N=n}\dfrac{(-\mu)^{|\alpha|}\prod_{j=1}^{n}a_j^{\alpha_j}}{\alpha!}$. As an aside, note that the

coefficient C_n is $\frac{1}{n!}$ times the exonential Bell partition polynomial $B_n(x_1, ..., x_n)$ evaluated at $\{x_i = -\mu a_i \cdot i!\}_{i=1}^n$. The exponential Bell partition polynomials are defined as

$$B_n = \sum \frac{n!}{k_1!(1!)^{k_1} k_2!(2!)_2^k \dots k_n!(n!)^{k_n}} x_1^{k_1} x_2^{k_2} \dots x_n^{k_n},$$

where the summation is over all partitions of n, i.e. over all nonnegative integer solutions $(k_1, ..., k_n)$ of the equation $k_1 + 2k_2 + ... + nk_n = n$. These functions are described in more detail in [57]-[58].

Theorem 5.4: *The coefficients a_n for $n \geq 2$ can be written as*

$$a_n = \lambda \sum_{i=1}^{n-1} \Big[\Big(\frac{i!}{n!} \Big) (-\gamma)^{(n-1)-i} C_i \Big] - \frac{(-\gamma)^{(n-1)} x_0}{n!}.$$

Proof. This can be shown through induction.

$$\begin{aligned} a_2 &= \lambda \sum_{i=1}^{1} \Big[\Big(\frac{i!}{2!} \Big) (-\gamma)^{1-i} C_i \Big] - \frac{(-\gamma)^2 x_0}{2!} \\ &= \lambda \Big[\frac{1}{2} \gamma_0 C_1 \Big] - \frac{\gamma^2 x_0}{2} \\ &= \frac{\lambda C_1 - \gamma^2 x_0}{2} \\ &= \frac{\Lambda C_1 - \gamma a_1}{2} \end{aligned}$$

Now assume that the hypothesis is true for a_{k-1}, $k \geq 3$. The formula needs to be verified for a_k to complete the induction.

$$\begin{aligned} a_k &= \frac{\lambda C_{k-1} - \gamma a_{k-1}}{k} \\ &= \frac{\lambda C_{k-1}}{k} + \frac{(-\gamma)}{k} \Big[\lambda \sum_{i=1}^{k-2} \Big(\frac{i!}{(k-1)!} \Big) (-\gamma)^{(k-2)-i} C_i - \frac{(-\gamma^{k-1}) x_0}{(k-1)!} \Big] \\ &= \frac{\lambda C_{k-1}}{k} + \Big[\lambda \sum_{i=1}^{k-2} \Big(\frac{i!}{k!} \Big) (-\gamma)^{(k-1)-i} C_i - \frac{(-\gamma^k) x_0}{k!} \Big] \\ &= \lambda \frac{(k-1)!}{k!} (-\gamma)^{(k-1)-(k-1)} C_{k-1} + \Big[\lambda \sum_{i=1}^{k-2} \Big(\frac{i!}{k!} \Big) (-\gamma)^{(k-1)-i} C_i - \frac{(-\gamma^k) x_0}{k!} \Big] \\ &= \lambda \sum_{i=1}^{k-1} \Big[\Big(\frac{i!}{k!} \Big) (-\gamma)^{(k-1)-i} C_i \Big] - \frac{(-\gamma)^{(k-1)} x_0}{k!}. \end{aligned}$$

□

The solution to the original IVP is

$$y(t) = \gamma x_0 t + \sum_{n=2}^{\infty} \left[\lambda \sum_{i=1}^{n-1} \left[\left(\frac{i!}{n!} \right) (-\gamma)^{(n-1)-i} C_i \right] - \frac{(-\gamma)^{(n-1)} x_0}{n!} \right] t^n$$

$$x(t) = e^{-\mu y(t)} \big(x_0 - 1 \big) + (1 - y(t)).$$

All solutions of this system with $x_0 > 0$ satisfy $\lim_{t \to \infty}(x, y) = (0, y^*)$. The time courses of N^p and N^d are given in terms of a formal power series. If convergence of the series can be proven, it would allow one to calculate (or estimate) the percentage of differentiation at any moment of time for this reduced system. Moreover, this would provide an estimate for the solution of the full system.

APPENDIX D. Derivation of the Lyapunov Function

Consider an ODE $\mathbf{y}' = \mathbf{f}(\mathbf{y})$ with critical point x^*. Let $V : R^n \to R$ be a scalar-valued function satisfying the following properties:

(1) V should be positive definite; that is, $V(x) \geq 0$ for all x in some neighborhood U around a critical point x^*, with $V(x^*) = 0$ and $V(x) > 0$ for all $x \in U \backslash \{x^*\}$, and

(2) V has continuous first-order partial derivatives at every point of U.

A function satisfying both of these properties is referred to as a *Lyapunov function* for the differential equation. Define $V'_*(\mathbf{y}) = \nabla_y V(\mathbf{y}) \cdot f(\mathbf{y})$, the time derivative of V with respect to the system $\mathbf{y}' = \mathbf{f}(\mathbf{y})$. Their usefulness is due to the following theorems ([8]):

Theorem C.1. *If there exists a scalar function $V(\mathbf{y})$ that is positive definite and for which $V'_*(\mathbf{y}) \leq 0$ (the derivative with respect to $\mathbf{y}' = \mathbf{f}(\mathbf{y})$ is nonpositive) on some region Ω containing the origin, then the zero solution of $\mathbf{y}' = \mathbf{f}(\mathbf{y})$ is stable.*

Theorem C.2. *If there exists a scalar function $V(\mathbf{y})$ that is positive definite and for which $V'_*(\mathbf{y})$ is negative definite on some region Ω containing the origin, then the zero solution of $\mathbf{y}' = \mathbf{f}(\mathbf{y})$ is asymptotically stable.*

Although the theorems are for the critical point $x = 0$, they can be easily generalized to any critical point. They can be considered to be a measure of the "distance" of points along the solution curve to the steady state, and as such are very useful in the study of stability of steady state solutions of nonlinear systems of ODEs. They are especially useful when linearized stability results are not valid for the nonlinear system.

Of interest here are the steady states of system (3.1). In particular, we are concerned with the stability of the curve of nonisolated steady states $T_2(s)$, as defined in Chapter 5. Linearized stability analysis is not valid in this case due to the three zero eigenvalues of the Jacobian matrix. Hence we need to use a Lyapunov function to investigate the long-term behavior.

There are many conservation laws for this system, and the only terms not appearing in multiple equations are the decay rate terms. We can make use of these conservation laws by looking for a Lyapunov function of the form

$$V(\vec{x}) = \alpha_1[A_i] + \alpha_2[R_{il}] + \alpha_3[A_a] + N^p(\alpha_4[A_s] + \alpha_5[\{A_a : R^p_{gp130}\}] + \alpha_6[\{A_s : R^p_{gp130}\}] + \alpha_7[J]) + \frac{1}{2}\Big(N_{max} - (N^p + N^d)\Big)^2$$

where $\vec{x} = ([A_i], [R_{il}], [A_a], [A_s], [\{A_a : R^p_{gp130}\}], [\{A_s : R^p_{gp130}\}], [J], N^p, N^d)$. Let $\phi(\vec{x})$ be a solution curve of system (3.1). Then the time derivative of $V(\vec{x})$ along $\phi(\vec{x})$ is

$$\begin{aligned}
V'_*(\vec{x}) &= \nabla_x V \cdot f(\vec{x}) \\
&= \alpha_1\frac{d[A_i]}{dt} + \alpha_2\frac{d[R_{il}]}{dt} + \alpha_3\frac{d[A_a]}{dt} + \frac{dN^p}{dt}\Big(\alpha_4[A_s] + \alpha_5[\{A_a : R^p_{gp130}\}] \\
&\quad + \alpha_6[\{A_s : R^p_{gp130}\}] + \alpha_7[J]\Big) + N^p\Big(\alpha_4\frac{d[A_s]}{dt} + \alpha_5\frac{d[\{A_a : R^p_{gp130}\}]}{dt} \\
&\quad + \alpha_6\frac{d[\{A_s : R^p_{gp130}\}]}{dt} + \alpha_7\frac{d[J]}{dt}\Big) - \Big(N_{max} - (N^p + N^d)\Big) \cdot \Big(\frac{dN^p}{dt} + \frac{dN^d}{dt}\Big) \\
&= (\alpha_1 + \alpha_2 - \alpha_3)\ell_{-1}[A_a] + (\alpha_3 - \alpha_1 - \alpha_2)\ell_1[A_i][R_{il}] + (\alpha_1 - \alpha_4)\widehat{k}_{-1}[A_s]N^p \\
&\quad + (\alpha_5 - \alpha_3)\nu_1[A_a][R^p_{gp130}]N^p + (\alpha_3 - \alpha_5)\nu_{-1}[\{A_a : R^p_{gp130}\}]N^p \\
&\quad + (\alpha_7 - \alpha_5)\nu_2[\{A_a : R^p_{gp130}\}]N^p + (\alpha_4 - \alpha_1)\widehat{k}_{-1}[A_i][R^p_{il}]N^p \\
&\quad + (\alpha_6 - 4)\widehat{\ell}_1[A_s][R^p_{gp130}]N^p + (\alpha_4 - \alpha_6)\widehat{\ell}_{-1}[\{A_s : R^p_{gp130}\}]N^p \\
&\quad + (\alpha_7 - \alpha_6)\widehat{\ell}_2[\{A_s : R^p_{gp130}\}]N^p - \Big(K_1(N^p, N^d) + K_2([J])\Big)\times \\
&\quad \Big(\alpha_4[A_s] + \alpha_5[\{A_a : R^p_{gp130}\}] + \alpha_6[\{A_s : R^p_{gp130}\}] + \alpha_7[J]\Big) \\
&\quad - \Big(N_{max} - (N^p + N^d)\Big)\Big[M_1N^p(1 - \frac{N^p + N^d}{N_{max}}\Big] - \alpha_1\mu_{ai}[A_i] \\
&\quad - \alpha_2\mu_{il}[R_{il}] - \alpha_3\mu_{aa}[A_a] - \alpha_7\mu_j[J]N^p.
\end{aligned}$$

In order to for this function to be nonpositive throughout Ω the coefficients α_i should satisfy

$$\begin{aligned} \alpha_1 &= \alpha_4 & \alpha_7 &\leq \alpha_5 \\ \alpha_4 &= \alpha_6 & \alpha_7 &\leq \alpha_6 \\ \alpha_3 &= \alpha_5 & \alpha_1 + \alpha_2 &= \alpha_3. \end{aligned}$$

We can convert this to a system of equations by introducing slack variables $s_1 \geq 0$ and $s_2 \geq 0$ to form

$$\begin{aligned} \alpha_1 &= \alpha_4 & \alpha_7 + s_1 &= \alpha_5 \\ \alpha_4 &= \alpha_6 & \alpha_7 + s_2 &= \alpha_6 \\ \alpha_3 &= \alpha_5 & \alpha_1 + \alpha_2 &= \alpha_3. \end{aligned}$$

Gauss-Jordan elimination can be used to solve this underdetermined system. There are an infinite number of solutions, and they can be represented parametrically as

$$\begin{aligned} \alpha_1 &= \alpha_7 + s_2 & \alpha_4 &= \alpha_1 \\ \alpha_2 &= s_1 - s_2 & \alpha_5 &= \alpha_3 \\ \alpha_3 &= \alpha_7 + s_1 & \alpha_6 &= \alpha_1 \\ \alpha_7, s_1, s_2 &\text{ arbitrary.} \end{aligned}$$

The solutions of interest here must satisfy $\alpha_i > 0$ for all i, $s_1 \geq 0$, and $s_2 \geq 0$. If we set $s_1 = 2$, $s_2 = 1$, and $\alpha_7 = 1$, we get the solution

$$\begin{aligned} \alpha_1 &= 2, & \alpha_3 &= 3, & \alpha_5 &= 3, & \alpha_7 &= 1, \\ \alpha_2 &= 1, & \alpha_4 &= 2, & \alpha_6 &= 2, \end{aligned}$$

These coefficients produce the function examimed in Chapter 5:

$$\begin{aligned} V(\vec{x}) = 2[A_i] + [R_{il}] + 3[A_a] + N^p(2[A_s] + 3[\{A_a : R^p_{gp130}\}] + 2[\{A_s : R^p_{gp130}\}] + [J]) \\ + \frac{1}{2}\Big(N_{max} - (N^p + N^d)\Big)^2. \end{aligned}$$

$V'_*(\vec{x})$ is clearly nonpositive when the concentration/densities of the species are nonnegative. It is shown in Chapter 5 that it is in fact a Lyapunov function, provided $N^p \geq \varepsilon > 0$.

APPENDIX E. Alternate Mechanisms Explored

This project initially began as an exploration of mechanisms that could explain the results in Table 1.1. Since IL6 was not initially hypothesized as the active molecule, there were many possible mechanisms explored, each with different responses to "active molecules". However, once IL6 was hypothesized, it was shown to be an important molecule in this mechanism (Table 1.2). Due to the importance of IL6, the focus in this appendix is on the modeling performed after IL6 was hypothesized as the active inducer of differentiation. Four mechanisms will be presented. Two are simplified versions of the IL6 mechanism, and another is an extension of the IL6 mechanism, including secretion of a protease. The first mechanism includes the effect of the laminin substrate on differentiation, based on the claim that both laminin and IL6 are needed for differentiation. It also includes a different activity for IL6 than is included in the other models.

Effect of the Extracellular Matrix

This first mechanism is a departure from the other mechanisms presented here, in that the response to IL6 does not occur on the AHPC iteself, but instead on the laminin substrate. Early discussions on the biological mechanism involved the possibility that laminin is necessary for (or at the least enhances) neuronal differentiation. In this mechanism, astrocytes secrete IL6 (C') which acts as a protease. It promotes differentiation by releasing a differentiation factor I from the laminin complex $\{F : I\}$. Astrocytes also inhibit differentiation by releasing

an inhibitor (A) of the differentiation factor I. These reactions can be summarized by

$$\{F:I\} \underset{l_{-1}}{\overset{l_1}{\rightleftharpoons}} F + I$$

$$C' + \{F:I\} \underset{\ell'_{-1}}{\overset{\ell'_1}{\rightleftharpoons}} \{C':F:I\} \overset{\ell'_2}{\to} C' + F + I$$

$$A + I_a \underset{\nu_{-1}}{\overset{\nu_1}{\rightleftharpoons}} I_i$$

$$I_a + N^p \overset{m_1}{\to} N^d.$$

Letting $\nu = \frac{\nu_1}{\nu_{-1}}$, and assuming the third reaction is at equilibrium, the population model corresponding to this mechanism is given by

$$\begin{aligned}
\frac{d[C']}{dt} &= b_1 N_a - \mu_{c'}[C'] \\
\frac{d[A]}{dt} &= a_1 N_a - \mu_a[A] \\
\frac{d[\{F:I\}]}{dt} &= -l_1[\{F:I\}] + l_{-1}[F][I] - \frac{\ell'_1\ell'_2}{\ell'_{-1}+\ell'_2}[C'][\{F:I\}] \\
&\quad + \lambda\Big(\frac{N^p+N^d}{N_{max}}\Big)[\{F:I\}]\cdot\Big(1 - \frac{[\{F:I\}]+[F]}{F_{max}}\Big) \\
\frac{d[F]}{dt} &= l_1[\{F:I\}] - l_{-1}[F][I] + \frac{\ell'_1\ell'_2}{\ell'_{-1}+\ell'_2}[C'][\{F:I\}] \\
\frac{d[I]}{dt} &= l_1[\{F:I\}] - l_{-1}[F][I] + \frac{\ell'_1\ell'_2}{\ell'_{-1}+\ell'_2}[C'][\{F:I\}] - m_1[I_a]N^p - \mu_I[I] \\
I_a(t) &= \frac{I(t)}{1+\nu[A]} \\
\frac{dN^p}{dt} &= M_1 N^p\Big(1 - \frac{N^p+N^d}{N_{max}}\Big) - m_1[I_a]N^p \\
\frac{dN^d}{dt} &= m_1[I_a]N^p.
\end{aligned}$$

Since AHPCs have been shown to express mRNA for the IL6 receptor ([41]), the more recent models under consideration have focused on mechanisms using the IL6 pathways for signal transduction. However, it could still be possible that integrin binding between AHPCs and laminin are necessary for the AHPC to differentiate in response to IL6.

Variants of the IL6 Mechanism

The IL6 mechanism presented in this dissertation has been shown to simulate all experimental results from Tables 1.1 and 1.2. However, it is still a simplification of the full IL6

mechanism. For example, it includes binding of activated IL6 to a gp130 dimer R^p_{gp130}, without any modeling of the process of dimerization. Simplifications are needed when modeling biological mechanisms due to the complexity of the mechanisms and the uncertainty of many of the parameters involved. When simplifying a model, one should always recall the words of Albert Einstein: "Everything should be made as simple as possible, but no simpler." In this section three alternate mechanisms are presented along with brief explanations of why they were not used for this dissertation.

The first mechanism under consideration includes the interactions among the soluble proteins, but does not include any of the surface receptors explicitly. Differentiation occurs by activated IL6 (A_a) binding to the AHPC. In this model, AHPCs do not express the receptor for inactive IL6 (A_i) on the membrane, but they may secrete R_{il}. These reactions can be summarized by

$$A_i + R_{il} \underset{l_{-1}}{\overset{l_1}{\rightleftharpoons}} \{A_i : R_{il}\} = A_a \overset{l_2}{\rightarrow} \text{degradation products}$$

$$A_a + G_p \underset{k_{-1}}{\overset{k_1}{\rightleftharpoons}} A_o \overset{\mu_{ao}}{\rightarrow} \text{degradation products}$$

$$A_a + N^p \underset{\nu_{-1}}{\overset{\nu_1}{\rightleftharpoons}} \{A_a : N^p\} \overset{\nu_2}{\rightarrow} N^d.$$

The population model corresponding to this mechanism is given by

$$\begin{aligned}
\frac{d[A_i]}{dt} &= S_{ai}(t) + a_1 N_a - l_1[A_i][R_{il}] + l_{-1}[A_a] - \mu_{ai}[A_i] \\
\frac{d[A_a]}{dt} &= S_{aa}(t) - (l_2 + l_{-1})[A_a] + l_1[A_i][R_{il}] \\
&\quad - \beta\nu_1[A_a]N^p + \beta\nu_{-1}[\{A_a : N^p\}] - k_1[A_a][G_p] + k_{-1}[A_o] \\
\frac{d[R_{il}]}{dt} &= S_{il}(t) + b_a N_a + b_p N^p - l_1[A_i][R_{il}] + l_{-1}[A_a] - \mu_{il}[R_{il}] \\
\frac{d[G_p]}{dt} &= S_{gp}(t) + s_a N_a - k_1[A_a][G_p] + k_{-1}[A_o] - \mu_{gp}[G_p] \\
\frac{d[A_o]}{dt} &= S_{ao}(t) + k_1[A_a][G_p] - (k_{-1} + \mu_{ao})[A_o] \\
\frac{dN^p}{dt} &= M_1 N^p\Big(1 - \frac{N^p + [\{A_a : N^p\}] + N^d}{N_{max}}\Big) - \nu_1[A_a]N^p + \nu_{-1}[\{A_a : N^p\}] \\
\frac{d[\{A_a : N^p\}]}{dt} &= \nu_1[A_a]N^p - (\nu_{-1} + \nu_2)[\{A_a : N^p\}] \\
\frac{dN^d}{dt} &= \nu_2[\{A_a : N^p\}].
\end{aligned}$$

This model does not account for the background differentiation. Unfortunately, this model was not able to numerically recreate all of the other experimental observations given in Tables 1.1 and 1.2 for biologically reasonable values. Parameter values often failed to recreate the dramatic increase observed for the noncontact coculture, or were unable to recreate the general behavior in Table 1.2. Moreover, although AHPCs express mRNA for the IL6 receptor ([41]), it is not known if they express the membrane receptor IL6R or secrete the soluble receptor sIL6Rα.

The second mechanism under consideration is similar to the first mechanism, but includes a more complicated response to A_a. The idea behind the response to A_a is based on a hypothesis in [49]. It is known that the complex of A_i, R_{il}, and the monomeric form of R^p_{gp130} (R^p_{mgp}) can exist as either the tetrameric complex $\{A_i : R_{il} : (R^p_{mgp})^2\}$ or the hexameric complex $\{(A_i)^2 : (R_{il})^2 : (R^p_{mgp})^2\}$. In other words, either one or two molecules of A_a can bind a gp130 dimer. In [49] it is hypothesized, based on previous research, that the transition between the tetrameric and hexameric state of this complex serves as a molecular switch between active and inactive receptor complexes. Binding of one A_a complex to a surface gp130 dimer on an AHPC initiates a signal transduction cascade resulting in differentiation of the AHPC. If two A_a complexes bind to the same gp130 dimer on the AHPC, the signal transduction cascade is not triggered. This effect can be modeled by the function $K_2([A_a]) = \dfrac{\kappa_1[A_a]}{\kappa_2 + [A_a]^2}$. The rate of differentiation initially increases with increasing concentrations of $[A_a]$, but as $[A_a]$ continues to increase, the likelihood of two complexes binding the gp130 dimer increases. Therefore, after a certain peak value, the rate of differentiation starts to decrease in response to increasing $[A_a]$. Figure E.1 shows the rate of differentiation in response to different concentrations of $[A_a]$. Letting $K_1(N^p, N^d)$ denote the coefficient for background differentiation as discussed previously, the population model corresponding to this mechanism is given by

$$\begin{aligned}
\frac{d[A_i]}{dt} &= S_{ai}(t) + a_1 N_a - l_1[A_i][R_{il}] + l_{-1}[A_a] - \mu_{ai}[A_i] \\
\frac{d[A_a]}{dt} &= S_{aa}(t) - (l_2 + l_{-1})[A_a] + l_1[A_i][R_{il}] - \beta K_2([A_a])N^p - k_1[A_a][G_p] + k_{-1}[A_o] \\
\frac{d[R_{il}]}{dt} &= S_{il}(t) + b_a N_a + b_p N^p - l_1[A_i][R_{il}] + l_{-1}[A_a] - \mu_{il}[R_{il}]
\end{aligned}$$

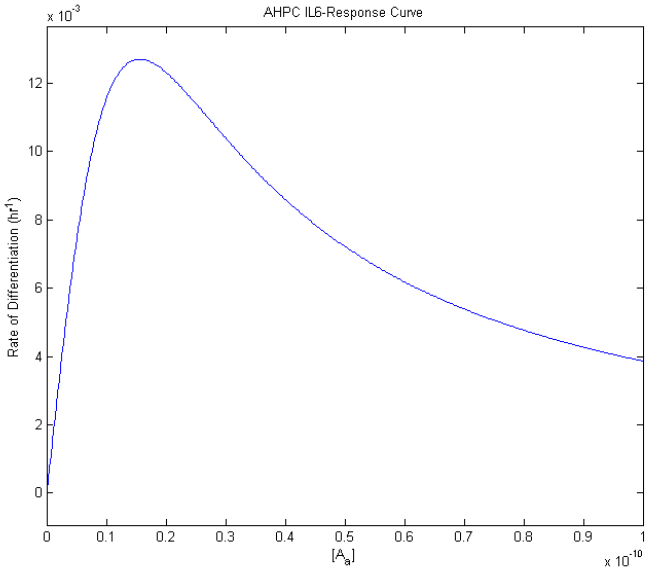

Figure E.1 *Coefficient governing the rate of differentiation for increasing concentrations of activated IL6.*

$$\frac{d[G_p]}{dt} = S_{gp}(t) + s_a N_a - k_1[A_a][G_p] + k_{-1}[A_o] - \mu_{gp}[G_p]$$
$$\frac{d[A_o]}{dt} = S_{ao}(t) + k_1[A_a][G_p] - (k_{-1} + \mu_{ao})[A_o]$$
$$\frac{dN^p}{dt} = -\Big\{K_1(N^p, N^d) + K_2([A_a])\Big\}N^p + M_1 N^p\Big(1 - \frac{N^p + N^d}{N_{max}}\Big)$$
$$\frac{dN^d}{dt} = \Big\{K_1(N^p, N^d) + K_2([A_a])\Big\}N^p.$$

This system of equations was able to simulate all results shown in Tables 1.1 and 1.2. (In fact, the concentration of $[A_a]$ yielding the maximum differentiation response corresponds to the concentration present during the noncontact coculture experiment.) To simulate the contact coculture results, contact would have to increase the secretion rates a_1 and b_a, lowering the rate of differentiation by increasing the inhibitory effect of overstimulation. However, a side effect of this response is that, when the astrocyte density N_a is decreased, $[A_a]$ will decrease, lessening the inhibitory effect, and leading to an increase in differentiation. This hypothesis was tested with biological experiments. However, the increase in differentiation due to decreasing astrocyte density was not observed.

Finally we consider an extension of the mechanism treated in this dissertation. One of the advantages of explicitly including both membrane receptor concentrations and cellular densities is that we can include molecules such as proteases that alter the number of receptors per cell but do not alter the number of cells. This is opposed to simply letting the cell density be proportional to the membrane receptor concentrations. In the final variant of the IL6 mechanism presented in this dissertation, we hypothesize that contact between the astrocytes and AHPCs induce the astrocytes to secrete a protease for R^p_{gp130}. The rest of the model is identical to that considered in the dissertation. Since this protease is only included in the contact coculture experiment, the model automatically matches the data from all of the other experiments. However, to simulate the drop in differentiation from $\sim 70\%$ in the noncontact coculture to $\sim 20\%$ in the contact coculture, one would need to cleave nearly 100% of the R^p_{gp130} present, which is most likely not occuring biologically. However, it is possible that this mechanism is occuring in conjunction with a decrease in secretion of IL6 and/or sIL6Rα. This combination of behaviors is an effect that can be explored in future work.

BIBLIOGRAPHY

[1] Alberts et. al., 2002. Molecular Biology of the Cell, 4th edition, *Garland Publishing, Taylor and Francis Group.*

[2] Alvarez-Buylla A., Garcia-Verdugo J.M., 2002. Neurogenesis in adult subventricular zone, *J Neurosci.*, 22(3):629-634.

[3] Anderson, T.W., 2003. An Introduction to Multivariate Statistical Analysis, 3rd edition, *Wiley-Interscience.*

[4] Bain and Engelhardt, 1992. Introduction to Probability and Mathematical Statistics, 2nd edition, *Duxbury Classic Series, Thomson Learning.*

[5] Barkho et.al., 2006. Identification of Astrocyte-Expressed Factors that Modulate Neural Stem/Progenitor Cell Differentiation, *Stem Cells Dev.* 15(3):407-421.

[6] Berg, 1993. Random Walks in Biology, expanded edition, *Princeton University Press.*

[7] Branicki, M. and Shimomura, Y., 2006. Dynamics of an Axisymmetric Body Spinning on a Horizontal Surface. IV. Stability of Steady Spin States and the 'Rising Egg' Phenomenon for Convex Axisymmetric Bodies, *Proc. R. Soc. A.* 464(2075):3253-3275.

[8] Brauer and Nohel, 1989. The Qualitative Theory of Ordinary Differential Equations: An Introduction, *New York, Dover Publications, Inc.*

[9] Bray, 2001. Cell Movements, 2nd edition, *Garland Publishing, Taylor and Francis Group.*

[10] Burden and Faires, 2000. Numerical Analysis, 7th edition, *Brooks Cole.*

[11] Carr, 1981. Applications of Centre Manifold Theory, 1st edition, *Springer-Verlag, Ney York, Inc.*

[12] Collins, Dan and Avissar, Roni, 1994. An Evaluation with the Fourier Amplitude Sensitivity Test (FAST) of Which Land-Surface Parameters Are of Greatest Importance in Atmospheric Modeling, *J. Climate.* 7:681-703.

[13] Cukier et.al., 1973. Study of the sensitivity of coupled reaction systems to uncertainties in rate coefficients. I Theory, *J. Chem. Phys.* 59:3873-3878.

[14] Cukier et.al., 1978. Nonlinear Sensitivity Analysis of Multiparameter Model Systems, *Journal of Computational Physics.* 26:1-42.

[15] Decker J.M., 2006. Cytokines, *University of Arizona Immunology 419.* http://microvet.arizona.edu/Courses/MIC419/Tutorials/cytokines.html, last accessed 1/5/09.

[16] Demmel, 1997. Applied Numerical Linear Algebra, *SIAM, Philadelphia, PA.*

[17] Eriksson P.S., et al., 1998. Neurogenesis in the adult human hippocampus, *Nat.*

Med. 4(11):1313-1317.

[18] Farlow, 1993. Partial Differential Equations for Scientists and Engineers, Reprint, *Dover Publications*.

[19] Garabedian, 1964. Partial Differential Equations, *John Wiley & Sons, Inc.*

[20] Gilbert, 2006. Developmental Biology, 8th edition, *Sunderland, Sinauer Associates*.

[21] Goodsell, 1998. The Machinery of Life, *Springer-Verlag New York, Inc.*

[22] Hackbusch, 1994. Iterative Solution of Large Sparse Systems of Equations, *Springer-Varlag New York, Inc.*

[23] Hammacher A., Simpson R.J., Nice E.C., 1996. The interleukin-6 (IL-6) Partial Antagonist (Q159E,T162P)IL-6 Interacts with the IL-6 Receptor and gp130 but Fails to Induce a Stable Hexameric Receptor Complex, *Journal of Biological Chemistry.* 271(10):5464-5473.

[24] Jostock et.al., 2001. Soluble gp130 is the natural inhibitor of soluble interleukin-6 receptor transsignalling responses, *European Journal of Biochemistry.* 268:160-167.

[25] Keller, Evelyn and Segal, Lee, 1971. Model for Chemotaxis, *J. Theor. Biol.* 30:225-234.

[26] Keller, Evelyn and Segal, Lee, 1970. Initiation of Slime Mold Aggregation Viewed as an Instability, *J. Theor. Biol.* 26:399-415.

[27] Kendall and Stuart, 1979. The Advanced Theory of Statistics, Volume 2, 4th edition, *Charles Griffin & Company Limited*.

[28] Kirschner et.al., 2008. A methodology for performing global uncertainty and sensitivity analysis in systems biology, *J. Theor. Biol.* 254:178-196.

[29] Krauss, 2001. Biochemistry of Signal Transduction and Regulation, 2nd edition, *Weinheim, Wiley*.

[30] LeVeque, 2002. Finite Volume Methods for Hyperbolic Problems, *Cambridge University Press*.

[31] Levine, Howard and Sleeman, Brian, 1997. A System of Reaction Diffusion Equations Arising in the Theory of Reinforced Random Walks, *SIAM J. Appl. Math.* 57(3):683-730.

[32] Lindmark E.L., Diderholm E., Wallentin L., Siegbahn A, 2001. Relationship Between Interleukin 6 and Mortality in Patients with Unstable Coronary Artery Disease, *JAMA*. 286:2107-2113.

[33] Liu, 2003. A First Course in Qualitative Theory of Differential Equations, 1st edition, *Pearson Education, Inc*.

[34] Lu, Yichi and Mohanty, Sitakanta, 2001. Sensitivity analysis of a complex, proposed geologic waste disposal system using the Fourier Amplitude Sensitivity Test method, *Reliab. Eng. Syst. Safety*. 72:275-291.

[35] Marz et.al., 1999. Neural activities of IL-6-type cytokines often depend on soluble cytokine receptors, *European Journal of Neuroscience*. 11:2995-3004.

[36] Mehler, Mark and Kessler, John, 1997. Hematolymphopoietic and inflammatory cytokines in neural development, *Trends Neurosci.* 20:357-365.

[37] Mistry S.K., Keefer E.W., Cunningham B.A., Edelman G.M., Crossin K.L., 2002. Cultured Rat Hippocampal Progenitors Generate Spontaneously Active Neural Networks, *PNAS.* 99(3):1621-1626.

[38] Mitchell and Griffiths, 1980. The Finite Difference Method in Partial Difference Equations, *John Wiley & Sons, Inc.*

[39] Murray, J.D., 2002. Mathematical Biology I: An Introduction, 3rd edition, *Springer.*

[40] Oh J., Recknor J.B., Recknor J.C., Mallapragada S.K., Sakaguchi D.S., 2009. Soluble factors from neocortical astrocytes enhance neuronal differentiation of neural progenitor cells from adult rat hippocampus on polymer substrates, *Journal of Biomedical Materials Research A.* 91(2):575-85.

[41] Oh J., McCloskey M., Blong C., Bendickson L., Nilsen-Hamilton M., Sakaguchi D.S. An Astrocyte-Derived Interleukin-6 Promotes Specific Neuronal Differentiation of Neural Progenitor Cells from Adult Hippocampus. (in press)

[42] Othmer, Hans and Stevens, Angela, 1997. Aggregation, Blowup, and Collapse: The ABC's of Taxis in Reinforced Random Walks, *SIAM J. Appl. Math.* 57(4):1044-1081.

[43] Perko, 2001. Differential Equations and Dynamical Systems, 3rd edition, *Springer-Verlag, New York, Inc.*

[44] Recknor J.B., Sakaguchi D.S., Mallapragada S.K., 2006. Directed growth and selective differentiation of neural progenitor cells on micropatterned polymer substrates, *Biomaterials,*. 27:4098-4108.

[45] Sachdev, 1991. Nonlinear Ordinary Differential Equations and their Applications, 1st edition, *Marcel Dekker, Inc.*

[46] Salamon, Sibani, and Frost, 2002. Facts, Conjectures, and Improvements for Simulated Annealing, *Society for Industrial and Applied Mathematics.*

[47] Saltelli, Tarantola, and Chan, 1999. A Quantitative Model-Independent Method for Global Sensitivity Analysis of Model Output, *Technometrics.* 41(1):39-56.

[48] Saltelli, Chan, and Scott, 2000. Sensitivity Analysis, 1st edition, *John Wiley & Sons, Ltd.*

[49] Schroers et.al., 2005. Dynamics of the gp130 Cytokine Complex: A Model for Assembly on the Cellular Membrane, *Protein Sci.* 14:783-790.

[50] Smiley, M.W., 2007. A Monotone Conservative Eulerian-Lagrangian scheme for Reaction-Diffusion-Convection Equations Modeling Chemotaxis, *Numerical Methods for Partial Differential Equations.* 23:555-586.

[51] Smiley, M.W., 2009. An Efficient Implementation of a Numerical Method for a Chemotaxis System, *International Journal of Computer Mathematics.* 86(2):219-235.

[52] Smiley, M.W. An Efficient Implementation of a Numerical Method for a Chemotaxis System, supplementary notes.

[53] Stein, Michael, 1987. Large Sample Properties of Simulations Using Latin Hypercube Sampling, *Technometrics*. 29(2):143-151.

[54] Taga and Kishimoto, 1997. gp130 and the interleukin-6 family of cytokines, *Annu. Rev. Immuno.* 15:797-819.

[55] Van Loan, 1992. Computational Frameworks for the Fast Fourier Transform, *SIAM, Philadelphia, PA*.

[56] Weyl, Hermann, 1938. Mean Motion, *Am. J. Math.* 60:889-896.

[57] Bell, E.T., 1927. Partition Polynomials, *Annals of Mathematics*. 24:38-46.

[58] Charalambides, 2002. Enumerative Combinatorics, *Chapman & Hall / CRC*.

ACKNOWLEDGEMENTS

I would like to take this opportunity to express my thanks to those who helped me with various aspects of conducting research and the writing of this thesis. First and foremost, I would like to thank professors Howard Levine and Michael Smiley for agreeing to be my advisors, and for all of the guidance, patience, and support they have given me over the years. I would like to thank professors Marit Nilsen-Hamilton, Jeffrey Essner, Tasos Matzavinos, and Khalid Boushaba for agreeing to serve on my committee. I would additionally like to thank the Co-P.I.'s of the research project that formed the basis of my research: Marit Nilsen-Hamilton, Don Sakaguchi, Surya Mallapragada, Howard Levine, and Michael Smiley. Your helpful commments and the discussions that we have had not only guided my research, but also helped improve my understanding of both biology and mathematics, and the interplay that exists between the two disciplines. Finally, I would like to thank my former professors Namyong Lee and Charles Waters for all of their help during my previous studies and for convincing me to continue on for my doctorate. If I had not continued with my education when I did, I likely would have never made it this far.